STRESSES AND DEFORMATIONS ON BRACED CUTS IN SANDS

Gunther Erwin Adolf Bauer, Ph.D.
Department of Civil Engineering
University of Ottawa, 1969

An experimental and analytical investigation has been conducted with the objective of finding a general relationship between the deformation of a braced cut in dense sand and the corresponding earth pressure distribution. The presently existing theories are scrutinized with respect to their applicability to the problem presented. A new solution is presented based on Dubrova's analysis (1963) which related qualitatively and quantitatively the active earth pressure distribution to the mode of deformation of the cut. The theoretical solution gives expressions for four different deformation patterns which can be possibly expected on a braced excavation. Different values of angles of internal friction and different wall friction angles are considered. In each type of movement the total active pressure is equal to the Coulomb value. The analytical investigation further examines the solutions for the coefficient of earth pressure at rest as proposed by Timoshenko (1934), Jaky (1944), and Hendron (1963).

The passive earth pressure is evaluated theoretically taking into account the roughness of the wall, plane and curved surfaces of sliding.

The phenomenon of soil arching is investigated and the two different concepts suggested by Terzaghi (1954) and Tschebotarioff (1952) are clarified.

The hydrodynamic conditions of the braced excavation are examined and compared to the theoretical and empirical solutions proposed by Bazant (1963), Marsland (1953), McNamee (1949), and Ordujanz (1954).

The experimental part was carried out on a full scale braced excavation which reached a depth of 50 feet. The quantities measured were; the earth pressures on two test piles, the pore water pressures, the horizontal deformations of the test section, and the strut loads. Field and laboratory tests supplied the necessary soil data.

The experimental results from the earth pressure cells lead to the conclusion that the lateral earth pressure distribution on the wall can be predicted by the theory outlined, if the deformation can be predicted and can also be controlled during construction.

After the excavation reached its final depth, the magnitude of the earth pressure can be calculated by Coulomb's theory.

The measured K-values assumed an average minimum value of 0.15 after a horizontal strain of 5 per cent was reached. It is therefore concluded that when this soil strain is exceeded the soil mass will be in a completely active state. It is held that this will be similar for other cuts in dense sand having similar soil properties and deformation behaviour.

The active earth pressure reached a minimum value after the wall had yielded a certain amount. Any further yield of the wall did not change the earth pressure. From this observation the shear strength does not appear to decrease with large strains and therefore the peak shear strength should be used.

The sheet pile penetration depth and the installed well point system did not prove entirely sufficient to prevent local boiling within the excavation.

STRESSES AND DEFORMATIONS ON

BRACED CUTS IN SAND

by

GUNTHER ERWIN ADOLF BAUER

B.A.Sc., University of Toronto, 1964

M.A.Sc., University of Waterloo, 1965

THESIS

Submitted in partial fulfillment of the requirements for the degree of Doctor of Philosophy in Civil Engineering in the Graduate School of the University of Ottawa, 1969.

Ottawa, Ontario

ACKNOWLEDGEMENT

This thesis was prepared under the direction and guidance of Dr. J.D. Scott, Chairman, Department of Civil Engineering, to whom the author wishes to express his most sincere gratitude for his continued advice, assistance and constructive criticism during the course of this investigation.

Professor N.E. Wilson, Department of Civil Engineering, McMaster University, initiated this investigation and was responsible for many of the ideas which contributed to the successful design and instrumentation of the test section.

The author is grateful to Mr. C. Christensen for considerable assistance with the field instrumentation and the gathering of the experimental data.

Special thanks are also due to Dr. S.S.-F. Ng, Department of Civil Engineering for assisting with the computer programme.

Acknowledgement is extended to Miss Nicole Renaud who has ably and patiently typed the manuscript.

The author also must acknowledge his indebtedness to the National Research Council for the financial assistance under Grant No. A-1183 and studentships which made this study possible.

Finally, the writer extends his sincere appreciation to his wife for her patience and continued encouragement throughout his entire education. To his beloved wife Irmgard this thesis is dedicated.

TABLE OF CONTENTS

LIST OF TABLES

LIST OF FIGURES

LIST OF FIGURES (continued)

LIST OF FIGURES (continued)

LIST OF FIGURES (continued)

LIST OF FIGURES (continued)

PRINCIPAL SYMBOLS

A_{st}	cross-sectional area of strut
B	width or halfwidth of excavation
C	constant
C_i	confinement index
D	grain size, diameter, depth of sheet pile penetration
D_{10}	effective grain size
D_r	relative density of cohesionless soil
E	modulus of elasticity
E_{st}	modulus of elasticity of strut
e	void ratio
e_{max}	void ratio in loosest state
e_{min}	void ratio in densest state
e_c	critical void ratio
F	reaction, resultant force, seepage force, factor of safety.
G	specific gravity of soil solids
H	depth of excavation, total thickness of soil layer
h	hydraulic head
i	hydraulic gradient, slope angle
i_c	critical hydraulic gradient
K	ratio between intensities of horizontal and vertical pressures at a given point in a soil mass

K_o coefficient of earth pressure at rest, measured or computed

K_A coefficient of active earth pressure, measured or computed

K_p coefficient of passive earth pressure, measured or computed

k coefficient of permeability

L length of excavation, length of flow path

M moment of a force

N number of blows on sampling spoon during performance of standard penetration test, normal reaction

n ratio between distance from bottom of retaining structure to point of application of earth pressure, and total height; porosity

P resultant pressure, normal force

P_A active earth pressure

P_p passive earth pressure

p pressure or normal stress

p_a intensity of active earth pressure

p_p intensity of passive earth pressure

p_o initial pressure, overburden pressure

Q total discharge per unit of time, concentrated load, strut load

q uniformly distributed load, surcharge per unit area, flow rate per unit length

r radius

r_o radius of logarithmic spiral

t time

U	total neutral stress, total pore water pressure
u	neutral stress, pore water pressure
V	total volume
v	discharge velocity
W	weight
W'	effective or submerged weight
z	depth
α	angle, coefficient
β	angle between horizontal and back of retaining structure
γ	unit weight of soil
γ'	submerged unit weight of soil
γ_d	dry unit weight of soil
γ_s	unit weight of solid constituents
γ_w	unit weight of water
Δ	increment
δ	angle of wall friction
ε	unit strain
ε_{xy}	unit shear strain
Θ	angle, central angle
ν	Poisson's ratio
ζ	angle between normal direction and resultant force of sliding surface
π	3.14159

σ	normal stress
σ_1	major principal stress
σ_3	minor principal stress
τ	shearing stress
τ_o	shearing stress along wall of retaining structure
ϕ	angle of internal friction, angle of shearing resistance
ϕ'	effective angle of internal friction
ψ	angle between vertical direction and total earth pressure

CHAPTER 1

INTRODUCTION

1.1 General

The problem of earth pressure on an engineering structure is one of the most basic and central topics of Civil Engineering. The design of retaining walls, braces for open cuts, the stability of natural slopes, or the determination of rock pressures on shafts or tunnel linings requires the solution of special earth pressure problems. In these different cases the knowledge and possible change of the magnitude and distribution of earth pressure is vital in the design of a safe and economic structure.

There are a variety of theories available for calculating earth pressures on retaining structures, such as theories based on the concept of elasticity and plasticity, extreme and empirical methods. But in order to be fully satisfactory a general earth pressure theory should enable a reasonable correct calculation corresponding to any assumed movement of the retaining structure. Therefore all theories and methods listed above will have to be scrutinized from this point of view.

Solutions based on the theory of elasticity are based on simplifying assumptions and do not fully describe the behaviour of the soil. Moreover, they are mathematically complicated and have the inherent defect of not giving any information about the safety against ultimate failure.

Theories based on the plasticity concept may be very valuable, but they are only correct when the boundary conditions are properly satisfied. They also assume a zone rupture and therefore cannot be applied to line ruptures.

Extreme methods have so far given the best results as compared to experimental facts as far as the magnitude of the earth pressure is concerned. The distribution is assumed to be independent of the soil strain.

Empirical methods may be very useful, but since they are neither based on any theoretical concepts nor are they generally applicable, their usefulness is limited to the conditions for which they were originally developed.

None of the above mentioned theories satisfy the requirements of a general earth pressure theory, at least not in their present form.

1.2 Statement of Problem

The design of the structural components of a braced excavation requires a knowledge of the forces and deformations transmitted from the soil to the structure. An evaluation of these forces and movements is necessary in order to guaranty an economical and safe structure. The complexity of this problem is further increased by the dependency of the stresses, with respect to magnitude and distribution, on the deformation behaviour of the structure.

At present, however, a systematic description of the stress-deformation behaviour of even dry granular material is not available. No satisfactory theoretical solutions exist to date which relate the earth pressure distribution to the deformation of the structure. The actual shape of the earth pressure distribution curve depends on the type and number of struts and the strain mobilized within the retained soil mass. Due to the deformation of the wall, the distribution as well as the magnitude of the earth pressure changes. Before a retaining structure collapses a considerable redistribution of stresses within the soil due to shear forces has taken place. This results in an increase of pressure on the less yielding parts of the structure and a corresponding decrease at the more flexible parts. This phenomenon imposes the important question of whether the sheeted structure should be designed for one pressure distribution only, should several types of distribution be considered, analogous to the different loading diagrams in structural engineering, or should an envelope containing any possible pressure distribution be used. A partial answer to this question can be found from measurements on a prototype structure.

There are many theories which the designer can employ to calculate the total earth pressure on the retaining structure. But no theory in soil mechanics should be adopted for practical use without ample proof by field observations that the theory will be at least reasonably accurate. As pointed out earlier the magnitude of earth pressure will also change with the deformation of the cut which in turn will depend to a large extent on the type of bracing and the construction methods. Recently; a number of new or improved techniques have appeared. Rarely can a theory take all these factors into consideration. But it is of extreme importance to know if the theory employed gives an upper or lower boundary value.

The mode of soil deposition and subsequent geological history will undoubtedly effect the magnitude and distribution of the earth pressure acting on the cut. Laboratory tests or large scale model tests cannot simulate or completely reproduce these conditions. Full-scale tests may evaluate these effects provided the soil profile is known and the geology is fairly simple.

To date only three reliable full-scale measurements have been made in sandy soils: in the Berlin Subway in 1936 (Spilker 1937), in the New York Subway (White and Prentis 1940), and in the Munich Subway (Klenner 1941). Only the strut loads on several sections were measured in these investigations. The earth pressure distribution was then computed from the strut loads neglecting the continuity of the sheet piles. Very little investigation was done concerning the soil condition and most of the soil parameters had to be estimated. The design criteria presently used for determining the structural components of a braced cut in sand, such as sheeting, wales, and braces, are based on these measurements (Terzaghi and Peck 1967) and on the results of large-scale model tests (Tschebotarioff 1951).

It is evident that the results from the measurements on the cuts (Berlin, Munich, and New York), which were obtained more than a quarter of a century ago, can only provide the answer with respect to the magnitude of earth pressure acting on the cut. The unknown factors had to be taken into consideration by allowing an additional factor of safety. Questions concerning the effect of stress history, influence of geological conditions, different construction methods, earth pressure distribution, settlements and deformations, and influences due to hydrodynamic conditions remained unanswered.

1.3 Objectives of the Study

The previous sections have indicated the prevailing state of limited knowledge in this field. The purpose of this investigation was to continue and to further the work toward a better understanding of the behaviour of braced cuts in sand.

The main objective was to find a theoretical and experimental relationship between the deformation of a braced cut and the corresponding earth pressure distribution. The solution to this problem should relate qualitatively and quantitatively the active earth pressure distribution to the mode of deformation of the cut. The theoretical relationship should be generally applicable considering different types of wall movements and a wide range of soil parameters. By controlling the deformation it should be possible to control the pressure distribution on the cut. The relation between pressure distribution and deformation as obtained from the experimental test should either prove or disprove the corresponding theoretical concept.

The second objective was to scrutinize and to evaluate the many existing earth pressure theories for calculating the magnitude of the active and passive earth thrust acting on the braced cut and to select or to propose a theory which can be used to safely predict these forces. Preference should be given to a theory which can be readily applied to different soil conditions, layered systems, and various construction methods. The experimental measurements of the forces due to the active and passive earth pressures were to show the validity of the proposed theory.

The soil at the test site consisted of medium to heavily overconsolidated dense fine sand and it was proposed to evaluate the effect of the mode of deposition and the previous stress history of the soil on the earth pressure, especially at the at-rest condition. The experimental results should compare with the existing theories.

The soil exploration prior to the construction indicated a very high water table and it was clear that controlling the seepage water would be a major problem. Therefore the construction of the cut would provide an ideal opportunity to study the hydrodynamic conditions and the adequacy of the sheet pile penetration depth.

The investigation also attempted to clarify the short comings in our knowledge of the behaviour of soil as derived from present testing methods. Suggestions were made as to what type of tests could be used in order to comply with the actual field behaviour of the soil.

The experimental investigation also served as a continuous check on the behaviour of the structure during construction.

1.4 Outline of Thesis

In the following chapter a general survey is given of the existing literature on the theories of earth pressures. Previous experimental work is also reviewed and discussed with respect to braced open cuts.

Chapter 3 gives a detailed review of the performance of open cuts. The construction procedures are outlined and their effect on wall movement is discussed. It is also clarified why from the theoretical point of view a braced excavation deforms approximately like a stiff retaining wall rotating about its top strut level.

Chapter 4 is divided into five main Sections. Section 1 is a general outline of the problem involved. Section 2 takes a critical view of present theories employed in calculating lateral pressures on braced excavations. The validity of assuming different forms of failure planes are investigated and compared to actual failure surfaces as determined from model tests. One method is emphasized which shows considerable merit and also takes into account the four basic modes of wall movement that could occur on a braced excavation. Lateral pressure distribution envelopes are plotted up for a range of internal friction and wall friction angles.

In Section 3 the stress-strain relationship for the cohesionless soil behind the vertical wall is established with respect to the deformation characteristic and the dilating properties of the cohesionless soil. The inadequacies of present laboratory tests are discussed which usually measure the axial strains whereas earth pressures problems involved lateral strains in two dimensions (plane strain). Further the difference in stress-paths of the prototype and the laboratory tests are evaluated. Usually constant strength parameters are assumed along the failure plane but it is shown that the angle of frictional resistance varies with the soil deformation due to wall displacement.

Much controversy exists about the concept of soil arching on retaining structures. It is hoped that Section 4 sheds some light on this controversy and new concepts of soil arching are proposed.

In Section 5, the hydrodynamic conditions are considered and a minimum depth of sheet pile penetration is suggested as a safeguard against bottom heave and boiling.

Chapter 5 describes the general geology soil conditions and excavation procedures at the excavation studied. The results from the field measurements are shown, such as, earth pressures, strut loads, water pressures, and sheet pile movements.

The results from the laboratory tests are discussed with respect to applicability to the problem presented and shear strength parameters for plane strain conditions are proposed.

The experimental results are discussed in Chapter 6 and correlations are also presented which qualitatively and quantitatively compare the actual behaviour of a full-scale braced sheeted cut and its lateral earth pressure distribution with the behaviour and distribution suggested by the theory presented in Chapter 4.

In the final Chapter, the summary and conclusions are presented. Future research which appears warranted as a result of this study is also suggested.

CHAPTER 2

HISTORICAL REVIEW OF EARTH PRESSURES ON RETAINING STRUCTURES

Earth pressure problems have intrigued and challenged engineers and scientists for the last few centuries and they still occupy a position of paramount importance in the field of Soil Mechanics. Even today hardly a year passes without the publication of a new earth pressure theory, but the basic question still remains: "What is the relationship between the movement of a partly or completely embedded structure and the resulting forces and stresses at the contact surfaces?"

There are three possible ways of finding a solution to this problem: from the theoretical point of view, from results based upon experimental investigation, or from utilizing the knowledge derived from practical experience. None should be given preference; they rather should be considered to supplement one another. Each approach has its limitations. Due to the complexity of the problem, simplifying assumptions have to be made in each category and most solutions obtained are only valid for a particular case of the problem. Much too often these assumptions have been and still are ignored or even forgotten by the practising engineer and the theory is applied with little regard to its range of validity. Even results from large scale model tests should be interpreted with care since a complete simulation of the prototype is hardly possible. The same is equally true for measurements of actual structures, each being exposed to different conditions and construction procedures.

A theoretical treatment of this problem was the most natural approach, because of the initial experimental difficulties and the desire to base any new concept on a sound theoretical foundation. To measure a stress there must be a certain strain and this deformation then falsifies the stress field in the environment of the measuring device. Coulomb in 1776 was the first person to supply a mathematical correct solution to the above question. His analysis was based on two main assumptions: firstly, that the failure surface was plane, and secondly, that the thrust on the wall acted in some known direction Once these assumptions had been made, the resultant thrust on the wall could easily be determined by simple considerations based on statics, Coulomb's theory, at least in its original form, has a considerable historical significance, since it was the first earth pressure theory to solve the problem correctly from the point of view of mechanics based on the frictional resistance of the soil, $\tau = C + \sigma \tan \phi$, which is also referred to as Coulomb's law of shearing resistance.

From the many possible failure planes through the toe of the wall one must choose the surface for which the earth pressure resultant attains an extreme value, a minimum for the passive pressure and a maximum for the active. Coulomb's method does not let us determine either the earth pressure distribution on the back of the wall or the location of the center of pressure. This difficulty is overcome by assuming a hydrostatic pressure distribution which assumes that the pressure on the wall increases linearly with depth. The laws of equilibrium for the soil wedge can only be satisfied if the distribution of pressure along the rupture surface is triangular, the ground surface horizontal and the back of the wall smooth. This means that either the earth pressure distribution is not hydrostatical, or the rupture-line is not straight, or both. Actually, Coulomb's method must be considered as an approximate means of calculation a zone-rupture; in this case the actual earth pressure distribution is hydrostatical, but the actual rupture line is usually not straight. It has been found from large and full scale measurements (Terzaghi 1934, Spilker 1937) that the active earth pressures calculated by means of Coulomb's equation are only a few percent smaller than the measured values, whereas in the passive case the calculated values may exceed the actual ones by 50% or more. Consequently, Coulomb's method should only be used for active cases and only then when certain deformation characteristics of the wall are satisfied and will bring about a state of failure at any point along the failure slip plane.

The earlist recorded experimental work was done in 1720, by the Frenchman Belidore, who concluded from his observations that the surface of rupture was on a slope 1:1, this was later modified by Mayniel

(1808) to a slope of two horizontal to three vertical, even though the natural slope of the material (angle of repose) was 1:1. Cauthey, in 1785, was probably the first scientist to perform a complete set of earth pressure experiments employing a wooden box 30 in. high and 12 in. wide. He succeeded in measuring a pressure at five different depths. The experimental earth pressures were increasing with depth. The same pressures were recorded for different sloping bottoms until it was tilted to 67.5 deg. to the horizontal. In this way he proved that the material below that plane had no effect on the pressure against the vertical wall. Most of the earlier experiments were done with small scale equipment in which the side effects were sometimes greater than the quantities to be measured. The earliest large-scale apparatus was built in Germany by Woltmann, in 1791, and consisted of a square box 1.15 m by 1.15 m by 1.72 m long. Until then the vertical test walls were usually hinged at the bottom to simulate the overturning of a stiff retaining wall. Woltmann has his wall hinged at the top and tested different materials such as sand, gravel and rye. The total lateral thrust obtained was approximately half of that given by Coulomb's equation. The vertical component was disregarded. Also no corrections were applied to compensate for the effect of side friction of the box. A friction correction of 2/11 of the measured earth pressure was proposed by Hagen later. Even taking this into account the total horizontal thrust is much too low as shown in later years by measurements using more refined apparata and measuring devices.

Hagen (1852) repeated Woltmann's test making one major change in allowing the fill to slope to each side in order to eliminate the effect of side friction. Due to this, the comparison with theoretical results was difficult. Lieutenant Hope, in 1845, built several full scale walls made of brick 2- ft. long and 10 ft. high having various cross-sections. Tests were carried out with dry and wet sand both in a loose and a dense state. He concluded that the Coulomb method gives the maximum pressure, and that also the line of intersection between the failure plane and the ground surface agreed closely with the wedge theory.

Collin, in 1848, made a study of the different failure surfaces and concluded that rupture did not occur along a predetermined surface but always along a definite surface approximating a plane. In Vienna, Forchheimer (1882) continued the experiments initiated by Winkler and determined the angle of the wedge rupture. Although he was experimenting with a very small test apparatus having different types of walls and mainly using very fine sand, his angles found agreed closely with the values as determined by the classical theory (Coulomb).

In 1857, Rankine found a mathematical solution using an entirely different approach than Coulomb. Considering the equilibrium conditions of an infinitely small element at failure in a semi-infinite cohesionless mass of soil, he could show that the rupture figure consisted of two systems of straight parallel lines, intersecting each other at angles of $90 + \phi$. In employing the Rankine theory it is usually assumed that the presence of a wall does not alter the stress in the soil. This implies, however, that only in special cases will the resulting stress on the wall have the exact direction consistent with the actual roughness of the wall. This is the most serious shortcoming of the Rankine theory. In the special case of a horizontal surface and a smooth vertical wall the same result is obtained as by means of Coulomb's theory. Since the horizontal displacement is supposed to have no effect other than to induce the slip, the factor "strain" does not appear in either Coulomb's or Rankine's theory. Very seldom is the concept of perfectly uniform lateral strain realized in a natural deposit which therefore limits this theory to a few special cases only.

The first tests in the United States were performed by Constable in 1784, but due to using peas as backfill material and a 16 in. wide test apparatus his results are questionable. An important step forward was made by Siegler in 1887, who was the first person to control the amount of motion of the test wall. He also measured the vertical pressure component. For a rotation about the top of the wall the resultant was a little above the lower one-third point and for rotation about the bottom the point of application of the resultant fell slightly below the one-third point.

The tests performed by Müller-Breslau, in 1905, in Germany are considered as examples of very carefully planned and executed tests in which he tried to check experimentally Coulomb's assumptions and results. The following conclusions can be drawn from these experiments:

(1) The total earth pressure was always smaller than calculated from Coulomb's equation when the angle of friction between the soil and the wall was greater than zero, i.e. $\delta > 0$.

(2) For $\delta = 0$ the observed values were smaller than the corresponding Coulomb values.

Müller-Breslau attributes these deviations to the non-linearity of the failure surface.

(3) The direction of the total thrust was in no way parallel to the ground surface as held by previous investigators. For rough walls δ could be as high as $3/4\ \phi$, but it was recommended to use lower values for design purposes.

(4) The point of application of the resultant ranged between 0.33 and 0.36 of the height of the wall if there was no surcharge. The effect of surcharge was to raise the center of pressure above the one-third point.

In 1908, the late J.C. Meem maintained on the basis of his vast experience in subway construction in New York City that the distribution of the earth pressure over the timbering of cuts is decidedly non-hydrostatic. His measurements showed that the forces in the top struts were much larger than in the lower ones, and that also the surface of sliding intersected the ground surface at right angles. His statements were corroborated by similar practical experiences described by Moulton (1920). Meem's observations have only a qualitative importance due to the crude measuring devices employed and the inadequate soil data supplied, but this was the first time that this phenomenon was recorded for braced open cuts.

Kötter in 1903 succeeded in deriving a differential equation relating the stresses on a slip surface to the curvature. Knowing the boundary conditions the stresses along any point of the rupture surface could be calculated. This decreased the degree of indetermination of the problem by one. The validity of Kötter's equation was originally derived for cohesionless soils but it also could be applied to soils with cohesion. Until 1940 very little use had been made of this because the theory is cumbersome and not quite simple. But with the help of modern computers this difficulty should be overcome.

Since 1910 the development of the different theories of plasticity was emphasized chiefly by Saint Venant (1871), von Mises (1913), Prandtl (1920, 1927), Nadai (1928), and Odquist (1934). Most of the theories put forward were developed for metals but were modified and also applied to the problem of earth pressures. Prandtl in 1920 solved the problem of earth pressure acting on a rough wall for a weightless or frictionless oil. In 1926 von Karman solved the corresponding problem for soil having both weight and internal friction.

At approximately the same time experimental work was carried out by Feld (1921) in America and by Fanzius (1924) and Krey (1926) in Germany. Jenkins in 1932 investigated the pressures exerted by dry granular materials and by submerged sand on retaining walls having many different shapes. He concluded that the resultant is inclined to the wall and the position may be much higher than the one-third point. Stability investigations and earth pressure calculations based on the extreme method principle, but assuming circular rupture lines, were made by Fellenius in 1927. The circular rupture line enables a simple analysis to be made for frictionless soil because the unknown stresses do not enter into the moment equation about the center of the circle. A corresponding calculation can be made for soils with internal friction when suitable logarithmic spirals are used as rupture lines. This is due to the fact that for such a spiral the angle between the radius vector and the normal is a constant, and when this angle is equal to ϕ the unknown normal stresses on the failure surface are directed towards its pole and consequently do not enter the moment equation about the pole. The first to make extensive use of this method was Reudulic (1935 and 1940), who succeeded in determining the general relation between the magnitude of the earth pressure on a smooth vertical wall and the location of its pressure center.

In 1934, Terzaghi published a series of five papers about tests performed in a 7 ft. high and 14 ft. wide earth pressure test apparatus at M.I.T. The wall was allowed to tilt around its lower edge or to move parallel to its original vertical position either against or away from the soil mass. The testing material consisted of dry sand in a loose or compacted state, saturated sand, fine-grained soils, partly saturated fill and glacial till. There was a marked difference between the behaviour of dense and loose sand, and the corresponding hydrostatic pressure ratios ranged from 0.35 to 0.70 depending on the relative density of the material. The maximum passive pressure was reached when the wall yielded inward through an average distance of about 0.1% of the wall height H. When the wall was moved outward by a distance greater than 0.8% of H, slip occured and the measured total pressure corresponded approximately with the Coulomb value. This was also in agreement with the results obtained by Müller-Breslau, Feld and others, where after the wall had undergone a relative small movement the magnitude of the earth pressure could be determined satisfactorily by the Coulomb theory. Exact agreement cannot be expected when dealing with materials like soils, due to the well known variation in physical characteristics because of non-uniformity. Of general interest is also Terzaghi's attempt to correlate the angle of internal friction to the movement of the wall. Substituting the horizontal component of the total earth pressure acting at an angle of δ to the normal of the wall into Coulomb's equation, the angle of internal friction was calculated for different wall movements. Well aware that the triangular earth pressure distribution did not hold true for braced cuts Terzaghi developed in 1936 a method taking the deformation into account. He introduced a factor "Ci", which he called the confinement index and depended on the relative density of the sand as well as on the mode of the lateral expansion of the wall. The form of the factor was given by $Ci = \frac{K - Kc}{Kc}$, where Kc is equal to the hydrostatic pressure ratio as determined by Coulomb's method and K is an assumed earth pressure coefficient which is greater than Kc. The denser the sand the larger Ci becomes and the pressure distribution becomes approximately parabolic. For $Ci = 0$ Terzaghi's equation will be identical with Coulomb's. This method proved to be unsatisfactory due to the difficulty in choosing the appropriate Ci value which depended both on the type of lateral expansion of the soil mass as well as on its intrinsic properties. A similar method for calculating the earth pressure distribution was derived by Hertwig (1939). In contrast to Terzaghi, who only utilized the two equilibrium conditions $\Sigma V = 0$ and $\Sigma H = 0$ as basis for his derivation, Hertwig in addition made use of the moment equation $\Sigma M = 0$. The results of both methods were similar.

After Terzaghi had concluded his large scale tests to establish the validity of Coulomb's theory, measurements were taken on two full-scale braced excavations in Munich and Berlin, Germany in 1936. From these results it was hoped to derive some basic rules applicable to the future designs of braced open cuts. On both structures it was observed that the earth pressure distribution was not at all triangular. Spilker, in 1937, reported the results from the Berlin subway. The tests performed by Lehmann in 1942 were supposed to clarify some factors which could not be controlled at the actual construction procedures in Munich and Berlin, such as the magnitude and type of wall movement, effect of surcharge, effect of vibration, roughness of the wall etc. He agreed with Terzaghi's conclusion that after a certain wall movement had been brought about the magnitude of the total earth pressure corresponded within 10% of the Coulomb value. Also the greater the wall roughness, the smaller was the measured lateral pressure component. The effect of vibration was to slightly increase the total pressure and the center of pressure was lowered.

In 1938 and 1948 Ohde in a series of publications derived the earth pressure distribution acting on the wall of a retaining structure. He assumed a circular line rupture and the horizontal component of the pressure distribution was basically of the form

$$e_x = \gamma h \left[C_1 \frac{y'}{h} - C_2 \left(\frac{y'}{h}\right)^n \right] \tag{2.1}$$

where y' is the depth at which e_x acts and C_1, C_2, and n are constants depending on the boundary conditions. The method proved to be far too complicated for universal practical application. Ohde differentiated between three "main types of wall deformations" as shown schematically in Figure 2.1. He used Kötter's equation to find the pressure distribution on the rupture surface and on the wall. Both distributions approximated parabolas for a wall rotating about its top. The circular sliding surface intersected the ground surface at right angles and also passed through the foot of the wall. The solution is an approximation only and the results exceeded Coulomb's value in some cases by as much as 25%. For wall movement "B" Ohde obtained a total lateral earth pressure which was 10% to 15% larger as compared to wall movement "A". For a flexible wall this difference was only about 5%. The whole soil body is assumed to remain

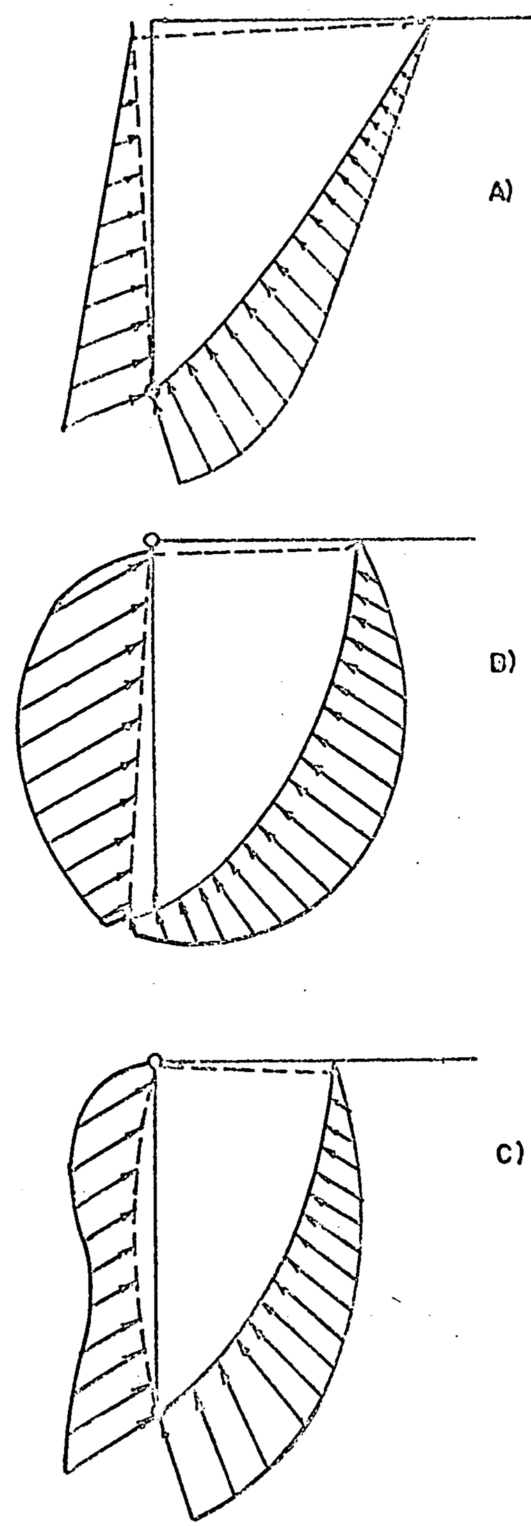

A) WALL ROTATING ABOUT TOE

B) WALL ROTATING ABOUT TOP

C) WALL ROTATING SIMUL- TANEOUSLY ABOUT TOP AND BOTTOM

FIG.2.1. MODES OF WALL DEFLECTION

perfectly elastic and the limiting equilibrium is only mobilized along the rupture surface (line rupture). The difference between Ohde's result and actual measurements is mainly due to the simplifying assumption of a circular sliding surface. A better approximation would be a doubly curved surface which however would make it extremely difficult to find a unique mathematical solution.

Since the agreement between Coulomb's and von Karman's theory of the active earth pressure case and between Ohde's rigorous and simplified theory of the passive earth pressure proved that a moderate departure of the assumed shape of the surface of sliding from the real one has little influence on the magnitude of the lateral earth pressure,Terzaghi (1941) substituted for the real surface of sliding Rendulic's logarithmic spiral with the polar equation:

$$r = r_o \, e^{\alpha \tan \phi} \qquad (2.2)$$

in which r_o = length of an arbitrary selected reference vector, α = angle between r and r_o, and ϕ = angle of internal friction. The spiral has to be chosen such as to pass through the foot of the wall as well as to intersect the horizontal ground surface at right angles and also to give a maximum value for the active and a minimum value for the passive earth pressure. For this method, known as the general wedge theory, the point of application of the total thrust must be assumed based on actual measurements and the total earth pressure exceeds Coulomb's value by approximately 10%.

In 1943, Peck published the systematic observations on the open-cut portions of the Chicago subway. It was the first thorough instrumentation and investigation of a full-scale structure. The results of the measurements were given together with a comparison of the measured earth pressures with generally accepted theories. He found that the magnitude of the total lateral pressure was in a satisfactory agreement with either the plane or the general wedge theories for purely cohesive soils having no effective internal friction but that the distribution of the pressure was non-hydrostatic, Measured movements of the sheeting were found to be in accordance with those theoretically necessary for non-hydrostatic distribution. He proposed a simple rule, based on the actual strut loads, applicable to the design of bracing for similar cuts in plastic clay deposits.

An extensive and most comprehensive research program was carried out by Tschebotarioff at Princeton in 1943 to 1948 sponsored by the Bureau of Yards and Docks, U.S. Department of the Navy. Most of his tests were performed with model flexible bulkheads anchored at the upper portion of the wall. The first series of model tests was performed in 1943 to 1945 with a 1:5 scale tank, which was essentially a concrete box, 18 by 13 by 9 ft, open at one end where it could be closed by the model steel bulkhead, which consisted of three independent vertical sections. The material employed ranged from clean sand of two different gradings to silty re-coloured clay and also mixtures of these two materials. The result of these tests were summarized by Tschebotarioff in 1949 in a special report. For most of these tests the backfill was deposited successively and no dredging took place in front of the wall. Since a theoretical treatment of anchored bulkheads was hardly existing at this time a comparison of the test results with theory was not possible.

Sokolovsky's first efforts (1939) in the field of earth pressure problems were directed towards the construction of a general method which could be used to examine the basic problems for a granular medium possessing weight where the lines of slip of both families are curved lines and the solutions would no longer have closed form. Various problems of critical equilibrium were formulated. The solution with a singular point and the fan of curved lines of slip which pass through the failure wedge have been extensively used. Between 1947 and 1953 he expanded his previous theories aiming at the solution of two problems: (1) the formulation of a general method for the examination of problems of critical equilibrium in a cohesive medium and (2) the development of a method which would simplify the calculation of various problems of the stress in an ideal granular wedge. But there are as yet certain difficulties connected with the construction of networks of slip lines because of the complexity and tediousness of the calculations.

A special theory of plasticity has recently been developed by Drucker and Prager (1951) under the name of "Limit Analysis", and they also have attempted to apply it to earth pressure problems. They defined first a statically admissable stress field by the conditions that it should satisfy the equilibrium equations and the yield inequality at any point, as well as the statical boundary conditions. Further, they defined a kinematically admissable velocity field which has to conform to the conditions of kinematics and, at any point, the equation:

$$\varepsilon_1 + \varepsilon_2 = \varepsilon_{nn} \sin \phi \tag{2.3}$$

where $\varepsilon_1 + \varepsilon_2$ represents the rate of dilatation and ε_{nn} the rate of maximum shearing strain. In order to calculate earth pressures by means of this method it is necessary to assume a fixed distribution of the earth pressure. If any statically admissable stress field can be indicated, the corresponding value of the earth pressure is an approximation which is somewhat on the conservative (safe) side. On the other hand, if any kinematically admissable velocity field can be indicated, the corresponding value of the earth pressure is an approximation which is somewhat on the unsafe side. Therefore it is possible to find theoretically an upper and lower bound value, the actual earth pressure must lie somewhere in between those two limits. Since statically admissable stress fields can be found for special cases only, one has usually to be content with kinematically admissable velocity fields which, as pointed out before, are on the unsafe side. Drucker and Prager consider the rupture line as a thin plastic zone, which necessitates that the rigid wedge can satisfy the above requirements only when the rupture line is a spiral rotating about its pole. The calculation of the corresponding case is executed in the same way as in Rendulic's method. The major shortcoming of this limit analysis is that it is based on the assumptions of continuous dilatation which does not seem to conform to experimental facts. The soil cannot go on dilating indefinitely. Instead, after a certain shear strain has been reached, incompressibility must be assumed in the narrow plastic zone which means that the rupture line must be a circle instead of a spiral.

Brinch Hansen in 1953 proposed a new method for calculation of earth pressures applicable to most problems in practical engineering. His method also could be extended to stability and foundation problems. It is based on the equilibrium principle. The unknown forces are determined by the statical equilibrium conditions of the structure and the soil mass. The stresses in an arbitrary rupture-circle are calculated by means of the Kötter equation and by means of certain boundary conditions in such a way that the equilibrium method will yield the same result as a corresponding extreme method. Before the earth pressure on the retaining structure can be calculated one or more figures of ruptures, i.e. a circle or a straight line or a combination of both, has to be chosen in agreement with the plastic deformations which are compatible with the movements of the structure. Like most calculation methods, Brinch-Hansen based his theory on several simplifying assumptions, sometimes of a merely tentative character. It is, therefore, most importance and necessary to compare the results of this method with suitable tests and general experience. Before this task has been accomplished his method should be used with suitable caution until tests by others will either prove or disprove the validity of this calculation method. Serious errors in applying this method should not be expected since it has been demonstrated repeatably that extreme-methods will produce very reliable results when used properly.

Rowe in 1952 carried out a remarkable series of tests with flexible, anchored sheetwalls. He studied the influence of surcharge, anchor level, anchor yield, dredge level, pile flexibility and soil density. He considered only cohesionless soils in his experiments. For yielding anchors Rowe agreed in principle, as did Tschebotarioff, with Coulomb's distribution of the active pressure, but with increasing flexibility the moments, and to a lesser degree the anchor pull, are reduced considerably which Rowe attributed chiefly to a rise of the passive earth pressure resultant. For yielding anchors, Rowe's method is probably the best available so far, but for unyielding anchors he suggested a reduction factor for the maximum bending moment based on Stroyer's (1935) experiments which does not seem quite satisfactory.

There are several other methods such as Christiani's method and the Danish Rules, which were based mainly on personal experience of

Skandinavian engineers and are applicable to special cases only.

Rowe and Briggs in 1961 reported the results of 29 tests with model strutted sheet pile excavations 3'-6" deep and 7'-0" long, using dry sand. The results demonstrated the general principle that stress is transferred from yielding to unyielding components of a composite structure. The total active load increased with the number of struts and the subsidence decreased. They established a direct correlation between subsidence and the angle of shearing resistance mobilized. They also claimed that for a sheeted excavation with more than one strut not even the active soil pressure may be computed on the basis of the failure parameters of the soil.

The Norwegian Geotechnical Institute published a special technical report in 1962 of the field data collected from measurements of the Oslo Subway construction. The observations were obtained from a test section of a strutted sheet pile excavation in clay. The instrumentation at the site consisted of the measurements of strut loads; earth and water pressures, ground settlements and pile movements. The purpose of the report was simply to record data, no interpretive conclusions concerning the field measurements were included. In 1961, Kane analysed a portion of the results obtained from the Oslo Subway construction.

In 1965 Müller-Haude and von Schreiber reported the results from measurements carried out since 1960 on the extension of the Berlin Subway construction. The scope of the measurements were to check out the existing empirical formulae so far available for braced excavations as well as to establish new design rules especially with respect to economy. The program included the measurements of foundations pressures, water level, strut loads, vertical earth pressures and temperature. From the measured strut loads the earth pressure distribution over the vertical wall was derived and found to be parabolic with the maximum lateral pressure occuring in the upper portion of the wall.

In 1966, Flaate investigated the results from most braced cuts in sand and in clay and made recommendations for future designs.

Presently other investigations of open cuts are being carried out in major cities in Europe and in North-American but no results have been made available to date according to the author's knowledge.

The foregoing review represents only a cross-section of the major publications in this field and is by no means complete. The author will refer to some of the work in more detail in the following chapters and as well make reference to other publications as need arises. A more extensive summary covering the experiments from 1720 to 1940 was given by Feld in 1940.

CHAPTER 3

BEHAVIOUR AND PERFORMANCE OF BRACED OPEN CUTS

The basic types of sheeting and bracing of excavations are confined to three main groups: vertical wood sheeting, soldier beams with horizontal timbers, and interlocking steel sheet-piles.

Vertical wood sheeting is the oldest and most inexpensive method. This type is normally limited to a depth from 16 to 20 feet, about the depth that can be driven at one time. For deeper excavations one has to resort either to driving of soldier beams and inserting horizontal timber laggings between the soldier beams immediately following excavation, or to interlocking steel sheeting. The former method is also referred to as the Berlin method because there it was used for the first time successfully for the subway excavation (Spilker 1937). The horizontal wooden timbers are spaced apart to provide drainage of the ground thus preventing the build up of hydrostatic pressure and therefore the systems can be designed considerably lighter than a steel sheeted one. The elimination of water pressure prevents a quick condition or boiling at the toe of the sheeting and drainage also reduces earth pressure by increasing the shearing resistance of the ground. The wooden laggings have to be spaced close enough together in order to prevent the sand from being washed through. Sometimes these spaces have to be plugged tight by straw or hay to stop the erosion of fine material below the water table. The sheeting can be placed on the rear flange of the soldier beams (usually H-piles) and the steel sections usually can be incorporated into the reinforcing for the wall. The horizontal sheeting can also be used as a back form for the permanent concrete wall particularly if wales are set back or eliminated by using braces to each soldier pile. In this way the horizontal sheeting and bearing pile can serve as an aid to the permanent structure.

Interlocking steel sheeting is usually the first type of sheeting considered by engineers. Its principal advantage is that it will penetrate to greater depths and is water tight and has excellent properties to resist bending especially in the Z-type piling. Steel sheeting, by preventing water from entering the excavation, causes hydrostatic pressure to build up which is much greater than that of a system retaining soil only. This requires a heavier system of wales and struts. It is also necessary that the cutoff below subgrade of the excavation be adequate to prevent bottom heave and blow-ups under the sheeting. For this reason it is desirable to seal the sheeting in an impervious layer such as clay, hard pan or rock. Interlocking sheet piles are difficult to drive in dense ground and should not be used in fill that has broken concrete, rip-rap, timbers, or in natural ground with boulders. The resistance of driving in dense sand is minimized by water jetting or using vibratory driving devices. But this has to be done carefully to insure water tightness and plumbness. If one sheet or interlock fails, the whole structure may fail. At the test site, interlocking steel sheet piles were used exclusively.

The normal construction procedure is to drive the piles to their full depths and then excavate the soil in front of them. Usually a row of struts is placed near the top of the excavation immediately after a small cut (stage 1, Figure 3.1) has been made. At this stage there is relatively little movement of the sheeting. Stage 2 is reached after a considerable amount of soil is excavated to allow the installation of the second row of struts. During excavation, movement of the wall takes place towards the cut. Because the upper part is restrained from movement by the struts already in place, movement is confined to the lower part of the cut only. Successive excavations will allow the wall to yield further towards the excavated pit. The placement of more struts at lower levels cannot prevent this deformation since their installation occurs after the deformation has already taken place. The number and spacing of strut levels depends on the depth of the cut and the headroom required for excavation. The final condition is shown in stage 3 of Figure 3.1, when the excavation has reached its full depth. The successive outward deflections of the cut are equivalent to a stiff wall rotating about its uppermost strut level. The total deformation of the braced open cut is usually sufficient to mobilize a rupture surface in the retained soil mass.

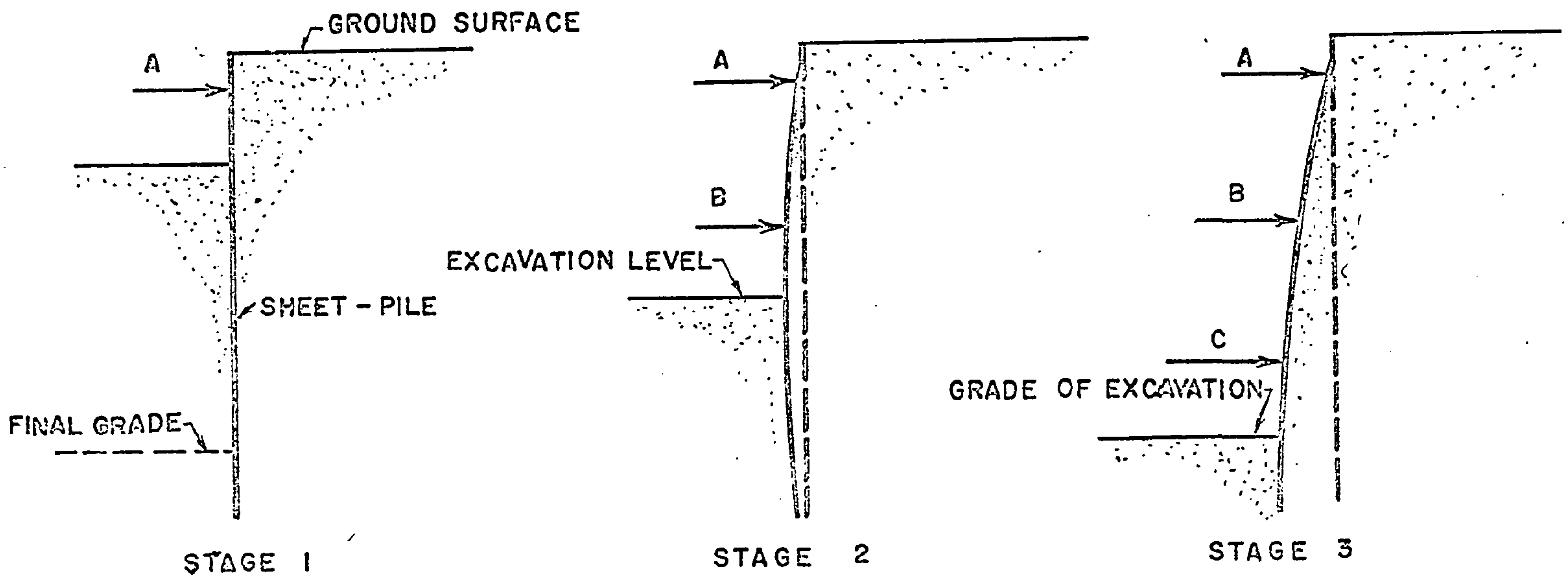

FIG. 3.1. DEFORMATION OF A BRACED OPEN CUT

The occurrence of the assumed rupture lines for the different stages has been indicated by Figure 3.2, and were shown experimentally by Lehmann in 1942.

The ideal deformation of the braced wall should be large enough for the earth pressure to become a minimum value and at the same time the resulting subsidence should be small enough not to cause any damage to adjacent structures. The elastic compression of the top strut has little effect on the final condition. The wall above the first strut will tend to move towards the soil located above this strut level.

In previous years it was assumed that the earth pressure distributions were influenced markedly by the wedging of the struts and wales, and it was also argued that the prestress in the struts were measured instead of the actual earth pressures exerted on the excavation wall. Theoretically it would be possible then to measure the passive earth pressure along the wall if the struts were wedged tight enough. This argument does not stand up to actual observations and measurements. The total earth pressure from strut load measurements has compared fairly well with either the classical theory or the general wedge theory for active earth pressures. Even when the struts were not wedged tight, an increase of earth pressure has been observed in the upper struts.

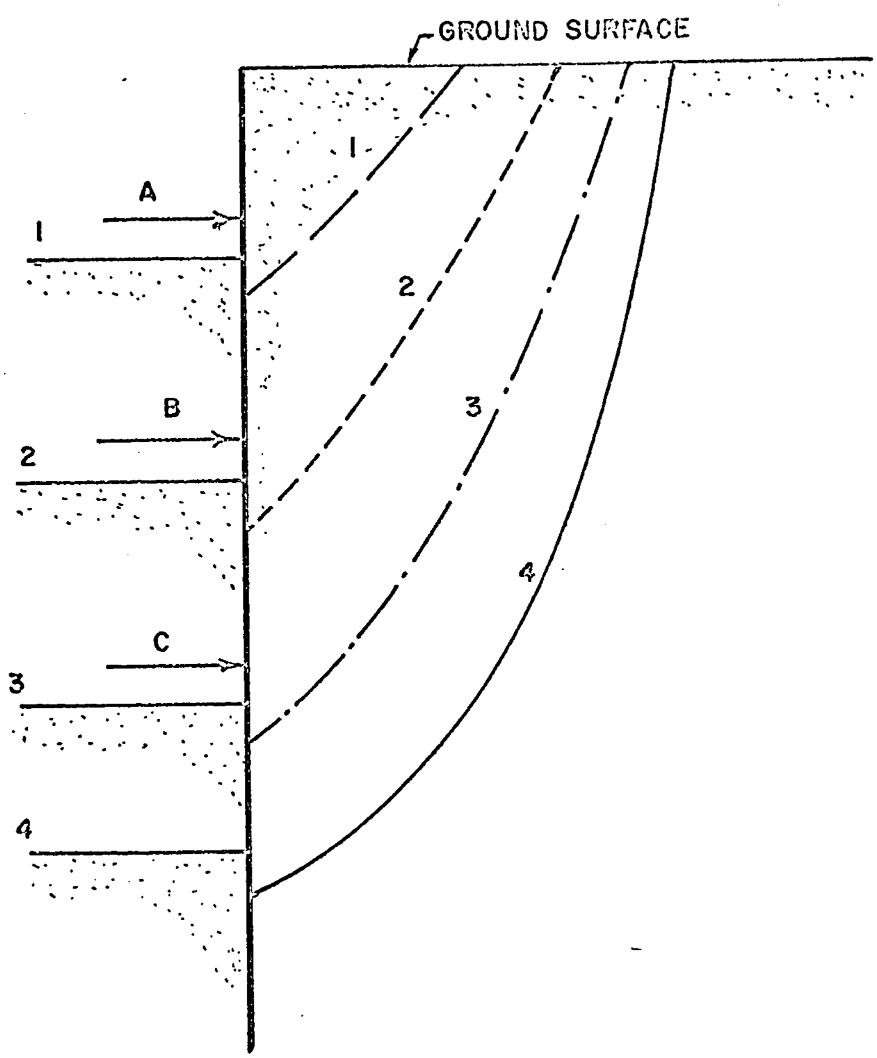

FIG.3.2. DEVELOPMENT OF SLIP SURFACES WITH PROGRESSING EXCAVATION

CHAPTER 4

THEORETICAL CONCEPTS FOR PREDICTING LATERAL EARTH PRESSURES IN SAND

4.1 General

In all braced structures a close relationship exists between the assumptions of design computations, the structural detailing and the construction procedures. All of which are of primary importance for the stability of the final product.

Most cuts would not have to be sheeted and braced if there was room to slope the sides as it is usually more economical to excavate the soil and backfill than to construct a sheeted cut. The necessity of maintaining neighbouring structures such as streets, buildings, utilities and sewers, requires that a system be installed that will retain and not interrupt these facilities near the excavation. Such a sheeting and bracing system can be constructed in an almost infinite variety of methods and designs to suit the type of ground encountered and structure to be built. There are numerous factors which have to be considered in designing bracing systems, such as, type of soil encountered, hydraulic conditions, closeness of buildings, the effect of heavy equipment operating on adjacent streets, allowable wall deformation and the resulting subsidence and last but not least the construction method. It also must be remembered that it is necessary to have a factor of safety as the bracing system is subjected to abuse of construction and braces can be damaged by blasting, dented by excavation equipment, and pressures may be greater than estimated because of leakage of water mains or sewers or improper pumping facilities. In a theoretical approach all of these factors cannot be taken into account but should be allowed for by providing an adequate factor of safety.

In this chapter the four major theoretical concepts in connection with the performance of braced cuts in sand are analysed. These concepts are: lateral earth pressures, stress-strain relationship, soil arching and hydrodynamic considerations. The order of dealing with these problems should not be interpreted as a rank of priorities. The concepts are of equal importance and more over they are interrelated.

4.2 Theoretical Lateral Earth Pressures

4.2.1 Plane Failure Surface

It is usually assumed that a sliding surface passes through the foot of the retaining structure and forms an earth wedge with the vertical wall and the ground surface. It is necessary then only to calculate the thrust which is necessary to maintain equilibrium.

Coulomb's theory utilizes a plane failure surface (Fig. 4.2.1) which necessitates one important condition. The retaining structure has to tilt outwards (away from the soil mass) about its foot. Only for such a deformation will the soil wedge ABC in Fig. 4.2.1 experience a uniform expansion, which would bring about an almost plane failure surface. The movement of the soil mass is resisted by the force Pa between the wall and the soil and by stresses along a plane AC. The limiting value of the force, Pa, is reached when the shear stress equals the shearing resistance along planes AC and BA, this is the active earth pressure Pa. For a cohesionless material the shearing resistance of the soil along plane AC and that between the soil and the wall along plane BA, are respectively

$$\tau = Q \tan \phi$$

and (4.2.1)

$$\tau_o = Pa \tan \delta$$

Coulomb (1776) postulated the assumptions listed below for his theory:

1. The sliding surface is a plane
2. The back of the retaining wall is vertical and the ground surface horizontal. Between the wall and the soil there exists no friction which makes the direction of the earth pressure horizontal (Fig. 4.2.1.a)

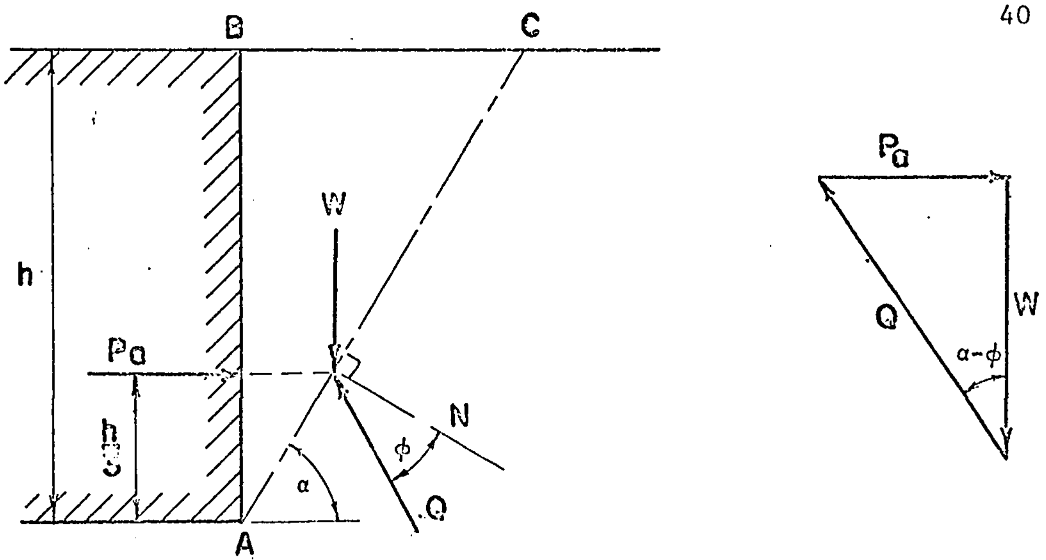

FIG. 4.2.1a COULOMB'S THEORY OF EARTH PRESSURE

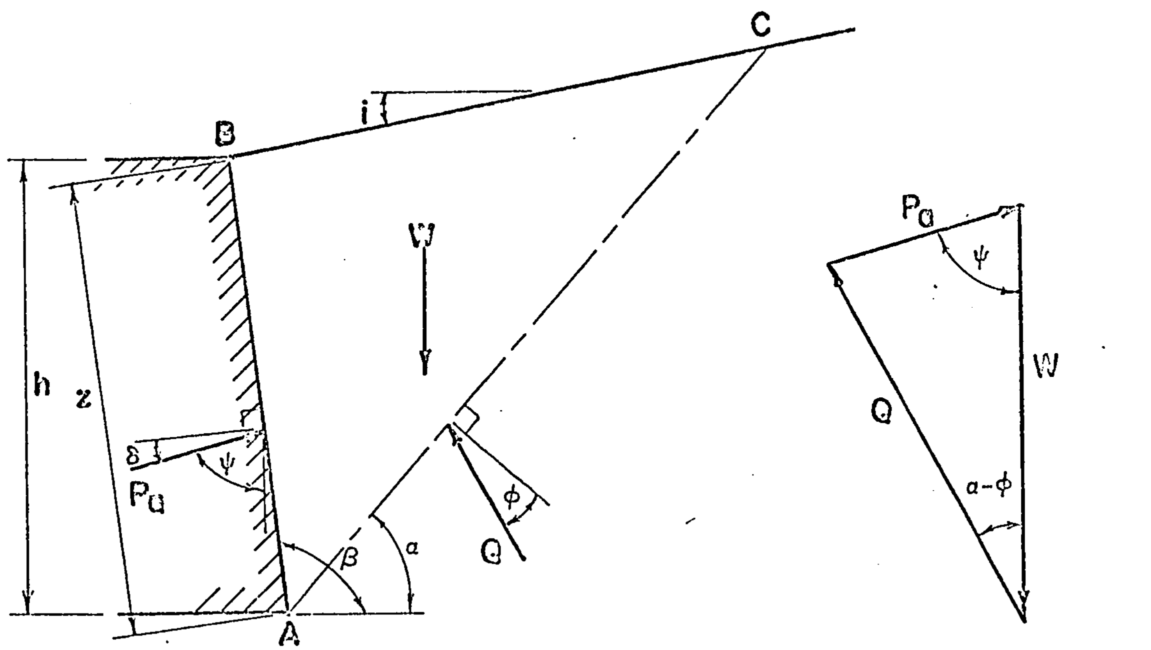

FIG. 4.2.1b GENERALIZATION OF COULOMB'S EARTH PRESSURE THEORY

3. Along the sliding surface Coulomb's condition of rupture is met (i.e. the maximum shear resistance is mobilized). The resultant force makes an angle of ϕ with the normal to the sliding surface.
4. There are infinite possibilities of sliding surfaces, the one chosen has to yield an extreme value for earth pressure.

From the force triangle (Fig. 4.2.1.a) one gets

$$Pa = W \tan (\alpha - \phi)$$

the weight of the soil mass is

$$W = \frac{h^2}{2} \gamma \cot \alpha$$

then

$$Pa = \frac{h^2}{2} \gamma \cot \alpha \tan (\alpha - \phi) \tag{4.2.2}$$

To get the extreme value for Pa

$$\frac{dPa}{d\alpha} = \frac{h^2}{2} \gamma \left[- \frac{\tan (\alpha - \phi)}{\sin^2 \alpha} + \frac{\cot \alpha}{\cos^2 (\alpha - \phi)} \right] = 0$$

whence

$$\alpha = 45 + \frac{\phi}{2}$$

substituting α into equation 4.1.2 results in

$$Pa = \frac{h^2}{2} \gamma \tan^2 (45 - \frac{\phi}{2}) = Ka \frac{h^2}{2} \gamma \qquad (4.2.3)$$

The point of application of the resulting thrust is obtained by differentiating Pa with respect to h, and the earth pressure distribution is:

$$pa = h \gamma \tan^2 (45 - \frac{\phi}{2}) \qquad (4.2.4)$$

which suggests a triangular pressure distribution with the resultant acting at the lower third point.

In a further development of Coulomb's theory by Müller-Breslau in 1906, the principle of a plane sliding surface was adhered to, but it was assumed that the wall was no longer frictionless (Fig. 4.2.1.b). The resultant earth thrust makes an angle of δ with the normal of the wall. δ is usually smaller than ϕ for cohesionless soils but may be as large as ϕ. Also the friction in the sliding surface is completely mobilized. In the general case it can be assumed that the ground surface slopes upward at an angle of i, the wall is inclined at an angle of β with the horizontal, and the earth thrust is inclined to the vertical at an angle of ψ. From the equilibrium conditions

$$Pa = W \frac{\sin (\alpha-\phi)}{\sin (\alpha-\phi+\psi)} = f (\alpha,\psi) \qquad (4.2.5)$$

The magnitude of the earth pressure is therefore a function of two variables. Assuming that the wall friction angle δ is known, then we can calculate, using Coulomb's fourth assumption (the earth pressure has to be an extreme value), the inclination of the sliding surface. Substituting this value into equation 4.2.5, the earth pressure is determined as

$$Pa = Ka \cdot \frac{z^2\gamma}{2} \tag{4.2.6}$$

where the coefficient of earth pressure:

$$Ka = \left[\frac{\sin(\beta-\phi)}{\sqrt{\sin(\beta+\delta)} + \sqrt{\dfrac{\sin(\delta+\phi)\ \sin(\phi-i)}{\sin(\beta-i)}}}\right]^2 \tag{4.2.7}$$

In the case where $\beta = 90^{\circ}$ and $\delta = i = 0$ we have the previous case

$$Ka = \left[\frac{\cos\phi}{1+\sin\phi}\right]^2 = \tan^2\left(45 - \frac{\phi}{2}\right) \tag{4.2.8}$$

The extreme value of the function $Pa = f(\alpha,\psi)$, (Eq. 4.2.5) is obtained by differentiating

$$dPa = \frac{\partial Pa}{\partial\alpha}\,d\alpha + \frac{\partial Pa}{\partial\psi}\,d\psi + 0 \tag{4.2.9}$$

Eq. 4.2.9 is satisfied when

$$\text{I.}\quad \frac{\partial Pa}{\partial \alpha} = 0 \qquad \text{and} \qquad \text{II.}\quad \frac{\partial Pa}{\partial \psi} = 0 \qquad (4.2.10)$$

Fig. 4.2.2 shows a graphical solution of the variation of earth pressure.

The function $Pa = f(\alpha, \delta)$ is shown in a three-dimensional plot. The surface is shaped like a saddle, the low point P of the saddle, determines the value of the earth thrust. From condition I (Eq. 4.2.10) the function has a maximum value and from II a minimum. Tables or a graphical solution are usually used in determining the Coulomb's earth pressure. For an irregular ground surface and a broken wall Culmann's graphical procedure is commonly employed.

Rankine in 1885 solved the same problem assuming a frictionless wall and a horizontal ground surface. His solution also yields straight failure planes based on the theory of plasticity. His ideal sand had the following characteristics:

1. The material was homogeneous and isotropic.
2. The Coulomb's law of shear resistance ($\tau = \sigma' \tan \phi$) is satisfied along each slip line.
3. The change in volume is negligible and at every point within the soil wedge the material yields plastically.
4. The friction between wall and soil mass is neglected.

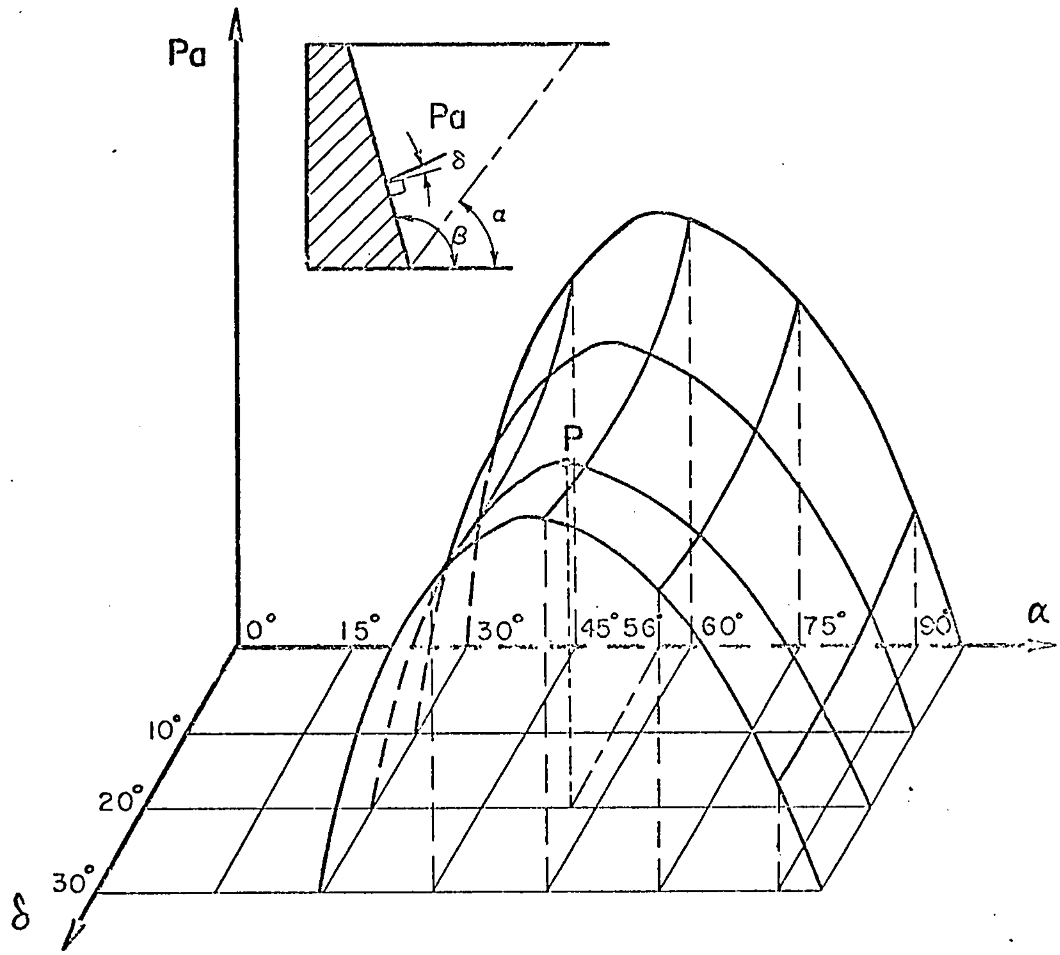

FIG. 4.2.2 REPRESENTATION OF THE EARTH PRESSURE AS A FUNCTION OF THE FAILURE SURFACE INCLINATION AND THE WALL FRICTION

The method should be applied only to specific cases in which the soil expands laterally and the frictional resistance along the wall is negligible. Both assumptions do not hold true for a braced excavation.

4.2.2 Circular Failure Surface

In 1927 Fellenius calculated the extreme value of the earth thrust on a vertical retaining wall based on a circular failure plane. His method is only applicable to frictionless soil ($\phi = 0$) and therefore cannot be considered for the problem studied here.

Ohde (1938 and 1948) published a series of papers calculating the earth pressure distribution for three modes of wall deformation as depicted in Fig. 2.1 (page 22). The lateral earth pressure distribution was parabolic as given by the general relationship Eq. 2.1. This equation yields for $\delta = 0$ and $\delta = \phi$ values for total lateral earth thrust which are up to 25 percent greater than experimental values (Lehmann 1942). In some instances Ohde's calculations produced values which were even higher than 50 percent of the test values. The calculations are also so mathematically involved that they could not be readily adopted for general practical applications.

4.2.3 Logarithmic Spiral Failure Surface

For soils possessing friction the actual failure surface is not a plane as Coulomb had assumed in his method but is slightly curved. Rendulic (1940) approximated the actual slip surface by a logarithmic spiral which has the advantage that all stresses inclined to the failure plane make an angle of ϕ with the normal to the surface and pass through the pole of the spiral. This method also makes use of the extreme condition of maximum earth pressure for the active case. As proof for his method Rendulic calculated in detail a case for which $\phi = 30^{o}$, the wall was rigid and smooth, and the ground surface was horizontal. He found a relationship between the magnitude of earth pressure and the point of application at the earth thrust.

Rendulic was the first person to solve the problem completely. The stress distribution on the back of the wall cannot be determined by this method, similar to any other method which assumes a single failure plane.

Terzaghi in 1941 published a method for computing the lateral earth pressure using a logarithmic spiral as a single failure surface (Terzaghi 1941). This method is now commonly known as the "General Wedge Theory" of earth pressure. Based on empirical observations the logarithmic spiral, with polar equation

$$r = r_o \, e^{\alpha \tan \phi} \qquad (4.2.11)$$

intersects the horizontal ground surface at right angles and passes through the foot of the vertical wall. He also assumed that the centre of the lateral pressure on a braced cut with a depth H in sand is somewhere between an elevation of 0.50 and 0.60 H from the bottom of the cut. The general wedge theory requires that the frictional resistance of the sliding surface is almost fully mobilized over the failure plane, BC, (Fig. 4.2.3). Taking moments about the pole of the spiral one obtains the following equation from the equilibrium condition

$$Pa = \frac{M_w + M_u + M_q - M_{w'}}{L_e} \qquad (4.2.12)$$

The moments of the various forces are M_w, the moment of the weight wedge; M_Q, the moment of the surcharge; M_u, the moment of the pore pressure acting on the failure plane; and $M_{w'}$, the moment of the force w'. M_w, M_Q, $M_{w'}$ and L_e may be calculated directly from the geometric relations in the figure. The increment M_u due to the pore water pressure acting on a portion of the failure plane between r_i and r_j, for which a uniform pressure can be assumed, can be calculated from

$$M_u \Big]_i^j = u \left(\frac{r_i^2 - r_j^2}{2}\right) \qquad (4.2.13)$$

The total value of M_u is found by the summation of all increments $M_u \Big]_i^j$

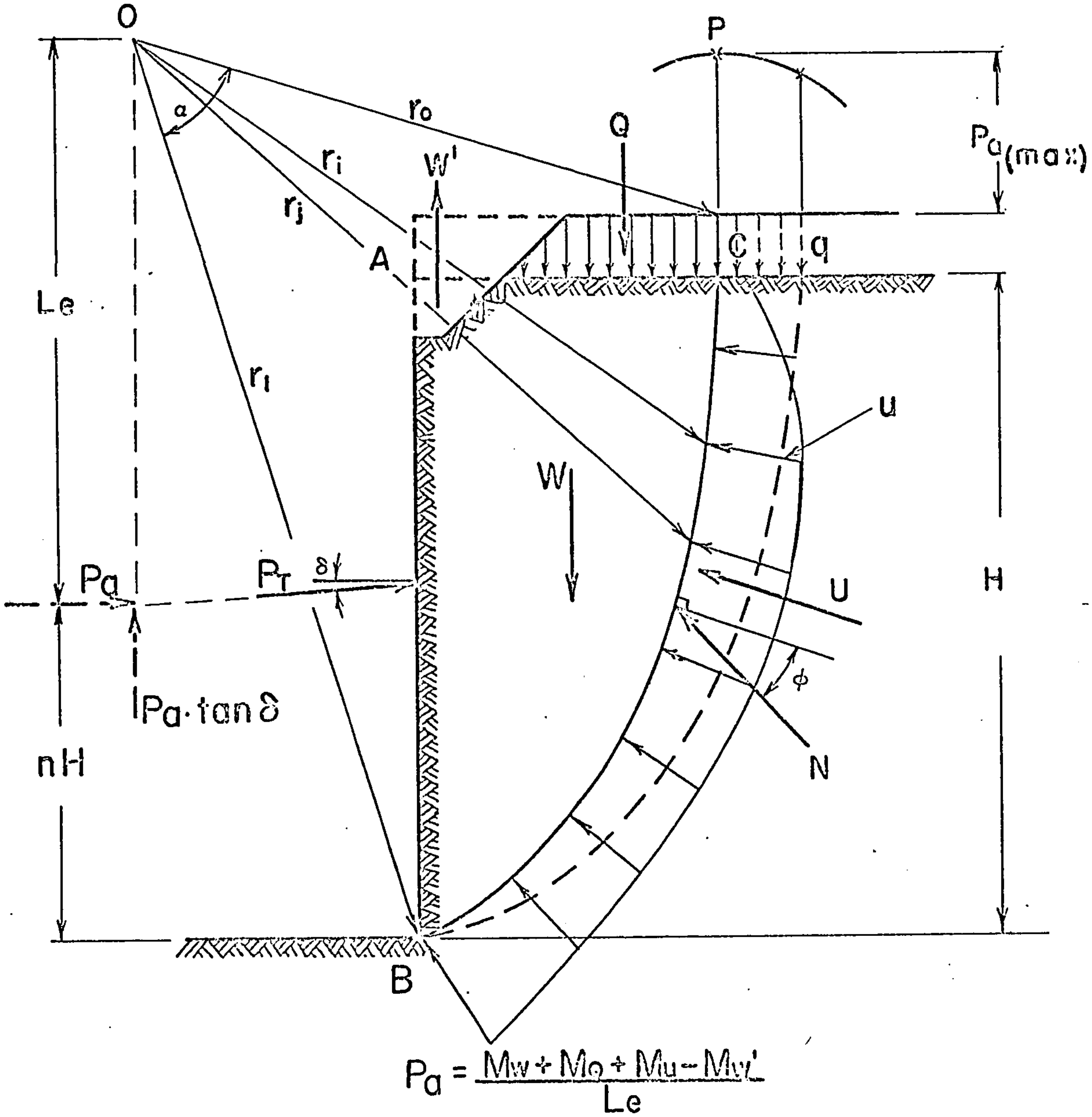

FIG. 4·2·3 APPLICATION OF THE LOGARITHMIC SPIRAL FAILURE SURFACE TO A BRACED CUT. (EFFECTIVE STRESS ANALYSIS) between r_o and r_1, the extreme radii of the spiral. It should be noted that all the incremental forces dN and their resultant N do not enter Eq. 4.2.12, since they all pass through point 0, the moment centre. The solution of Eq. 4.2.12 can be handled in a similar manner to Culmann's graphical solution of Coulomb's method. The active pressure, Pa is then equal to the ordinate of the highest point P on the curve and the position of the corresponding surface of sliding is determined by point C on the ground surface. The value of Pa depends to a certain extent on n or the height at which the resultant thrust is assumed to act. An increase of n from 0.45 to 0.55 increases Pa by 8% for values of $\phi = 38^o$ and $\delta = 0$. If n is taken as 0.55 then Pa = 1.1 Pc, where Pc is the lateral thrust obtained from Coulomb's solution. Since the General Wedge Theory cannot give the pressure distribution on the back of the wall and one has to assume the point of application of the resultant earth pressure it appears no more advantageous than the Coulomb solution, except for cross-sections of irregular shape in which a graphical solution appears less cumbersome.

4.2.4 Effect of Wall Movement on Lateral Earth Pressures

The nature of deformation of a braced excavation was described in Chapter 3 and illustrated in Fig. 3.1. It consisted basically of an outward rotational movement of the wall as a stiff unit about its upper strut level. Neither Coulomb's nor Rankine's theory were based upon this deformation criterion. Theoretical and experimental investigations regarding the type of failure caused by a tilt of the lateral support about its upper edge have led to the conclusion that the surface of sliding starts at the foot of the wall at an angle of $45 + \frac{\phi}{2}$ with the horizontal for a smooth wall and that it becomes steeper until it intersects the ground surface at right angles (Terzaghi 1941).

The distribution of pressure against a lateral support as found from field measurements and laboratory investigations is roughly parabolic instead of triangular. Because of this, the active earth pressure distribution against the cut cannot be computed be means of Coulomb's or Rankine's theory. A method must be developed that takes into consideration the influence of deformation conditions on the type of failure. The first attempt was made by Terzaghi (1936) as discussed in Chapter 2, but his method never gained the recognition it deserved because it was hampered by the difficulty in determining or choosing the proper "confinement index", c_i, which depended both on the type of lateral expansion of the soil mass as well as on its intrinsic parameters. Ohde's attempt in 1938, as outlined in the foregoing section, was mathematically far too complicated to find popular acceptance by the practising engineer.

Another method that appears to have considerable merit will be proposed here. It is based on Dubrova's (1963) solution as discussed by Harr (1966) and has been modified in some instances to comply with any mode of movement a braced excavation might undergo. Fig. 4.2.4, diagrams a, b, d and e illustrate the four modes of deformation a stiff braced retaining wall might have undergone during the time the cut was excavated to grade. Usually the first row of struts are installed near the top after the soil has been excavated to a small depth. In movement A (Fig. 4.2.4.a) it is assumed that the braces are installed very close to the top of the wall and wedged tightly or even prestressed so that no lateral yield towards the excavation will occur. If the upper strut level is installed at a distance $\frac{1}{4}$ H below the original ground surface and no lateral yield is allowed the wall will have tilted about this level as shown by movement B in Fig. 4.2.4.b. The portion of the retaining structure which lies above the point of rotation will be slightly pressed into the soil in the case of a fairly inflexible wall. This is not an unreasonable assumption to make when using stiff steel sheeting or H-pile soldier beams.

For both modes of rotation it is further assumed that the limiting active state is mobilized at the bottom and the resultant force F on the rupture line passing through the foot of the wall will be inclined at an angle $\bar{\phi}$ to the normal as shown in Fig. 4.2.4.b. This is invariably true for most practical cases except for piles which are embedded to such a depth below grade to prevent any lateral movement of the wall at the foot. As will be explained in Section 4.3.3 below, the degree to which shear strength can be mobilized is directly dependent on the amount of soil strain.

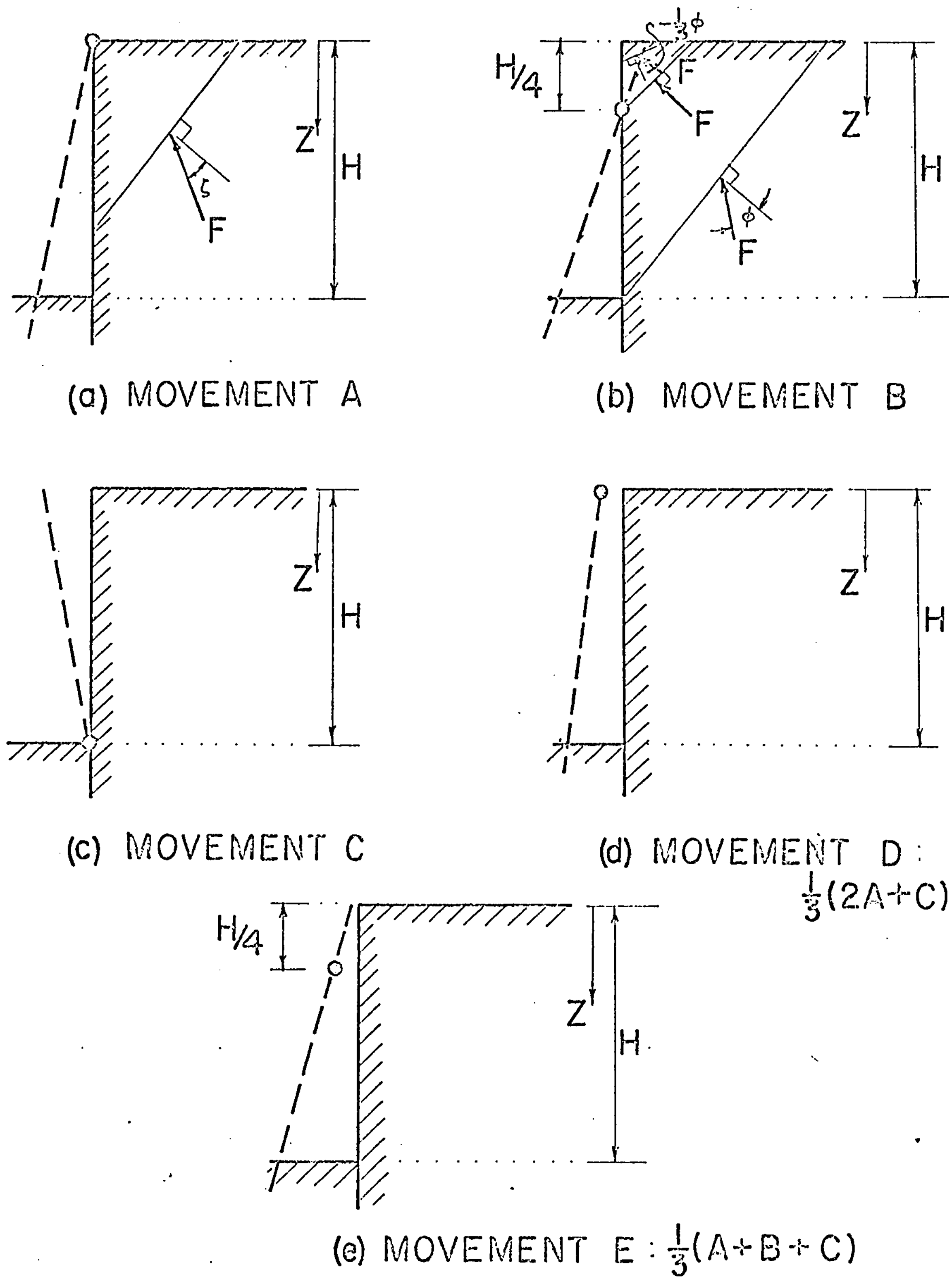

FIG. 4·2·4 DIFFERENT MODES OF WALL MOVEMENT

At the point of wall rotation no lateral strain occurs and no friction is mobilized along the rupture line passing through this point. The resultant force F necessarily is normal to this quasi-rupture line. The angle between the normal and the force on any rupture line is ξ and it is further assumed that this angle varies linearly with depth z. This assumption is similar to Terzaghi's (1936) approach in which the coefficient of earth pressure was assumed to vary linearly with depth. In the case of the wall rotating outward about its top (movement A)

$$\xi = \frac{z}{H}\,\phi \tag{4.2.14}$$

For movement B, ξ will vary as

$$\xi = \left(\frac{4}{3}\,\frac{z}{H} - \frac{1}{3}\right)\phi \tag{4.2.15}$$

which would mean for $z = 0$, $\xi = -\frac{1}{3}\,\phi$, or one - third of the passive resistance is mobilized at the top of the wall simultaneously as the full active strength is mobilized at the bottom. This condition is illustrated in Fig. 4.2.4.b. For the case of a wall rotating about its bottom as in Fig. 4.2.4.c, movement C,

$$\xi = \left(1 - \frac{z}{H}\right)\phi \tag{4.2.16}$$

This type of movement has never been observed to occur on braced cuts but will be employed in combination with movements A and B to simulate deformations as discussed below.

In movement D, Fig. 4.2.4.d, the cut is rotating about its top and also moving out laterally. This type of deformation has been observed as will be discussed in Chapter 5, Section 5.2.5 and is mainly due to loose wedging of the struts which would allow lateral movement. Movement D is taken as the average deformation of twice the movement A and movement C. Similarly movement E, where the wall yields laterally and also rotates about a point H/4 below the ground surface, is taken as the average of movements A, B, and C. In most properly constructed excavations the deformation should correspond either to movement A or movement D.

According to field and experimental measurements (Spilker 1937, Peck 1943, and Lehmann 1942) and theoretical calculations (Terzaghi 1936 and 1941) the total active lateral earth thrust was in close agreement to or exceeded the Coulomb's value by not more than 15 percent. Therefore the assumption of the validity of Coulomb's solution for calculating the total force exerted by the earth wedge method is not unreasonable. Coulomb's solution was given in Section 4.2.1 as

$$Pa = \frac{H^2}{2} \gamma \tan^2 (45 - \frac{\phi}{2}) = Ka \frac{H^2}{2} \gamma \qquad (4.2.3)$$

A more general solution was obtained by Müller-Breslau in 1906, as mentioned in Section 4.2.1. Combining Eqs. 4.2.6 and 4.2.7

$$Pa = \tfrac{1}{2}\,\gamma\,H^2 \left[\frac{\csc\beta \,.\, \sin(\beta-\phi)}{\sqrt{\sin(\beta+\delta)} + \sqrt{\dfrac{\sin(\phi+\delta)\,\sin(\phi-i)}{\sin(\beta-i)}}} \right]^2 \qquad (4.2.17)$$

where i = angle of slope of backfill, and

β = inclination of back of wall with the horizontal

For the case of a vertical wall and a horizontal ground surface as in most braced cuts, Eq. 4.2.17 simplifies to

$$Pa = \tfrac{1}{2}\,\gamma\,H^2 \left[\frac{\cos\phi}{\sqrt{\cos\delta} + \sqrt{\sin(\phi+\delta)\,\sin\phi}} \right]^2 \qquad (4.2.18)$$

or

$$Pa = \frac{\gamma H^2}{2\cos\delta} \left[\frac{1}{\dfrac{1}{\cos\phi} + \sqrt{\tan^2\phi + \tan\phi \,.\, \tan\delta}} \right]^2 \qquad (4.2.19)$$

Eqs. 4.2.18 and 4.2.19 give the total active force which is inclined at an angle of δ with the normal to the wall. The horizontal component is

$$Px = Pa\cos\delta \qquad (4.2.20)$$

or

$$Px = \frac{\gamma}{2} \left[\frac{H}{(\frac{1}{\cos \phi}) + \sqrt{\tan^2 \phi + \tan \phi \tan \delta}} \right]^2 \qquad (4.2.21)$$

The definition of ξ as given in Eqs. 4.2.14, 4.2.15, and 4.2.16 can now be substituted for ϕ in Eq. 4.2.21. Then the horizontal component of the force against the wall for any depth z will be

$$Px = \frac{\gamma}{2} \left[\frac{z}{(\frac{1}{\cos \xi}) + \sqrt{\tan^2 \xi + \tan \xi \tan \delta}} \right]^2 \qquad (4.2.22)$$

To find the lateral distribution of the pressure against the back of the cut, the proper substitution for ξ has to be made, depending on the type of wall movement anticipated, and then Eq. 4.2.22 has to be differentiated with respect to z. For movement A, where $\xi = \frac{z}{H} \phi$ (Eq. 4.2.14) the derivative of Eq. 4.2.22 is

$$\frac{dPx}{dz} = px = \gamma \left[\frac{z \cos^2 \xi}{(1 + t \sin \xi)^2} - \frac{z^2 \phi \cos \xi}{H(1 + t \sin \xi)^2} (\sin \xi + \frac{1 + t^2}{2t}) \right]$$

(4.2.23)

where $t = (1 + \tan\delta/\tan \phi)^{1/2}$ multiplying both sides of Eq. 4.2.23 by the factor $1/\gamma$ H to make the relationship dimensionless we get

$$\frac{px}{\gamma H} = (\frac{z}{H}) \frac{\cos^2 \xi}{(1+ t \sin \xi)^2} - (\frac{z}{H})^2 \frac{\phi \cos \xi}{(1+ t \sin \xi)^3} (\sin \xi + \frac{1+ t^2}{2t}) \qquad (4.2.24)$$

Similarly for movement B and C the relation will become, respectively

$$\frac{px}{\gamma H} = (\frac{z}{H}) \frac{\cos^2 \xi}{(1 + t \sin \xi)^2} - \frac{4}{3} (\frac{z}{H})^2 \frac{\phi \cos \xi}{(1 + t \sin \xi)^3} (\sin \xi + \frac{1 + t^2}{2t}) \qquad (4.2.25)$$

and

$$\frac{px}{\gamma H} = \frac{z}{H} (\frac{\cos \phi}{1 + t \sin \phi}) \qquad (4.2.26)$$

A computer programme was written and used in order to evaluate Eqs. 4.2.24, 4.2.25, and 4.2.26 for different values of z/H ranging from 0 to 1.0 in 0.1 intervals and also for different ϕ and δ values. The results are shown graphically in Figs. 4.2.5 to 4.2.25 inclusively.

Figs. 4.2.5 to 4.2.9 show the variation of lateral earth pressure with depth of a wall rotating about the top (movement A). Generally each diagram shows five curves, one for each particular angle of internal friction which varies from 0 to 50° in 10° intervals. For $\phi = 10^{\circ}$ the pressure distribution approximates a hydrostatic distribution and it

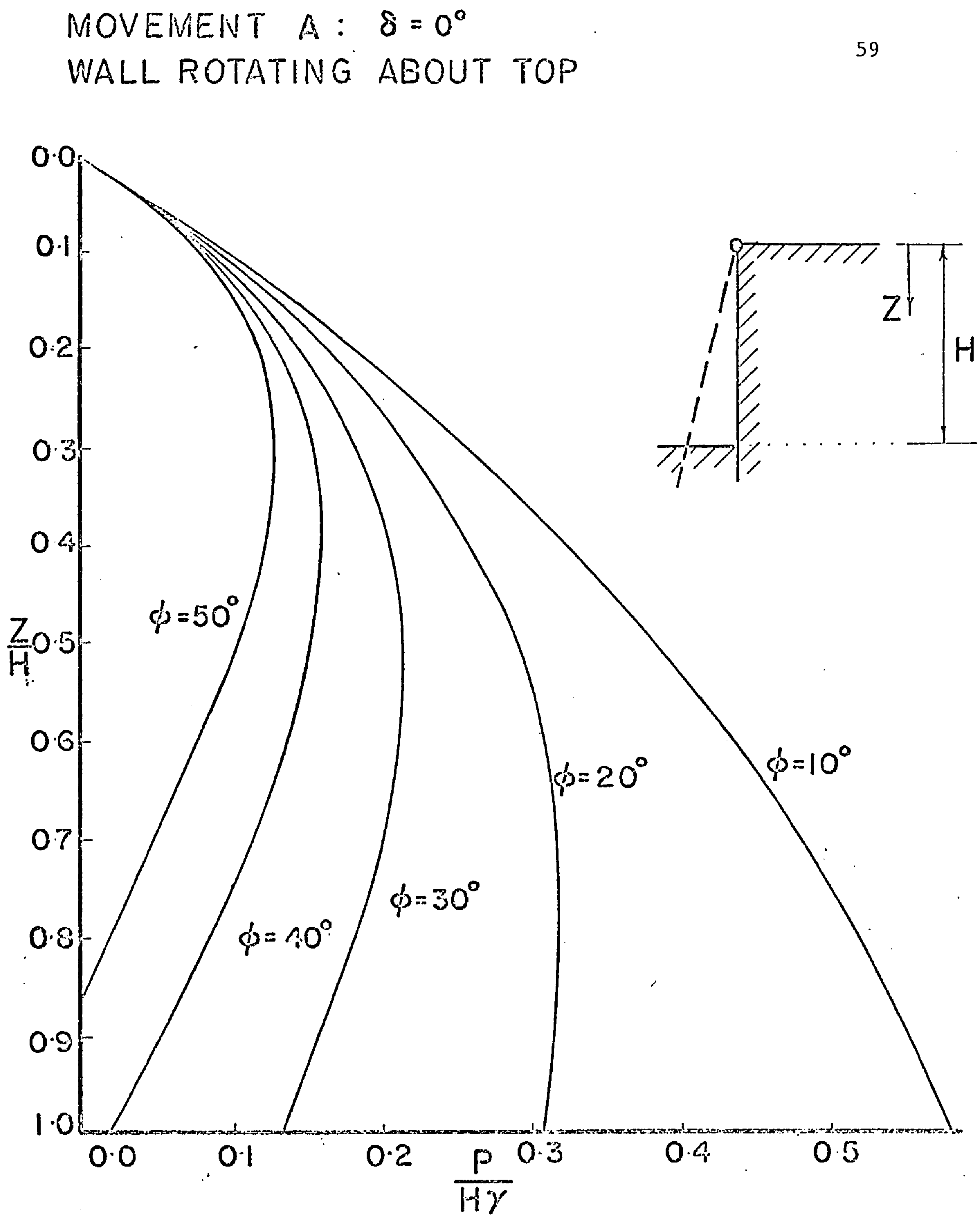

FIG. 4·2·5 LATERAL EARTH PRESSURE DISTRIBUTION

MOVEMENT A : $\delta = \frac{1}{3}\phi$
WALL ROTATING ABOUT TOP

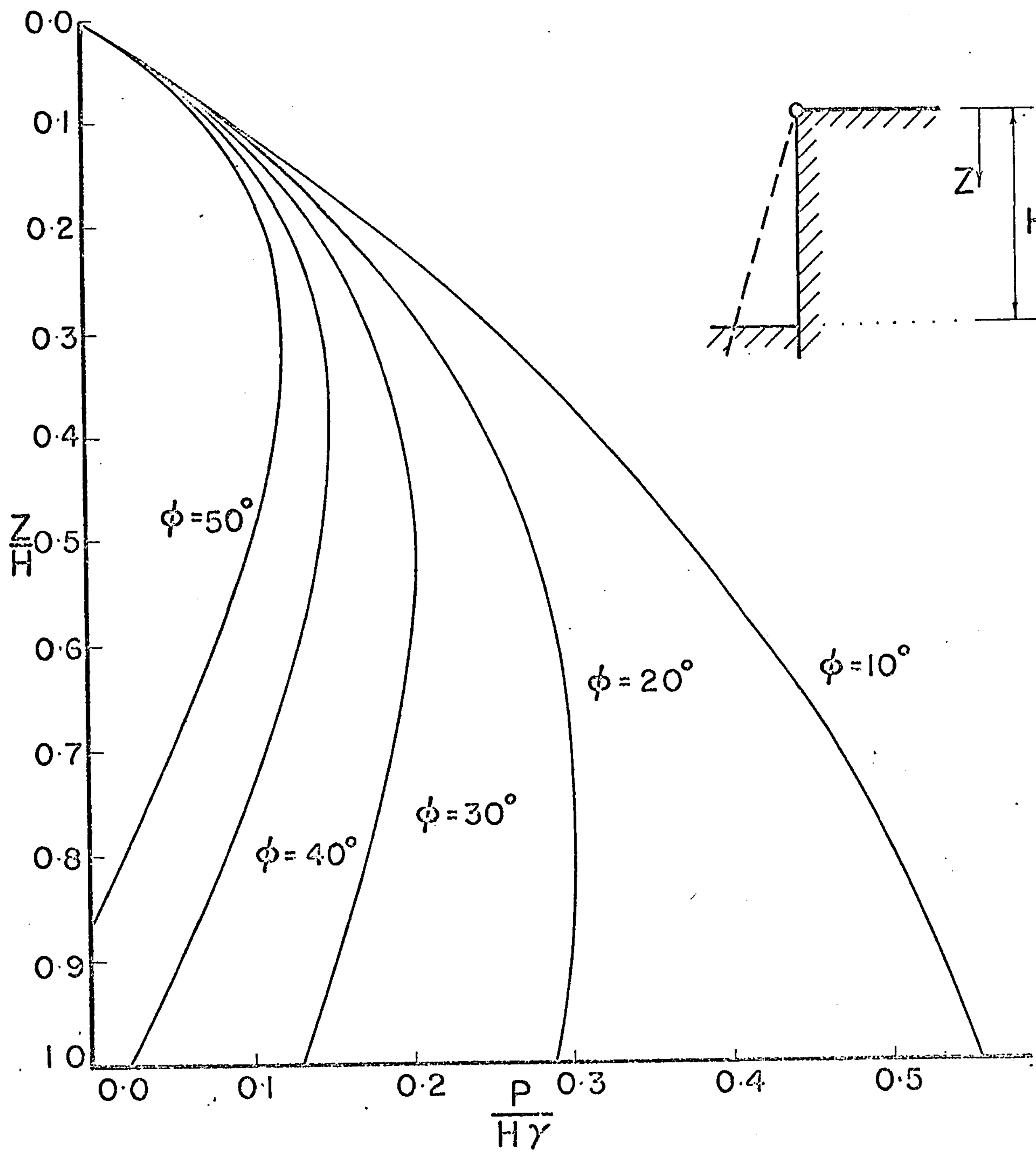

FIG. 4·2·6 LATERAL EARTH PRESSURE DISTRIBUTION

MOVEMENT A : $\delta = \frac{1}{2}\phi$
WALL ROTATING ABOUT TOP

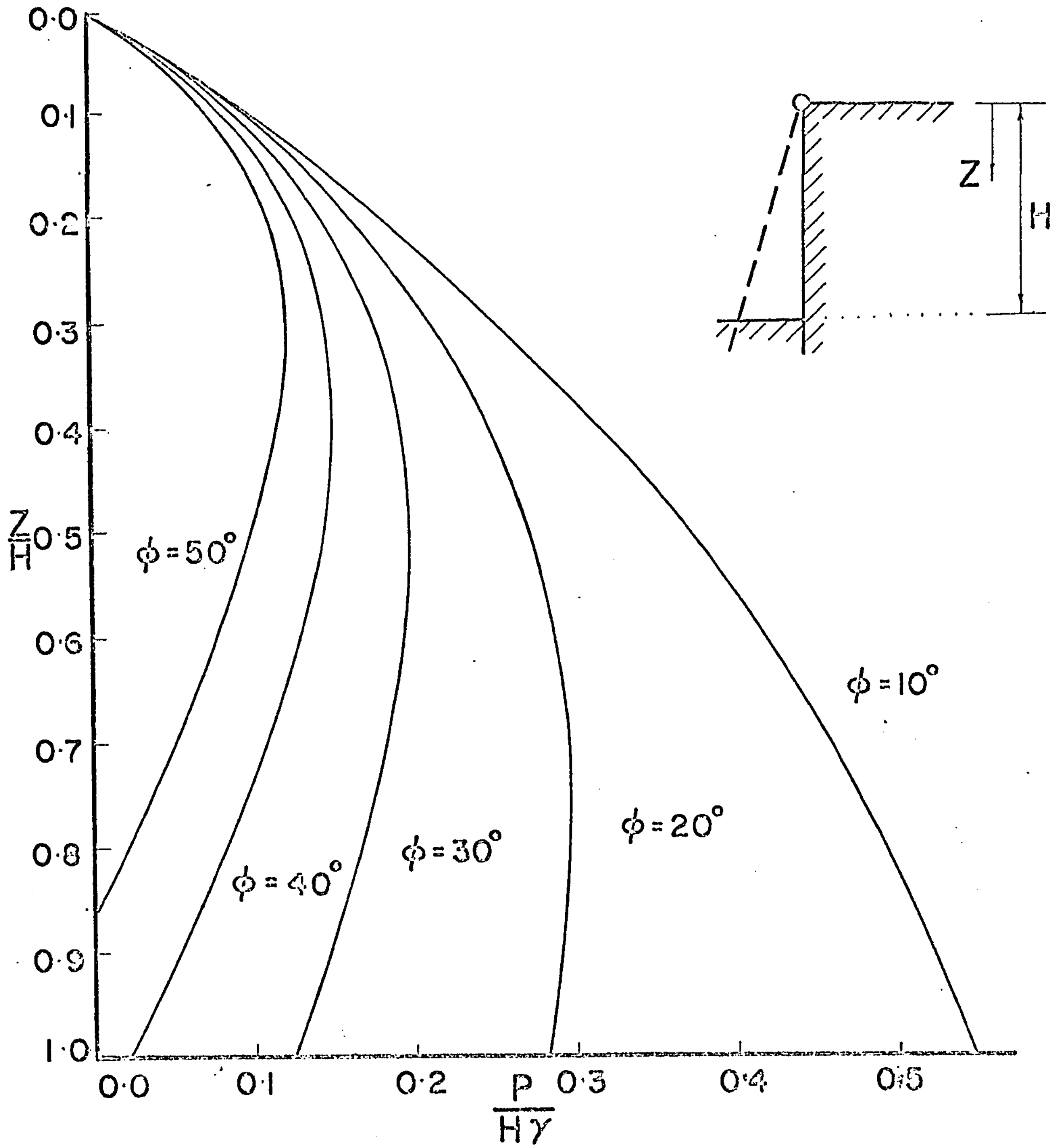

FIG. 4·2·7 LATERAL EARTH PRESSURE DISTRIBUTION

MOVEMENT A: $\delta = \frac{2}{3}\phi$
WALL ROTATING ABOUT TOP

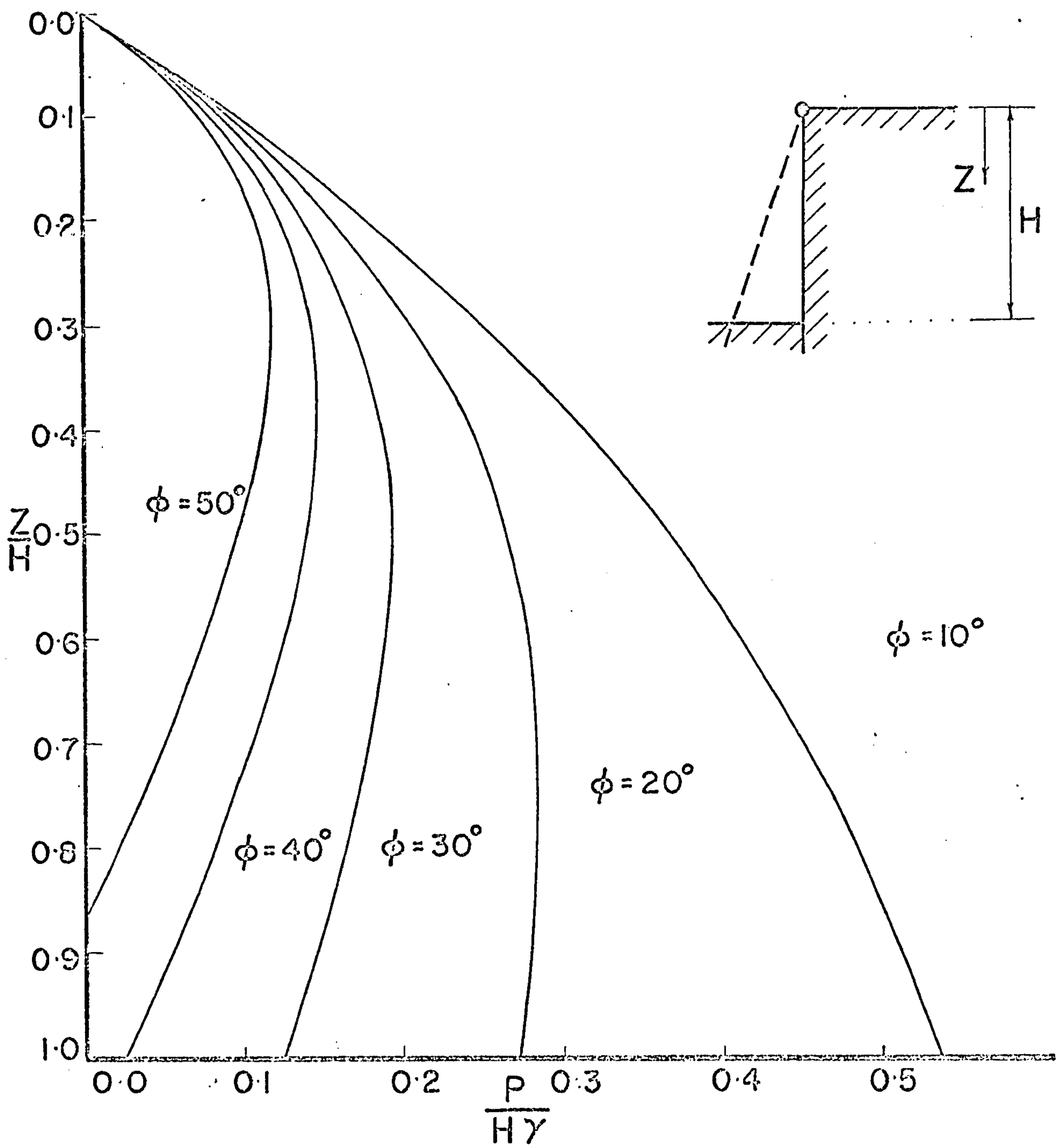

FIG. 4·2·8 LATERAL EARTH PRESSURE DISTRIBUTION

MOVEMENT A : $\delta = \phi$

WALL ROTATING ABOUT TOP

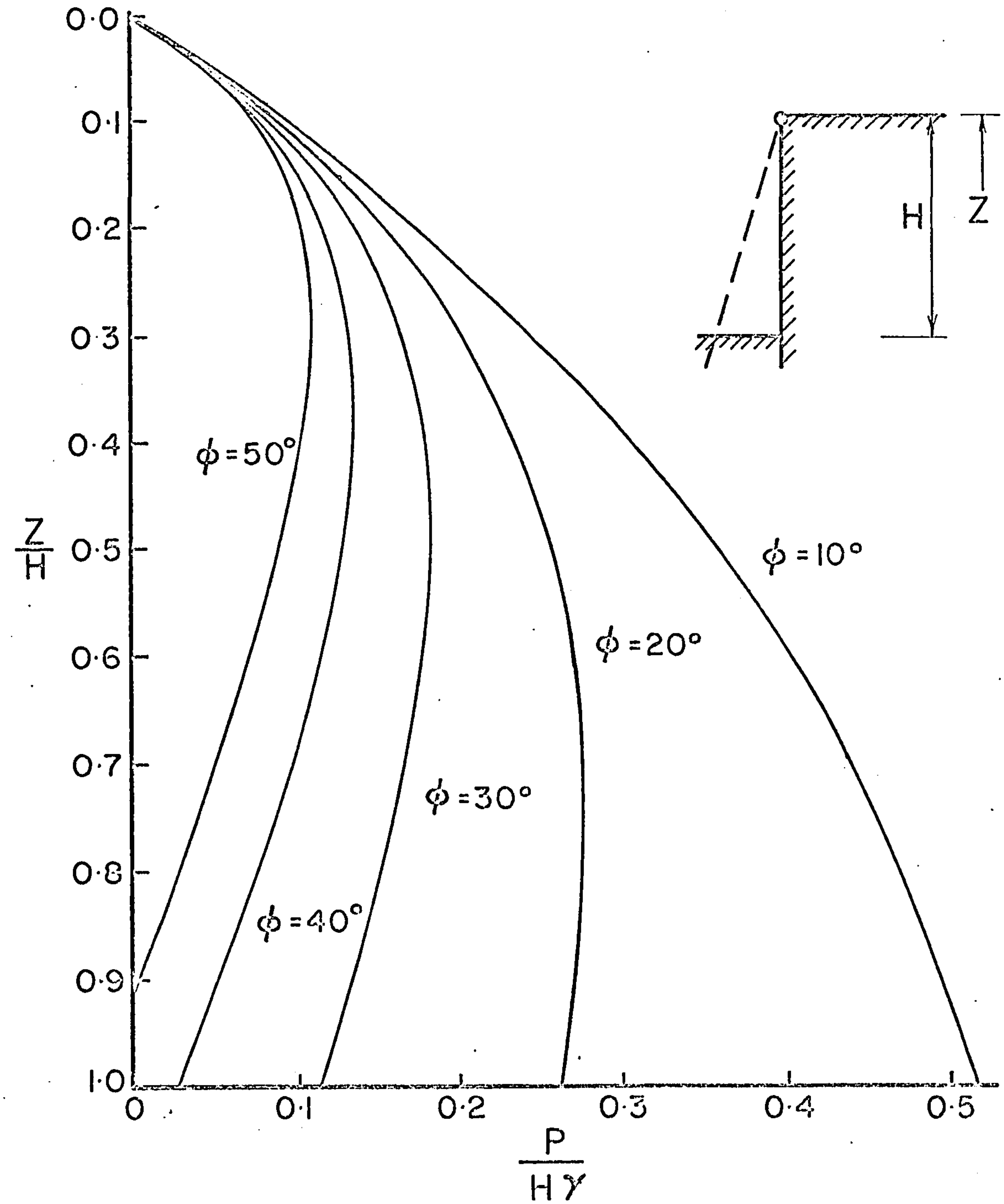

FIG·4·2·9 LATERAL EARTH PRESSURE DISTRIBUTION would be truly hydrostatic if the material had no shear strength at all, that is, $\phi = 0$. For higher values of internal friction the distribution becomes more and more parabolic or pear-shaped and the total earth thrust becomes smaller. Also the maximum pressure abscissa and the point of application of the resultant move upwards with increasing shear strength parameters. For movement A all distribution curves become tangent in the upper part to the curve of $\phi = 10^{\circ}$.

The higher the wall friction the smaller will be the total horizontal pressure on the wall. For any case the total thrust will be equal to the corresponding Coulomb value. For a certain wall movement five different wall friction values have been taken into account, 0, $(\phi/3)$, $(\phi/2)$, $(2\phi/3)$, and ϕ. The effect of the wall friction on the total value of earth pressure has been illustrated in Fig. 4.2.25. As an example movement A and a value of internal friction of $\phi = 30^{\circ}$ was chosen. The difference between the total lateral forces for $\delta = 0$ and $\delta = \phi$ is approximately 10 to 15%. Therefore no appreciable error will be introduced by neglecting the wall friction, since it is on the safe side to do so. Neglecting the effect of wall friction will bring the theoretical value closer to the experimental one. Spilker (1937) and Lehmann (1942) found that their observations never exceeded corresponding Coulomb values by more than 15%.

For movement B (the wall is rotating about a point H/4 below its top) the shift of the resultant horizontal pressure towards the

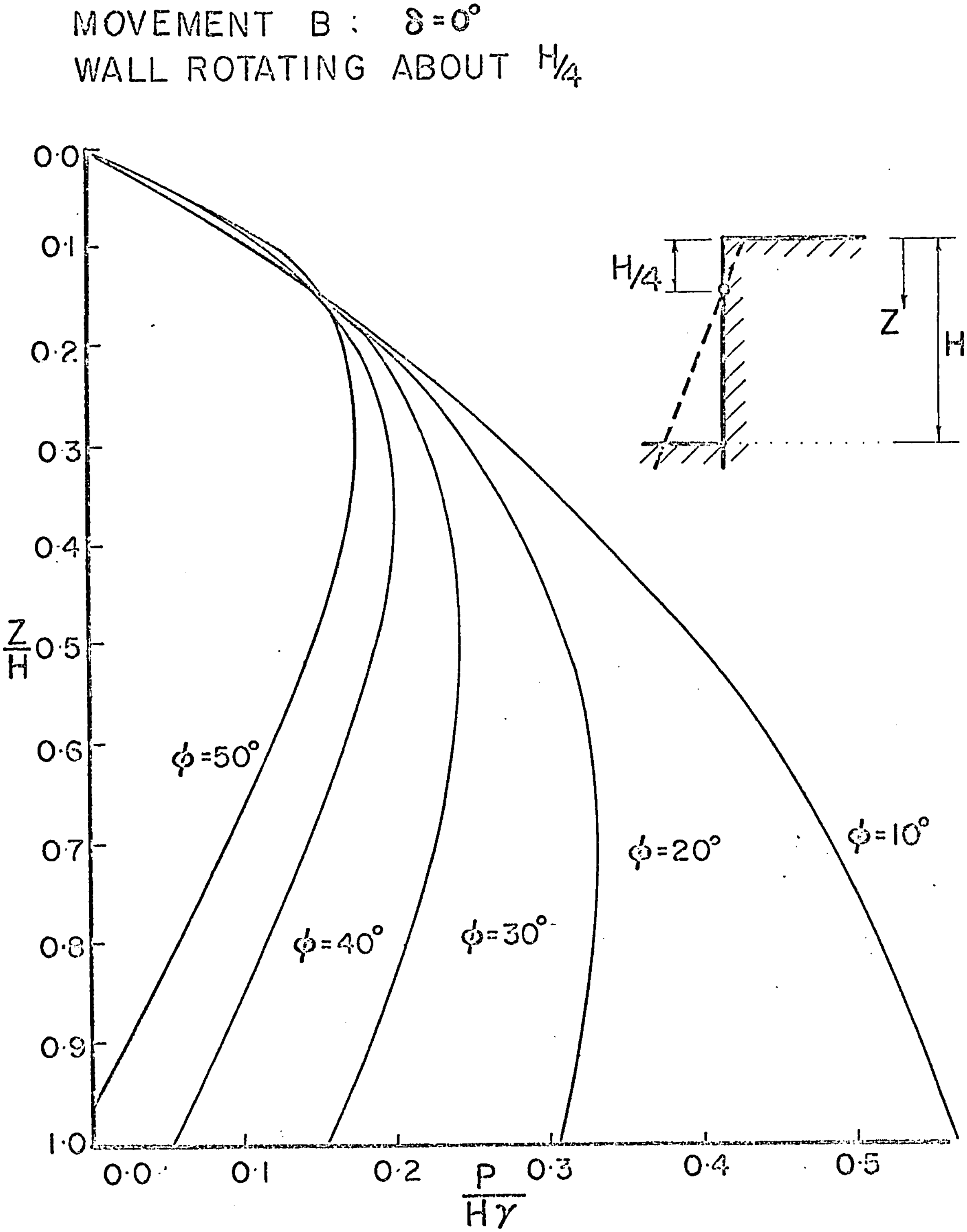

FIG. 2·4·10 LATERAL EARTH PRESSURE DISTRIBUTION

MOVEMENT B: $\delta = \frac{1}{3}\phi$

WALL ROTATING ABOUT H/4

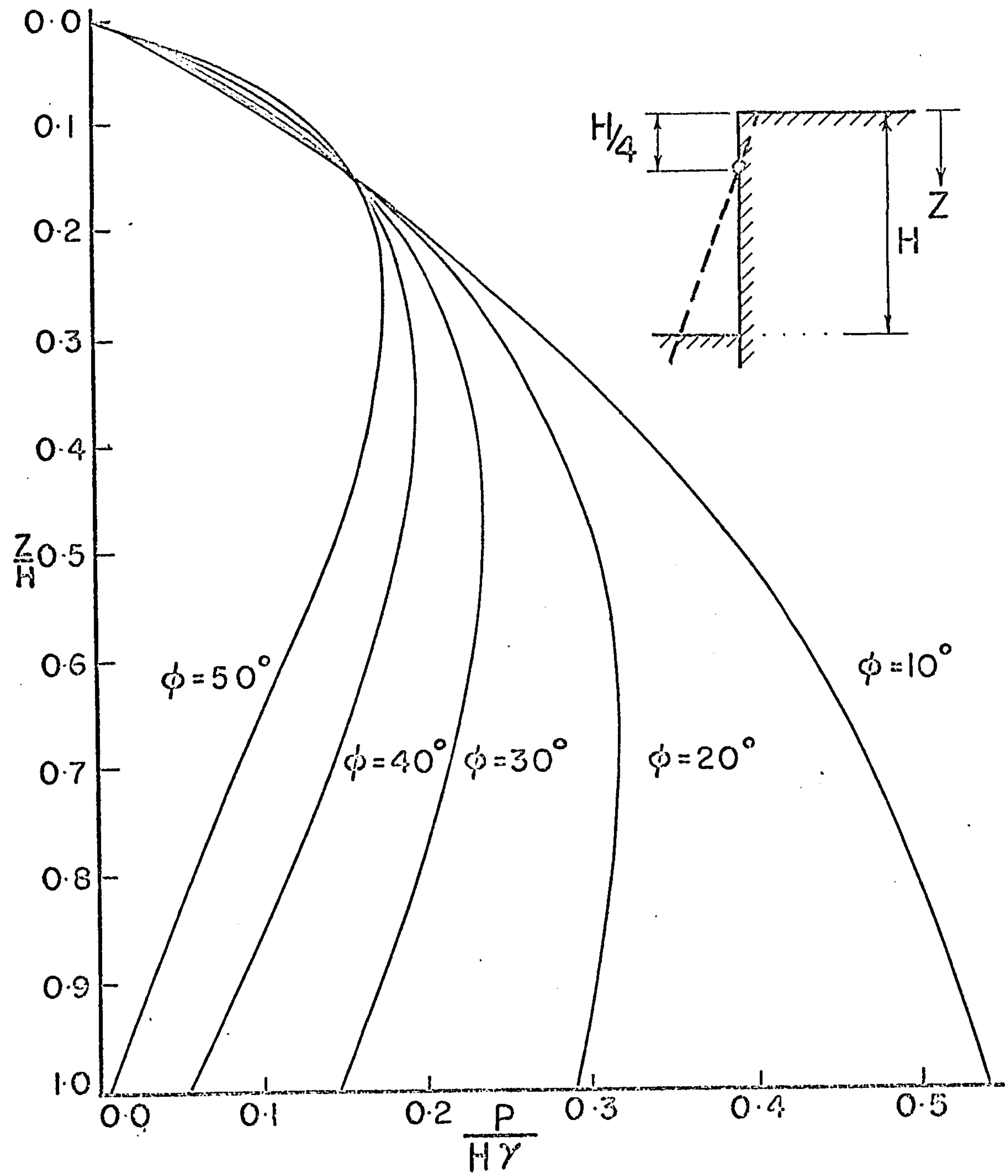

FIG. 2.4.11 LATERAL EARTH PRESSURE DISTRIBUTION

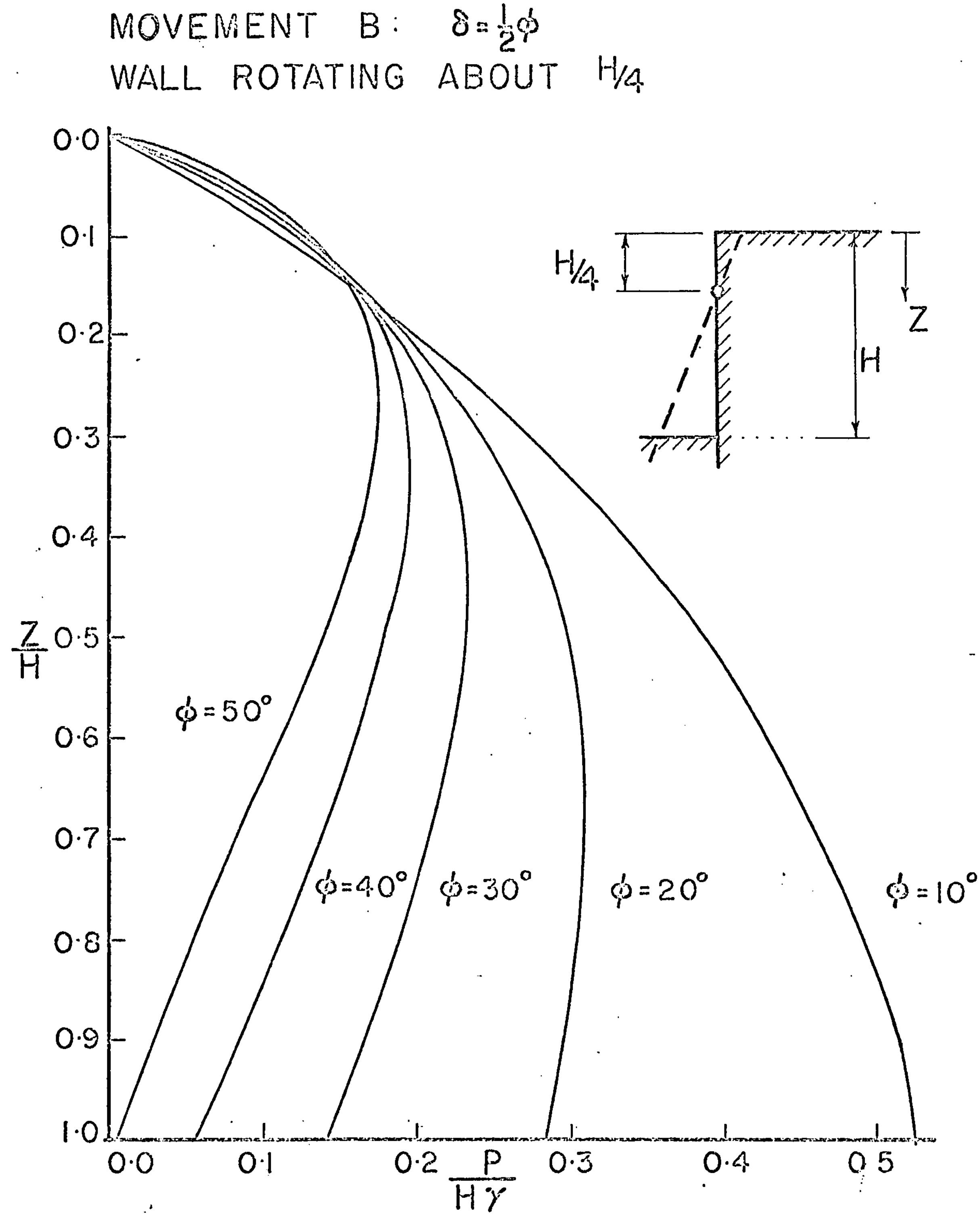

FIG. 4·2·12 LATERAL EARTH PRESSURE DISTRIBUTION

MOVEMENT B: $\delta = \frac{2}{3}\phi$
WALL ROTATING ABOUT $H/4$

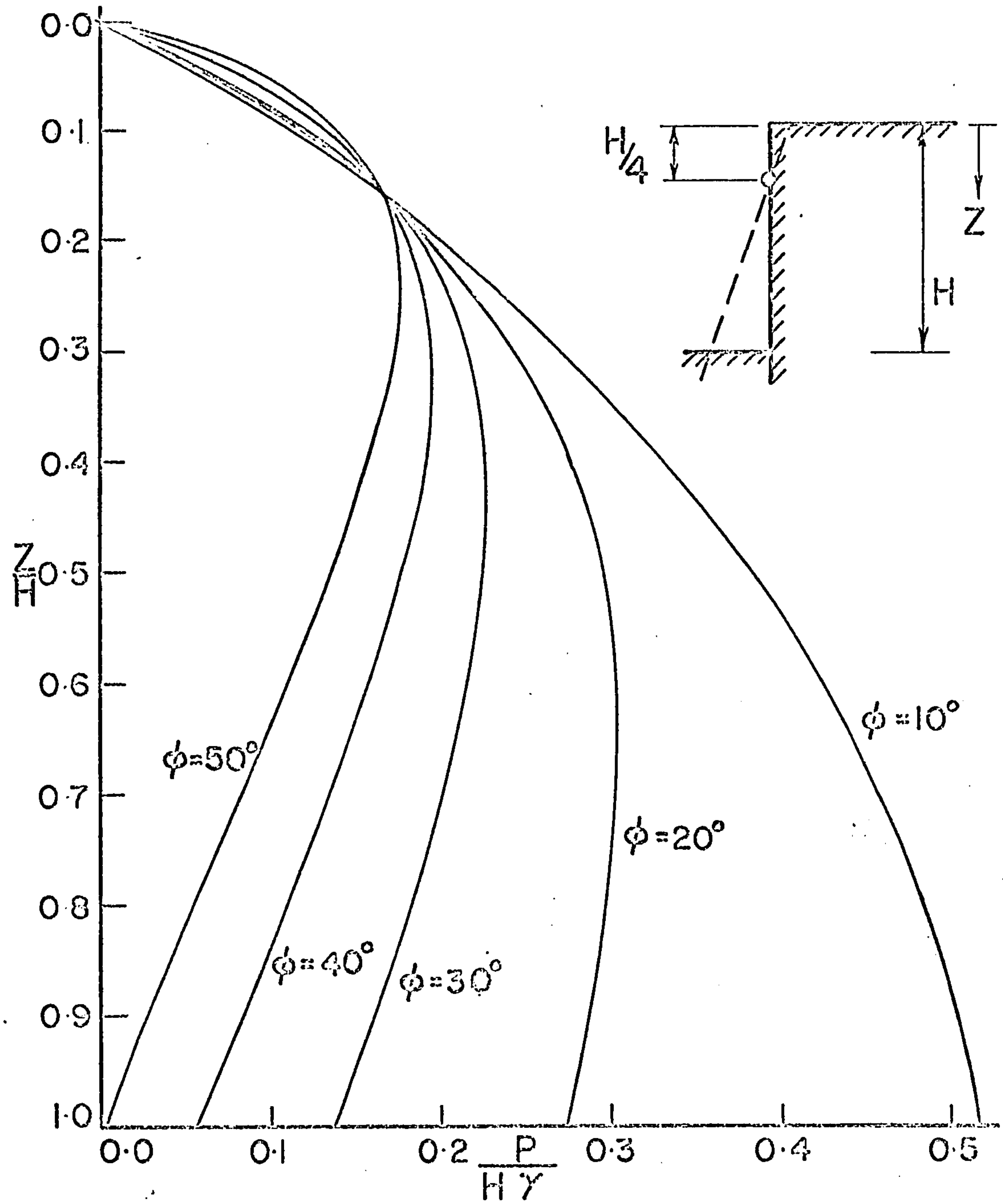

FIG.4.2.13 LATERAL EARTH PRESSURE DISTRIBUTION

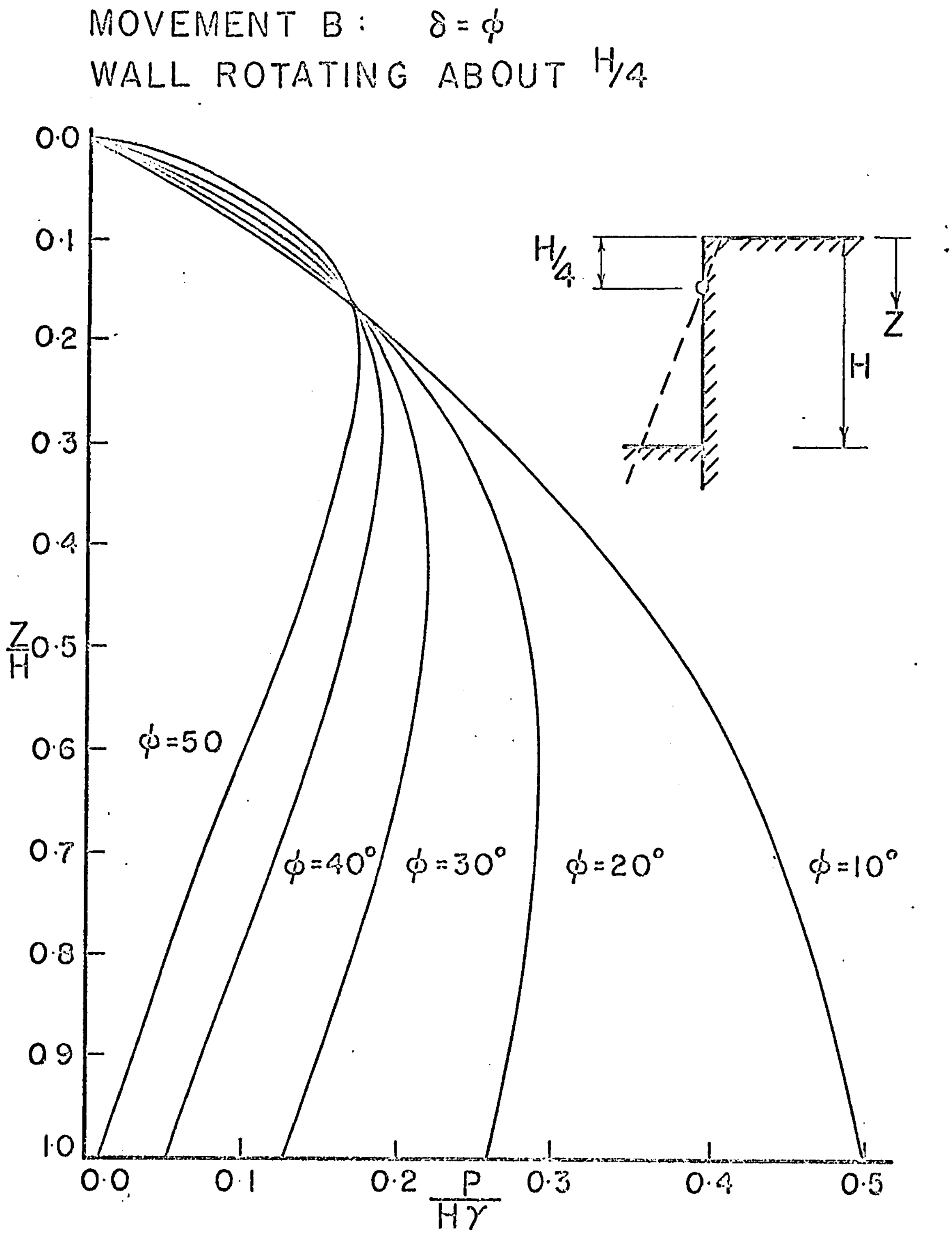

FIG. 4.2.14 LATERAL EARTH PRESSURE DISTRIBUTION

upper part becomes more pronounced due to the partial mobilization of the passive state of the soil above the pivot point of the rotating wall. The point of application is always higher than the lower third point and even is above the half depth for higher internal friction values. The curves for the higher ϕ values are no longer tangent to the $\phi = 10^{o}$ curve but intersect it and lie above it at a z/H ratio of about 0.17. For most braced excavations the first strut level is installed between the top and a point one-quarter of the depth of the cut. The question whether the wall remains stiff and whether the portion of the wall above the point of rotation will be pushed into the soil depends on the stiffness of the sheet piles and on the orderliness and method of constructing the braced excavation. The derivation of the theory was based on the assumption that the wall rotates as a stiff rigid unit and it is reasonable to venture the assumption that for a light steel pile section a hinged could be formed at the pivot point.

The different pressure distributions for movement C (wall rotating about toe) have not been illustrated in this thesis. For this particular deformation the mobilization of ϕ varies linearly with the height of the wall corresponding to the well known triangular pressure distribution of Coulomb's theory. But this distribution was used in deriving movements D and E.

The lateral pressure for movement D increases at a decreasing rate with depth, (Figs 4.2.15 to 4.2.19). This is due to the pre-

MOVEMENT D: $\frac{1}{3}(2A+C)$ $\delta = 0°$
WALL ROTATING ABOUT TOP AND MOVING OUT LATERALLY

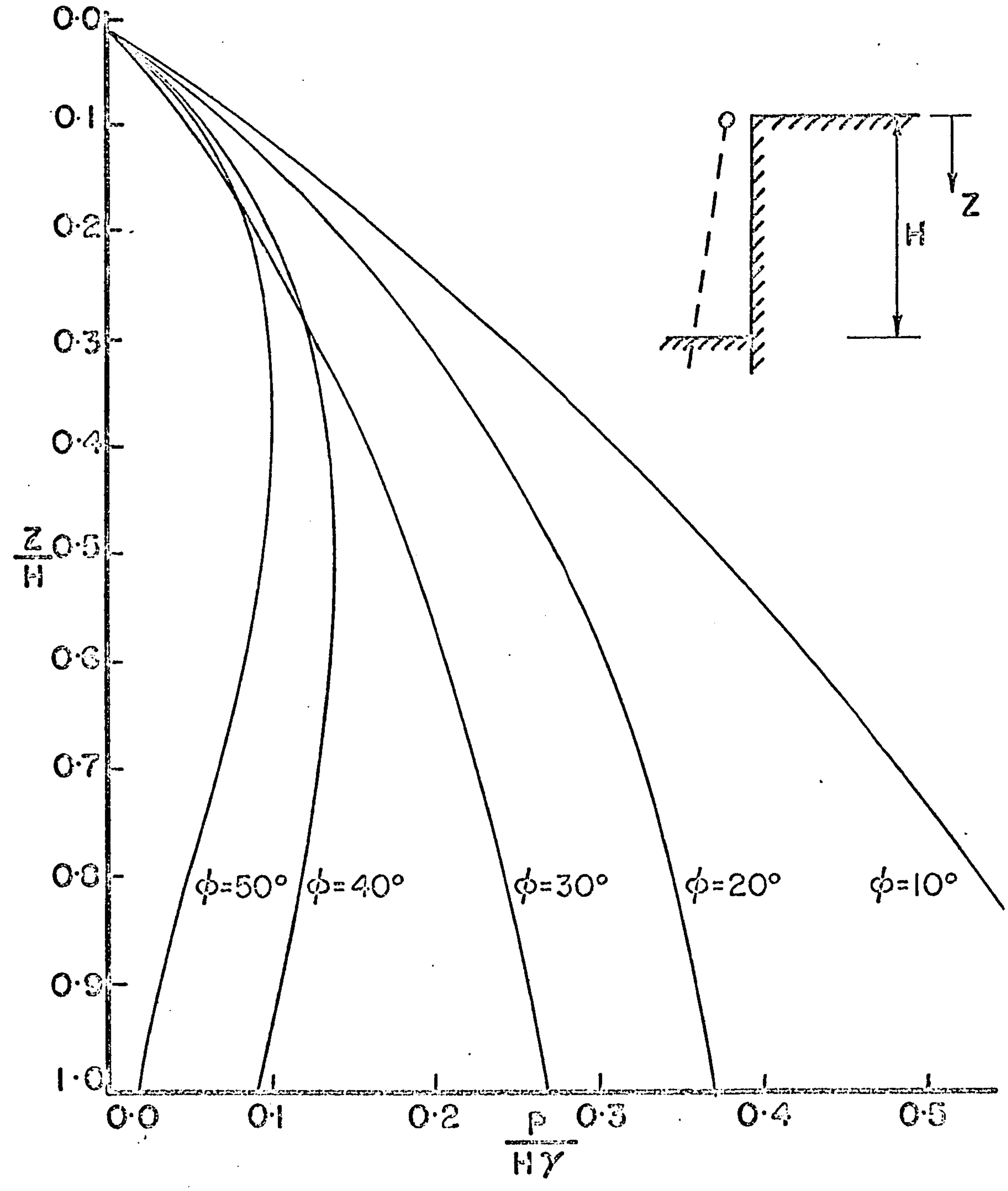

FIG.4·2·15 LATERAL EARTH PRESSURE DISTRIBUTION

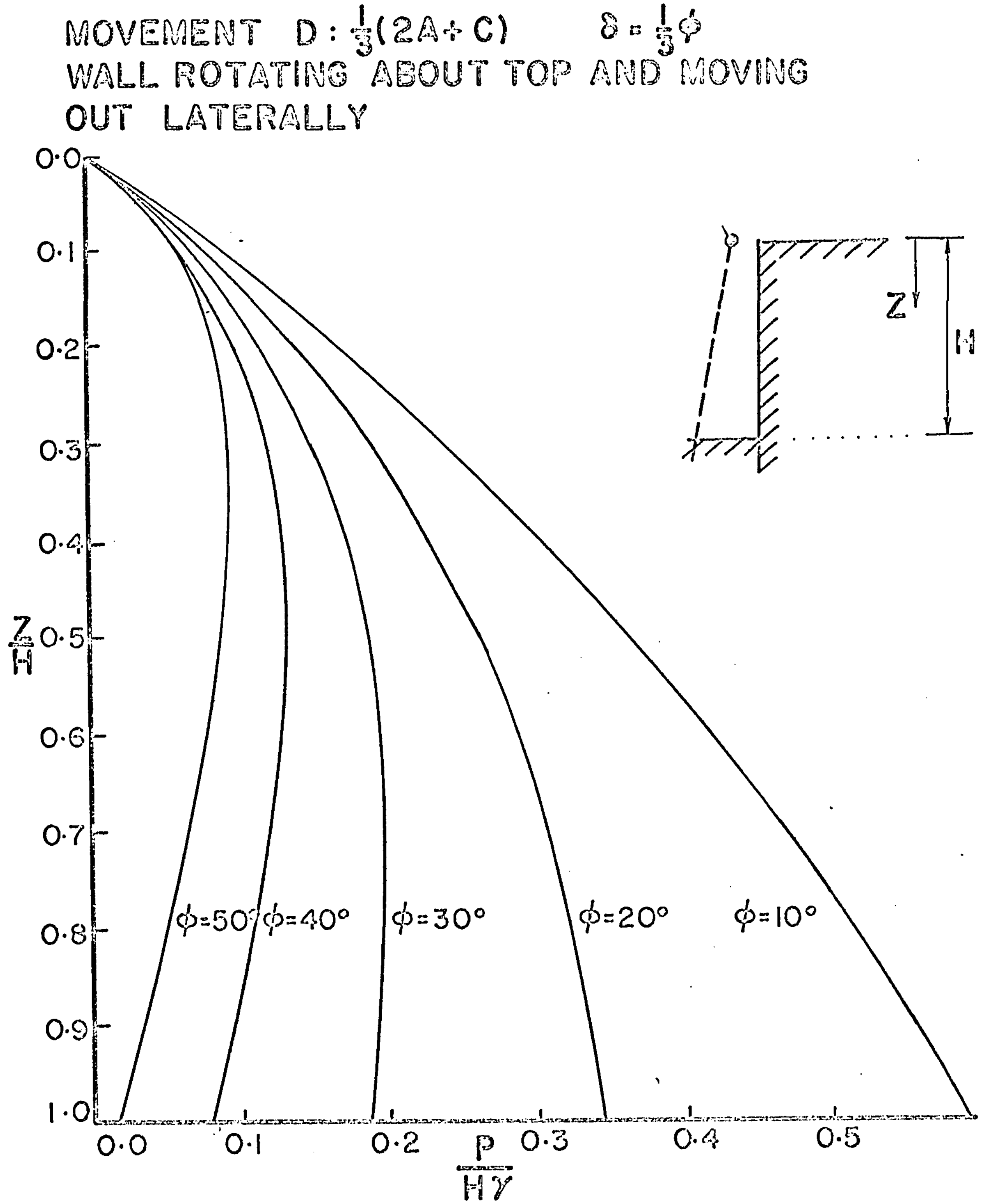

FIG. 4·2·16 LATERAL EARTH PRESSURE DISTRIBUTION

MOVEMENT D : $\frac{1}{3}$(2A + C) $\delta = \frac{1}{2}\phi$

WALL ROTATING ABOUT TOP AND MOVING OUT LATERALLY

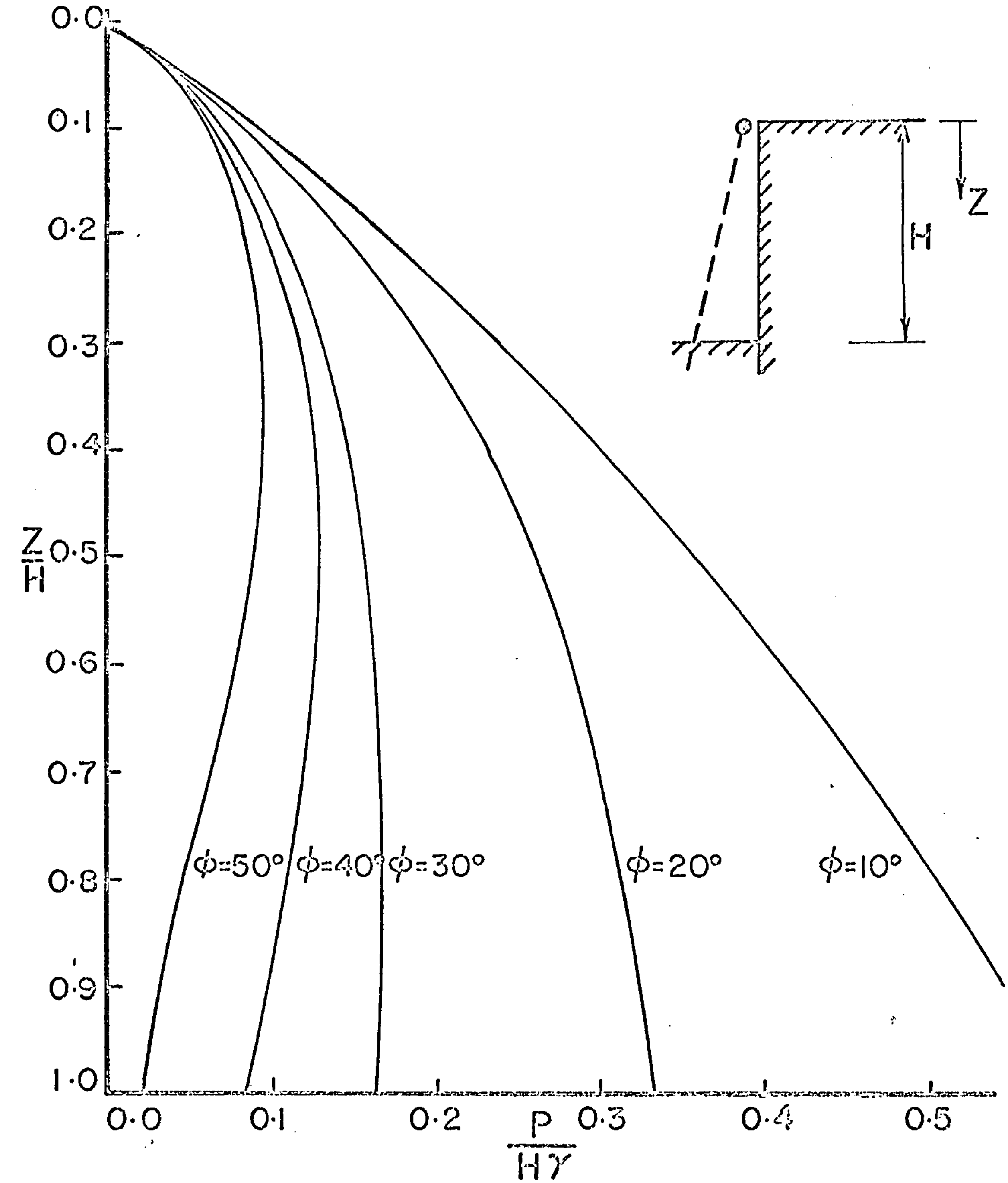

FIG. 4·2·17 LATERAL EARTH PRESSURE DISTRIBUTION

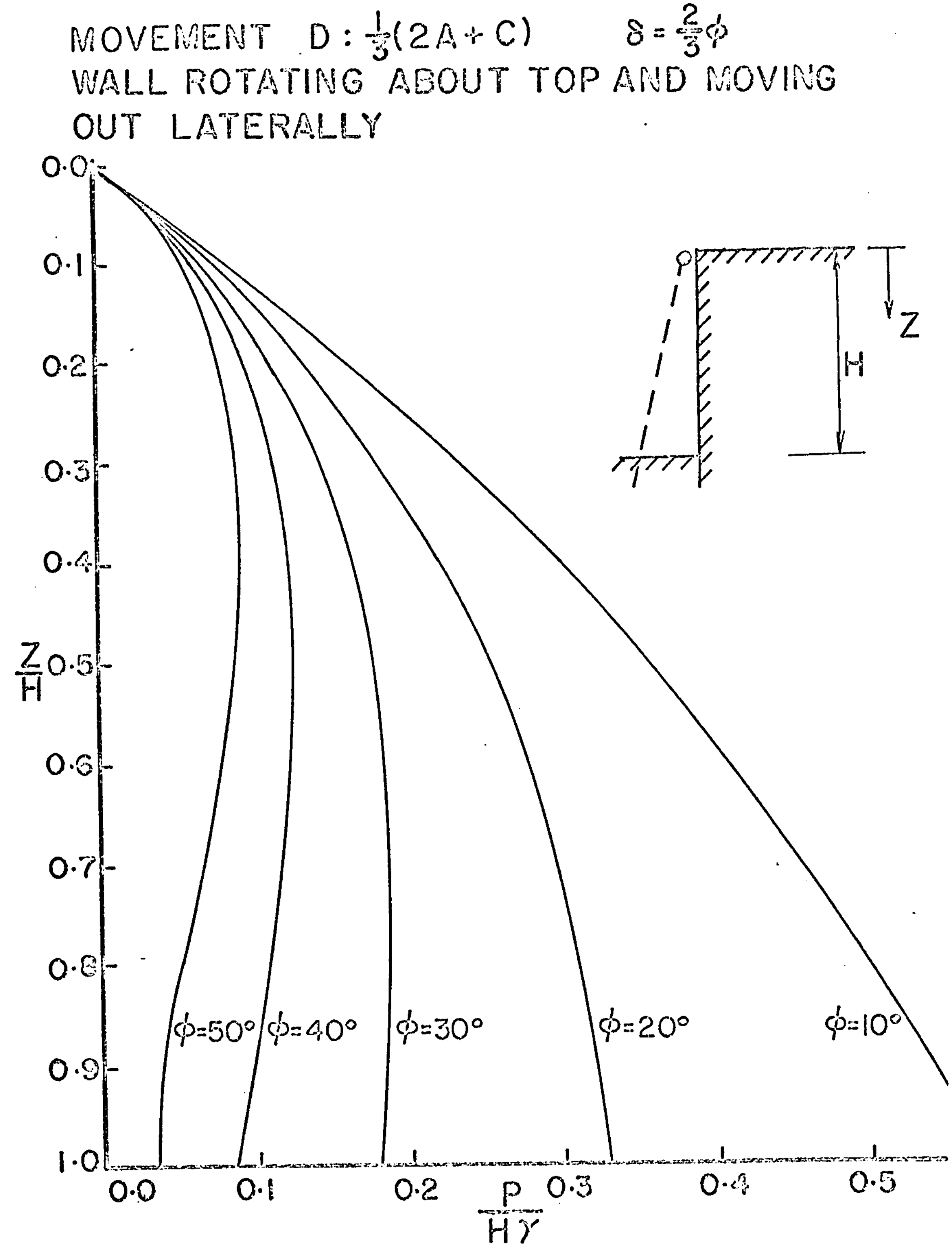

FIG. 4·2·18 LATERAL EARTH PRESSURE DISTRIBUTION

MOVEMENT D: $\frac{1}{3}$(2A+C) $\delta = \phi$
WALL ROTATING ABOUT TOP AND MOVING OUT LATERALLY

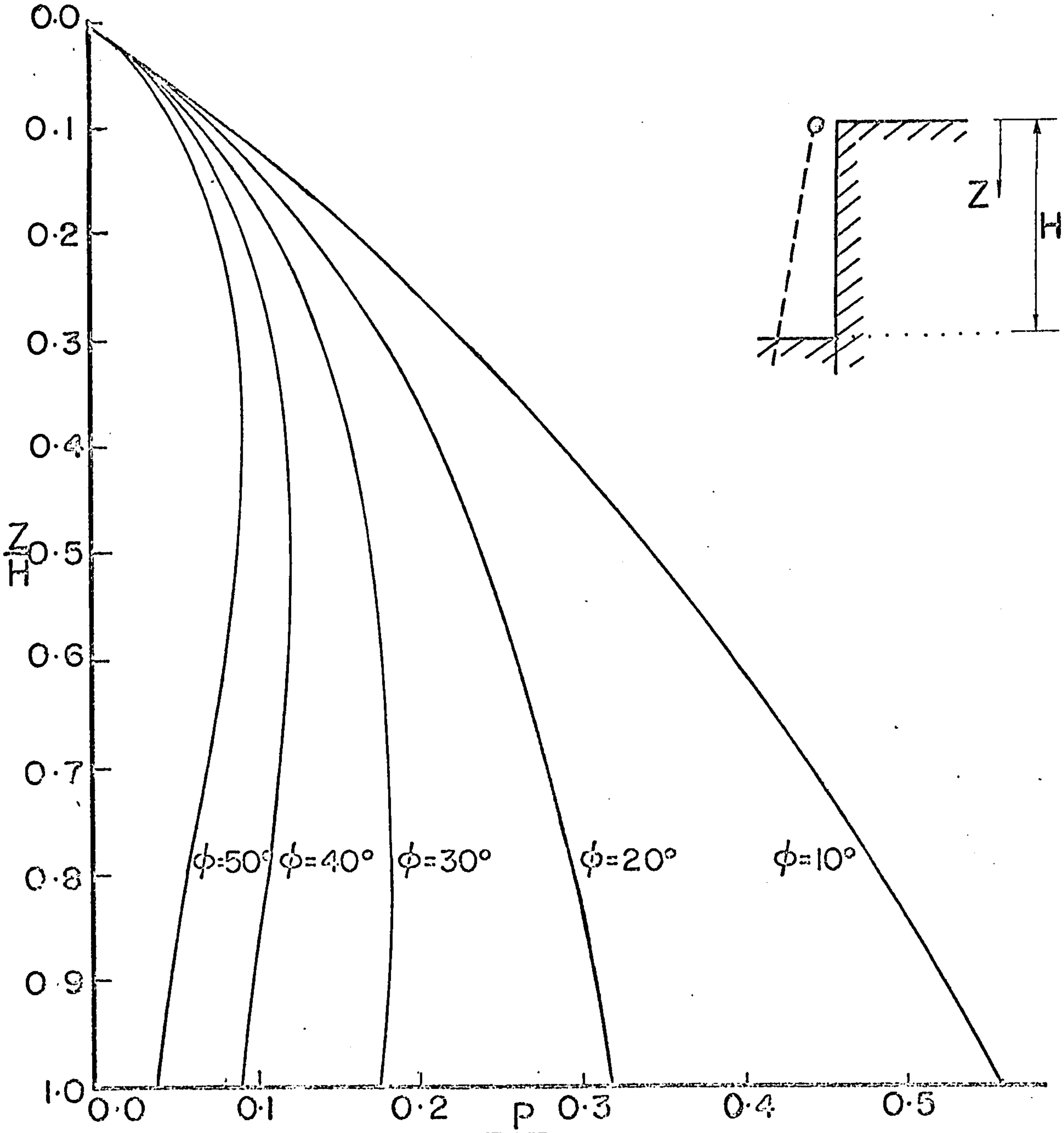

FIG. 4.2.19 LATERAL EARTH PRESSURE DISTRIBUTION

dominance of the linear increase of pressure with depth of movement C, which is overriding the contributions of pressure ordinates from movement A and B. The question of whether a braced cut will translate sufficiently to fully mobilize the active state at the top of the wall is open to argument. This depends to a large extent on the construction method employed. If the struts are not prestressed then they have to be slightly shorter than the length at which the two walls are spaced, otherwise they would not fit in. But even before the struts can be installed the wall had a chance to move away from the soil due to the unbalanced earth pressures. Proper wedging will only prevent additional movement. It is therefore quite feasible to assume in some cases that the top of the wall will yield sufficiently to have the shear strength at this point fully mobilized. For movement D all curves are tangent to the $\phi = 10^{\circ}$ curve for low values of z/H (Figs. 4.2.20 to 4.2.24).

The lateral pressure distribution curves of movement E are similar to those of movement D except the points of application of the resultant earth pressures are slightly higher than those of the corresponding ones of movement D. The point of application varies from a height of cut of 0.35 to 0.50, the higher values corresponding to greater internal friction angles. The effect of different wall friction angles on the total lateral earth pressure is even less obvious and the difference seems to be less than 10 per cent (Fig. 4.2.25).

MOVEMENT E: $\frac{1}{3}$(A+B+C) $\delta = \frac{2}{3}\phi$
WALL ROTATING ABOUT H/4 AND MOVING OUT LATERALLY

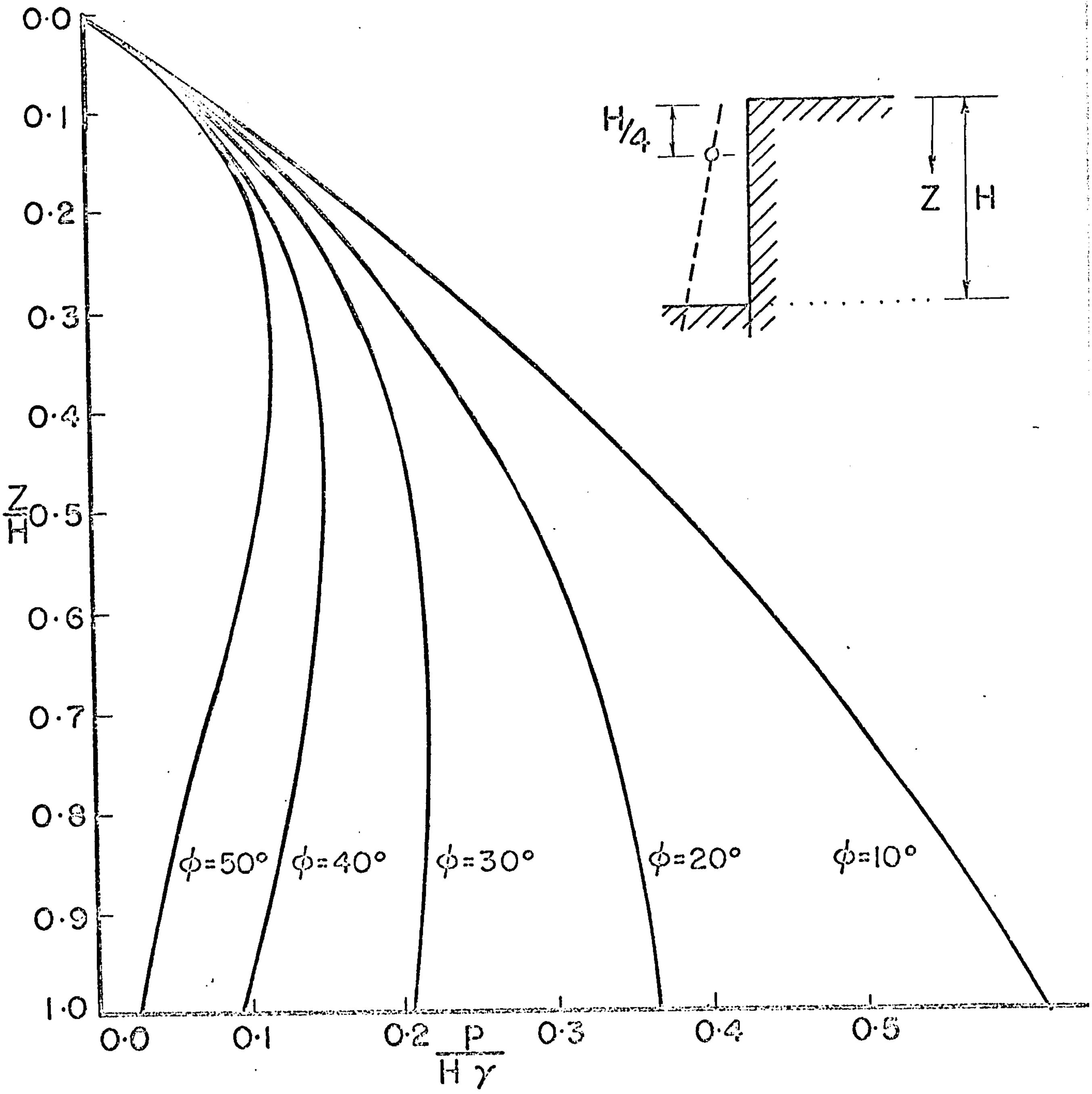

FIG. 4.2.20 LATERAL EARTH PRESSURE DISTRIBUTION

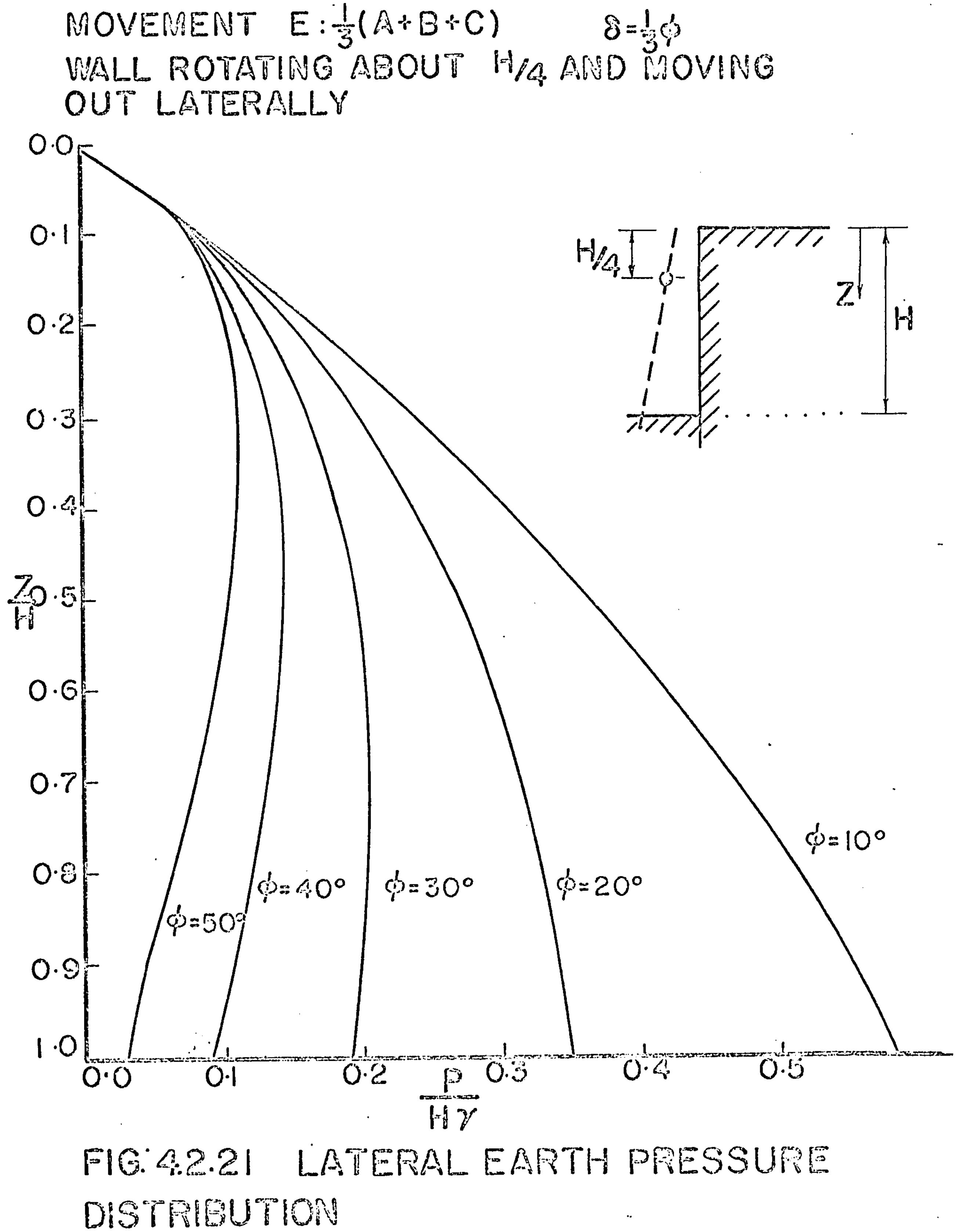

FIG. 4.2.21 LATERAL EARTH PRESSURE DISTRIBUTION

MOVEMENT E: $\frac{1}{3}$(A+B+C) $\delta = \frac{1}{2}\phi$

WALL ROTATING ABOUT H/4 AND MOVING OUT LATERALLY

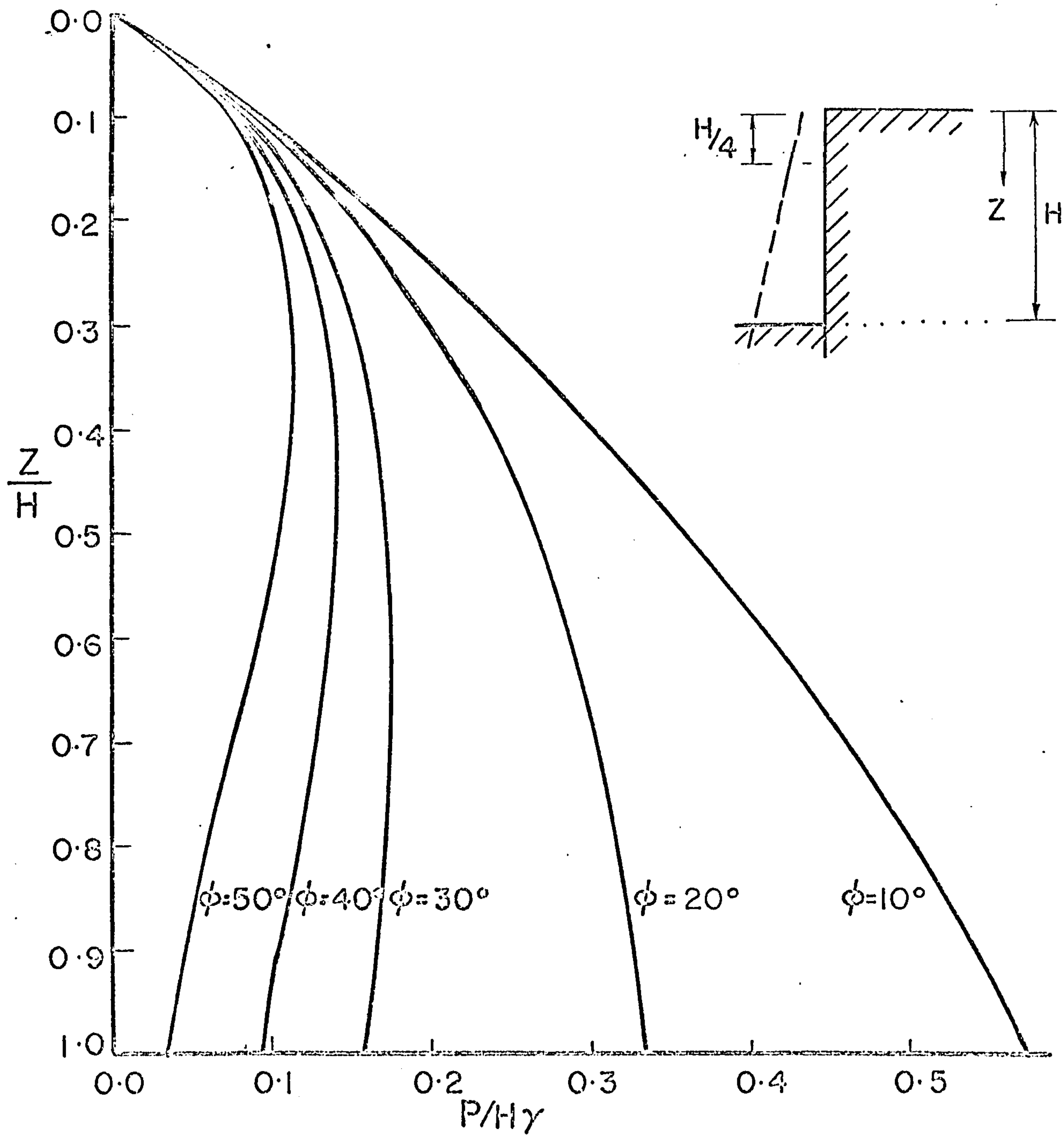

FIG. 4.2.22 LATERAL EARTH PRESSURE DISTRIBUTION

MOVEMENT E: $\frac{1}{3}$(A+B+C) $\delta = \frac{2}{3}\phi$

WALL ROTATING ABOUT H/4 AND MOVING OUT LATERALLY

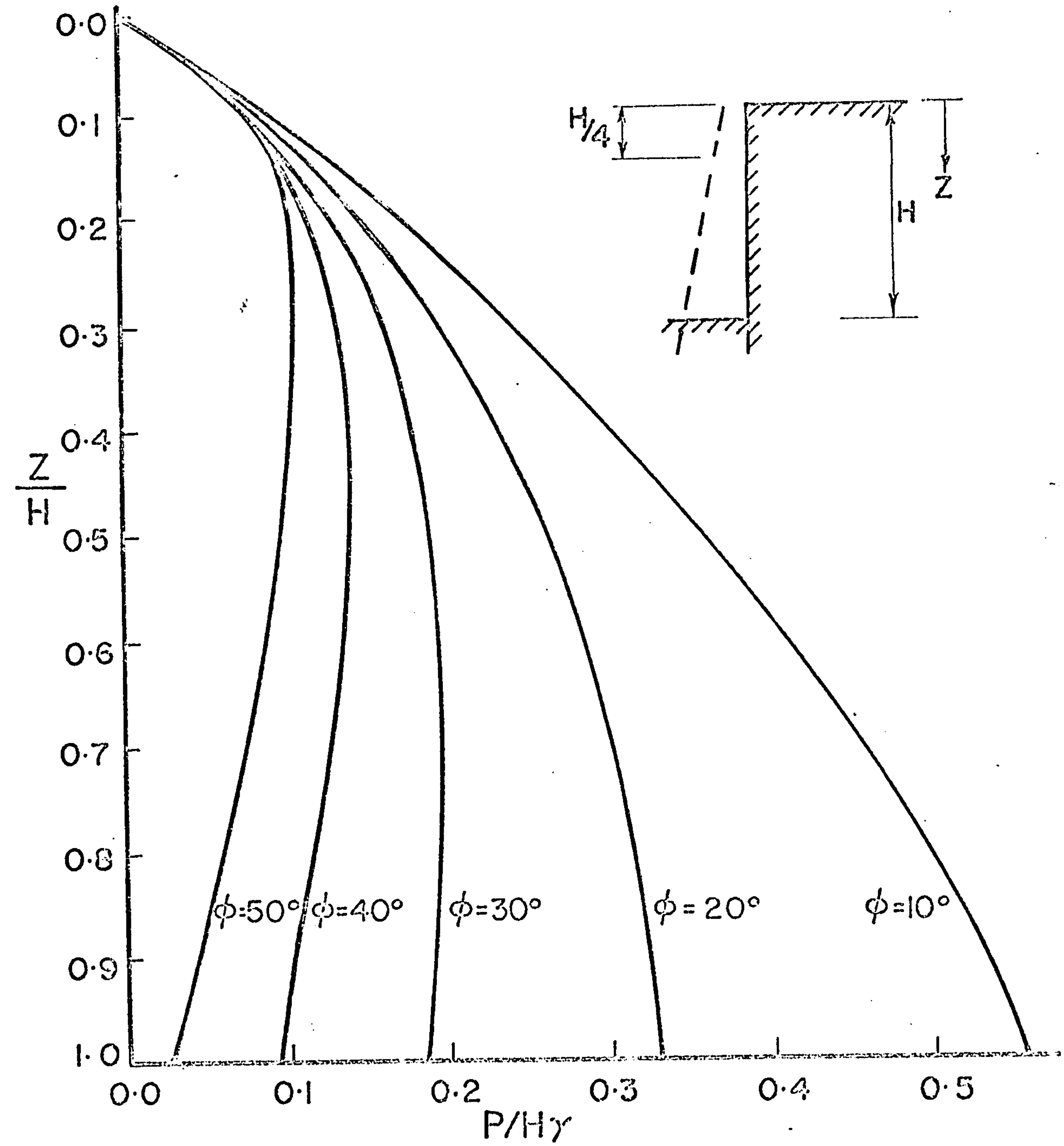

FIG. 4.2.23 LATERAL EARTH PRESSURE DISTRIBUTION

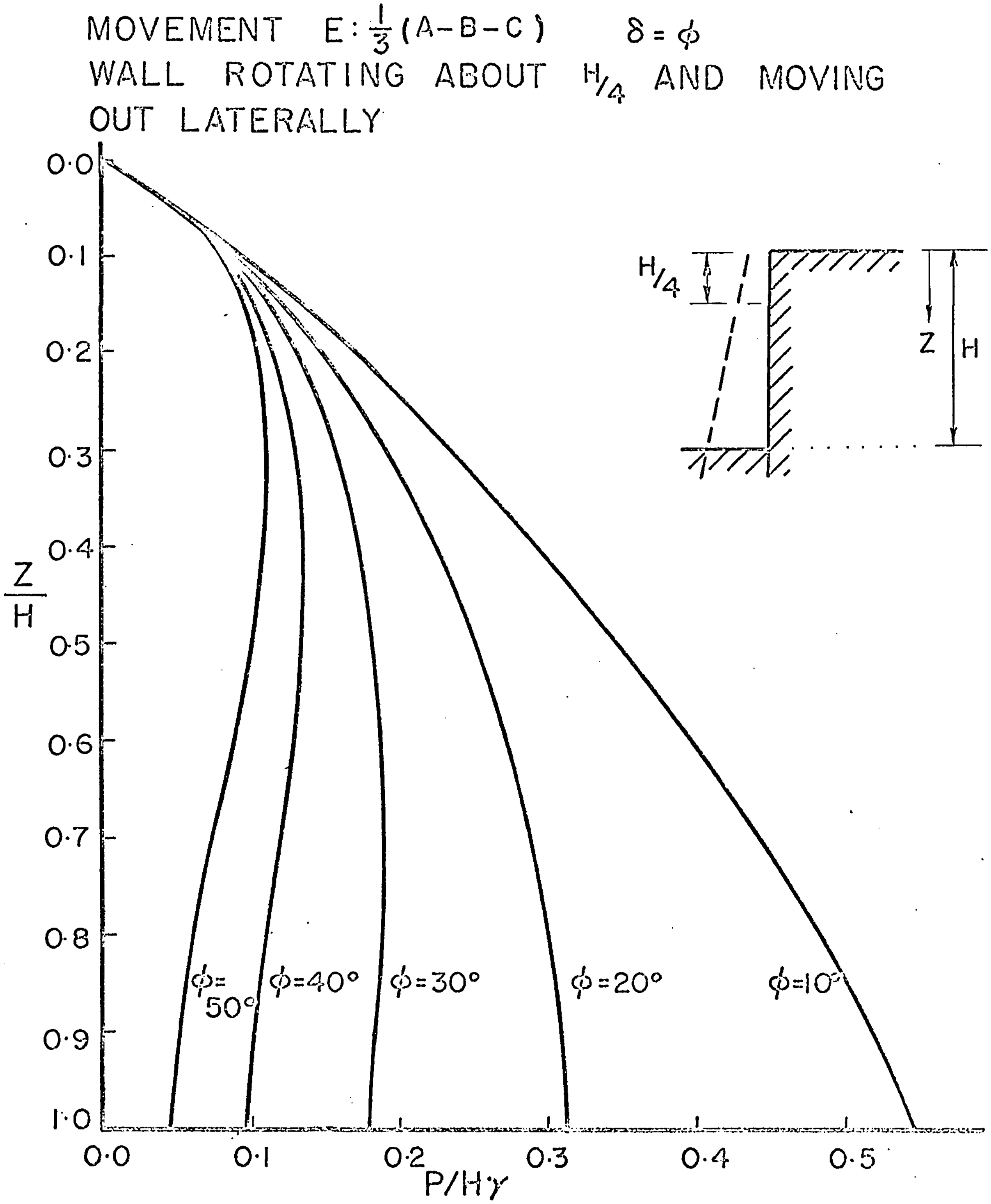

FIG. 4.2.24 LATERAL EARTH PRESSURE DISTRIBUTION

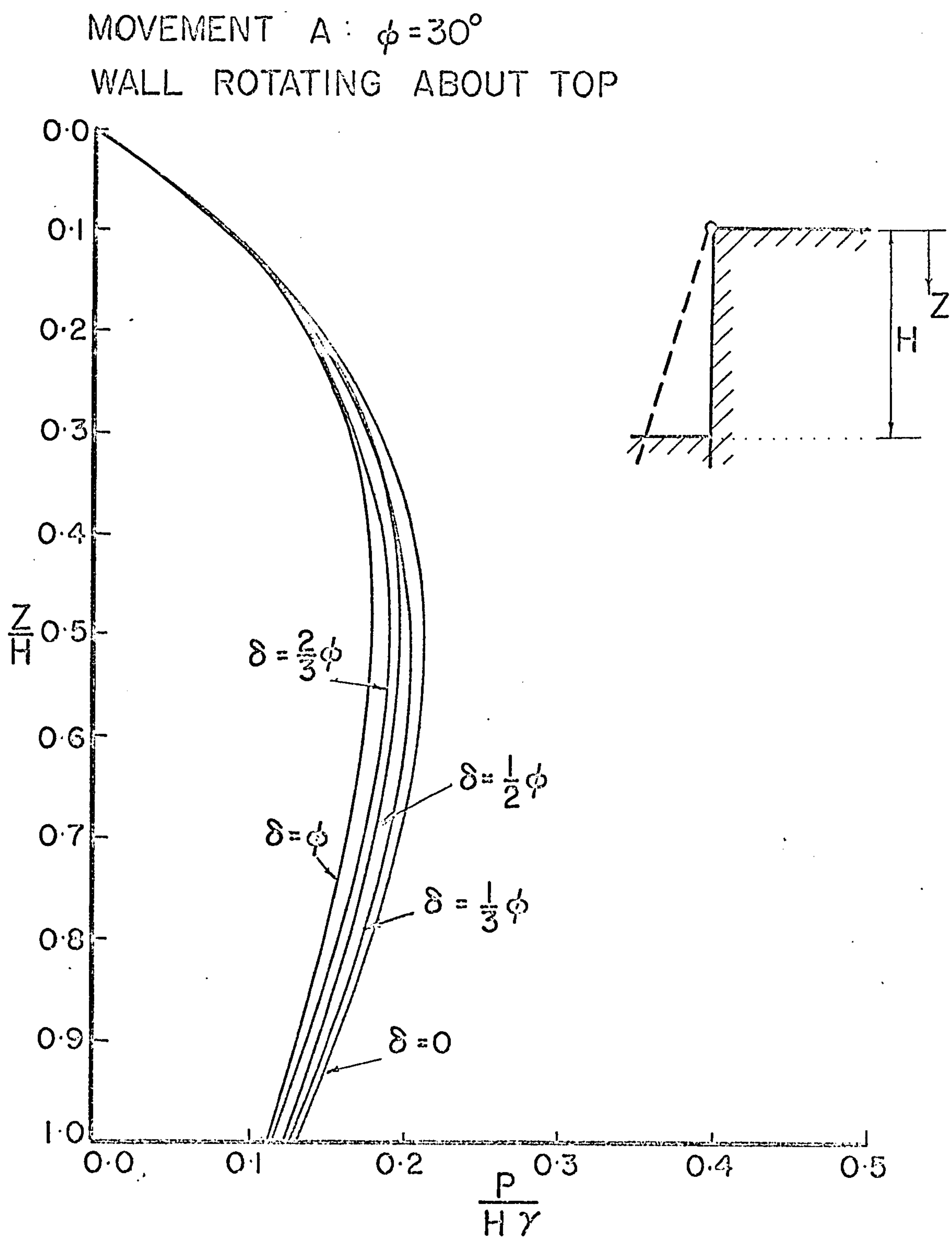

FIG.4·2·25 LATERAL EARTH PRESSURE DISTRIBUTION

The deformation of a properly executed braced excavation should correspond to either movement A, or movement B, or movement D. For these movements the resulting lateral earth pressure distribution is parabolic or pear-shaped.

4.2.5 The Coefficient of Earth Pressure at Rest

An element of soil mass which is in a state of static equilibrium is acted on by stresses which cannot produce failure as long as the soil properties and loads remain unchanged. The initial relationships between the principal stresses are influenced by the soil characteristics and by the manner in which the soil has arrived at its present position. In natural soils, the principal stress ratio will be governed by the nature of the sedimentation processes which have produced the soil and by the stress history of the formation, differing according to the degree of consolidation.

A point at a depth z in a semi-infinite mass of soil having an effective unit weight, γ, will have an effective stress on a horizontal plane due to the weight of the overburden equal to γz. The stress on the vertical plane (considering a two dimensional state of stress) is given as Ko z, in which Ko is termed the coefficient of earth pressure at rest, as introduced by Donath (1891).

In order to calculate the lateral earth pressure at-rest condition the value of Ko has to be determined. As first step in that direction Terzaghi (1920, 1925) undertook an experimental study for the purpose of determining the value of the at-rest coefficient, that is, the value of K coefficient where no lateral yield of the soil is taking place. Two thin strips of metal were embedded in a soil mass, one horizontally, the other one vertically and then pulled out. The forces required to make them move were measured. It was considered that the ratio of the forces P_h/P_v represented the value of the coefficient of earth pressure at rest, Ko. The values Terzaghi obtained were:

sands: Ko = 0.42

clays: Ko = 0.70 to 0.75 (remoulded and reconsolidated)

Later investigations, however, have shown that the above values of Ko for sand is too low in some cases, and that the values given for clays are too high (Tschebotarioff 1948).

Timoshenko (1934) established the following relationship for the lateral unit strain, ε_3, within an elastic body:

$$\varepsilon_3 = \frac{1}{E}\left[\sigma_3 - \nu\ (\sigma_1 + \sigma_2)\right] \qquad (4.2.27)$$

For a semi-infinite mass of soil the lateral pressures σ_3 and σ_2 can be considered to be equal, that is, $\sigma_3 = \sigma_2$. Further in the at-rest condition there is no lateral yield, that is, $\varepsilon_3 = 0$. Then Eq. 4.2.27 reduces to

$$\sigma_3 - \nu\sigma_3 - \nu\sigma_1 = 0 \qquad (4.2.28)$$

from which the coefficient of earth pressure at rest can be determined

$$Ko = \frac{\sigma_3}{\sigma_1} = \frac{\nu}{1-\nu} \qquad (4.2.29)$$

For a completely incompressible material the Poisson ratio ν was its maximum value $\nu = 0.5$, and the corresponding value of Ko = 1.0 as has been actually measured for saturated semifluid unconsolidated clays. For sands a value of Poisson ratio between 0.35 and 0.45 is assumed which corresponds to a range of Ko between 0.54 and 0.82. No reliable method for the direct measurement of Poisson ratio of soils has yet been developed. Therefore the theory of elasticity cannot yet be used for any direct determinations of the values of lateral earth pressure.

Experimental investigations to find the Ko values for different soils were carried out by Tschebotarioff and Welch (1948) in a specifically constructed lateral earth pressure meter. Their values for sand ranged from 0.1 to 0.5, with the high value obtained from the lateral pressure measurements at the top of the 1.5 ft. high circular tank. The low value of 0.1 was close to the bottom of the tank. It appears that no considerations were given to the side friction on the inside wall of the tank, which would explain the large difference of the Ko values obtained from the bottom and top of the tank.

Bishop and Henkel (1957) outlined a procedure to determine the Ko value from sample specimens in the triaxial test apparatus.

The puzzling part of determining the coefficient of earth pressure at rest lies in the absence of any apparent generally valid relationship between the measured Ko ratios and the values of the internal friction angle, ϕ, of different soils as determined in the laboratory by different testing procedures.

Jaky (1944) suggested the following relationship

$$Ko = 1 - \sin \phi \tag{4.2.30}$$

It was derived from stress conditions along the centre line of an embankment with slopes forming the angle ϕ with the horizontal, so that there is a variation of the horizontal shearing stress with the distance from the centre line. Jaky's proposed equation fits many of the experimental results since with $\phi = 30^{\circ}$, Ko $= 0.50$. However, the basic assumptions on which the derivation of the above equation is based do not appear tenable for an infinite mass of soil with a horizontal surface.

Hendron (1963) related the coefficient at rest and the angle of internal friction for a face - centred cubic array of round spheres as follows:

$$Ko = \frac{1}{2}\left[\frac{1+\frac{1}{2}\sqrt{3}-\frac{1}{2}\sqrt[3]{6}\sin\phi}{1-\frac{1}{2}\sqrt{3}-\frac{1}{2}\sqrt[3]{6}\sin\phi}\right] \tag{4.2.31}$$

The relationship given in Eq. 4.2.31 suggests that Ko decreases as ϕ increases, which is similar qualitatively to Jaky's relationship but not numerically identical. A plot of Eqs. 4.2.30 and 4.2.31 is shown in Fig. 4.2.26 which indicates the relationship between Ko and sin ϕ as proposed by Hendron and Jaky.

4.3 Stress - Strain Relationship and Strength of Sands

4.3.1 General

At the present time, design methods for plane strain problems use the values of shearing resistance determined by triaxial compression or direct shear test. Sufficient evidence is already available, including correlation with actual failures in the field, to suggest there is unlikely to be radical changes in strength under different strain conditions for sands (Bishop and Eldin 1950). Therefore, the versatile and comparatively simple triaxial test will continue to be fa-

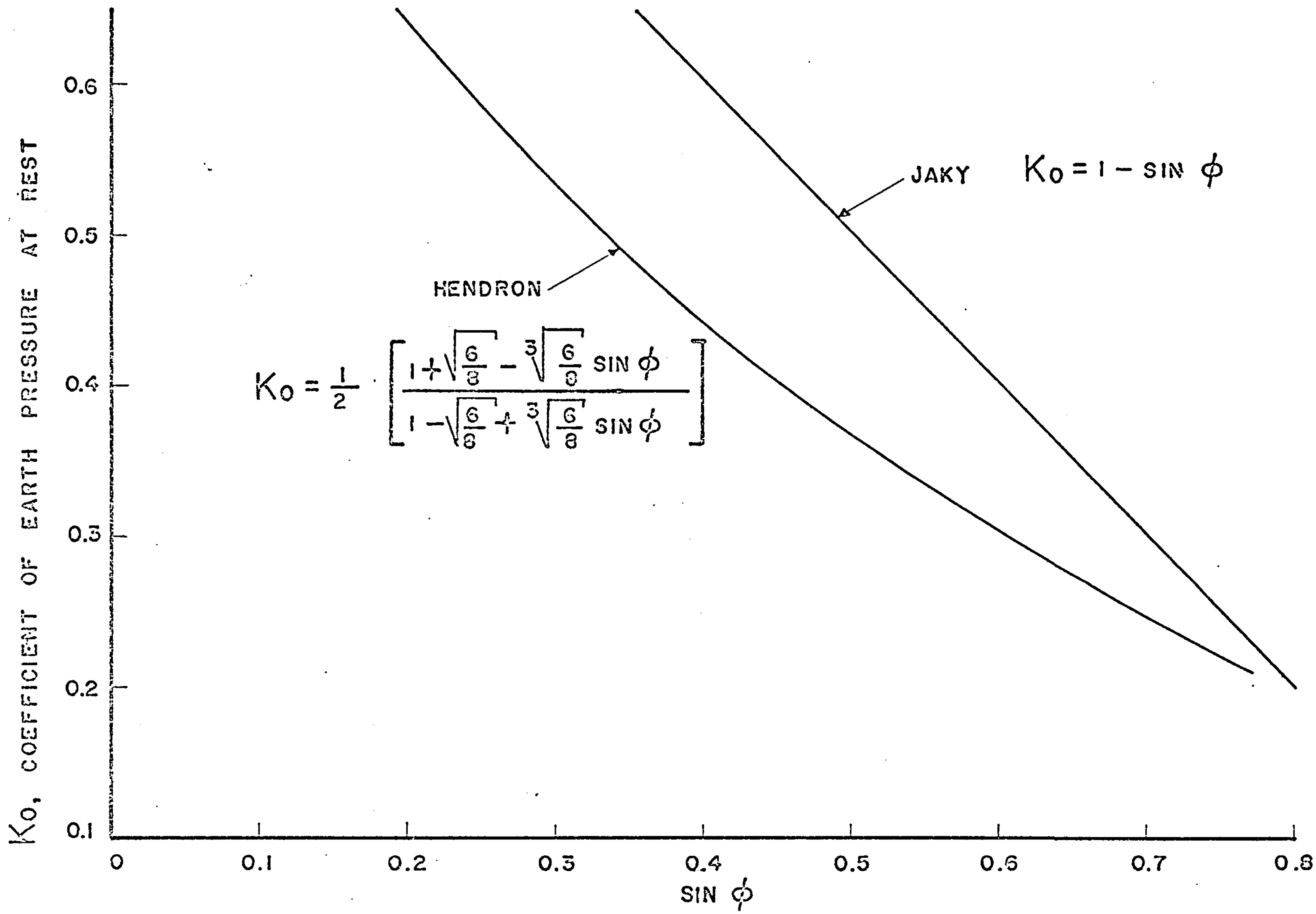

FIG 4.2.26 VARIATION OF K_o WITH SIN ϕ

voured by most commercial laboratories for measuring soil strength and other properties.

Valuable information can be obtained by observing or deliberately producing stability failures in the laboratory or on the construction site. The stability analysis under failure has a known safety factor of 1.0. However, the conclusions or improved design procedures which result from these measurements will be more valuable if the soil strength parameters used in the computations are known to correspond with the strain conditions of the structure.

4.3.2. Stress-Strain Relationship

Based upon the results of large-scale earth pressure tests, Terzaghi published a paper (1936) in which his first conclusion was as follows: "The fundamental assumptions of Rankine's earth pressure theory are incompatible with the known relation between stress and strain in the soils, including sands." For a retaining structure in contact with sand and rotating about its upmost point the condition of the affected sand mass is not at a state of failure at each and every point. The theories of elasticity also cannot be applied to this problem, since the sand mass is composed of individual particles, incapable of taking tension, dependent upon confining pressure in a non-linear manner for its strength, and having properties which vary with its stress history.

There are available, however, satisfactory theories of the states of stress in a soil mass, as discussed in Section 4.2, which require only a knowledge of the angle of internal friction for their solution. At failure this value has been know but, for soil that is not in a state of complete failure, it is necessary to determine a relation between the value of this friction angle mobilized and the soil deformation, then to relate the deformation to the boundary movements imposed by the structure.

In the laboratory a stress-strain or shear stress-shear strain relationship is obtained from a triaxial and/or direct shear test. From these results the shear strength parameters can be found by utilizing Mohr - Coulomb's failure envelope. In a triaxial compression test the axial stress and strains are easily measured and the values plotted as a stress-strain curve to obtain maximum and ultimate stress values and a modulus of elasticity. Such a curve is shown in Fig. 4.3.1 for a typical sand. Curve A designates the shear stress in relation to shear strain for a dense sand whereas curve B shows the same relationship for a loose sand. It is also possible for an initially dense sand in the lower portion of a cut to follow the dotted line C as the wall rotates about the top point whereas the sand in the upper part follows curve A during the same rotational movement. Sofar this has not been taken into consideration in the calculation of the earth pressure and its effect on the earth pressure distribution is not known. In the classical theories, as well

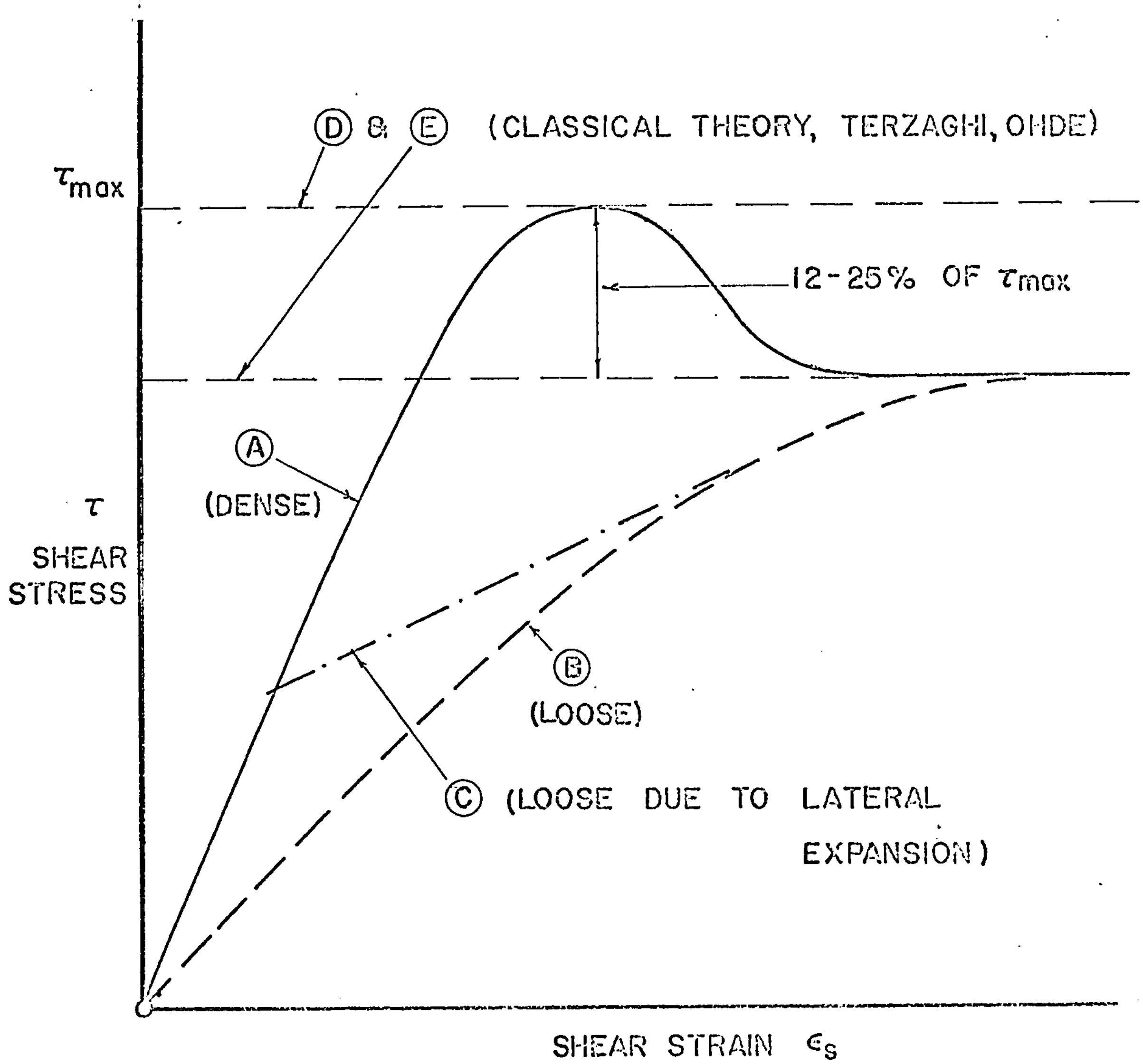

FIG.4.3.1 STRESS - STRAIN RELATIONSHIP

as in Terzaghi's General Wedge Theory and in Ohde's calculations τ_{max} was usually assumed for the shearing resistance.

Another factor which is usually not taken into consideration is that in triaxial compression tests the axial strains only are recorded whereas the lateral strains are seldom if at all measured. The difference between the axial and lateral strains and the resulting E may be significant. Earth pressure problems involving the modulus of elasticity are concerned with lateral strains, hence to obtain a reliable solution for such a problem the lateral strains should be determined. If the calculation of the wall movement to obtain the active pressure condition is based upon the customary modulus of elasticity, as determined from the axial strain, the movement is likely to be much greater (two times or more) than that which is actually required.

The problems of earth pressure on open cuts is virtually two-dimensional. The structure and soil do not change laterally considerably from section to section. While the stresses change in all three principal directions the strains are limited to two dimensions. The strain parallel to the wall, therefore, can be considered to be equal to zero (plane strain condition). The effect of different strain conditions on the shear strength parameters will be discussed in Section 4.3.4.

4.3.3 Strength Parameters

To calculate the lateral earth pressure one has to assume or determine the coefficient of earth pressure which is a function of the internal friction angle. The strength of sand is conventionally determined by direct shear or triaxial compression tests performed on samples which have been formed in the laboratory to the desired conditions.

Several investigations have been carried out (Chen 1948, Nash 1953, Kirkpatrick 1957, Jakobsen 1957, Bjerrum et al 1961, and Cornforth 1964) to correlate the shear strength of fine uniform sand using different testing apparatus.

Nash (1953) concluded from his experiments that the compressibility and the angle of shearing resistance is the same regardless of whether dry or wet sand was used. He also found that at a porosity of 42 per cent the shear box and triaxial test gave approximately the same angle of shearing resistance. Below this porosity the shear box gave an angle of about 10 per cent higher, and above this porosity it gave an angle of 5 per cent lower.

Cornforth (1964) compared drained strength results from triaxial tests with tests carried out in a specially constructed plane strain apparatus. At a porosity of 44 per cent both testing procedures yielded approximately the same angle of shearing resistance. Below this porosity the plane strain results were as much as 10 per cent higher. These results will be discussed in more detail in Chapter 5 under Results of Laboratory Measurements with regards to test data found in this work.

4.3.4 Stress Path

The manner in which the stresses in the soil change during changes on loading has a marked influence on the test results. In order to derive meaningful soil parameters in the laboratory we have to simulate the stress path the soil sample would have undergone in the field. The sequence in which a stress changes from point A to point C or from point A to point B and then to point C has a major effect on the test result even though the final stresses are the same.

The basic principle of the stress path method is: because strain, porewater pressure, and the strength of a soil element depend on the stress path, the engineer should consider the field stress paths (or field strains, or both) in selecting the soil testing procedure and method of analysis for a given problem. Frequently, the stress paths and the behaviour of the soil in the actual problem are such that conventional testing and conventional analytical techniques are sufficient. In certain problems, however, special testing and analytical techniques will be needed.

A stress path is a line drawn through points on a plot of stresses. The particular stress point used in the stress path method is that of maximum shear stress on a Möhr circle diagram, as shown in Fig. 4.3.2. Thus, a stress path is the locus of points of maximum shear stress

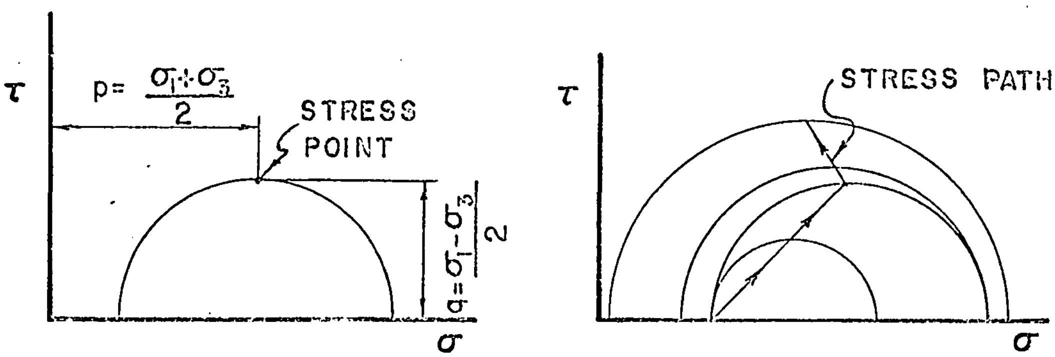

a) DEFINITION OF STRESS PATH

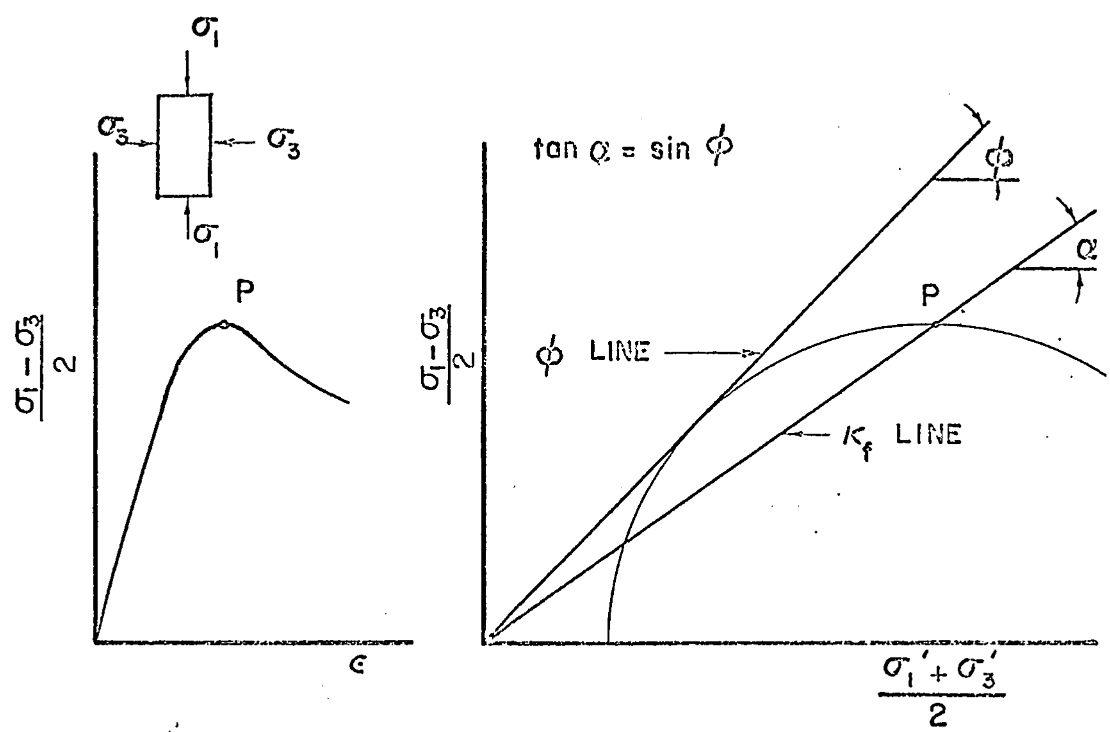

b) THREE-DIMENSIONAL COMPRESSION

FIG. 4.3.2 STRESS PATH CONCEPT

experienced by an element in going from one state of stress to another.

For determining the shear strength parameters the triaxial test has proved to be the most commonly used stress-strain test. Fig. 4.3.3 shows stress paths for four types of tests that can be performed without any difficulty with the triaxial apparatus. The paths shown are for drained tests on sand. The effective stress paths are depicted only, the total stress path can easily be drawn knowing the pore water pressure. Each total stress path is parallel to the corresponding effective stress path and displaced to the right a distance equal to the static pore pressure, which in case of a laboratory test is the static back pressure.

Commonly a triaxial compression test is performed in order to evaluate the cohesion intercept and the angle of internal friction. A constant chamber pressure is left on the sample throughout the whole test and the sample is brought to failure by increasing the axial load. The change of stress during this test is indicated by the stress path AB in Fig. 4.3.3. The stress change of an element at point 1 of the braced cut in Fig. 4.3.3 follows a quite different stress path. Initially the soil is at Ko condition. It is assumed that the soil element at point 1 lies below the ground surface on the failure plane, which means that the shear stress will be less or equal to the shear strength. It should be pointed out that this element does not represent the average element of the wall. During excavation the vertical stress remains unchanged ($\Delta\sigma_1 = 0$), the

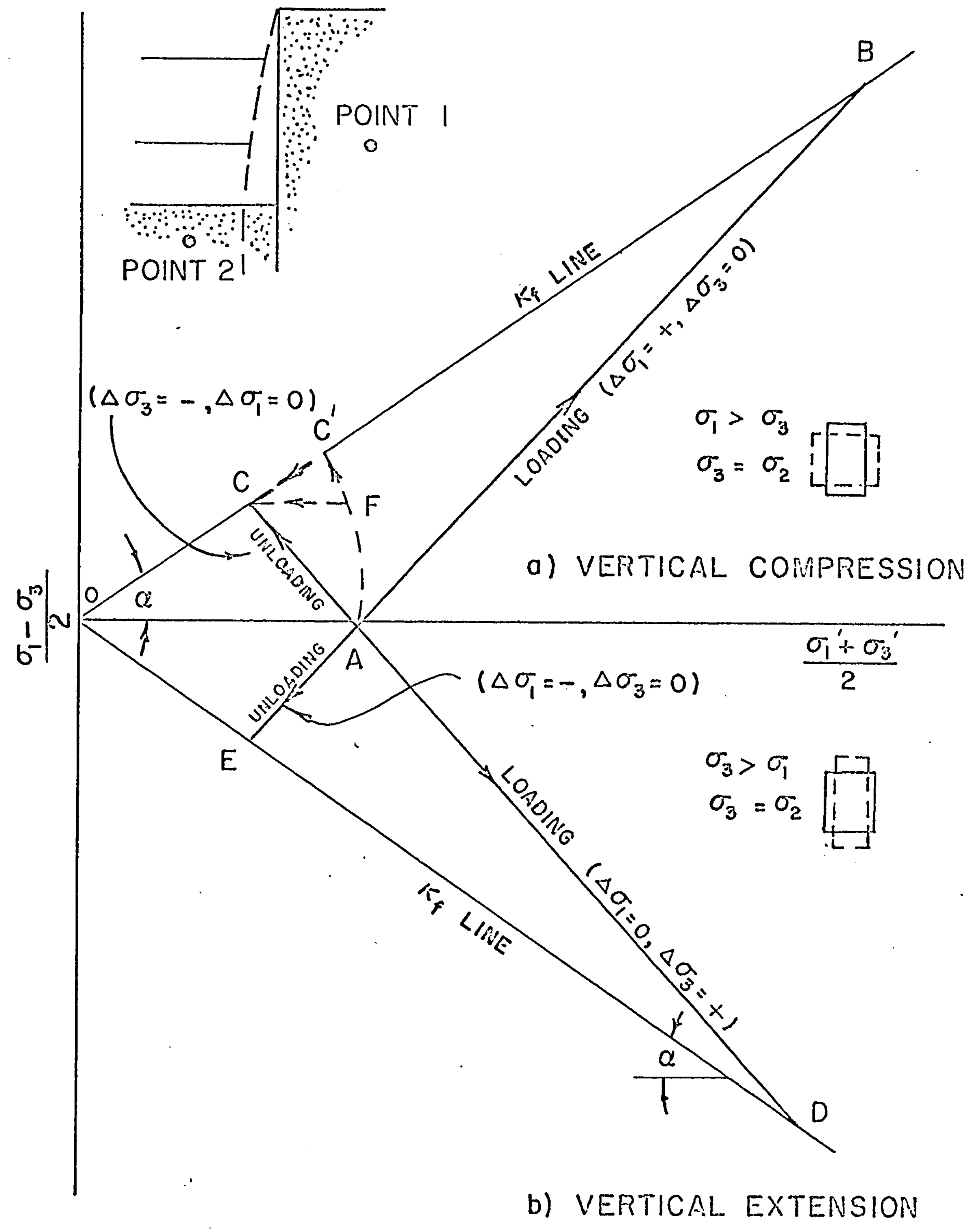

FIG. 4.3.3 STRESS PATH FOR TRIAXIAL TEST AND FIELD BEHAVIOR

horizontal stress, σ_3, is decreasing and the effective stress path will change from point A to point C. The exact stress path which the element follows going from the initial point A to the final point C depends on the drainage condition. Shown are the effective stress paths for three drainage conditions of going from A to C. The minimum strain occurs by going from A to C in drained shear. The maximum strain occurs from going from A to C' in undrained shear and then from C' to C in drained shear. An intermediate amount of strain occurs from the stress path AFC. Thus the strain associated with developing active stress in element 1 depends on the drainage condition and on the loading path.

The field element reaches its maximum shear stress at point C and the sample tested in a conventional triaxial compression test will reach its maximum shear stress at point B. the slope angle, α, of the K_f line will be identical for both tests whereas the stress paths are quite different and also the stress levels and the magnitude of strains differ quite considerably.

As the excavation proceeds the wall of the cut deforms away from the soil mass. An element of soil at point 2 will undergo a state of lateral compression. The overburden pressure remains unchanged, $\Delta\sigma_1 = 0$, and the lateral stress, σ_3, will be increased until failure occurs on a stress circle passing through D. This stress path, AD, can be simulated by a vertical extension test in the laboratory with keeping the vertical stress constant and increasing the lateral pressure.

Retaining wall problems can for all practical purpose be considered as a plane strain problem and it is recommended to use plane strain tests, rather than triaxial tests. If triaxial tests are used, a correction should be applied to the parameters obtained.

4.4 Concept of Soil Arching

4.4.1 General

It appears that the significance of the arching phenomenon was first observed in connection with the bracing of open cuts. During the construction of the New York subway system at the turn of the century, field measurements of strut loads in open cuts disagreed with Coulomb's hydrostatic distribution of lateral earth pressures (Meem 1908). Higher loads were measured in the top struts of braced, open cuts. Similar results were observed by Terzaghi (1941) in connection with lateral earth pressure measurements in open cuts during the construction of the Berlin subway.

The deviation of lateral earth pressure distribution from the hydrostatic distribution was generally attributed to the phenomenon of arching. The actual mechanism of arching, if any, has not been solved yet adequately. Most of the existing theories of arching deal with the pressure of dry sand on yielding horizontal strips. All these theories

(Engesser 1882 , Bierbaumer 1913, Caquot 1934, and Vollmy 1937) are in accordance with experience in that the pressure on a yielding, horizontal strip with a given width increases less rapidly than the weight of the mass of sand located above the strip and approaches assymptotically a finite value.

The investigation of the effect of arching on the pressure of sand on a vertical support is much more difficult. The first attempt to investigate this effect was made on the simplifying assumption that the surface of sliding is plane (Terzaghi 1936). This investigation gave a satisfactory general conception of the influence of the different factors involved, but failed to give information regarding the effect of arching on the intensity of the lateral pressure.

In the following section it is attempted to define arching and to explain its mechanism and also to evaluate its influence, if any, on the lateral earth pressure distribution.

4.4.2 Theoretical Considerations

A unique definition of arching in soils does not exist since this concept is very complex and some authors define "arching" as any deviation from the straight line earth pressure distribution. The best general definition was probably given by Terzaghi (1954):

"If one part of the support of a mass of soil yields while the remainder stays in place the soil adjoining the yielding part moves out of its original position between adjacent stationary masses of soil. The relative movement within the soil is opposed by a shearing resistance within the zone of contact between the yielding and the stationary masses. Since the shearing resistance tends to keep the yielding mass in its original position, it reduces the pressure on the yielding part of the support and increases the pressure on the adjoining stationary part. This transfer of pressure from a yielding mass of soil onto stationary parts is commonly called arching effect, and the soil is said to arch over the yielding part of the support. Arching alos takes place if one part of a yielding support moves out more than the adjoining parts."

Terzaghi associated arching with the yielding of the soil mass, whereas Tschebotarioff (1952) assumed continuous tightly wedged sand grains for his soil arch, that is a true arch is an elastic and not a plastic condition. The very high K-values (coefficient of earth pressure), which were observed frequently in the uppermost portion of a rotating wall, served Tschebotarioff as support of his theory.

The basic difference then between Terzaghi's "arching effect" and Tschebotarioff's "true arch" is, therefore, that in the former case the sand grains are free to move, whereas in the latter they are wedged tightly with one another. Arching effect, therefore, can be defined as the transfer of pressure by shearing stresses from a yielding part to a stationary or less yielding part. A physical or structural arch is not necessarily formed. True arching occurs when individual hard soil grains are wedged together in order to form a selfsupporting structural arch, similar to a masonary arch. It is almost impossible to push dense sand out of a sampling tube no matter how high pressures are applied. This is an example of true arching.

So far the problem of arching cannot be treated satisfactorily quantitatively because of the present impossibility to differentiate numerically between the two above causes of redistribution of lateral earth pressures. It will be illustrated later, however, that true horizontal arching, which relieves the lateral stress at the lower portion of the cut, seldom occurs in actual practice.

There are several different types of arching effect which may occur in a braced open cut in dense sand. They are illustrated in Fig. 4.4.1. Fig. 4.4.1.a shows arching effect occuring between struts due to the slight deflection of the wales. The stress is increased at the supports and at the same time decreased towards the centre of the bay. This effect is more pronounced the more dense the sand. It should be noted that the total pressure is not altered. Horizontal arching effect may also occur in a plane perpendicular to the sheet pile wall as indicated in Fig. 4.4.1.b. A wall rotating about its upper point results in an

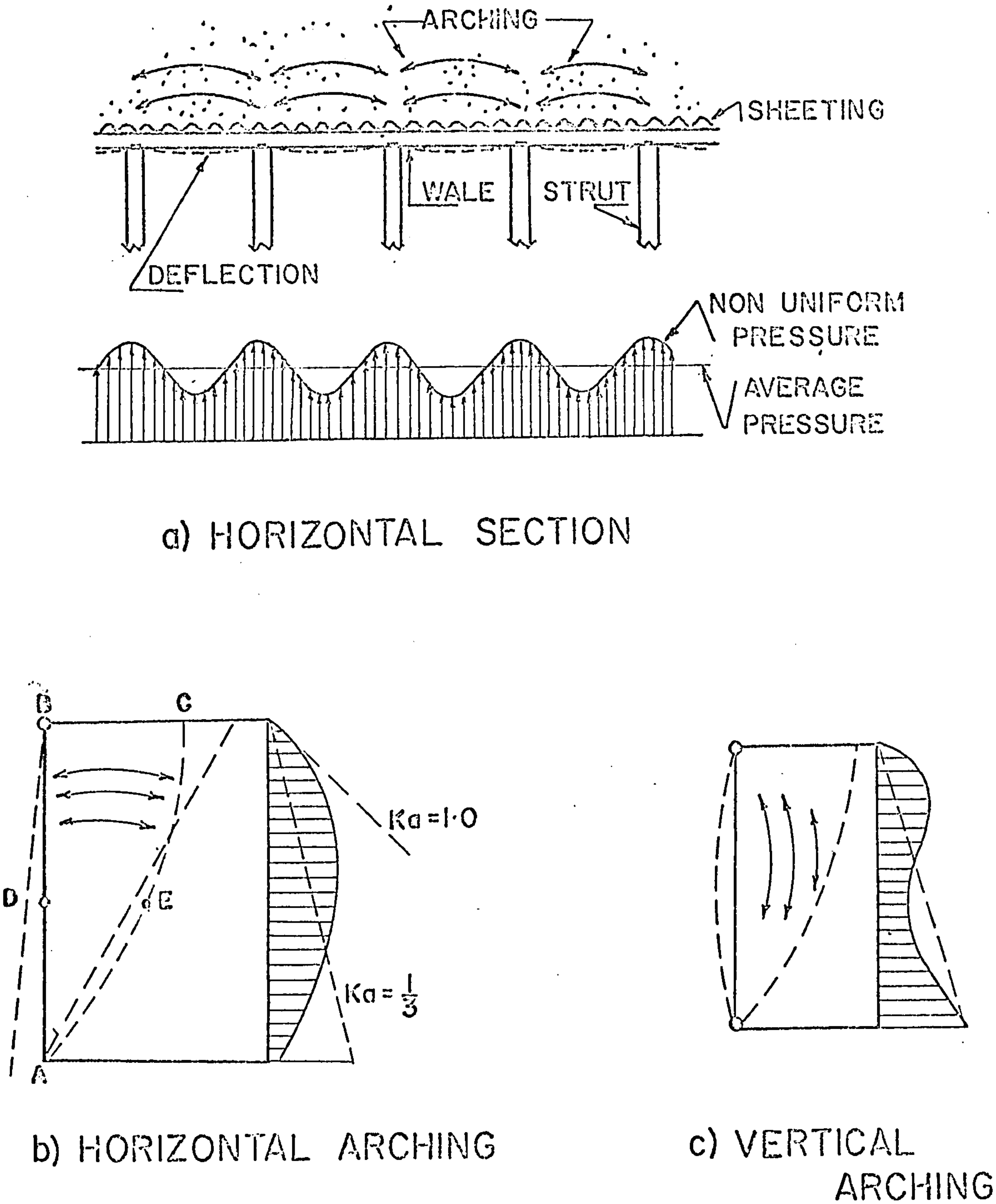

FIG.4.4.1 ARCHING ACTION IN A BRACED OPEN CUT

energetic expansion of the lower part of the wedge, DAE, which in turn causes the upper part of the wedge, BDEC, to descend. This downward movement mobilizes the frictional resistance of the soil along the slip surface AC. Once the frictional resistance along AC is fully mobilized, the total lateral pressure automatically assumes the theoretical Coulomb value, regardless of what the state of stress within the wedge ABC may be (Terzaghi 1936). The earth pressure acting on a horizontal plane of the lower part, such as DE, is equal to the weight of the overlying soil minus the vertical frictional components which are mobilized along the slip surface AC, on one side and on the wall-soil interface, AB, on the other. The wall and the slip surface will provide the two stationary masses required for an arching effect to be present.

Arching on a smaller scale also occurs across the troughs of the sheeting and to an even smaller extent across the deflected membrane of the pressure transducer.

Fig. 4.4.1.c shows the effect of vertical arching and the resulting lateral pressure distribution. Lateral pressures are transferred from the highly deflected centre part of the wall to the stationary parts at the two extremities of the wall.

Tschebotarioff (1952) assumed that the true arches are parabolic and self supporting. For a true arch of parabolic shape (Fig. 4.4.2.a) the following general relationships hold, according to conventional struc-

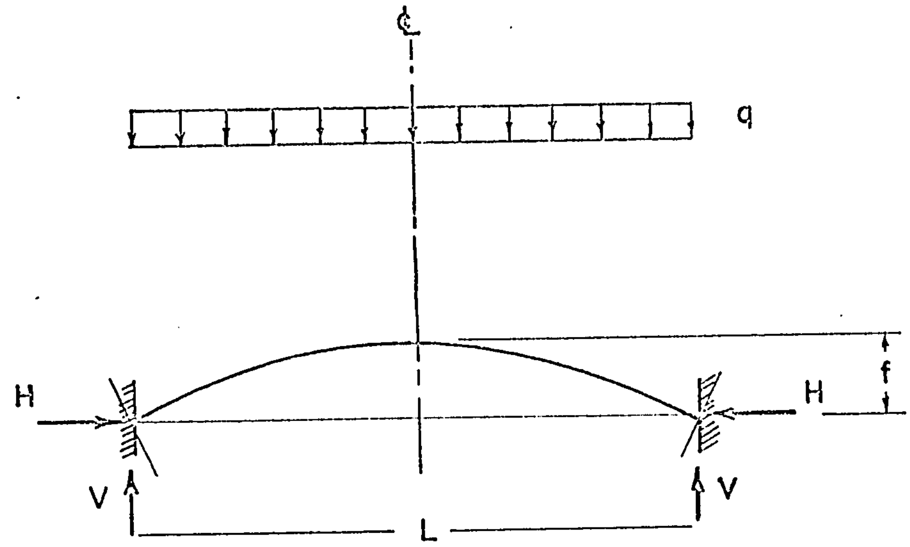

a) DIMENSIONS AND FORCES ON TRUE ARCH

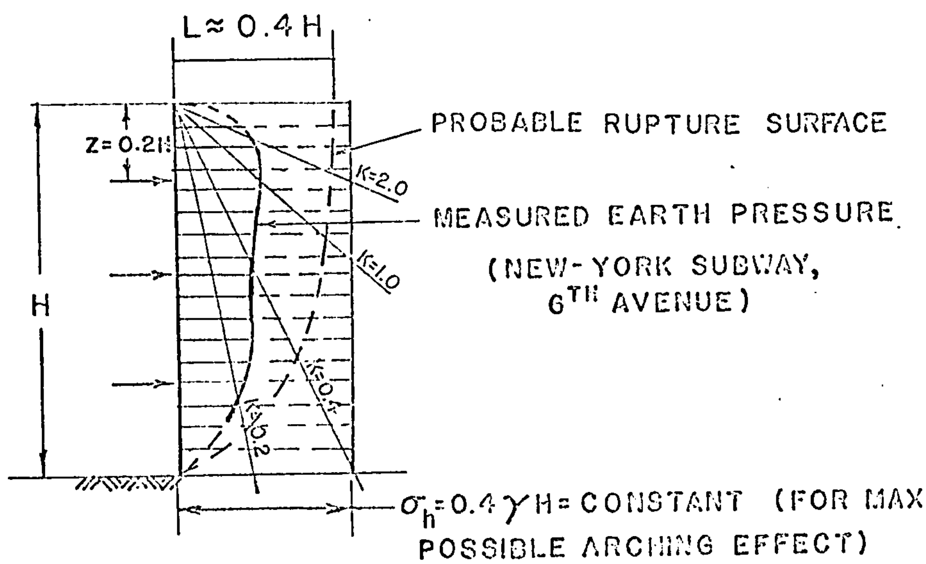

b) COMPARISON OF TRUE ARCHING AND ACTUAL MEASUREMENTS

FIG 4.4.2 TRUE ARCHING AFTER TSCHEBOTARIOFF tural theory: For a uniformly distributed vertical unit load the vertical reaction is

$$V = \frac{q\,L}{2} \tag{4.4.1}$$

The horizontal reaction is

$$H = \frac{q\,L^2}{8f} \tag{4.4.2}$$

If the vertical reaction is to be supported by friction only, then

$$V = H \tan\,\phi \tag{4.4.3}$$

Solving Eqs. 4.4.1, 4.4.2, and 4.4.3 for f, we obtain

$$f_{(max)} = \frac{L\,\tan\phi}{4} \tag{4.4.4}$$

Thus a relatively flat, horizontal arch may support its own weight by friction at its abutments, provided the grains are hard and tightly wedged to form an arch, and provided the two abutments do not yield. Tschebotarioff assumed then that one of the successive horizontal arches, located at a depth z below the soil surface, has a cross section of unity and carries its own weight only. In that case $q = \gamma(1.0)^3$, and therefore the horizontal stress

$$\sigma_h = \frac{H}{A} = \frac{AL^2}{8f} \; \frac{1}{A} = \frac{\gamma L^2}{8f} \tag{4.4.5}$$

At a depth z, the coefficient of active earth pressure K_A will be

$$K_A = \frac{\sigma_h}{\gamma z} = \frac{L^2}{8fz} \tag{4.4.6}$$

For $\phi = 30^o$, by substituting $\tan\phi = 0.577$ into Eq. 4.4.4 to obtain f, we get

$$K_A = \frac{L^2}{8(0.144)\ Lz} \qquad \frac{L}{z} \tag{4.4.7}$$

If we assume now as a maximum value $L = 0.4\ H$, where H is the full depth of the cut, the hydrostatic earth pressure ratio becomes

$$K_A = 0.4\ \frac{H}{z} \tag{4.4.8}$$

Thus, at a depth $z = 0.10\ H$, $K_A = 4$; if $z = 0.20\ H$, $K_A = 2.0$; if $z = 0.4\ H$, $K_A = 1.0$. Actual observations on cuts in sand (Spilker 1937, White and Prentice 1940), however, show lesser pressures at these elevations. This indicates that true arching in the case of cuts in sand does not reach its maximum possible value.

Fig. 4.4.2.b shows a comparison of Tschebotarioff's arching theory and an actual measurement of lateral earth pressures against braces of a subway excavation at Sixth Avenue and 16th Street, New York (White and Prentice 1940). From this it is obvious that Tschebotarioff's solution yields a total lateral earth thrust very much in excess as compared to actual measurements and the constant theoretical pressure distribution is also not in accordance with actual observations.

4.4.3 Critical Evaluation of Soil Arching

All concepts of arching try to explain the non-linear distribution of earth pressures by postulating certain thoeries. So far they all fall short with respect that they cannot even come close to the actual pressure distribution as observed on large-scale models or actual structures. In Figs. 4.4.3 and 4.4.4 an attempt is made to approach the problem step by step from the opposite end. The type of pressure distribution is taken to be "known" and by a sequence of diagrams it is tried to draw a physical picture how a transfer of stresses has to take place from the "upper" arches to the lower ones to obtain the observed pressure distribution. The following is considered to be a visualization of certain events and not a proof of a new theory, but important deductions will be

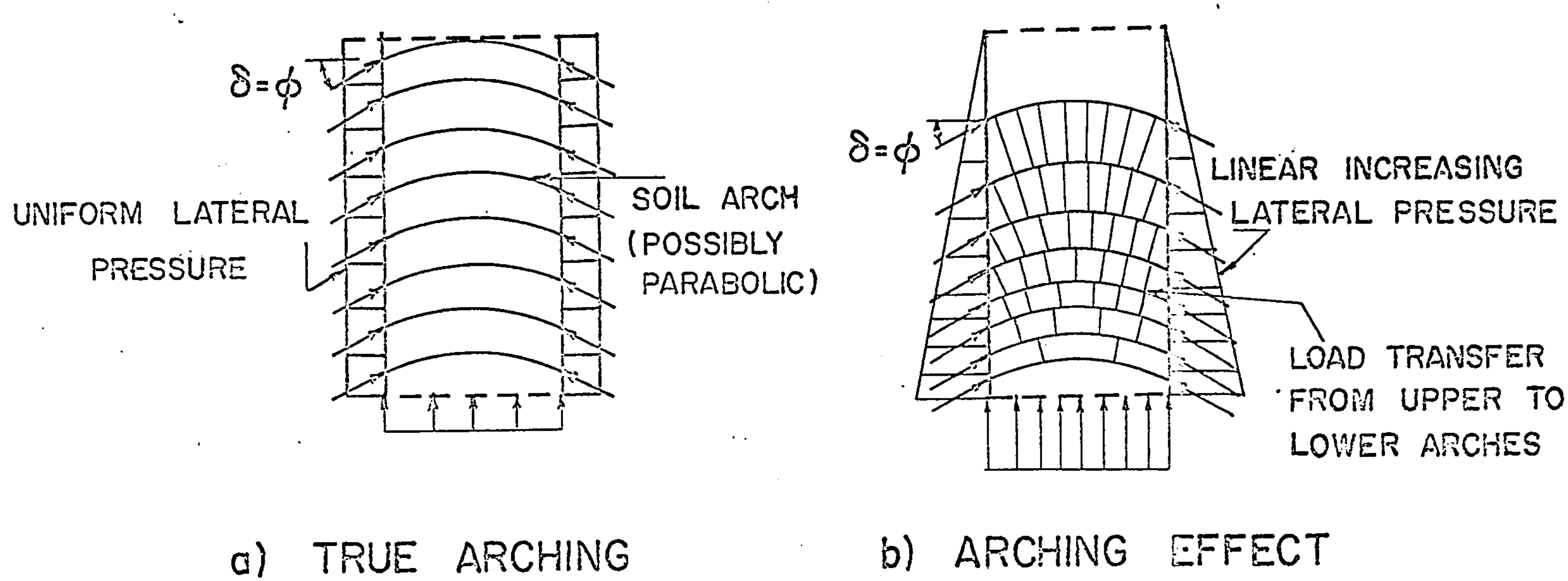

FIG. 4.4.3 TRUE ARCHING AND ARCHING EFFECT

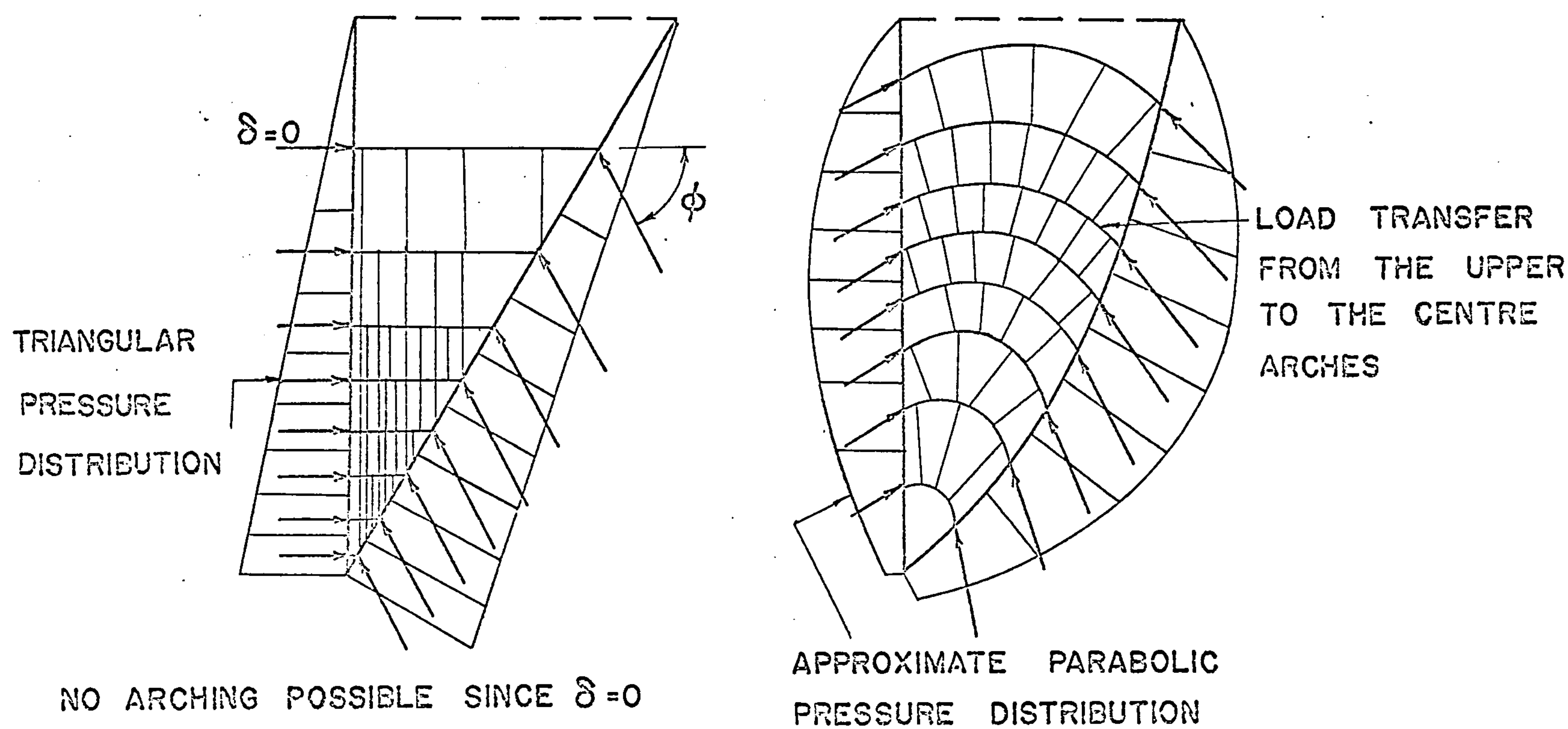

a) RANKINE'S CASE

b) WALL ROTATING ABOUT TOP

FIG. 4.4.4 SOIL ARCHING

made from it. All diagrams have been drawn for a constant horizontal reaction. Fig. 4.4.3.a shows two parallel walls without bottom having a uniform lateral pressure distribution. For simplicity sake the wall friction was assumed to be equal to the internal soil friction. As an example eight arches are shown. Each arch is supporting 1/8 of the total weight, true and complete arching is possible.

In Fig. 4.4.3.b the arches are deeper in the upper portion since each arch can support only 1/8 of the soil weight, the portion over and above this has to be transferred to the lower not yet fully loaded arches.

For the case where there is only one vertical wall, as for a sheet pile wall, the second wall necessary as reaction for the soil arch is provided by the rupture surface. For the Rankine case, Fig. 4.4.4.a there is no arching possible since the frictionless wall cannot support a vertical reaction, the failure surface on the other hand could supply a vertical reaction but there is no such thing as a cantilever arch for uncemented individual soil grains. The formation of a soil arch always occurs between the wall and the sliding surface which supply the two reactions necessary. This kind of reasoning agrees also with Terzaghi's definition of arching effect; the pressure is transferred from the yielding to the less yielding part. Fig. 4.4.4.b shows the parabolic lateral pressure distribution and the load transfer from the upper to the center arches. The radial lines indicate the transfer of the weight of soil to the lower arches. The horizontal reaction of all the soil arches is

$$H = \frac{qL^2}{8f} = \text{constant}$$

Since for concentric arches $\frac{L}{8f}$ is constant, Lq also has to be constant which means that the upper arches which have a large L, can support only a small q and have to transfer the remaining soil weight to the lower arches.

From these observations it is hardly justifiable to speak of vertical arching, because vertical arches would require more or less fixed supports in a horizontal plane and these are not present for a braced open cut.

Fig. 4.4.5 indicates how the soil arches would have to form to give the respective lateral pressure distribution. From Fig. 4.4.5 it can be deduced that for a small friction angle and small wall friction the centre of gravity of the area of the earth pressure distribution has to lie lower due to the small vertical reaction components at the wall on one side and the sliding surface on the other, yielding in higher pressures at the lower part of the wall. Further it has been shown (Lehmann 1942) that for higher vertical stresses, brought about by surcharge loading, the lateral earth pressure increased considerably at the upper portion of the wall, which is equivalent to a shift of the centre of gravity of the pressure area towards the top.

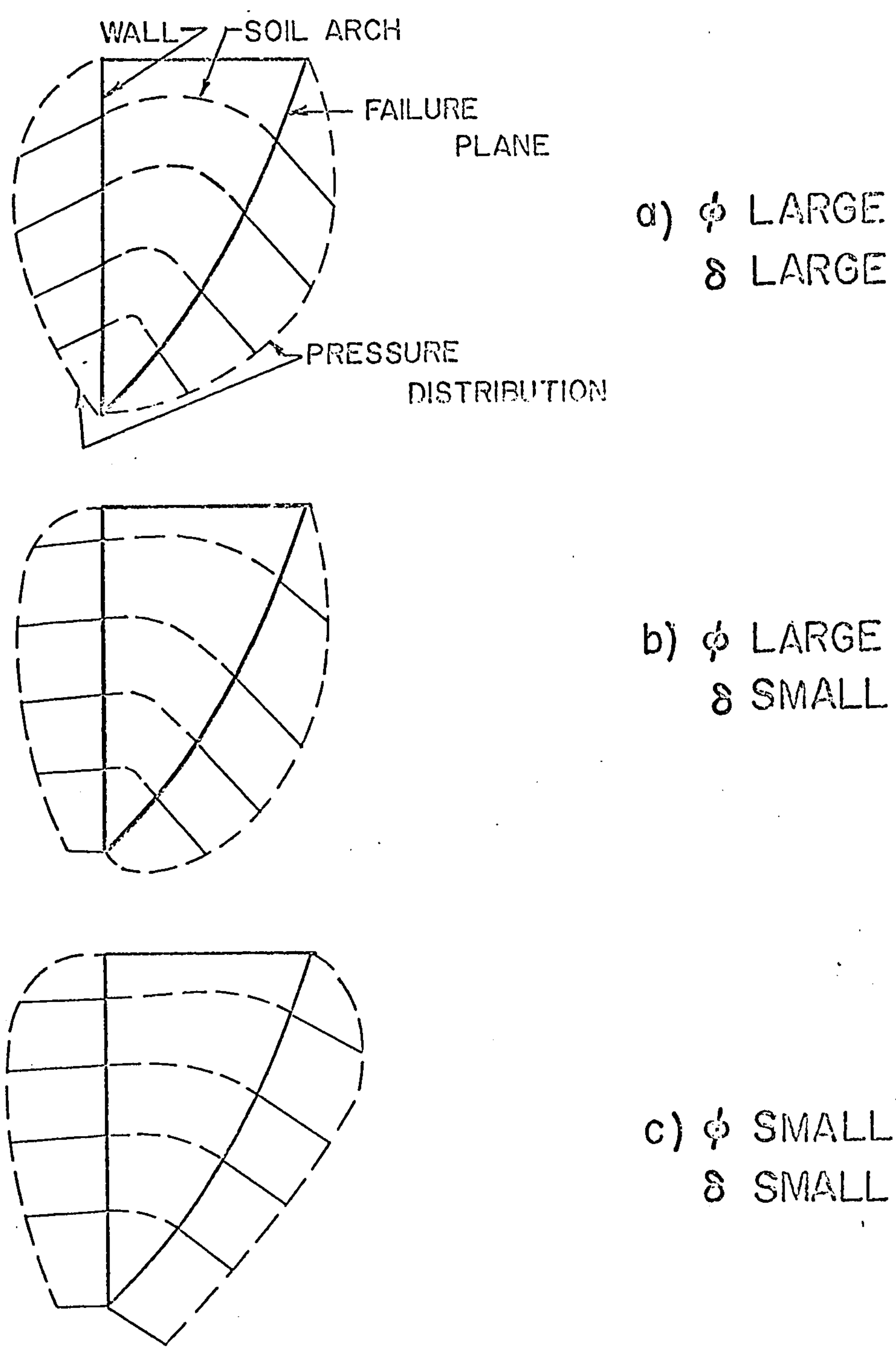

FIG. 4.4.5 POSSIBLE EARTH PRESSURE DISTRIBUTION

4.5 Hydrodynamic Considerations

4.5.1 Water Pressure

Water is one of the most important factors influencing earth pressures. The mechanism is complex; however, for most problems in Soil Mechanics it can be represented by the concept of effective stress. This concept can be considered adequate for earth pressure analyses.

There are many different causes of water pressure, among the most important are hydrostatic, changes in pore volume, capillary tension, and various molecular forces. Because the actual areas of soil grain contact with an engineering structure are extremely small, virtually the full water pressure is exerted on the structure. Since the effective weight of the soil is reduced by submergence, the pressure exerted by the soil grains is reduced proportionally. The total active pressure is greatly increased, 2.5 to 3 times the dry soil pressure for typical sands. In the case of passive pressure, the combined effect is usually a reduction in the total pressure. The effect on at-rest pressure of a cohesionless soil is an increase, similar to that for active, but not so pronounced.

The effect on the active earth pressure of a cohesionless soil is illustrated in Fig. 4.5.1. The water table is taken a distance H_1 below the ground surface and assuming no flow conditions the porewater pressure in the soil is the hydrostatic pressure. The earth pressure is

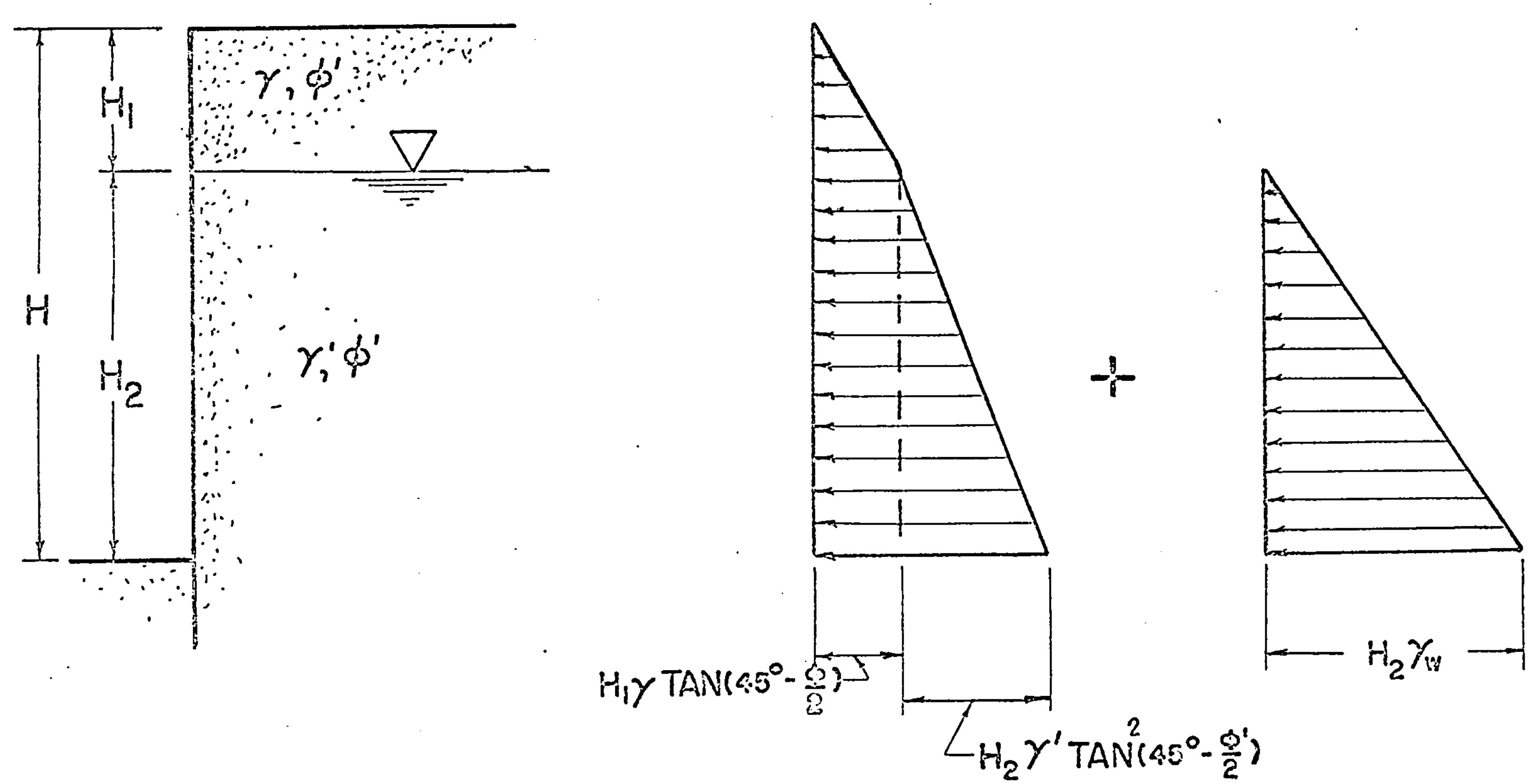

FIG. 4.5.1 EFFECTIVE STRESS IN EARTH PRESS. CALCULATIONS

calculated with the total unit weight γ above the water table and the submerged unit weight γ' below it. Since we are considering the effective stress, the shear strength parameter is ϕ'. The calculated earth pressure is that exerted by the solid particles on the wall. The total force on the wall consists of this earth pressure plus the hydrostatic pressure. The positive pore pressure produces a reduced effective stress and thus a reduced strength. The effect of the loss in strength is an increase in the active earth pressure. If the pore water pressure becomes negative, as induced by capillary tension, the shear strength is increased. The negative water pressure, -u when inserted in the effective stress equation

$$\sigma' = \sigma - u$$

becomes

$$\sigma' = \sigma - (-u) = \sigma + u$$

which means an increase in shear strength, regardless of whether the effect is expressed in effective or total stresses. Similarly, capillary tension produces an increase in modulus of elasticity. In such a state the active earth pressure is correspondingly reduced and the passive increased. This is a temporary condition and can be destroyed by either drying or saturation.

4.5.2 Seepage

An important consideration in the design of a braced open cut is the hydrodynamic analysis of the seepage conditions. The information obtained from such an analysis may often be put to very practical use, and the total cost of sheeting and bracing, which are temporary and incidental to the construction of permanent structures, may be materially reduced.

The basic principles of flow through soils and the flow net method of analysis represent so far the only approach which is satisfactory, from a scientific standpoint for the determination of the laws governing the nature of flow through soils. The analysis permits a prediction of the quantity, velocity, and direction of seepage flow, as well as of seepage pressures. Tests and experience have proved this to be a good guide.

The theory of seepage flow in porous media is based on a generalization of Darcy's law (1856). This law was derived from an experimental study of the rectilinear flow of water through sand filters and stated that the quantity of water flowing through a unit area of sand is proportional to the hydraulic gradient. Hence v is the average velocity of flow, we have

$$v = k\, i \quad (4.5.1)$$

where i denotes the hydraulic gradient and k is a factor of proportionality which is generally termed the coefficient of permeability.

When the excavation is open at the bottom, that is the sheet piles are not terminated in an impermeable layer, provisions have to be made to remove the quantity of water seeping into the excavation. The amount depends on the hydrostatic head, which is the difference of water levels on the inside and outside of the excavation and on the permeability of the soil. For a rough approximation Karafláth (1953) proposed the following equation

$$q = 2\ k\ H \left[\frac{1}{\pi} \quad \ln \left[\frac{B}{2D} \sqrt{\left(\frac{B}{2D}\right)^2 + 1} \right] \right] \qquad (4.5.2.)$$

where k = coefficent of permeability

H = hydrostatic head

B = half width of excavation

1 = distance from center of excavation to horizontal water table

D = depth of penetration of sheet pile below bottom of excavation

In order to compute the rate of flow of water through soils, it is necessary to determine the intensity and distribution of the pore-water pressures. These pressures can very conveninently be determined from a flow net, which represents the flow of water through an incompressible soil. Fig. 4.5.2.a shows such a graph in which the flow lines and

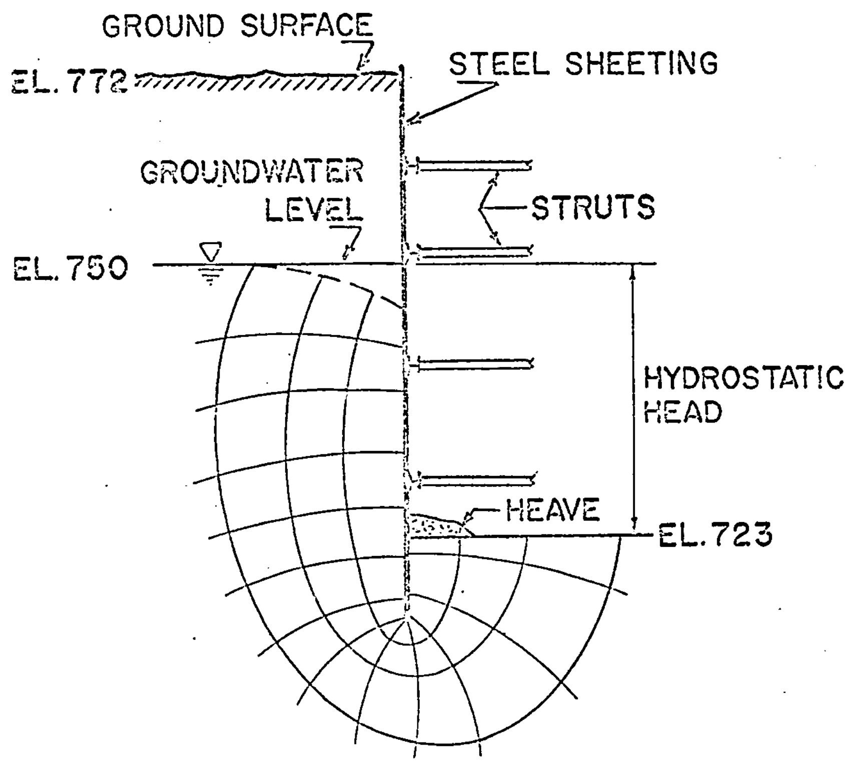

a) FLOW NET FOR STEEL SHEETING

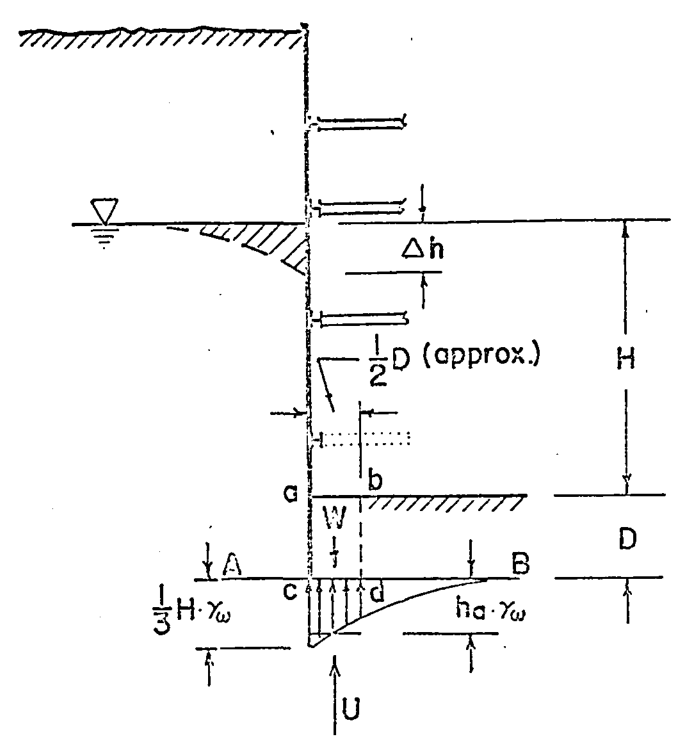

b) FORCES ACTING ON SAND ZONE abcd OF POTENTIAL HEAVE

FIG. 4.52 CALCULATION OF SEEPAGE FLOW AND FACTOR OF SAFETY AGAINST BOTTOM HEAVE equipotential lines run in a predominantly vertical and horizontal direction, respectively. Using this concept and Darcy's law the amount of flow per unit length of sheet pile wall is given by

$$q = \frac{N_f}{N_d} \; k \; H \tag{4.5.3.}$$

where N_f = number of flow channels

N_d = number of equipotential spaces.

Molnar (1957) determined by the electrical analogy method the flow pattern for a perfectly watertight sheet pile wall. The assumption with respect to watertightness corresponds to the actual behaviour of a well constructed prototype. The wall always yields somewhat towards the excavation and this movement will tighten the joints. The deposition of fine soil particles between the joints will further increase the watertightness of the steel sheeting.

Molnar (1957) proposed the following equation to approximate the quantity of water inflow per unit length of wall

$$q = \frac{2B \; k \; H}{h + 2D} \tag{4.5.4}$$

where B = half width of excavation

Of course the total quantity of water (Q) is obtained by multiplying the unit inflow by the perimeter of the excavation or

$$Q = 2\ q\ (L + 2B) \qquad (4.5.5)$$

in which L = length of excavation and

B = half width of excavation.

This quantity should be increased by some factor due to the increased inflow (bunching of flow lines) at the corners.

4.5.3 Piping and Bottom Heave

The excavation of a cofferdam is, if possible, done in the dry which means that the waterlevel inside the cofferdam has to be kept at or below the bottom of the excavation. As the excavation proceeds the inside waterlevel has to be kept lower and lower and the effective head of the seeping water is increased which increases the danger of formation of boils and heaves. It is necessary to calculate the factor of safety with respect to piping. This condition is shown in Fig. 4.5.2 which is a section through a single wall sheet pile cofferdam. As soon as there is a hydrostatic head developed water starts to flow downwards through the sand on the left side of the sheet piles and upwards on the right, Fig. 4.5.2.a. If D is the depth of sheet pile penetration below the excavation grade then it was found by model tests (Terzaghi - Peck 1967) that the rise of sand occurs within a distance of D/2 of the sheet pile. The zone of danger is confined to the prism abcd. Considering the forces acting on a horizontal section through the tip of the sheet piles such as AB, Fig. 4.5.2.b, at the instant of failure the effective or intergranular stress becomes equal to zero on or above section cd. The soil grains do not offer any resistance to the water flowing upwards and the sand rises with the water as one mixture and at the same time the effective lateral stress at the sides of the prism is approximately equal to zero. The sand within the prism has lost all its supporting capacity for objects having a greater unit weight than the soil water mixture. To determine the pore water pressures at section AB it is necessary to plot a flow net, Fig. 4.5.2.a. It should be noted that for this particular case one-third of the loss of head occured within the cofferdam. The average excess hydrostatic pressure on the base of the prism cd is γ_w ha. From the condition of equilibrium at this section we have the total excess hydrostatic force acting upwards, which is

$$U = \frac{1}{2} D \quad \gamma_w \, h_a$$

and the submerged or buyant weight of the prism of sand acting downward.

$$w' = \frac{1}{2} \; D^2 \; \gamma'$$

Therefore the factor of safety with respect to piping is given by

$$F = \frac{W'}{U} = \frac{D\,\gamma'}{h_a\,\gamma_w} \qquad (4.5.6)$$

The flow path of the water can be increased by increasing the depth of penetration of the sheet pile, which results in a smaller hydraulic gradient and a lower flow velocity.

The penetration depth necessary to guaranty an adequate factor of safety against boiling was also given by Ordujanz (1954). Bottom heave in the excavation is imminent when the submerged unit weight of the soil is equal to the flow pressure directed vertically upwards. From Fig. 4.5.2.b the hydraulic gradient is

$$i = \frac{H}{H + 2D}$$

To consider a factor of safety, F, with respect to bottom heave the equation will be

$$\frac{\gamma'}{F} = i\,\gamma_w = \frac{H}{H + 2H}\,\gamma_w$$

from which

$$\frac{\gamma'}{F}\,H \quad \frac{2D\,\gamma'}{F} = H\,\gamma_w$$

or

$$D = \frac{H}{2}\left(\frac{F\ \gamma_w}{\gamma'} - 1\right) \qquad (4.5.7)$$

A factor of safety of 1.5 to 2.0 is usually considered to be adequate for this type of structure.

From the English Civil Engineering Code Practice No. 4, pp. 93, the following minimum values for the sheet pile penetration depth were given:

For an open cut

$B > H, \quad Dmin. = 0.4H$

$B = H, \quad Dmin. = 0.5H$

$B = 0.5H, \quad Dmin. = 0.7H$

As can be seen the penetration depth, D, does not only increase with an increase of hydrostatic head but also increases with a decrease of cut width. Similar experimental observations were also made by Bazant (1963).

Marsland (1953) undertook extensive model studies and concluded that for excavations in dense homogeneous sands, failure occurs when the exit gradient equals the critical gradient of flotation, i_c, and also that for loose homogeneous sands, failure occurs when the pressure difference between the pile tip and the excavation base is sufficient to lift the column of submerged sand adjacent to the inside of the sheeting. He suggested also values of the penetration required for various factors of safety for narrow excavations in loose and dense sand as given in Fig. 4.5.3. In all cases the water levels were taken to be at the corresponding sand levels, inside and outside the excavation.

McNammee (1949) summarized the work done at the Building Research Station and presented his conclusions in form of graphs. He concluded that it is difficult to determine by a priori considerations of whether boiling or heaving is more likely to occur in any particular problem. There are, however, some guiding principles. In homogeneous sands it seems likely that boiling will be the criterion of safety against seepage pressures when the excavation is very wide and that heaving is more likely to occur in narrow excavations. Fig. 4.5.4 gives the penetration depth required for excavations of different width for factors of safety ranging from 1.0 to 2.5.

A valuable nomograph was developed by Mandel (1951). He considered the equilibrium at the instant of failure at a point directly below the tip of the sheet pile. He found the following relationship between the forces p_1 and p_2 (Fig. 4.5.5):

$$p_1 \quad G = V_B \ (p_2 + G)$$

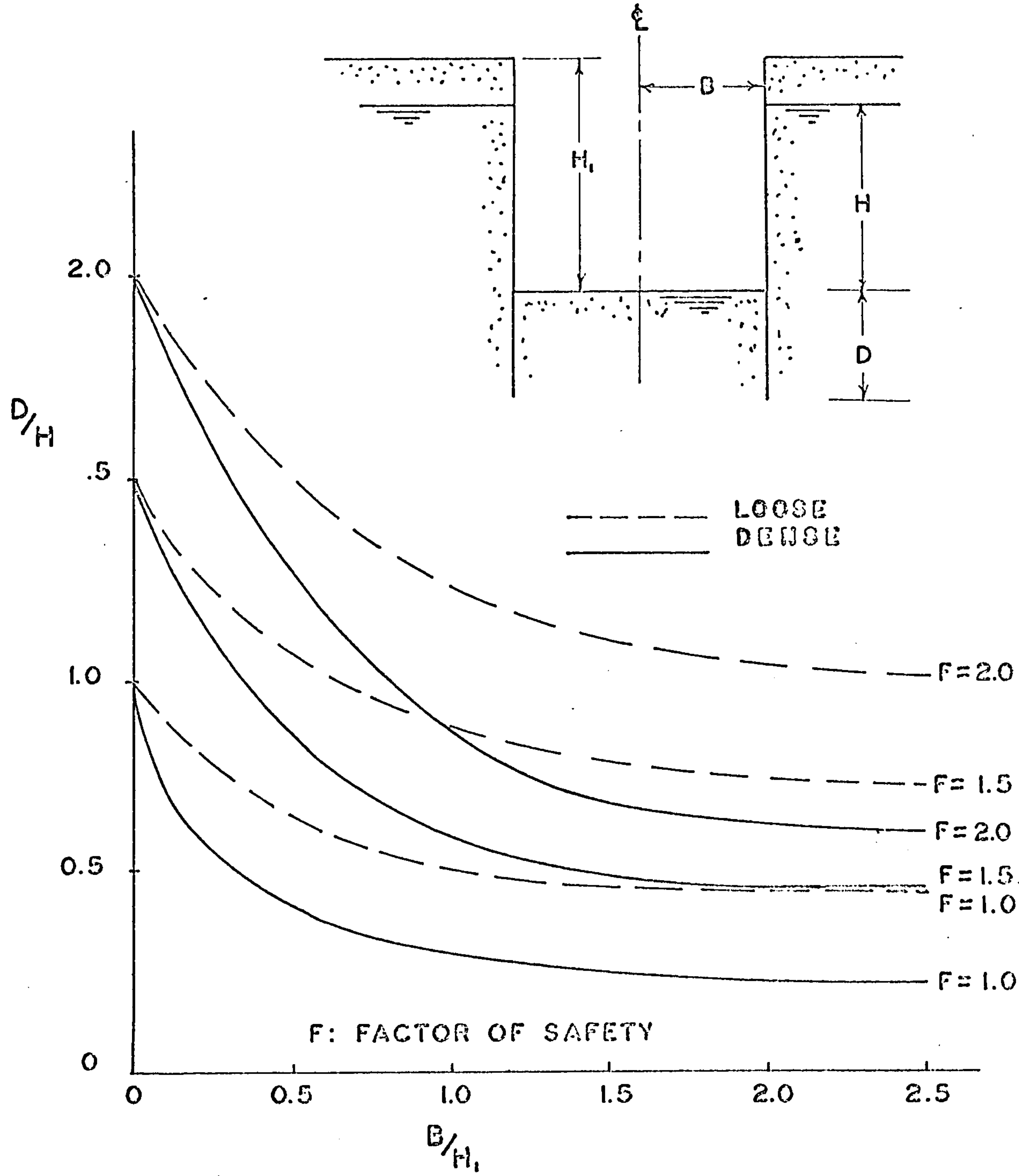

FIG. 4.5.3 PENETRATION REQUIRED FOR EXCAVATIONS IN HOMOGENEOUS SANDS OF INFINITE DEPTH (AFTER MARSLAND 1953)

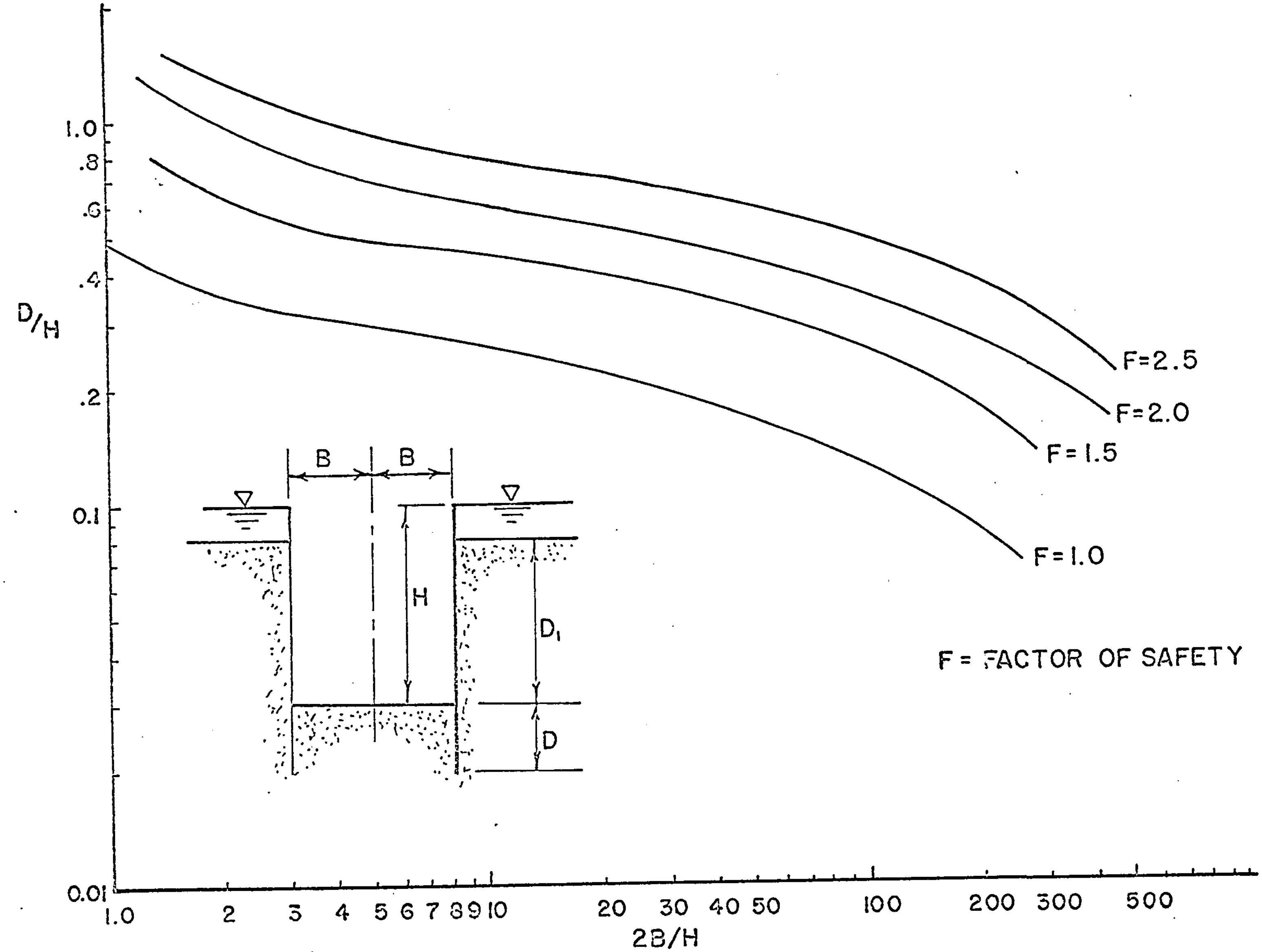

FIG. 4.5.4 PENETRATION REQUIRED FOR EXCAVATIONS OF DIFFERENT WIDTH (AFTER McNAMEE 1949)

in which

$$G = C \cdot \text{ctg}\ \phi$$

and

$$V_B = e^{\pi \tan \phi} \cdot \tan^2 (45 - \frac{\phi}{2})$$

and further

$$P_1 = P + \gamma_w \gamma D - \gamma_w (D + iH)$$

$$= P + \gamma_w (\gamma' D - iH)$$

from which he derived the necessary penetration depth

$$D = \frac{D}{\gamma_w \gamma'} \left[\frac{P}{V_b - 1} - G \right] + \frac{i}{\gamma'} H \tag{4.5.9}$$

For a sheeted excavation

$$P = \gamma_w \left[\gamma (H - H_1) + \gamma' H \right]$$

Using the above equations as a basis Mandel obtained a graphical solution in form of a nomograph as shown in Fig. 4.5.5, in which

$$\left.\begin{aligned} Z_1 &= \frac{1}{(\gamma - 1)H} \left[\frac{P}{V_b - 1} - C \text{ ctg } \phi \right] \\ Z_2 &= \frac{1}{\gamma - 1} \quad , \quad \gamma = (\gamma_s - 1)(1 - n) + 1 \\ Z_3 &= T/H \\ Z_4 &= D/H \end{aligned}\right] \tag{4.5.10}$$

from which is obtained.

At the London site the conditions were as shown in Fig. 4.5.2. The ground surface was at an elevation of 772 ft. and the grade of the excavation at elevation 722.9 ft. The hydrostatic head averaged 27 ft. and the sheet pile penetration depth was 9 ft. with the pile tip elevation at 714.0 ft. At several times during construction local boils occurred. Therefore it is of paramount interest to analyse this case using the different methods and procedures outlined above firstly with respect to a factor of safety against a hydraulic failure and secondly to check the required sheet pile penetration depth for different factors of safety.

(DIMENSIONS IN METRIC TONS AND METERS)

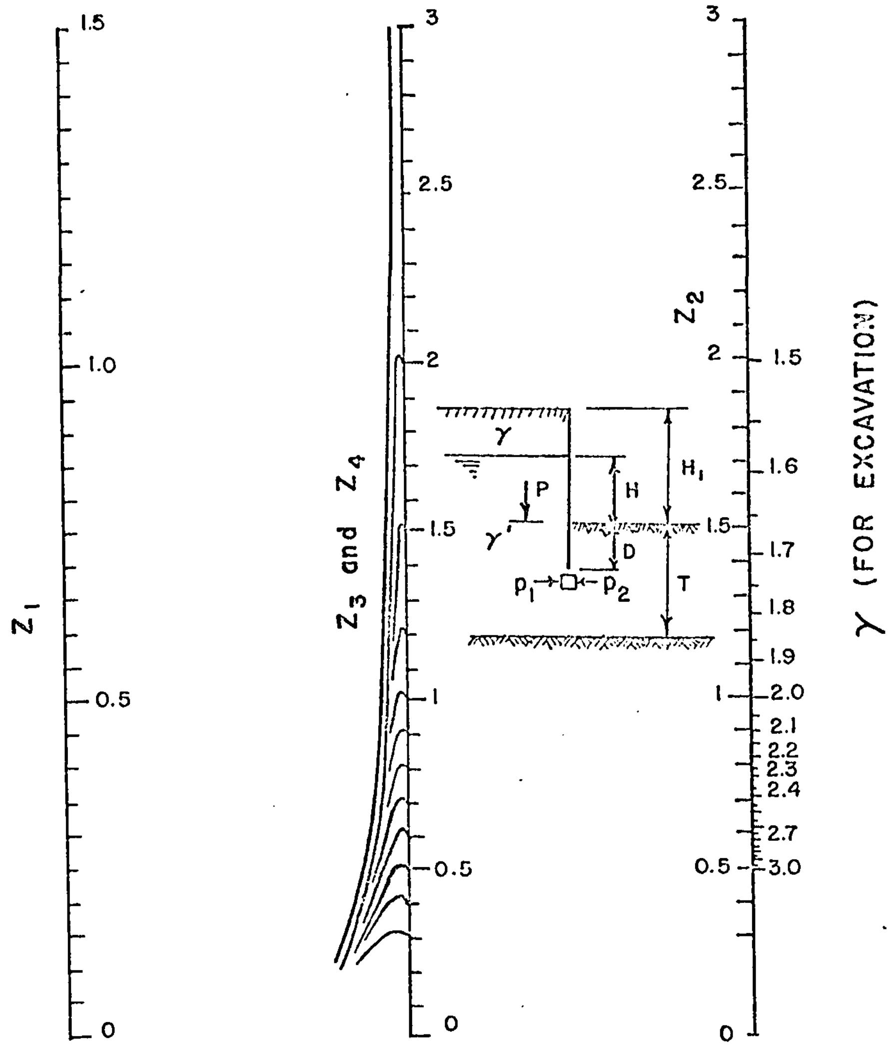

$$Z_1 = \frac{1}{(\gamma - 1)H}\left[\frac{P}{V_b - 1} - c\cot\phi\right] \qquad Z_2 = \frac{1}{\gamma - 1} \qquad Z_3 = \frac{T}{H} \qquad Z_4 = \frac{D}{H}$$

FIG. 4.5.5 NOMOGRAPH FOR DETERMINING THE PENETRATION DEPTH D (after Mandel 1951)

From Terzaghi's Eq. 4.5.6 the factor of safety with respect to piping is for $D = 9$ ft., $\gamma' \cong \gamma_w$ and $h_a = 1/3H$, where $H = 27$ ft.,

$$F = \frac{D\ \gamma'}{h_a\ \gamma_w} = \frac{9(1)}{1/3\ (27)} = 1$$

which indicates that piping is imminent. Assuming a factor of safety of 1.5 the required sheet pile penetration depth would be

$$D = \frac{F\ h_a\ \gamma_w}{\gamma_w} = \frac{1.5\ (27)\ (1)}{3} = 13.5 \text{ ft}$$

Ordujanz' solution yields

$$(\frac{\gamma_w}{\gamma'})\ F = 2\ \frac{D}{H} + 1 \quad \text{and} \quad F = 2\ \frac{9}{27}\ (1) + 1 = 1.67$$

which seems unrealistically high considering that local boiling did occur in the excavation. The required penetration depth for $F = 1.5$ should then be

$$D = \ (\frac{\gamma_w}{\gamma'})\ F - 1 \quad \frac{H}{2} = \ (1)\ 1.5 - 1 \quad \frac{27}{2} = 6.75 \text{ ft}$$

It seems that the solution proposed by Ordujanz is unsafe as applied to the test site conditions.

From Marsland's proposal, Fig. 5.4.3 we obtain for $D/H = 1/3$ and $B/H_1 = \frac{42}{50} = 0.84$, $F = 1$ indicating boiling is occurring. For $F = 1.5$ the required penetration should be

$$D = 0.65\ H = 0.65\ (27) = 17.5 \text{ ft}$$

McNamee's graph, shown in Fig. 4.5.4 yields for $D/H = 1/3$ and $2B/H = \frac{84}{27} = 3.1$ a factor of safety $F = 1$. Or considering $F = 1.5$ the penetration depth should be

$$D = 0.55\ H = 0.55\ H = 14.9 \text{ ft.}$$

In order to use Mandel's nomograph Fig. 4.5.5, all dimensions and soil parameters have to be converted into metric units

$$H = 8.2 \text{ m}$$

$$\gamma = 2.08 \text{ t/m}^3$$

$$P = 1.0 \left[2.08 \ (3.94) + 1.0 \ (8.2)\right] = 16.4 \text{ t/m}^3$$

$$V_b = e^{\pi \tan 52^o} \tan^2 (45 + 52/2) = 303$$

$$Z_1 = \frac{1}{(2.08 - 1) \ 8.2} \left[\frac{16.4}{303 - 1} - 0\right] = 0.006$$

$$Z_2 = \frac{1}{2.08 - 1} = 0.93$$

$$Z_3 > 3$$

The value of Z_4 is obtained from the nomograph as 0.48 and the penetration depth is

$$D = Z_4 \times H = 0.48 \times 8.2 = 3.94 \text{ meters}$$

or

$$D = 13 \text{ feet}$$

Unfortunately Mandel does not specify the factor of safety he has assumed for his graphical solution.

The English Civil Engineering Code will give $D_{min} = 0.5$ H or $D_{min} = 13.5$ feet.

Concluding it can be said that the methods discussed above yield consistent results, except for Ordujanz' method, and that the sheet pile penetration depth should have been approximately 15 feet to provide a factor of safety F = 1.5. The use of an adequate well point system would, of course, decrease this penetration depth.

CHAPTER 5

EXPERIMENTAL MEASUREMENTS AND RESULTS

5.1 Description of Excavation

5.1.1 General

During the period from December 1963 to July 1964 a systematic programme of measurements was undertaken at an open braced cut at the Greenway Pollution Control Centre in London, Ontario. It was considered of importance to determine the nature and magnitude of the forces and of the movements of the soil mass associated with the excavation, and to obtain definite information concerning the safety of the bracing of the temporary structure. Furthermore, it was desirable to obtain quantitative data which could be used as the basis for economical design of bracing systems for future excavations in similar soil.

The roughly L-shaped excavation measured 68 by 42 feet for the longest leg, the other leg was 30 by 23 feet. A plan of the location of the site is shown in Fig. 5.1.1.

Continuous sheet piling was driven around the perimeter of the excavation and consisted of 225 interlocking U-shaped Larssen III_N steel piles from 41 to 55 feet long as well as horizontal wales and struts. The maximum depth of excavation was approximately 50 feet below the ground surface elevation of 772. The three main strut levels A, B, and C were at elevations 753.0, 741.0, and 729.0 feet, respectively. Additional sloped braces were installed at elevations 762.0 and 772.0 feet.

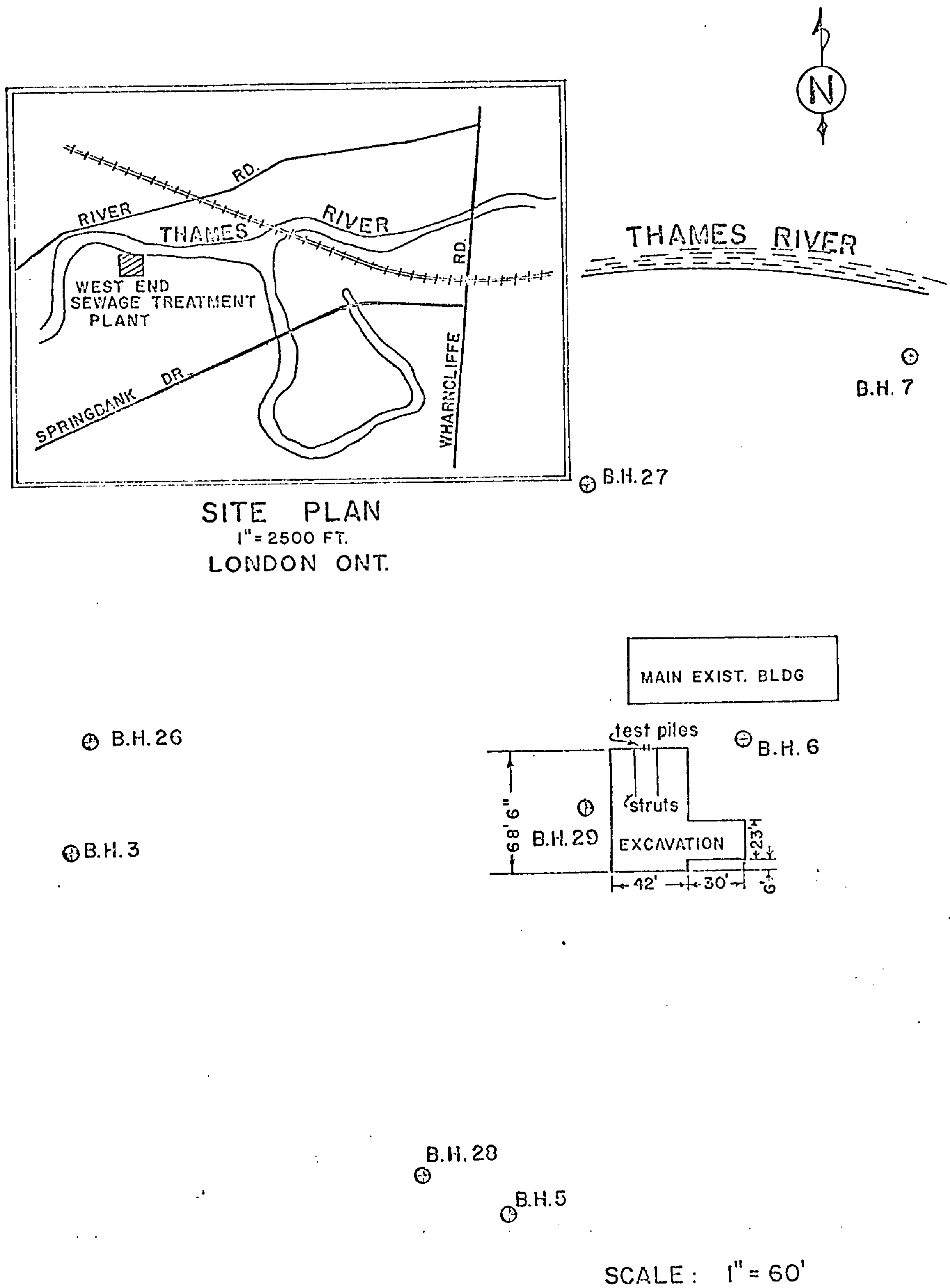

FIG. 5.1.1 LOCATION OF BOREHOLES

5.1.2 Geology

The area of the site lies within an ancient glacial spillway which underlies the western part of the surrounding territory of the city of London. These spillways were built either by a broad tongue of ice advancing through the lowlands of Lakes Ontario and Erie or by an ice sheet advancing from the north to meet this ice tongue and pushing forward as a lobe from the basin of Lake Huron (Chapman and Putnam 1966). North of Lake Ontario the bulky Oak Ridge moraine stands at the meeting point of the two conflicting movements of ice, while west of the Niagara escarpment interlobate deposits are found in several places around London. These are sandy moraines with drainage channels running through them lengthwise.

The highest glacial lake (Lake Maumee) of the Erie and Huron basins emptied westwards into the Mississippi. During the early life of this lake the Huron and Erie ice lobes contacted each other just west of London. The finer sediments give way to stream gravels along either branch of the Thames River. Irregularities in the deposits, due to the glaciofluvial origin are not uncommon. Soil fractions of all sizes may be present, but the clay content is usually not significant. The underlying bedrock is of sedimentary origin from the Devonian Age, mainly limestone. It was encountered in one borehole at a depth of 97 feet (elevation 675). Presumably the bedrock is flat lying, its surface generally being almost horizontal in this region.

5.1.3 Soil Condition

The subsoil within the depth of the excavation consisted almost exclusively of uniform fine to medium sand. The grain size analyses curves of seven samples are shown in Fig. 5.1.2. The locations where the samples were taken are shown in Table 5.1. The location of the boreholes are indicated in Fig. 5.1.1 and the borehole logs are given in Fig. 5.1.3. The holes were wash bored and lined with BX casing. Standard penetration test samples were taken. The N values from the penetration resistance are also shown on the borehole logs in Fig. 5.1.3. Below the watertable which was located approximately at elevation 753 feet (15 to 20 feet below the ground surface) the N values were generally greater than 100 or very close to it, which classified the soil as very dense. Field densities were obtained during excavation at seven locations. The greatest dry unit weight was 125.3 pcf at an elevation of 753.0 feet. Table 5.1 lists the field densities and the locations from where the samples were taken. Above an elevation of approximately 740 feet the sand had an average dry density of 103 pcf whereas below this elevation the dry density averaged 123 pcf for the same type of soil.

5.1.4 Water Table

The ground water level at different locations before the start of construction of the excavation are indicated on the borehole logs

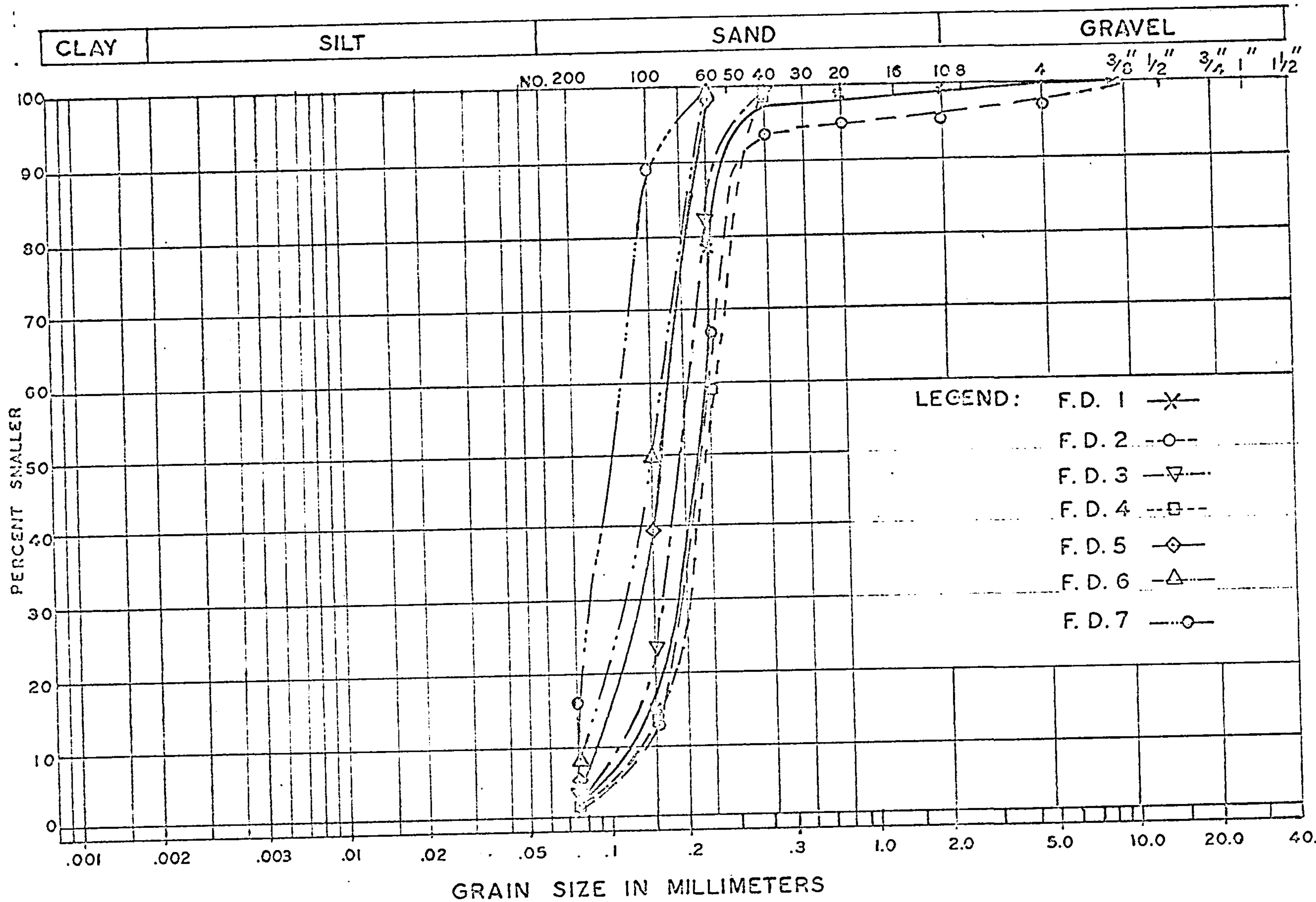

FIG. 5.1.2 GRAIN SIZE DISTRIBUTION CURVES

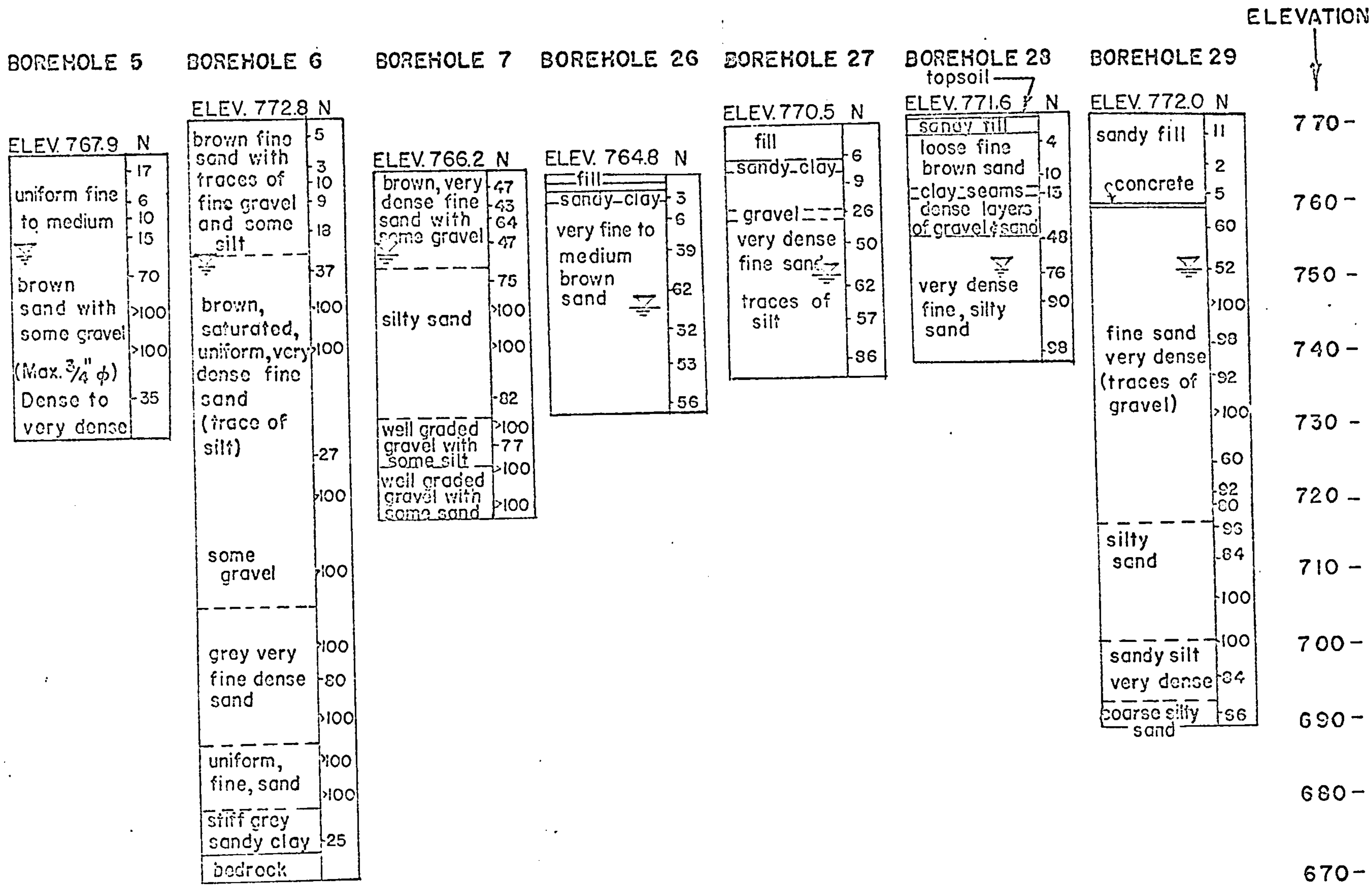

FIG. 5.1.3 BOREHOLE LOGS

Sample No.	Location	Elevation Feet	Spec. Grav.	Dry Density, pcf Field	Max.	Min.	Rel. Dens. D_r %
F.D. 1	6' south of pile No. 19	747.0	2.69	99.8	125.2	88.0	41.2
F.D. 2	6' south of pile No. 11	747.0	2.70	105.3	127.1	86.4	56.0
F.D. 3	7' south of pile No. 14	743.0	2.71	103.0	126.4	87.3	49.4
F.D. 4	13' south of pile No. 18	735.0	2.69	124.5	126.1	90.0	96.4
F.D. 5	4' north of south wall at pile No. 7	735.0	2.71	125.3	125.8	85.5	99.5
F.D. 6	7' south of pile No. 7	728.5	2.71	122.4	125.3	87.1	95.0
F.D. 7	18' south of pile No. 18	728.0	2.70	122.2	122.2	89.0	100

Table 5.1 Location and Densities of Soil Samples

in Fig. 5.1.3. Boreholes 3 to 7 were made in September 1960. The water table was at an approximate elevation of 753 feet. Boreholes 25 to 29 were made in October and November 1961 and the average water level in these holes was at 750 feet. The first water level measurements were taken several days after completion of the borehole to allow the water table to reach static equilibrium.

Borehole No. 6 which was located just north of the excavation and the three piezomaters installed on sheet pile No. 13 were taken as indicative of the ground water table in the soil just north of the north wall.

The change of water levels during the excavation period is shown in the corresponding figures of Section 5.2.

5.1.5 Instrumentation

5.1.5.1 General

Uncertainties concerning the behaviour of soils during and after construction are usually taken into consideration by using conservative design procedures or construction methods that increase the cost of the work while not necessarily assuring anticipated safe performance. In some cases, this type of job can be more realistically approached by installing measuring instruments, observing closely the behaviour of the structure, and altering the construction procedures if the results of the measurements indicate that this might be necessary. The experience thus gained, which is recorded in the form of measurement data, can also frequently be of value for future design problems. Although the purpose of this instrumentation was to obtain field data concerning the magnitude and the distribution of earth and water pressures as well as information on the deformation behaviour of a strutted excavation in sand as a research project, the strut load measurements were used during construction to estimate the safety of the bracing system.

In order to conveniently refer to structural members the sheet piles of the north wall were numbered consecutively from west to east as indicated in Fig. 5.1.4. The north wall was chosen for instrumentation because it was the deepest part of the excavation (approx. 50 feet deep) and the ground surface was level.

5.1.5.2 Struts

The bracing system of the north wall is shown in Fig. 5.1.4. The three main strut levels A, B, and C were at elevations 753.0, 741.0, and 729.0 feet, respectively. Auxiliary inclined braces (rakes) were installed at elevations 762.0 and 772.0 feet and were braced against the east and west walls for support.

A ten foot deep excavation inside the periphery of the structure was made before the Larssen III_N piles were driven. Additional H-piles with wooden laggings

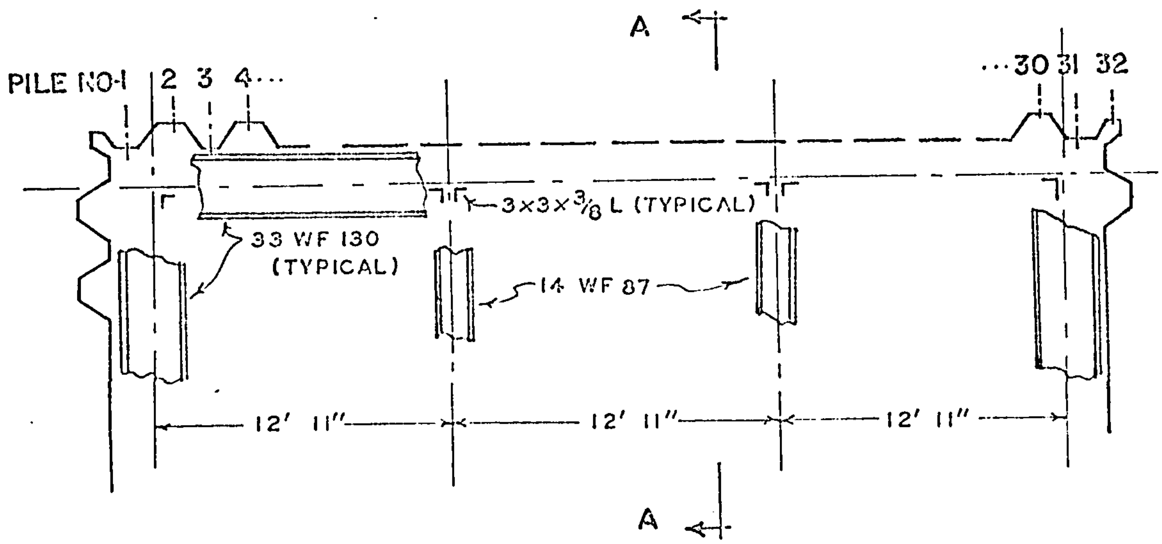

PLAN

STRUTS AT ELEVATIONS 762.0', 753.0', 741.0' AND 729.0' WERE EQUIPPED WITH STRAIN GAUGES FOR LOAD MEASUREMENT.

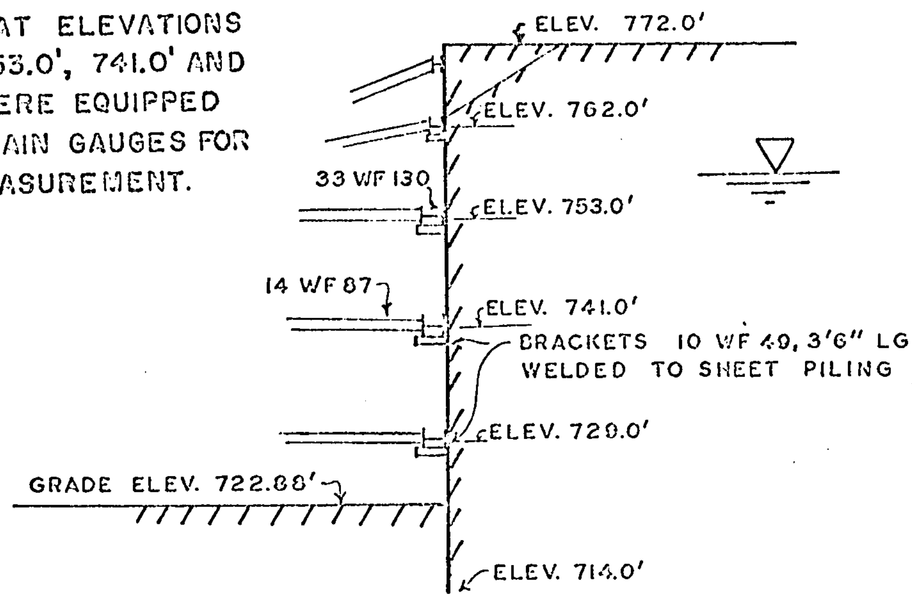

SECTION A-A

FIG. 5.1.4 BRACING SYSTEM FOR NORTH WALL were welded to the top of the first piles to bring the north sheet pile wall up to the original ground surface at elevation 772.0. The excavation outside the north wall then was backfilled with loose sand. The inclined top strut at elevation 772 had the purpose to hold the backfill in place and carried practically no load.

The struts of the main levels were 14 WF 87 and were welded to the wales. The 33 WF 130 wales were supported by 3.5 feet long 10 WF 49 brackets welded to the sheet piles. To ensure a tight contact between the troughs of the piles and the wales, wooden wedges were driven between them.

The loads in the struts of the north wall (Fig. 5.1.4) were determined by measuring the strains in the struts with a Whitmore dial gauge. All the struts, except the top inclined braces at elevation 772, which were practically load free, were instrumented with strain gauge points. The forces in the instrumented struts were measured by measuring the strains over an eight inch gauge length. The strain gauge points were mounted five feet from the welded connections to keep away from concentrated stresses at the connection. A dummy gauge welded to the strut was used for reference and temperature correction. The strains were measured on either side of the neutral axis of the strut and the average strain was multiplied by the product of the cross-sectional area of the strut and the modulus of elasticity of the steel in order to obtain the load. One division on the

Whitmore dial gauge corresponded to a strain reading of $1.25\ (10)^{-5}$ in/in for an eight inch gauge length. For the 14 WF 87 strut this corresponded to an axial load of 9.2 kips for a modulus of elasticity of 29,000 ksi.

For the inclined struts at elevation 762 feet the total force was measured. Knowing the angle of inclination the horizontal or lateral force component was computed. The gauge points were protected from corrosion and damage by grease and by a plywood cover. With these precautions only one set of gauge points was lost. These were replaced taking as zero reading the previous load measurement.

5.1.5.3 Water Levels

Three water pressure gauges were mounted on sheet pile No. 13. These gauges consisted of plastic tubing with an open end and were attached to the pile during the excavation. The ground water level was also determined from borehole and stand pipe observations. The location of the piezometers are shown in Fig. 5.2.40 (page 198). Pressures were measured by observing the height of water level in the plastic tubes or in the case of the boreholes by determining the water level by means of an electric probe.

5.1.5.4 Sheet Pile Movements

Sheet pile movements were measured directly from a baseline which was located south of the north wall. To measure the movement of the top of the piles, reference points were marked at the top of piles 2, 4, 6... to 32 as indicated in Fig. 5.1.4. The deflections of piles 13 and 15 in the vertical plane were measured directly by establishing reference points on these piles at approximately 3 foot vertical intervals. The distances between these points and a plumb line suspended in the vertical plane of the baseline were measured by means of a scale. These measurements could only be taken down to the bottom of the excavation. The order of accuracy of these direct measurements was 0.1 in.

The subsidence of the soil behind the north wall could not be measured because the soil surface was disturbed during construction and because of the location of the adjacent administration building.

5.1.5.5 Pressure Cells

The earth pressure transducers used were of the vibrating-wire type and were developed by the Norwegian Geotechnical Institute for the Oslo Subway Construction in the late 1950's.

The gauges with prefixes "G" were cells on loan from the Division of Building Research of the National Research Council and the "W" gauges were identical except they were manufactured in the machine shop of the University of Waterloo. The cells had a relatively stiff membrane at the back of which the vibrating wire was affixed. The membrane was sealed into the housing by an O-ring. The electric cables were brought up to the ground surface inside a tubing protected by a steel angle welded to the sheet pile and terminated in a switchbox. The tubing was necessary to allow atmospheric pressure inside the cells.

A description of the mechanical and electrical details of the cells is given in Appendix A. This appendix also gives an evaluation of the performance and reliability of this transducer.

A total of thirteen cells were installed at various elevations on sheet piles No. 14 and No. 15. The cells, leads, and steel angles were attached to the two test piles at the machine shop of McMaster University under the direction of Professor N.E. Wilson before the piles were brought to the site. Fig. 5.1.5 shows the location of the cells on these two test piles. Due to the particular U-shape of the pile sections, the cells on pile No. 14 were mounted on the recessed face or trough of the section, whereas the cells on pile No. 15 were mounted on the front face. It was suspected that the pressure transducers mounted in the trough of pile No. 14 would register low and those located at the front face of pile No. 15 would register high due to arching effect occurring across the trough. In order to obtain the average earth pressure, therefore, two adjacent piles were chosen for instrumentation. One cell, G-7, on pile No. 14 was located below the bottom of the excavation with the membrane facing to the inside to measure the passive earth pressure. All gauges

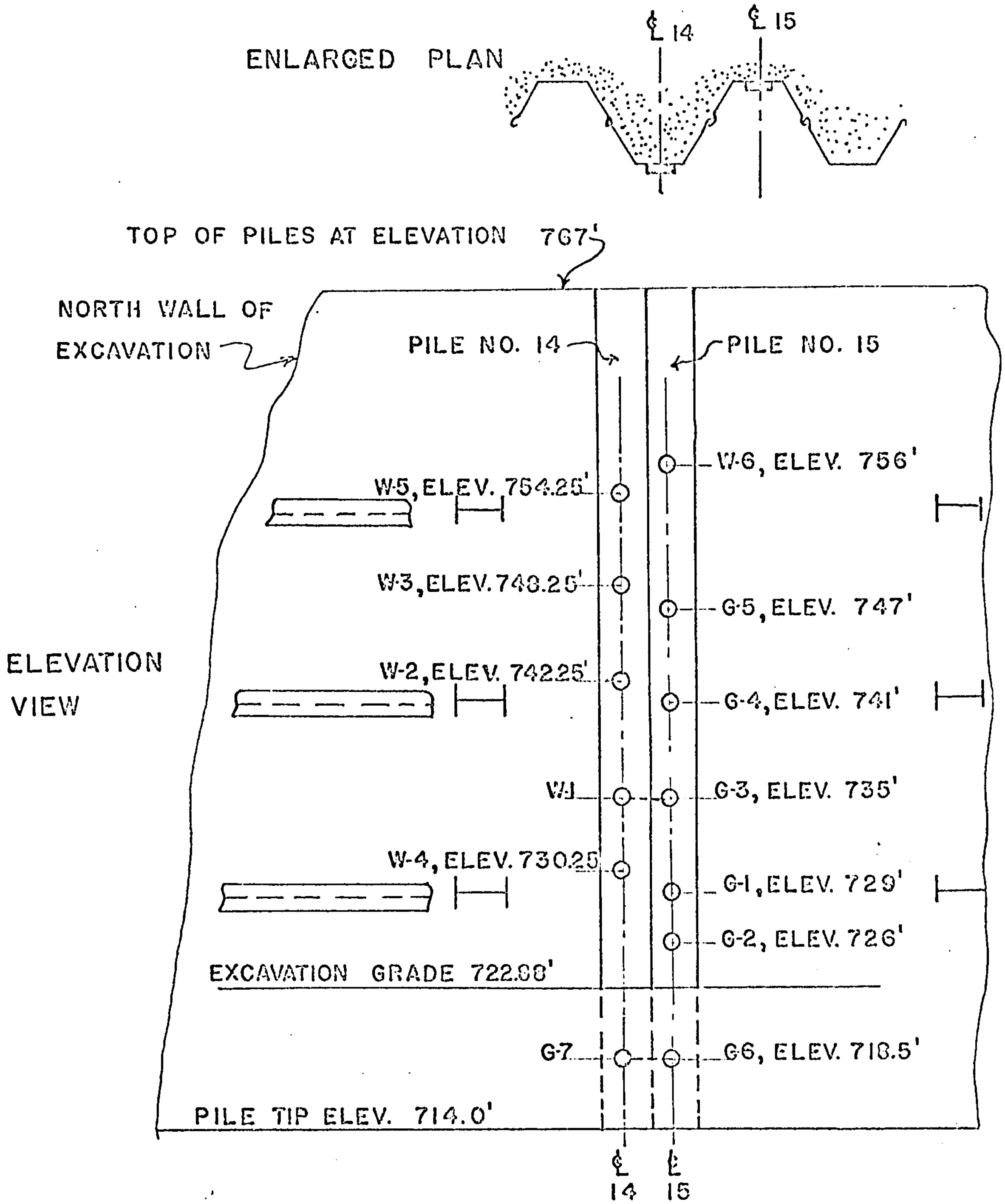

FIG. 5.1.5 LOCATION OF EARTH PRESSURE CELLS ON PILES NO. 14 AND NO. 15

were calibrated in the laboratory and zero readings were taken before and during pile driving as long as they were above the ground surface.

5.1.6 Construction Procedures

The simplest form of an open cut is that of an excavation with surrounding sloped banks in a stable condition and provided with an adequate drainage system consisting of pumps, sumps, and drainage ditches, or a system composed of well points. Where there is room for the slopes, this is the most economical solution, but where the excavation has to be made in built-up areas the engineer has to resort to a vertical sheeting and bracing system or to a combination of both.

At the London site interlocking sheet piles were employed because of the proximity of adjacent structures and the high ground water level. Construction started in January 1964 and the reinforced concrete slab at elevation 722.9 feet was poured in July 1964. The intermediate excavation stages along a vertical section through the north wall at the centre bay are shown in Fig. 5.1.6. The excavation level close to the north wall and the time of installation of the bracing members are indicated in Fig. 5.2.2 to Fig. 5.2.16 inclusively. The original ground elevation at the north wall was at elevation 772 feet. The area inside the excavation boundaries was excavated to a general elevation of 762 feet, then a two foot deep trench was excavated around the perimeter of the whole excavation.

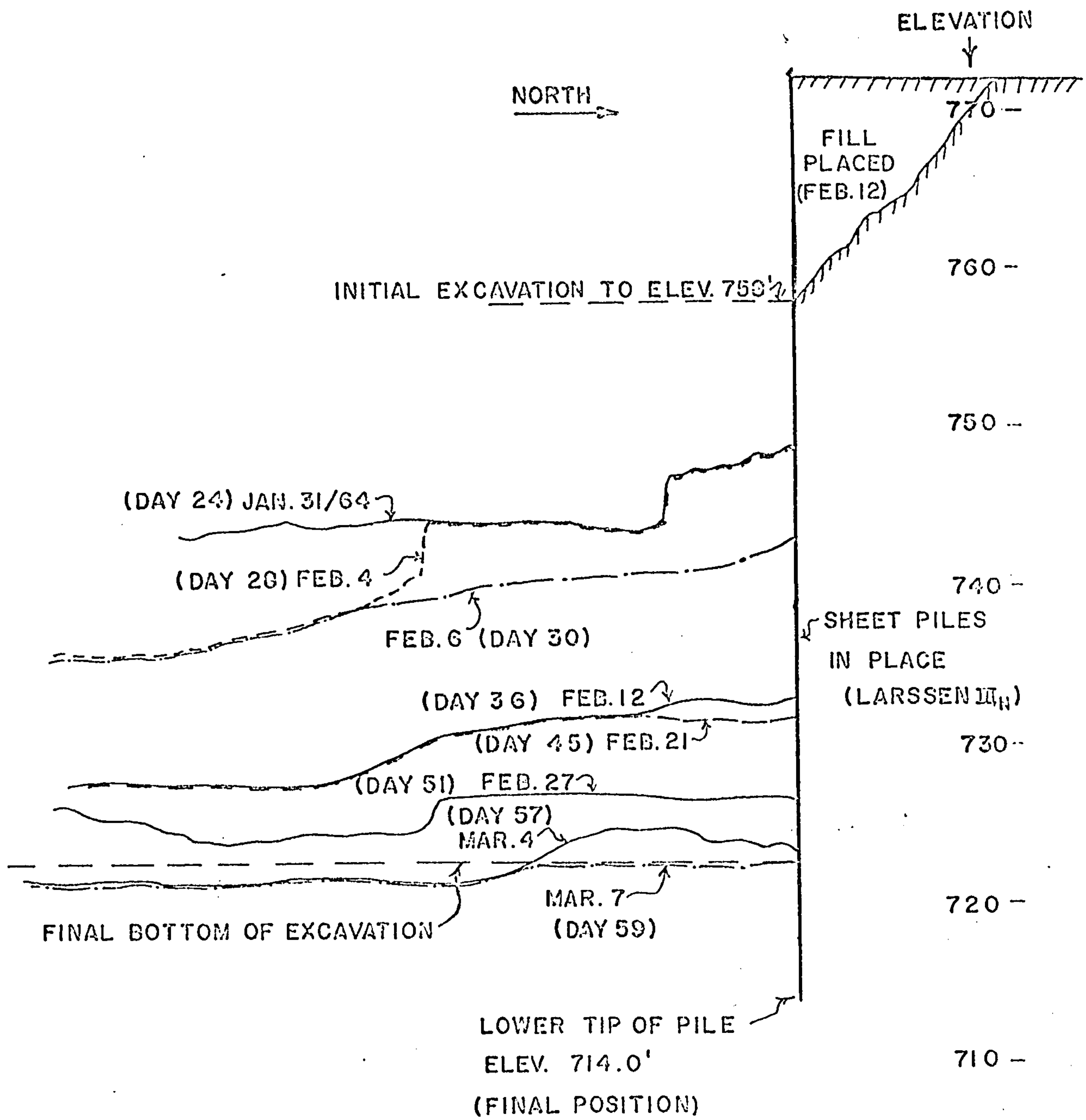

SECTION THROUGH CENTRE BAY OF NORTH WALL

FIG. 5.1.6 PROGRESS OF EXCAVATION

For convenience in referring to particular times, the days have been numbered consecutively starting with zero on January 6th, when the pile driving operation at the north wall began. Thus day 1 is January 7th, day 2 is January 8th, and so forth.

The Larssen III_N sheet piles were positioned in place at the bottom of the trench and driven down approximately four to five feet and then the driver was moved to the next pile. This procedure was followed around the excavation in order to prevent opening of the joints and buckling of the free standing section of the pile. To hold the piles in vertical alignment a steel template was used. The first ten feet were driven with a Delmag D-12 diesel hammer and then a 5.5 ton vibratory driver Model Foster Vibro, having a maximum frequency of 1,000 cycles per minute, was used to drive the piles to grade. The tip elevation of the piles when fully driven was at elevation 714.0 feet. When the resistance to driving became too severe, a 2-inch pipe with a 1-inch nozzle was pushed down the piles just ahead of the pile tip and the soil was loosened by a jet of water.

Excavation to a level slightly below the A-level at elevation 753.0 feet was accomplished with a clam shell before wales and struts were installed. The soil of the whole excavation was removed by clam shell with the trimming close to the sheet pile wall being done by hand shovels. When the excavation reached a strut level, steel brackets 3.5 feet long were welded at 13 feet centres to the piling and the wale was placed on top of them. It was then welded to the wales along the adjacent sides of the excavation to form a continuous section. The struts were welded to the wales. None of the braces were prestressed.

On day 37 (Feb. 13) as the excavation level at the north wall reached elevation 733 feet with the B - level struts at elevation 741 feet already in place, the large iron water main running north of the north wall broke. This was probably due to the deformation of the wall causing the sand to exert excessive bending stresses in the pipe. The break in the water main caused the water level directly behind the sheeting to rise to an elevation of 759 feet, as was indicated by the newly installed standpipe at pile No. 13. Subsequently boiling occurred in the excavation opposite piles 10 and 12 of the north wall. It was found that pile No. 10 had a broken weld at elevation 726 where the two sections of this pile had been joined. The sections were now separated allowing the water to pipe into the excavation. This soil disturbance did not affect the cell readings on the two test piles. It took several days to repair the damage.

On day 45 (Feb. 21) well points at 3 foot centres were installed just inside the sheet pile wall. Up to this day the water level in the excavation was controlled by pumping from sump pits. The newly installed well point system did not prove to be adequate. Fine sand plugged up the filters and the discharge from the pumps was comparatively small. Localised boiling could be observed in the lowest parts of the excavation.

On March 5th (day 58) the excavation had reached elevation 724 feet when the south-west corner failed by piping. The inrushing water filled the excavation to an elevation of 730 feet. The concrete aeration tank adjacent to the west wall of the cut cracked and settled, probably due to removal of sand from under the tank. Two days later the damage was repaired and the water level inside the excavation was drawn down by a combination of well points and sump pumps in order to complete the excavation. The final trimming to grade (elevation 722.9 feet) was done by hand equipment and was completed by March 7th (day 59).

The well point system at this time was still not functioning adequately. The water level within the excavation was therefore kept at elevation 730 feet to reduce the hydraulic head while an attempt was made to improve the well point system by placing a filter around the well points. The improved system was still not satisfactory because localized boiling could be observed at the bottom of the excavation as the water table was drawn down again. The excavation was flooded again and the water level was kept at elevation 730 feet and no further work took place up to approximately April 15th (day 99).

After April 15th the excavation was flooded to the outside water level at elevation 748.5 feet. The old well point system was removed and a new system was installed. In June the new system was completed and functioned well. The water level was drawn down below the bottom of the excavation and construction operations resumed. In July the concrete mat was poured onto the floor of the cut. Before the concrete walls were poured, using the sheeting as back form, the earth pressure cells above the bottom of the excavation were removed from sheet piles No. 14 and No. 15. They were taken back to the laboratory for recalibration.

5.2 Results of Field Measurements

5.2.1 General

The measurements at the London site represent the first known efforts to measure earth pressures directly on the sheet piles of a braced cut in sand. At the same time the strut loads were measured and used to deduce the pressure distribution on the back of the wall to permit an internal check on the lateral earth pressure distribution obtained from the cell readings. Therefore it is of prime importance to establish the reliability of the measurement techniques and instruments used. Considerable time and effort has been spent in evaluating all factors affecting the obtained readings. This was especially true for the earth pressure cell readings as discussed in Appendix A. The water pressures have been claculated from flow nets based on standpipe observations at different locations outside and inside of the excavation as well as directly on the sheet piles. The results have been represented in a graphical form to indicate the general trend of measurements on a time base and also to allow one to become familiar with the construction sequence and its effects upon the behaviour of the excavation.

5.2.2 Earth Pressures

The results of the thirteen earth pressure cells mounted at different elevations on sheet piles No. 14 and No. 15 are tabulated in Table 5.2.1 (a) and (b). Observations over a period of 175 days are shown with respect to construction progress. The pressure cells recorded total pressures with the effective stresses being obtained by subtracting the water pressure on the cell. The results are depicted graphically in Figs. 5.2.1 to 5.2.16 inclusively. These vertical sections, plotted for different days, show the lateral effective earth pressure distribution, the water pressure behind the wall, the extent of excavation as well as the progress of strut installation. The methods used to interpret the cell readings and the factors affecting these and their accuracy limits are discussed in Appendix A.

5.2.3 Strut Loads

The strut loads were calculated from strain measurements in the struts. It was assumed that each strut carried the total pressure contributed from an area of one half of the bay's width to each side of the strut and the distance halfway to the next adjacent strut level. From this an apparent pressure distribution diagram was derived after subtracting the total water force from the strut load. The strut forces are shown in Figs. 5.2.17 to 5.2.38 and are the average loads from the

Day	Date 1964	Air Temp F^{o}	Earth Pressures - psi					
			W-5	W-3	W-2	W-1	W-4	G-7
1	Jan. 7	32	0	0	0	0	0	24.5
7	Jan. 14	20	0	0	0	0	0	23.7
8	Jan. 15	18	0	0	0	0	0	9.5
14	Jan. 21	39	0	0	0	1.2	11.1	9.6
21	Jan. 28	42	2.2	2.0	3.7	-	7.5	7.6
24	Jan. 31	35	3.8	1.0	3.6	-	5.2	7.6
28	Feb. 4	42	4.0	1.0	2.8	-	5.7	8.7
30	Feb. 6	37	3.6	-	2.2	-	5.8	8.5
36	Feb. 12	32	3.7	4.9	2.1	-	7.5	10.6
37	Feb. 13	35	2.6	7.1	7.5	-	3.7	9.5
45	Feb. 21	25	4.5	6.4	5.2	-	2.7	6.5
57	Mar. 4	47	9.0	-	7.5	-	-	3.2
60	Mar. 7	45	13.5	-	8.3	-	-	7.2
76	Mar. 23	43	9.0	8.9	9.2	-	-	1.0
86	Apr. 2	40	9.2	-	8.3	-	-	1.6
111	Apr. 27	54	8.8	-	5.6	-	-	2.5
168	June 23	94	8.1	1.2	3.8	-	2.4	5.9
175	June 30	95	3.9	4.9	5.0	-	0.3	9.4

NOTE: A "zero" reading indicates cell is above ground surface

TABLE 5.2.1(a)

EARTH PRESSURES ON SHEET PILE NO. 14 -

RESULTS OF MEASUREMENTS FROM EARTH PRESSURE CELLS

Day	Date 1964	Air Temp F°	Earth Pressures - psi						
			W-6	G-5	G-4	G-3	G-1	G-2	G-6
1	Jan. 7	32	0	0	0	0	0	3.4	5.0
7	Jan. 14	20	0	0	0	0	0	3.6	4.4
14	Jan. 21	39	0	0	0	1.4	5.0	8.9	10.1
17	Jan. 24	42	-	-	-	-	-	-	-
21	Jan. 28	20	3.0	2.6	3.3	9.0	13.8	11.7	15.6
24	Jan. 31	35	2.9	1.7	2.9	6.7	13.4	9.5	12.9
28	Feb. 4	42	3.0	1.9	3.3	6.5	12.5	9.4	13.3
30	Feb. 6	37	3.0	1.9	3.4	4.7	11.7	9.4	13.2
36	Feb. 12	32	3.7	5.8	5.2	5.7	5.5	5.3	14.9
37	Feb. 13	35	5.4	6.4	7.1	3.0	3.8	2.0	13.3
45	Feb. 21	25	3.2	6.3	4.5	2.7	4.4	1.5	11.0
50	Feb. 26	34	6.1	1.5	2.2	1.4	3.4	3.2	8.1
57	Mar. 4	47	7.7	1.0	3.4	2.1	4.6	1.7	8.8
60	Mar. 7	45	7.9	0.6	3.6	2.4	4.1	3.9	8.9
76	Mar. 23	43	7.1	1.1	4.6	4.7	5.1	3.4	5.6
86	Apr. 2	40	6.5	1.1	4.2	3.2	4.3	2.5	5.3
111	Apr. 27	54	5.0	1.2	2.7	3.2	5.8	3.3	6.0
168	June 23	94	5.4	1.1	3.1	7.1	11.5	8.3	10.0
175	June 30	95	5.4	1.5	3.3	2.3	10.9	7.7	9.4

TABLE 5.2.1(b)

EARTH PRESSURES ON SHEET PILE NO. 15 -

RESULTS OF MEASUREMENTS FROM EARTH PRESSURE CELLS

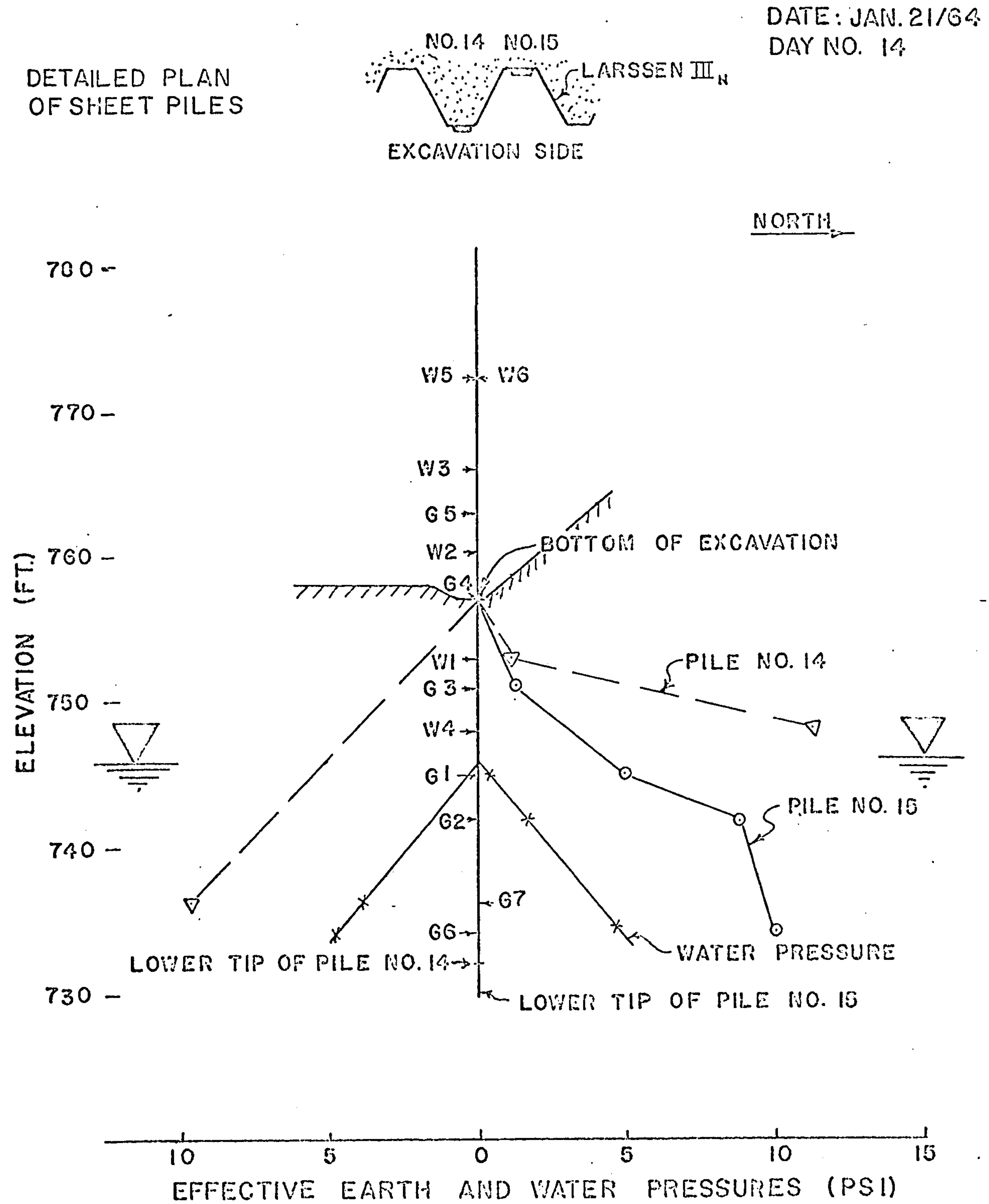

FIG. 5.2.1. EFFECTIVE EARTH PRESSURE DISTRIBUTION, SHEET PILE NO. 14 AND NO. 15

DATE: JAN. 28/64
DAY NO. 21

FIRST READING AFTER PILES FULLY DRIVEN

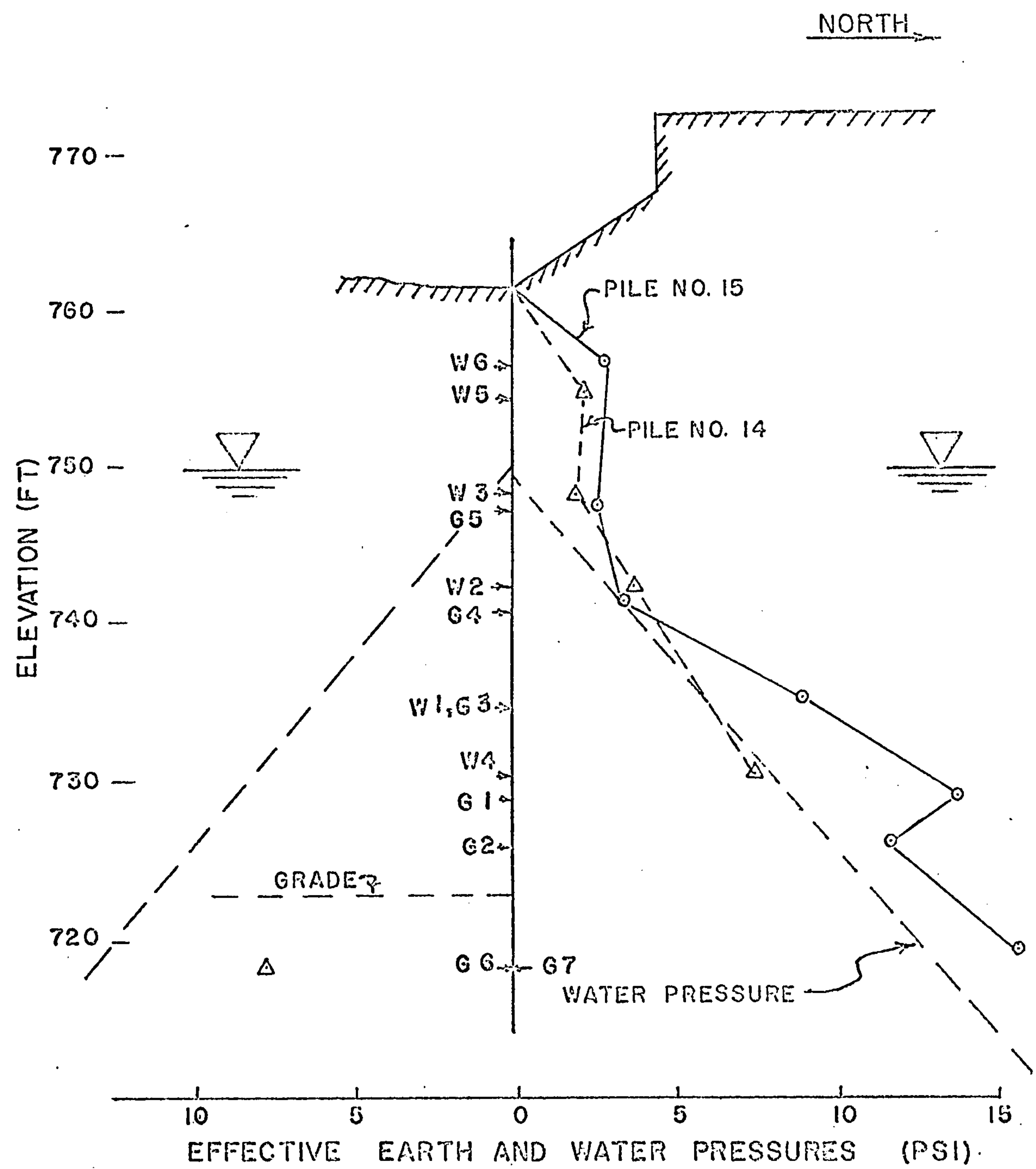

FIG. 5.2.2 EFFECTIVE EARTH PRESSURE DISTRIBUTION, SHEET PILE NO.14 AND NO. 15

DATE: JAN. 31/64

DAY NO. 24

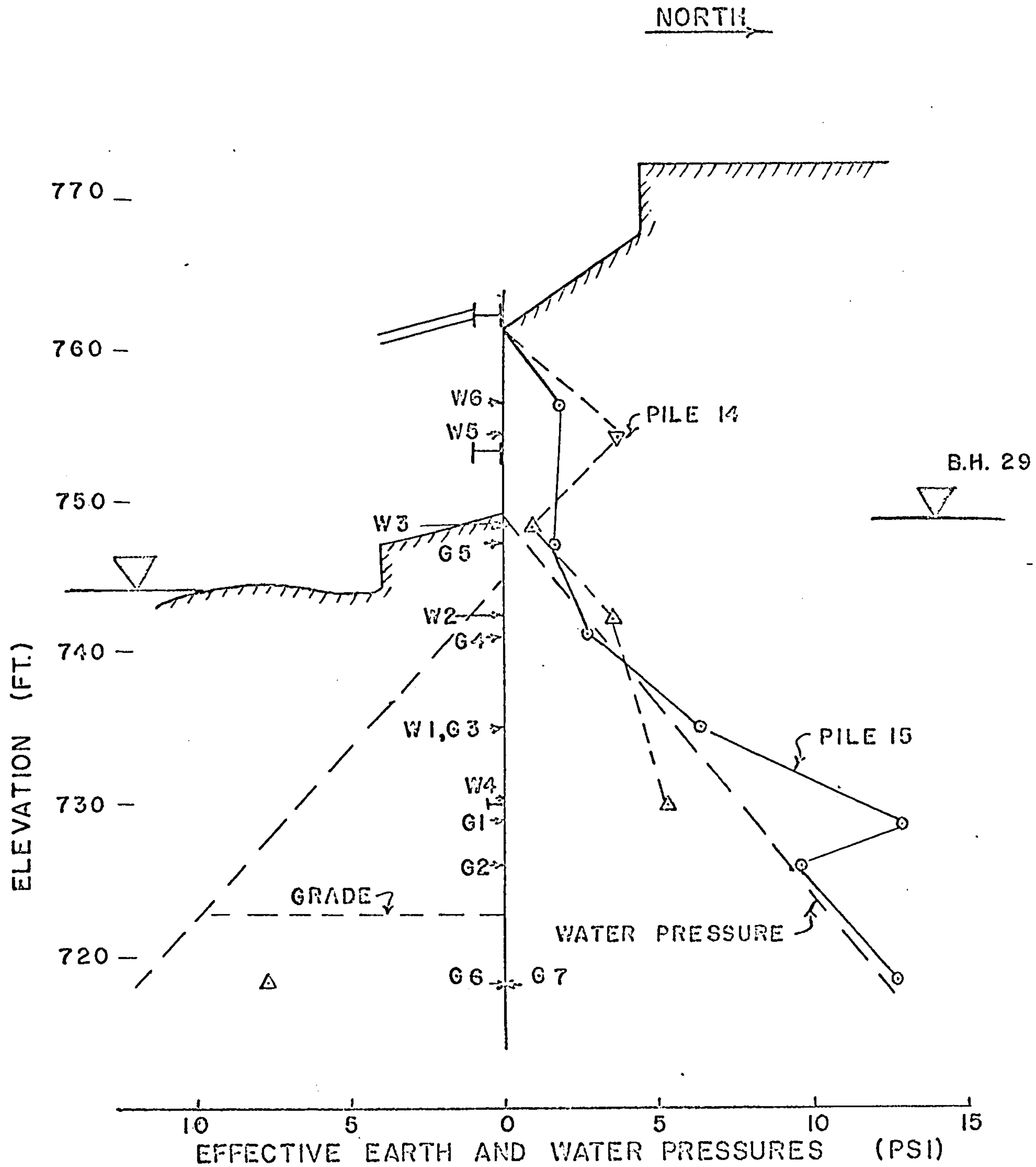

FIG. 5.2.3 EFFECTIVE EARTH PRESSURE DISTRIBUTION, SHEET PILE NO.14 AND NO.15

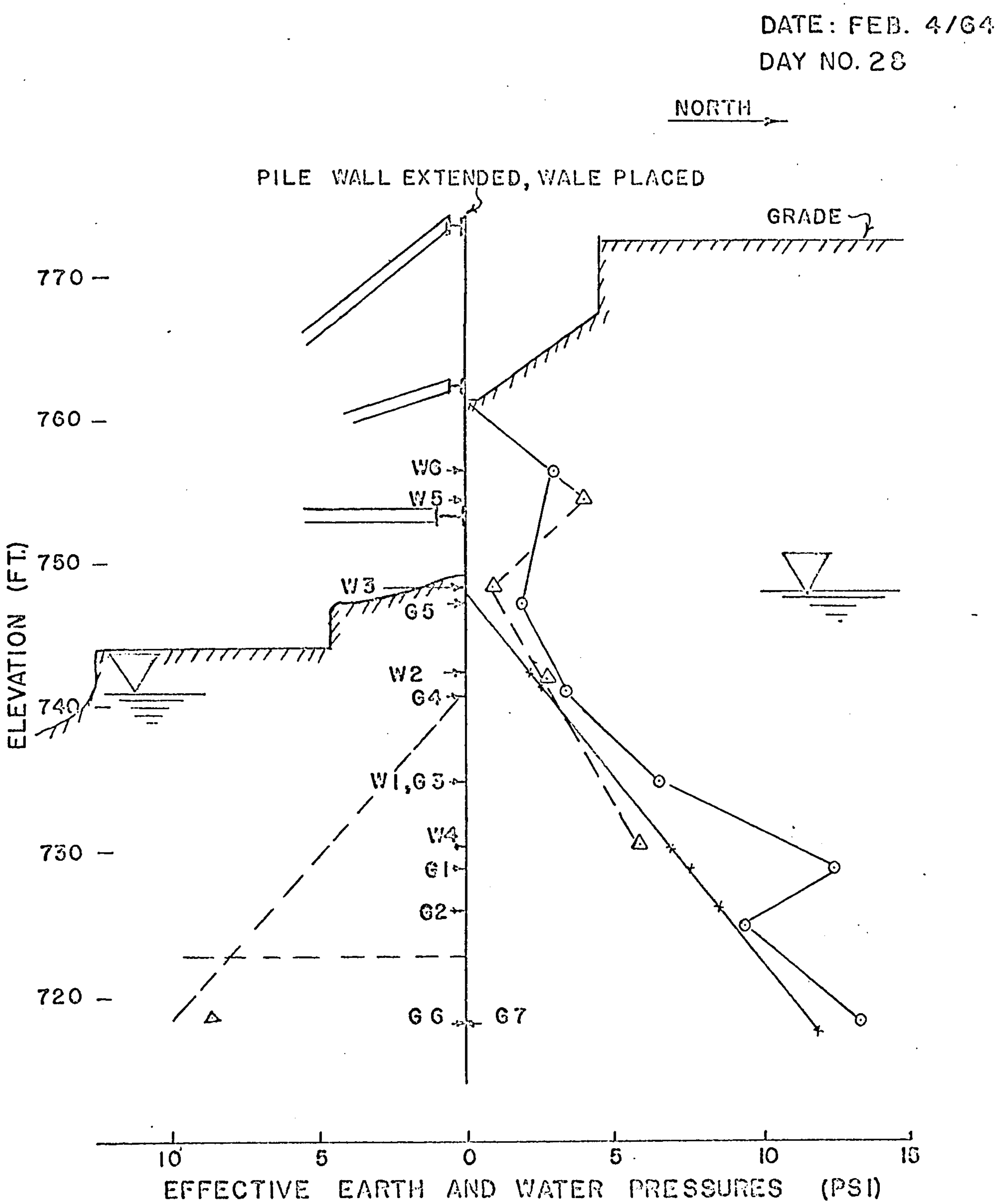

FIG. 5.2.4. EFFECTIVE EARTH PRESSURE DISTRIBUTION, SHEET PILE NO.14 AND NO.15

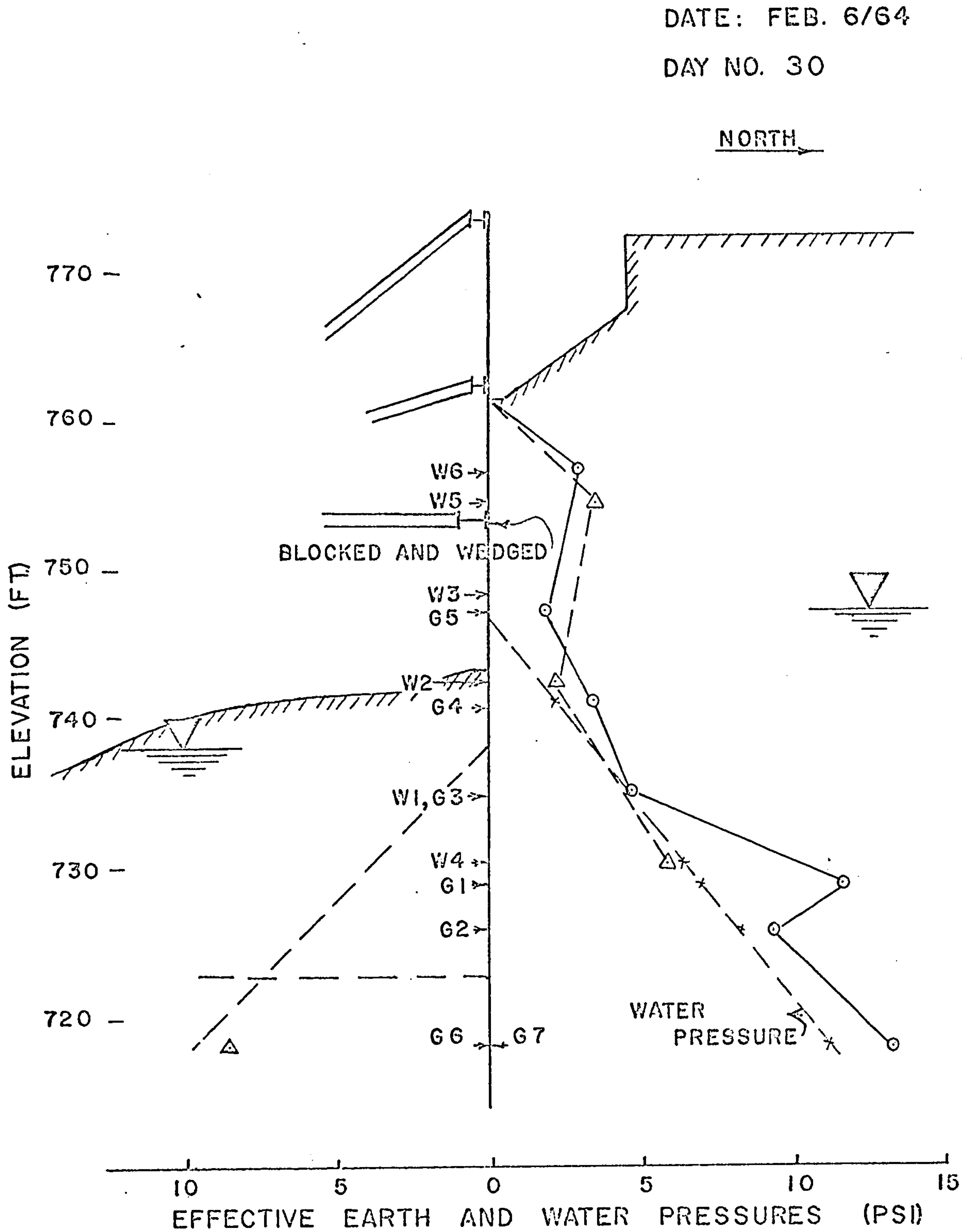

FIG. 5.2.5 EFFECTIVE EARTH PRESSURE DISTRIBUTION, SHEET PILE NO. 14 AND NO. 15

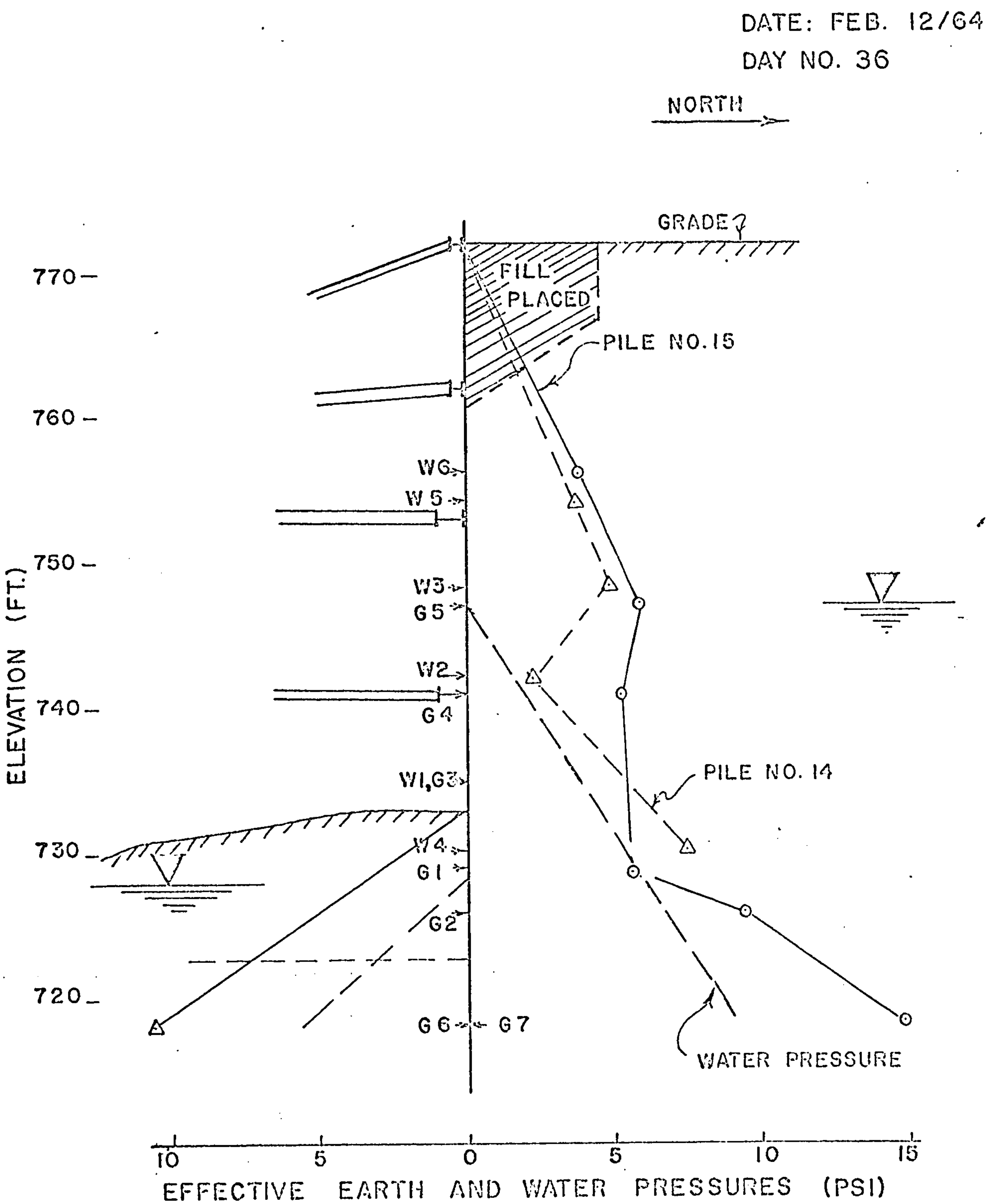

FIG. 5.2.6 EFFECTIVE EARTH PRESSURE DISTRIBUTION, SHEET PILE NO. 14 AND NO. 15

DATE: FEB. 13/64
DAY NO. 37

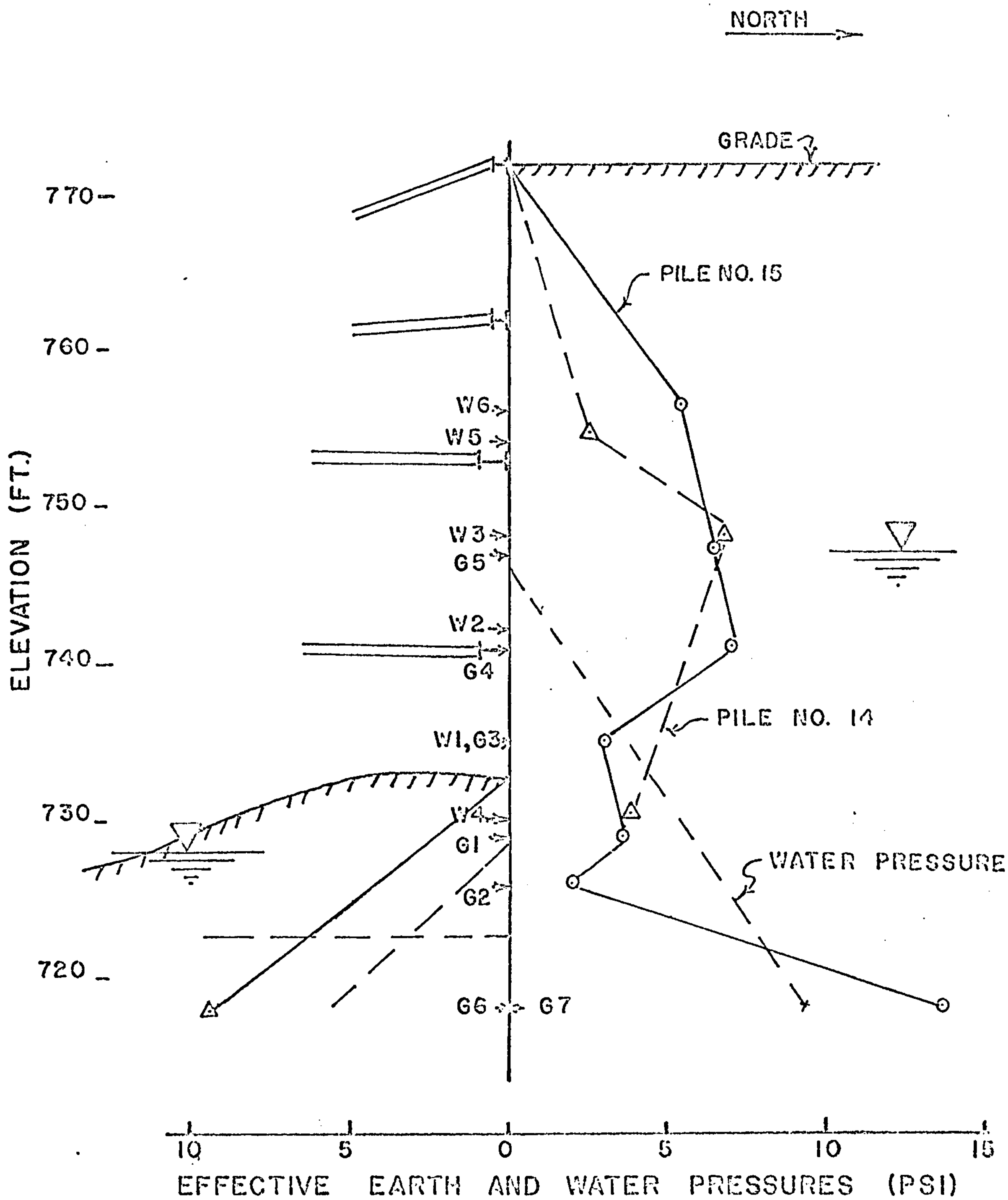

FIG. 5.2.7 EFFECTIVE EARTH PRESSURE DISTRIBUTION, SHEET PILE NO. 14 AND NO. 15

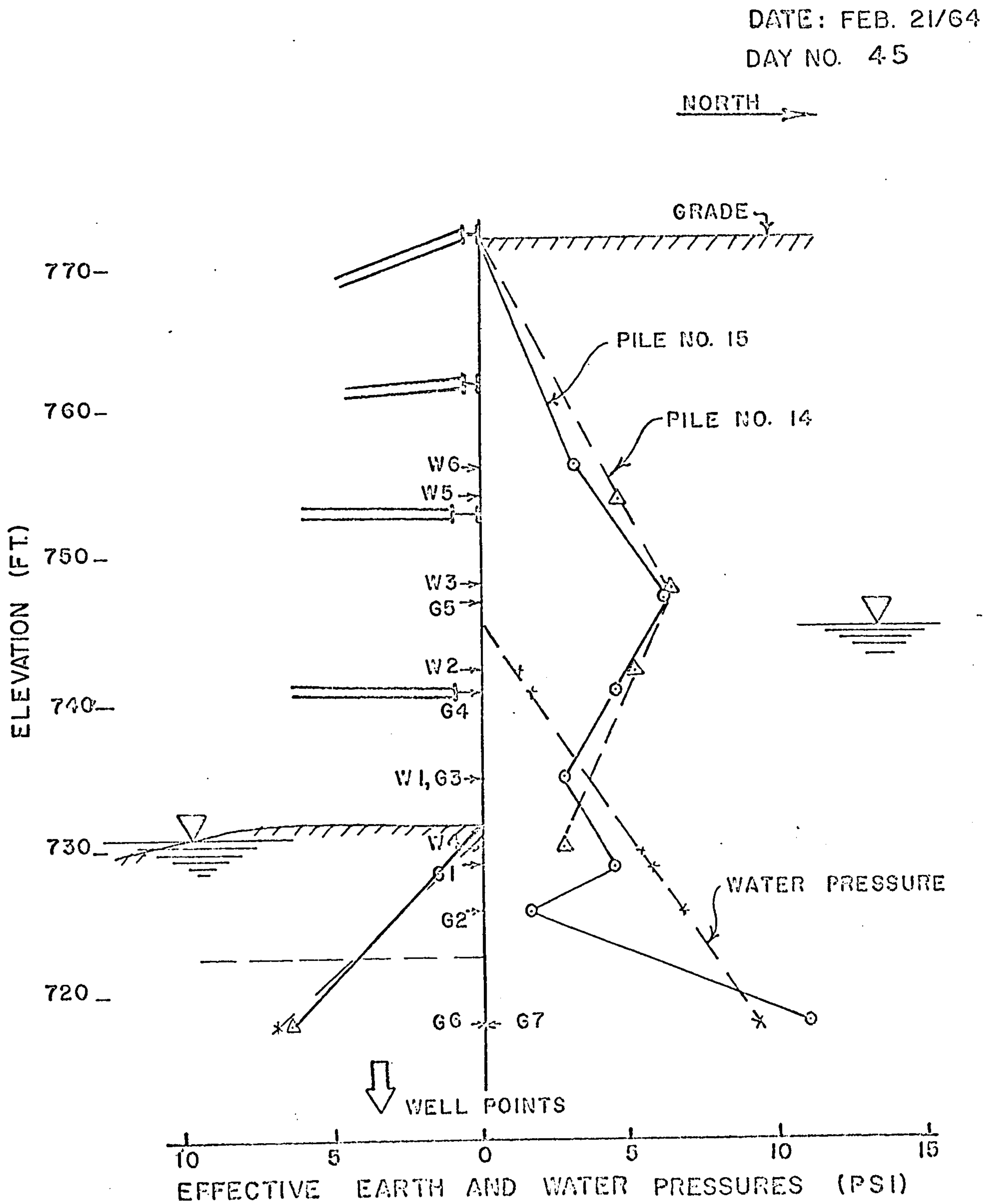

FIG. 5.28 EFFECTIVE EARTH PRESSURE DISTRIBUTION, SHEET PILE NO. 14 AND NO. 15

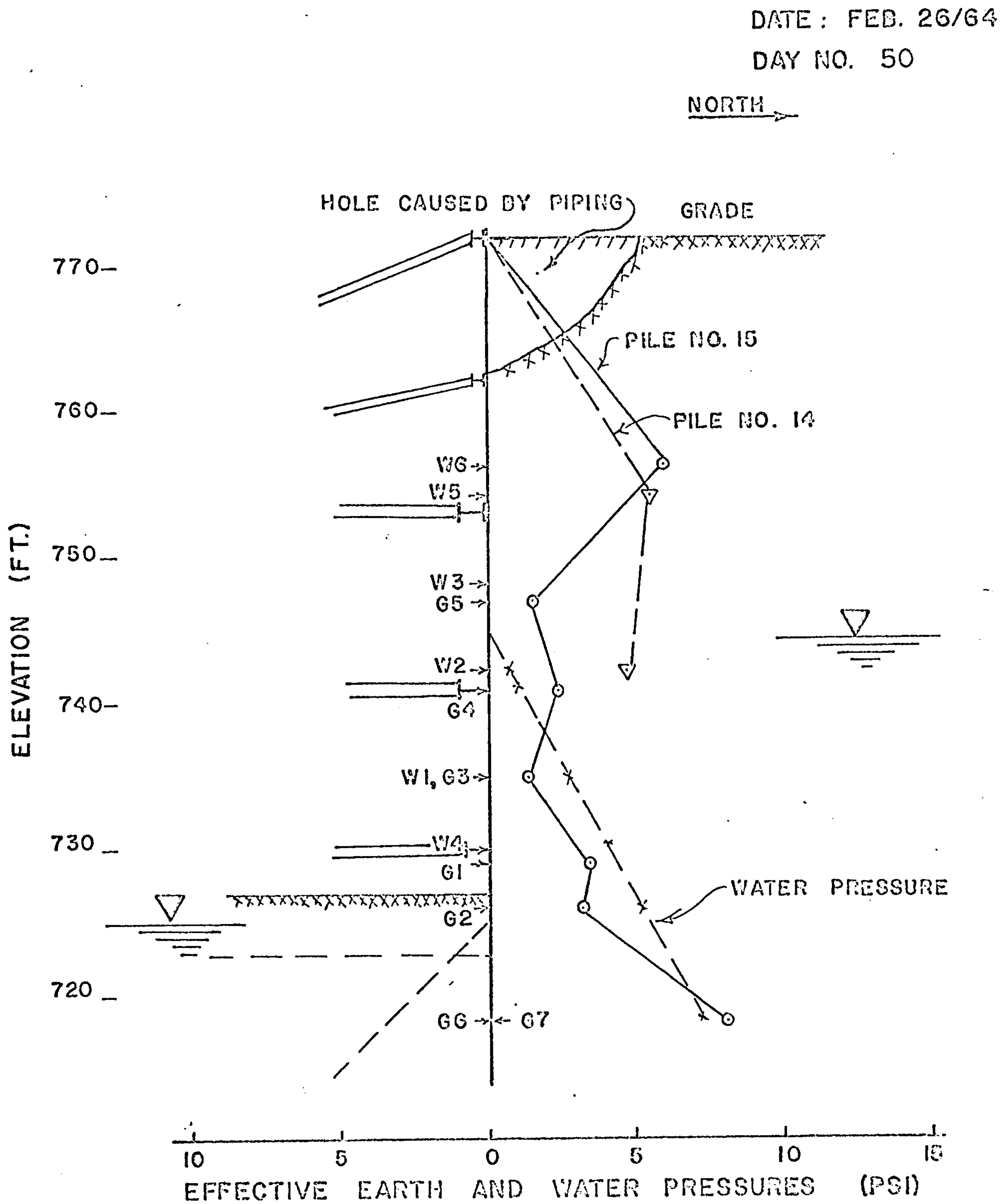

FIG. 5.2.9 EFFECTIVE EARTH PRESSURE DISTRIBUTION, SHEET PILE NO. 14 AND NO. 15

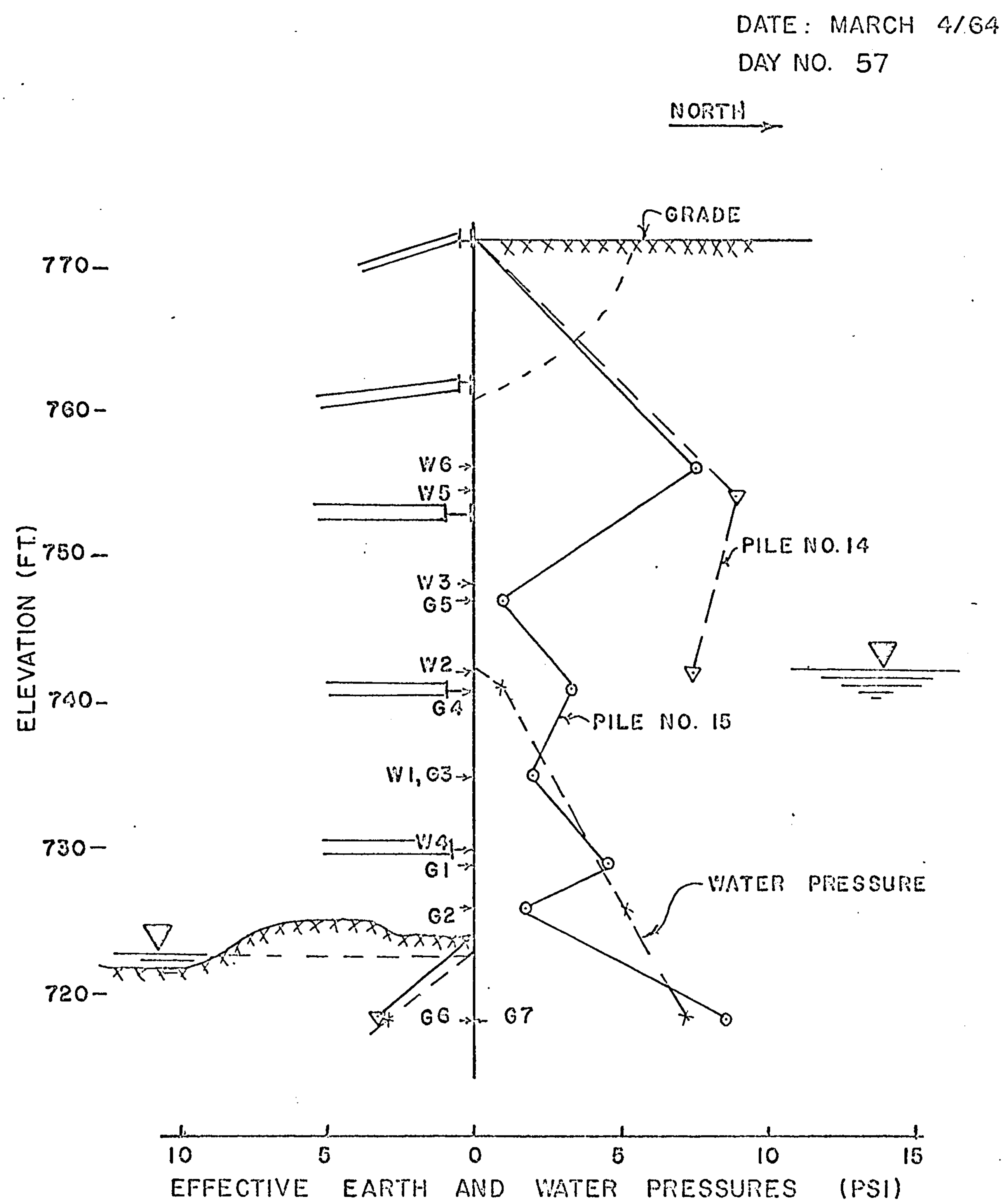

FIG 5.2.10 EFFECTIVE EARTH PRESSURE DISTRIBUTION, SHEET PILE NO. 14 AND NO. 15

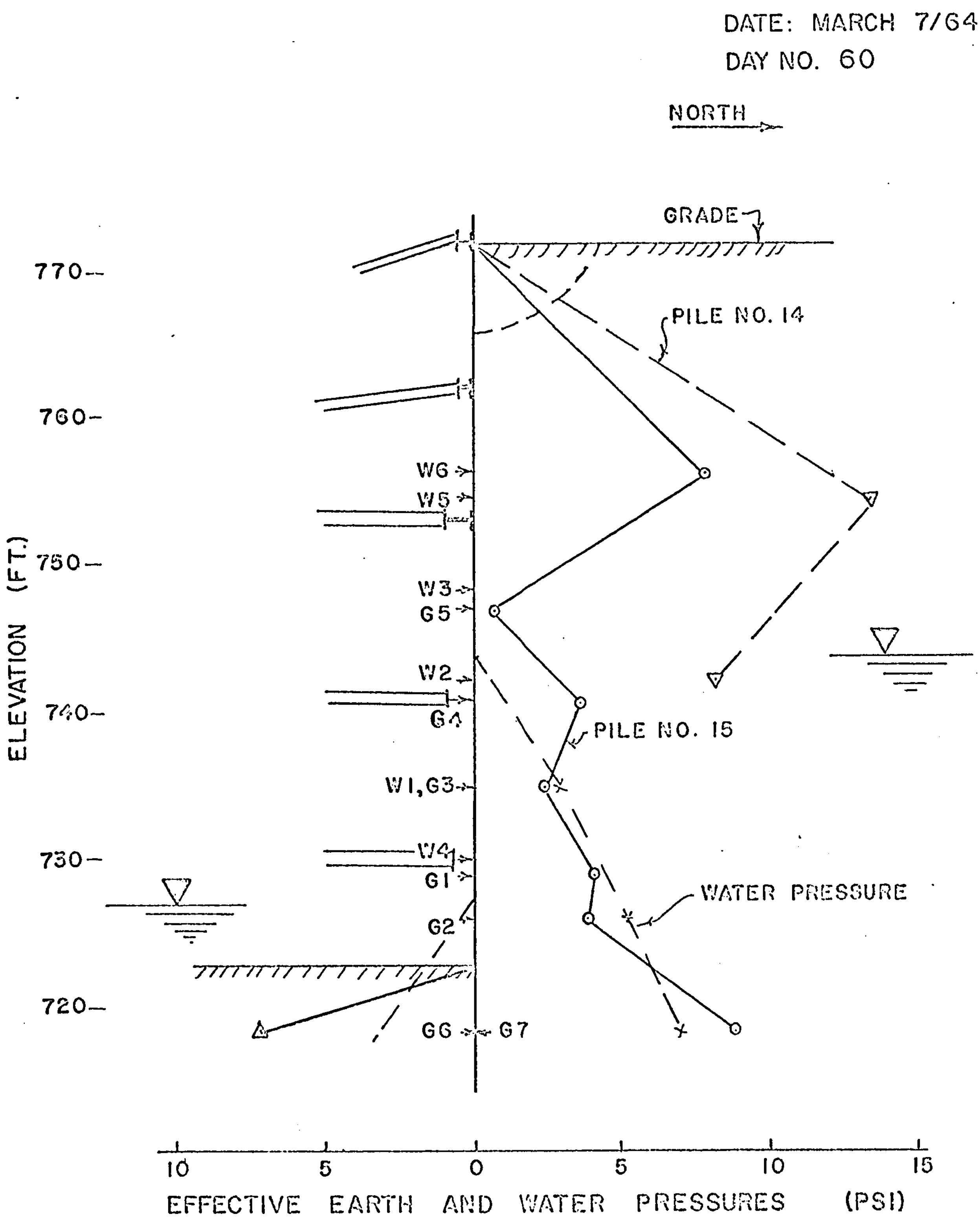

FIG. 5.2.11 EFFECTIVE EARTH PRESSURE DISTRIBUTION, SHEET PILE NO. 14 AND NO. 15

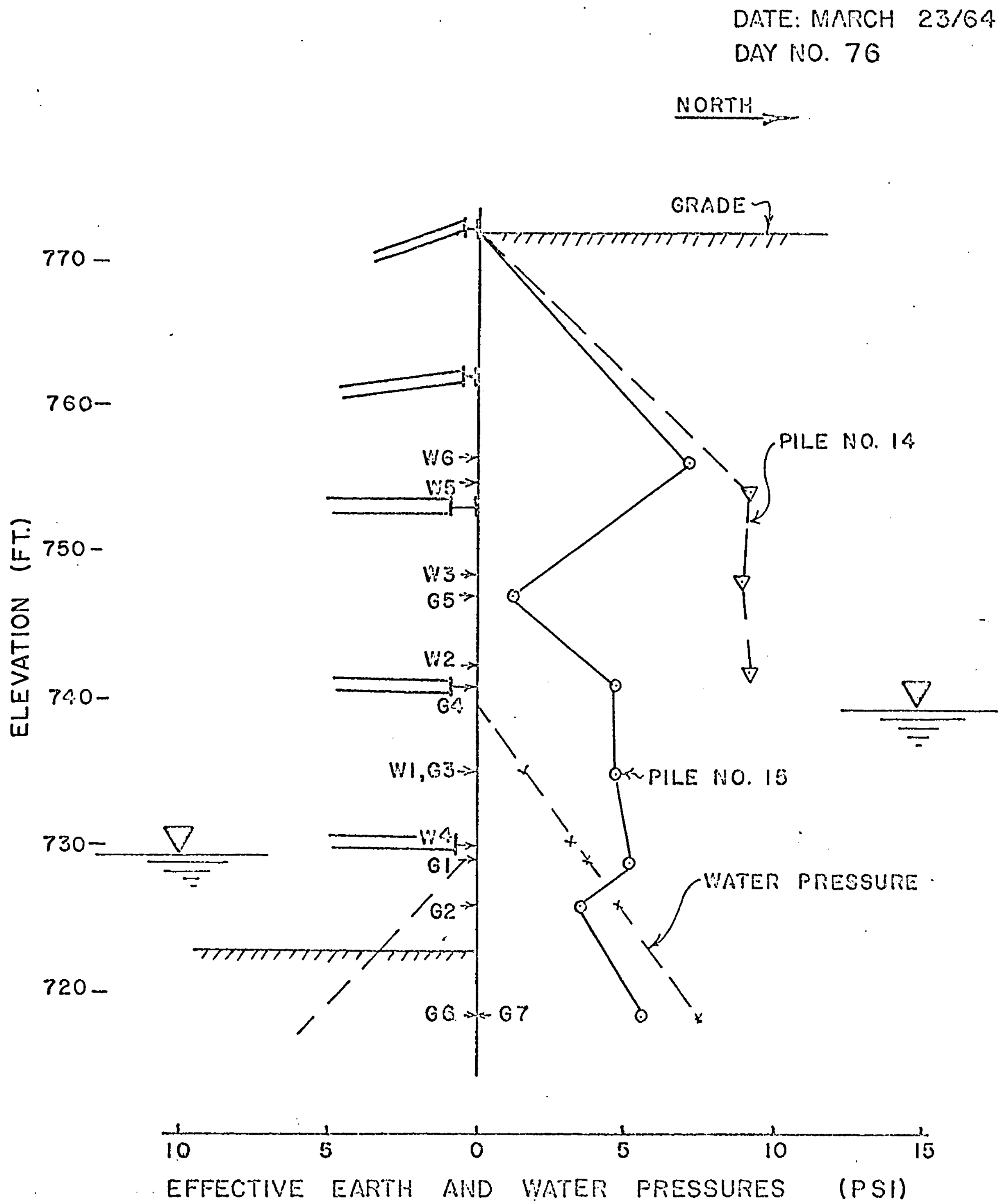

FIG. 5.2.12 EFFECTIVE EARTH PRESSURE DISTRIBUTION, SHEET PILE NO. 14 AND NO. 15

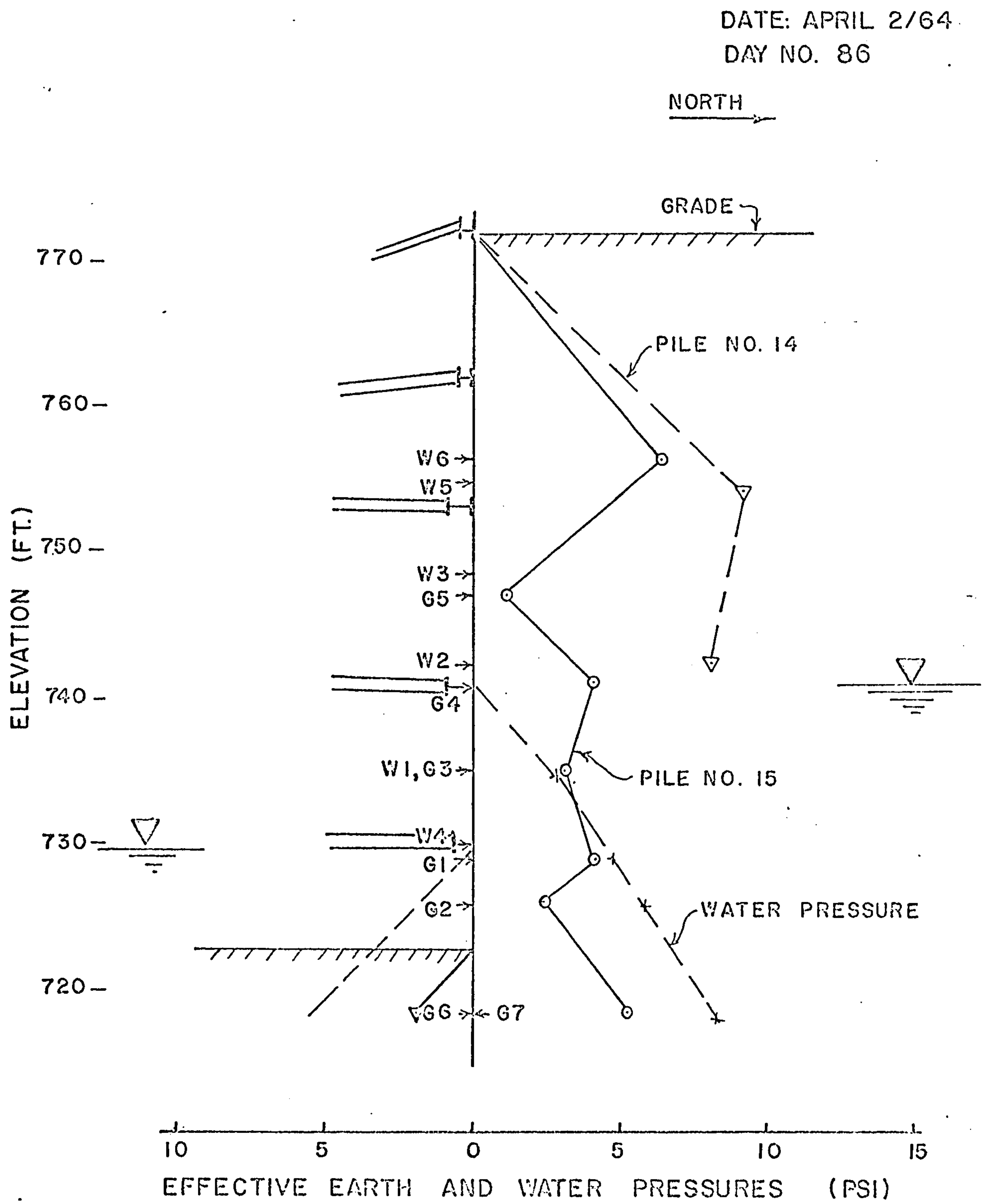

FIG. 5.2.13 EFFECTIVE EARTH PRESSURE DISTRIBUTION, SHEET PILE NO. 14 AND NO. 15

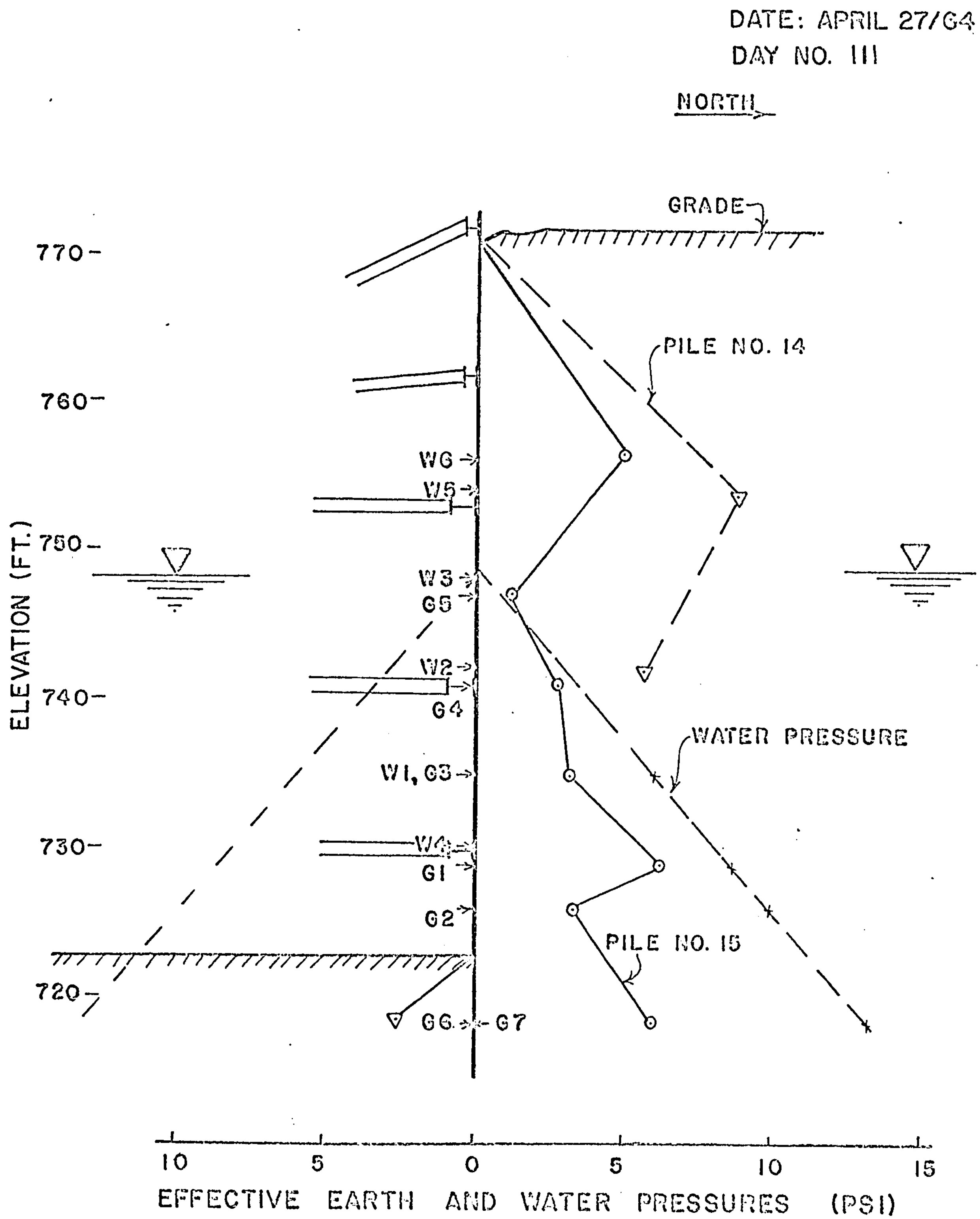

FIG. 5.2.14 EFFECTIVE EARTH PRESSURE DISTRIBUTION, SHEET PILE NO. 14 AND NO. 15

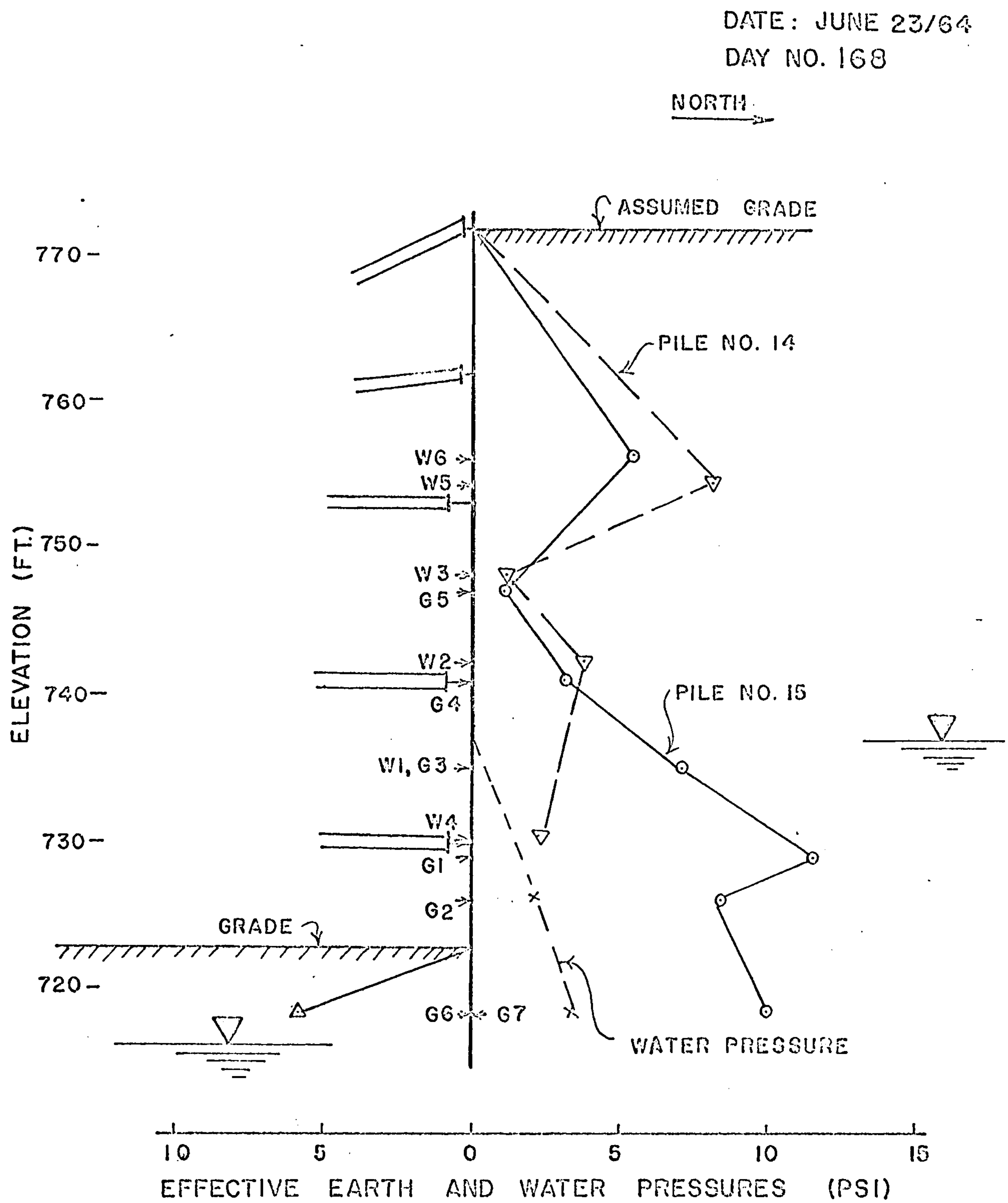

FIG. 5.2.15 EFFECTIVE EARTH PRESSURE DISTRIBUTION, SHEET PILE NO. 14 AND NO. 15

DATE: JUNE 30/64
DAY NO. 175

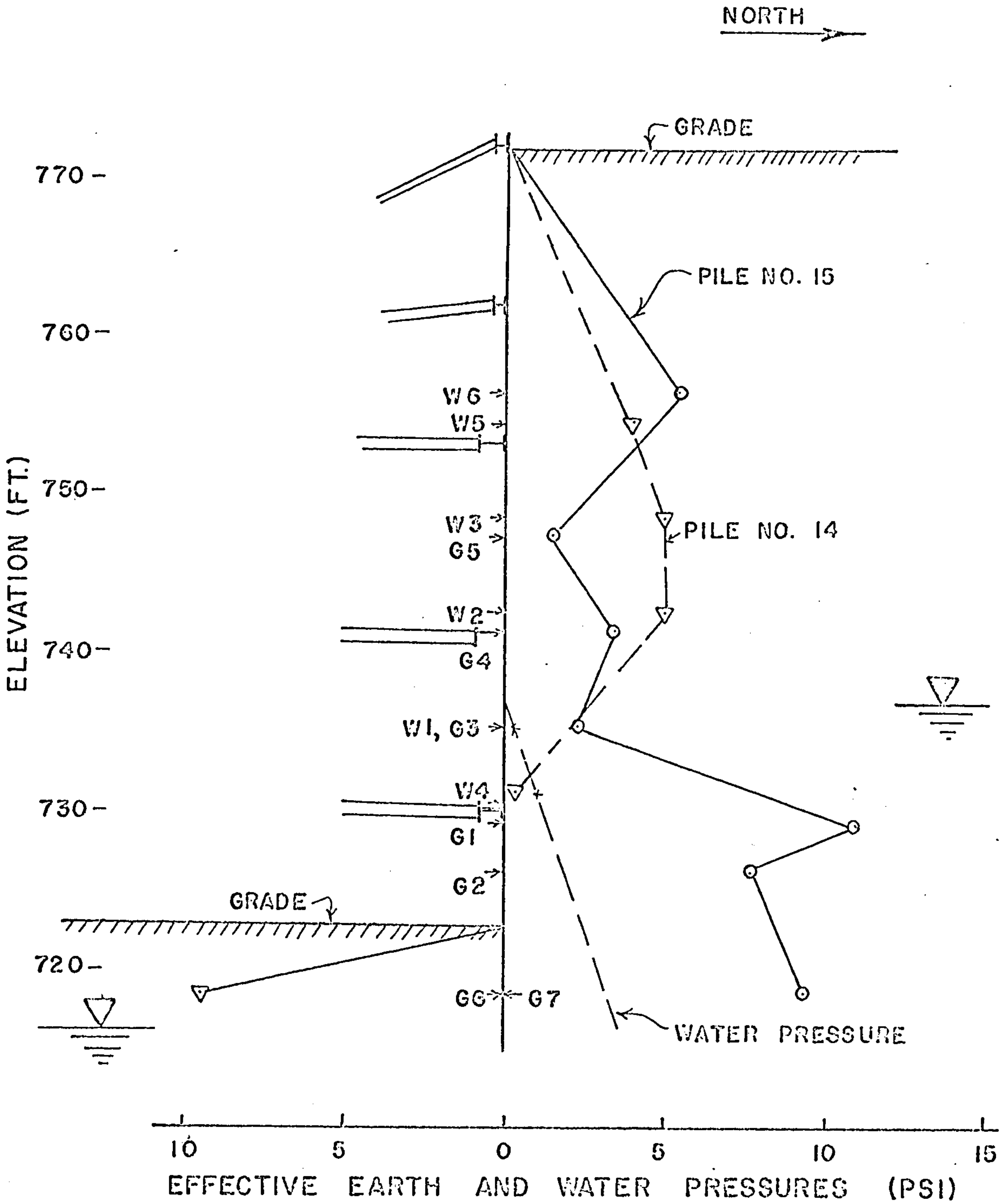

FIG. 5.2.16 EFFECTIVE EARTH PRESSURE DISTRIBUTION, SHEET PILE NO. 14 AND NO. 15

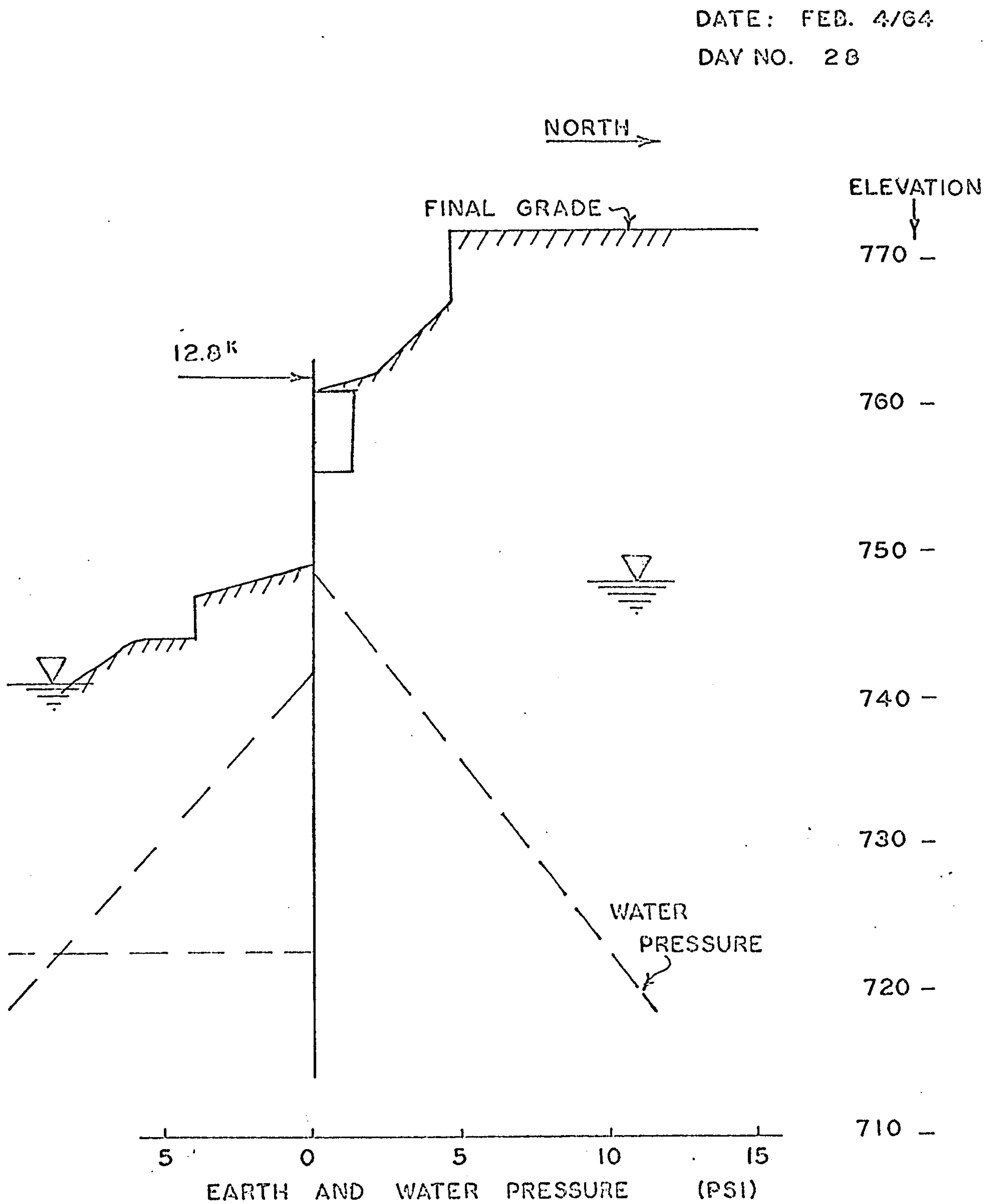

FIG. 5.2.17 STRUT LOADS

DATE: FEB. 6/64

DAY NO. 30

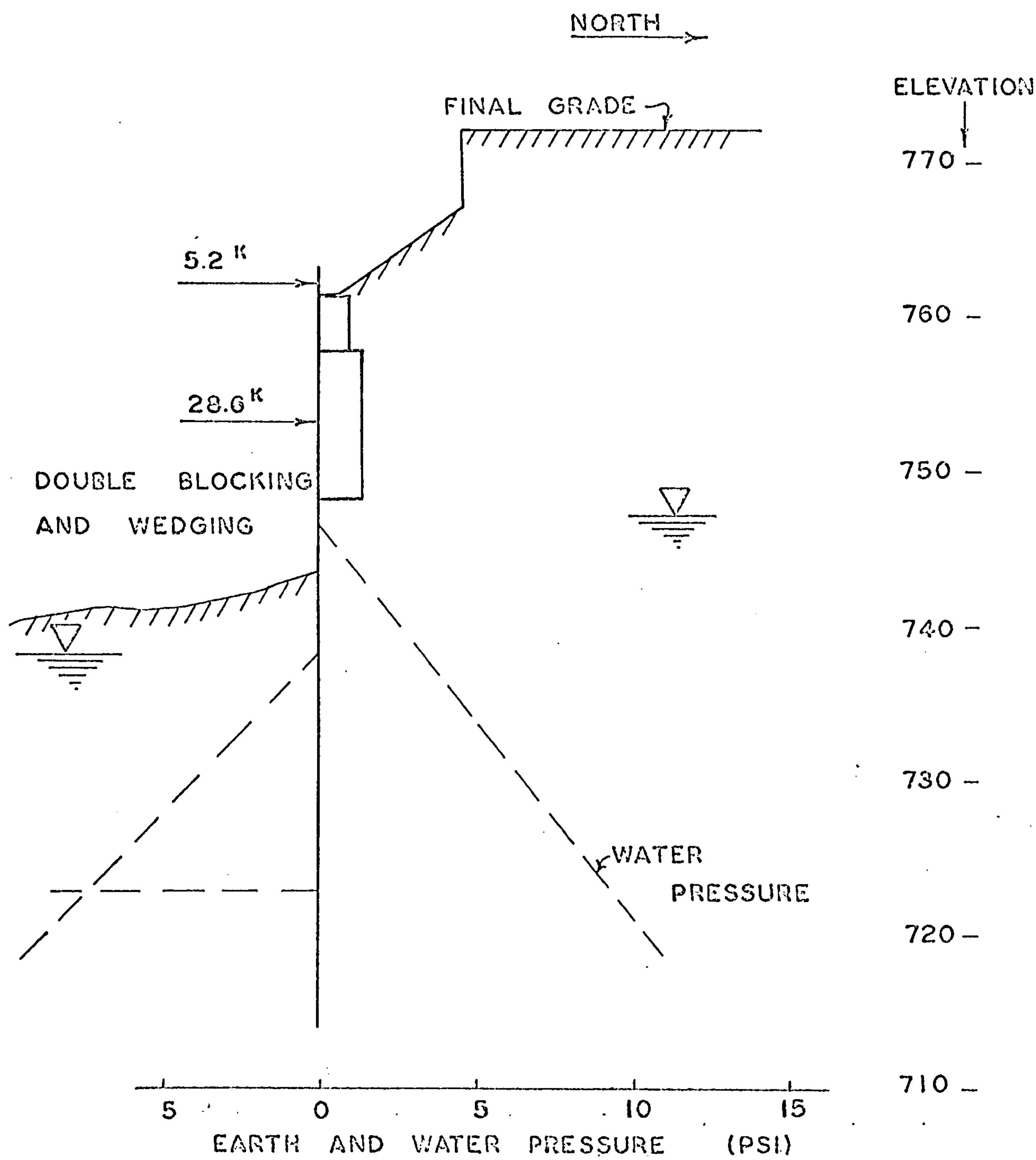

FIG. 5.2.18 STRUT LOADS

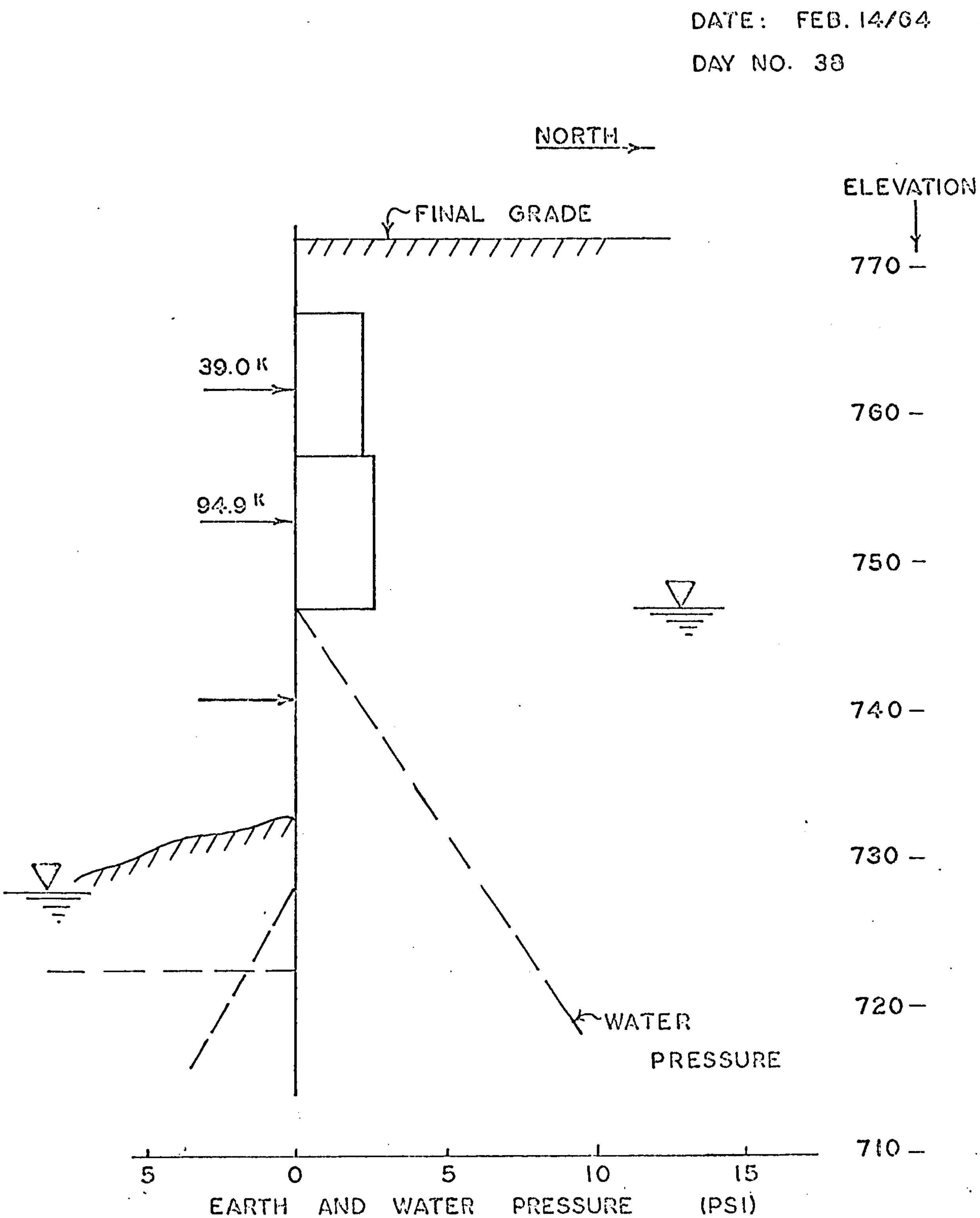

FIG. 5.2.19 STRUT LOADS

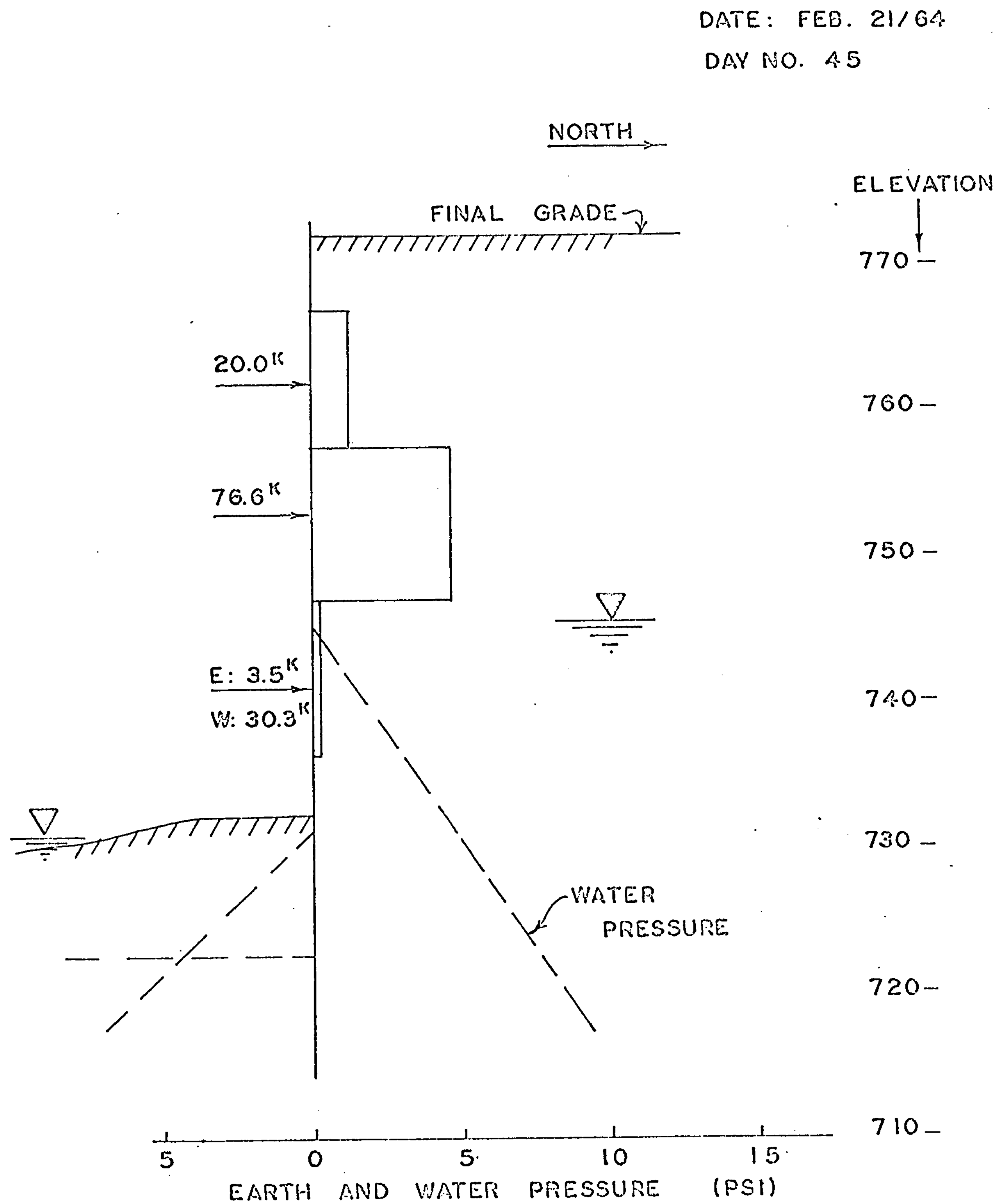

FIG. 5.2.20 STRUT LOADS

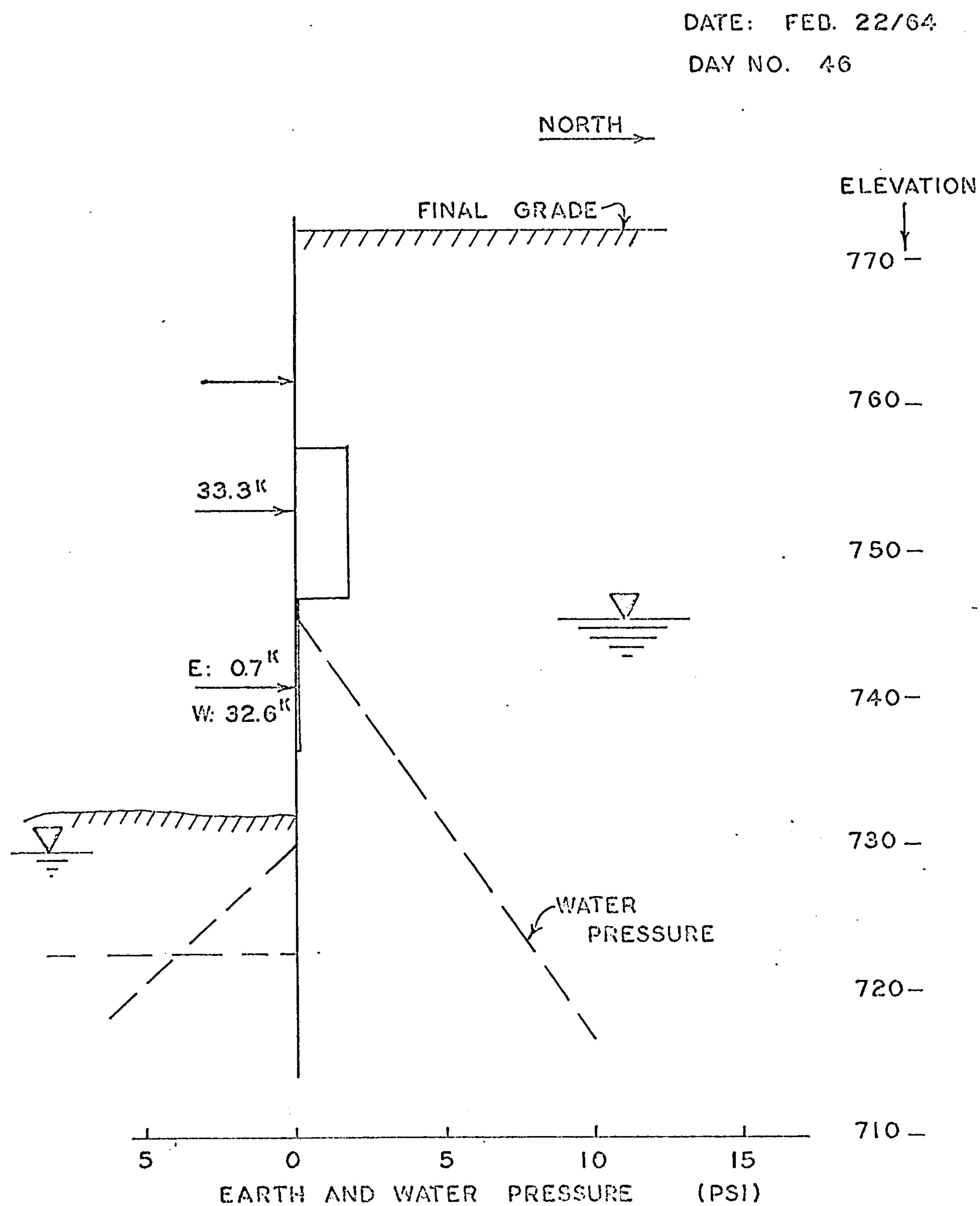

FIG. 5.2.21 STRUT LOADS

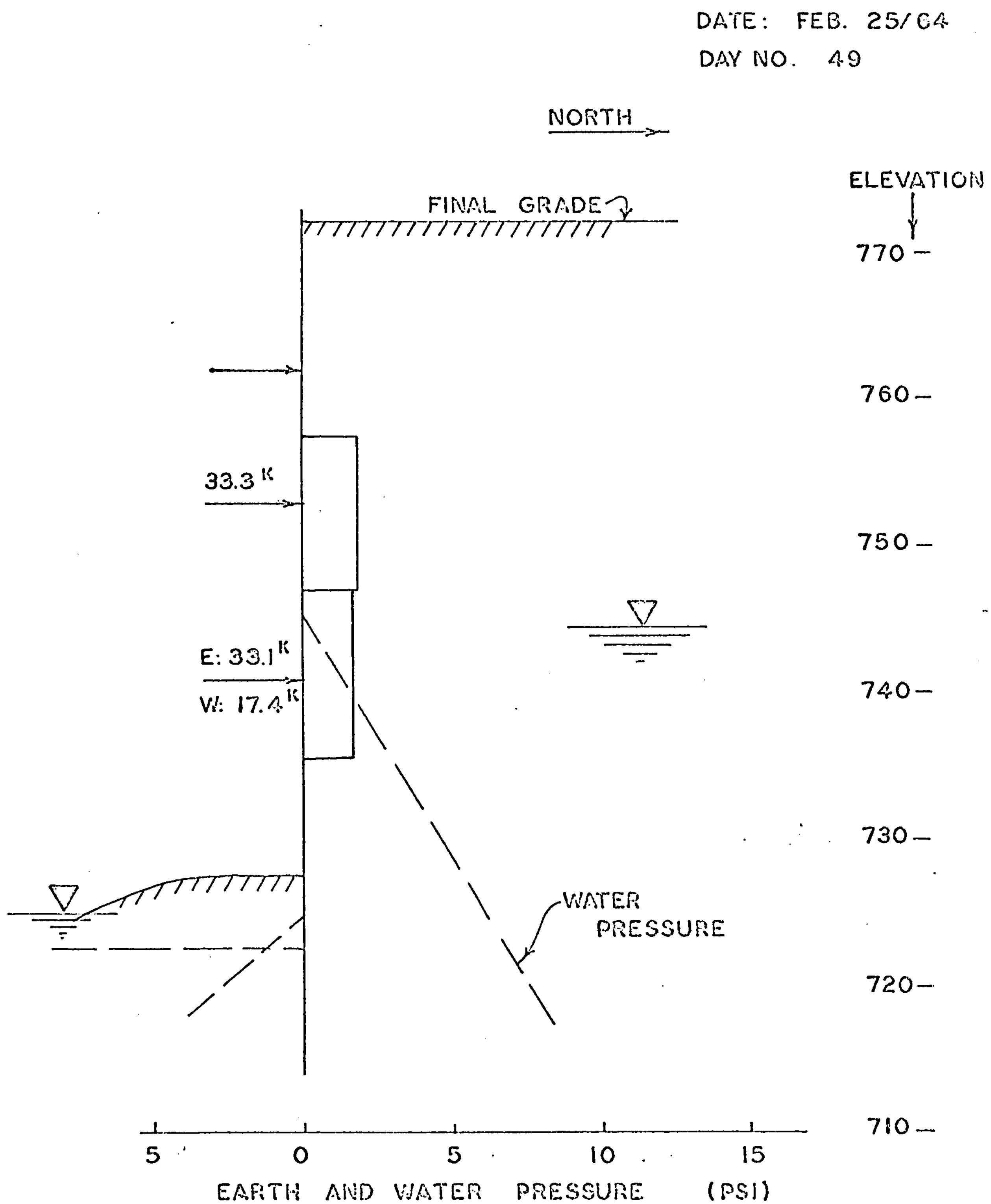

FIG. 5.2.22 STRUT LOADS

DATE: FEB. 26/64
DAY NO. 50

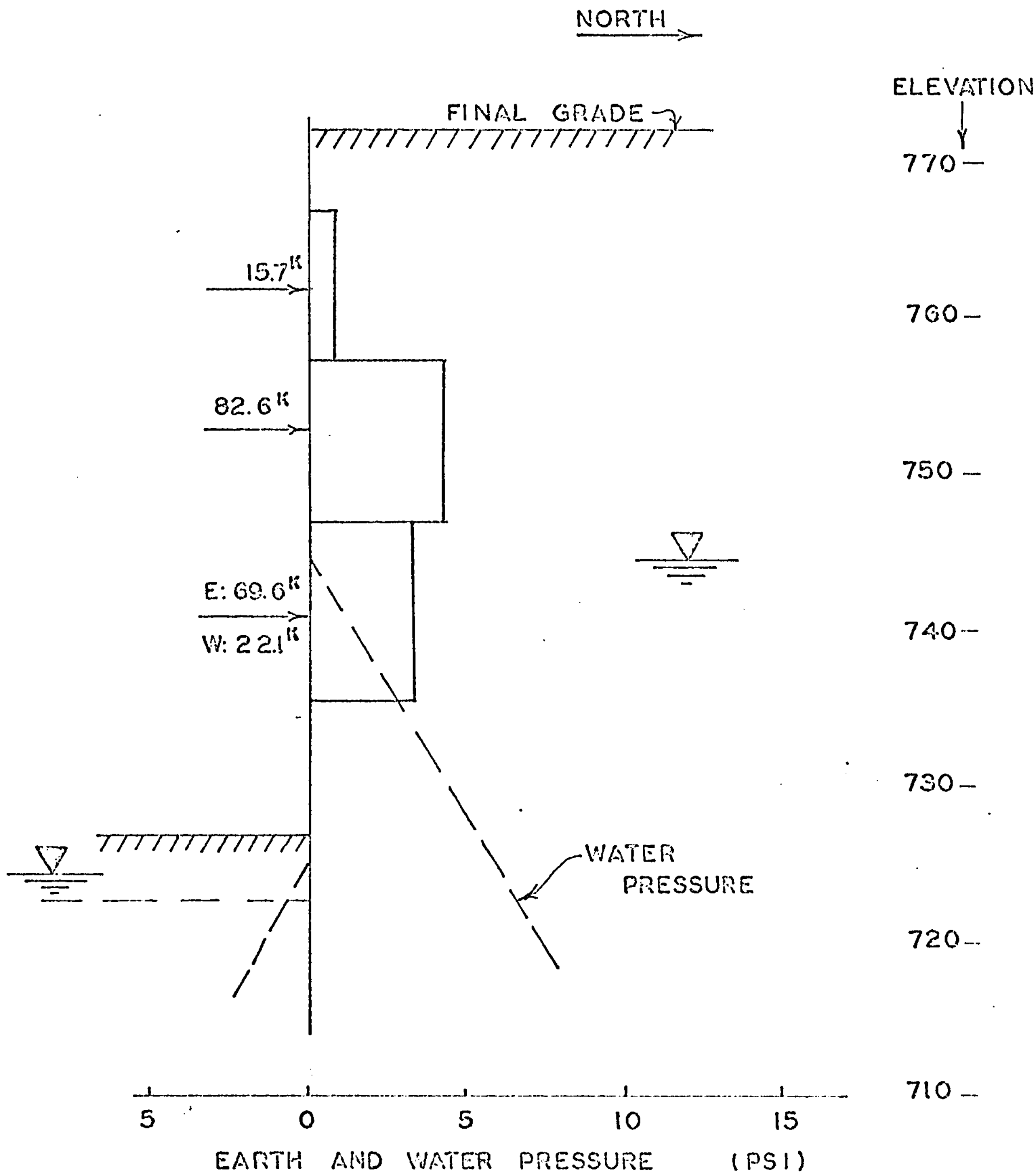

FIG. 5.2.23 STRUT LOADS

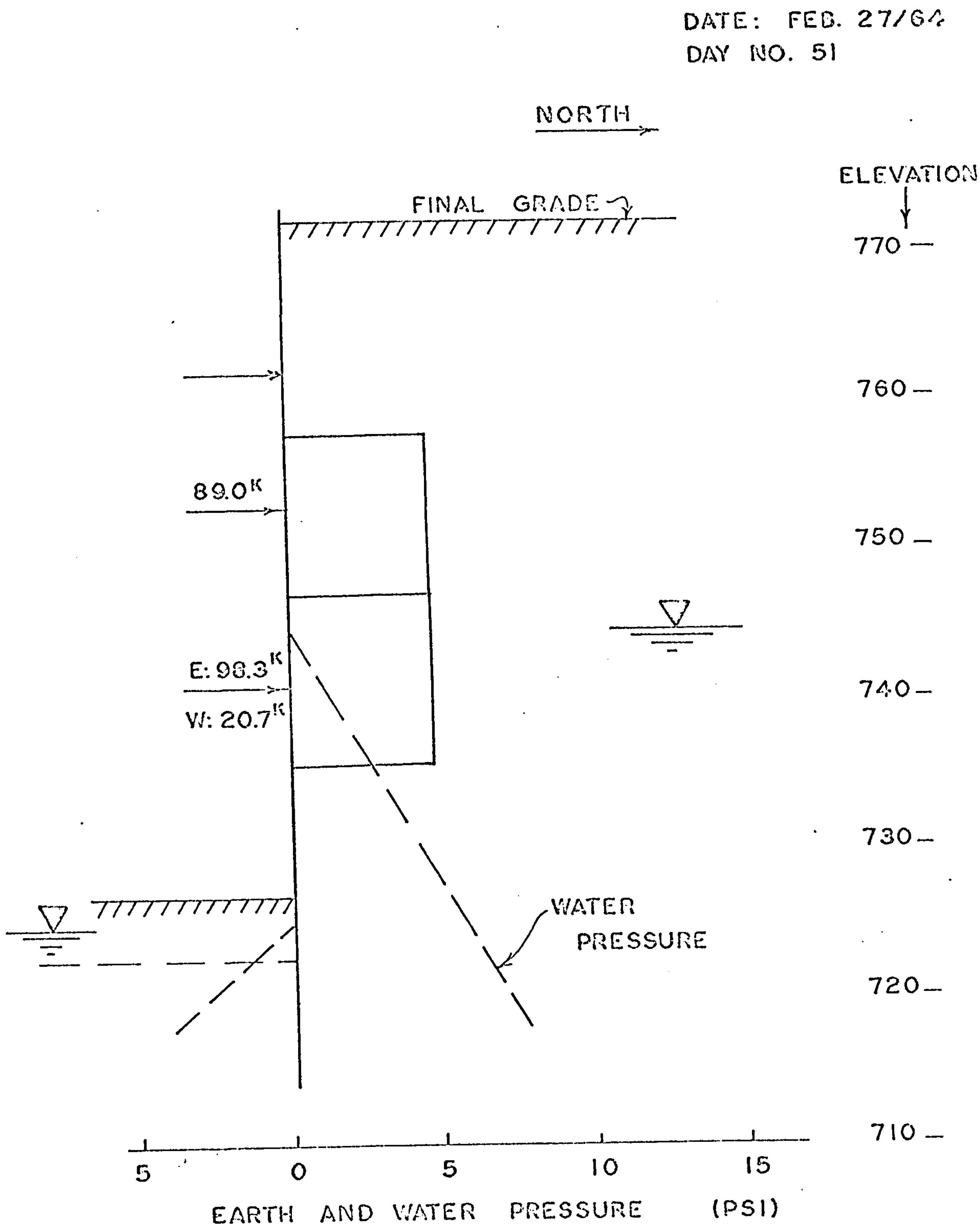

FIG. 5.2.24 STRUT LOADS

DATE: MARCH 2/64
DAY NO. 55

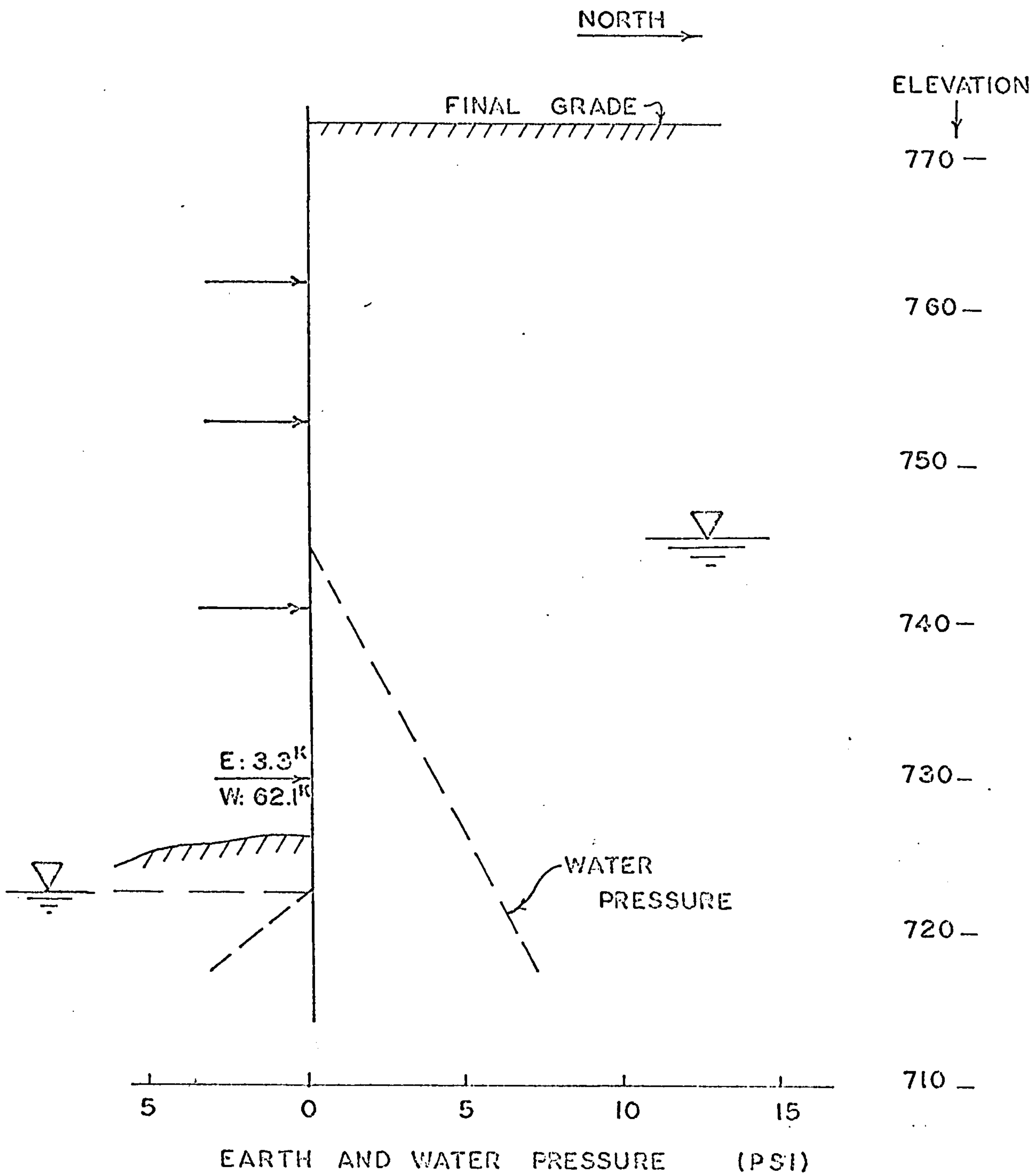

FIG. 5.2.25 STRUT LOADS

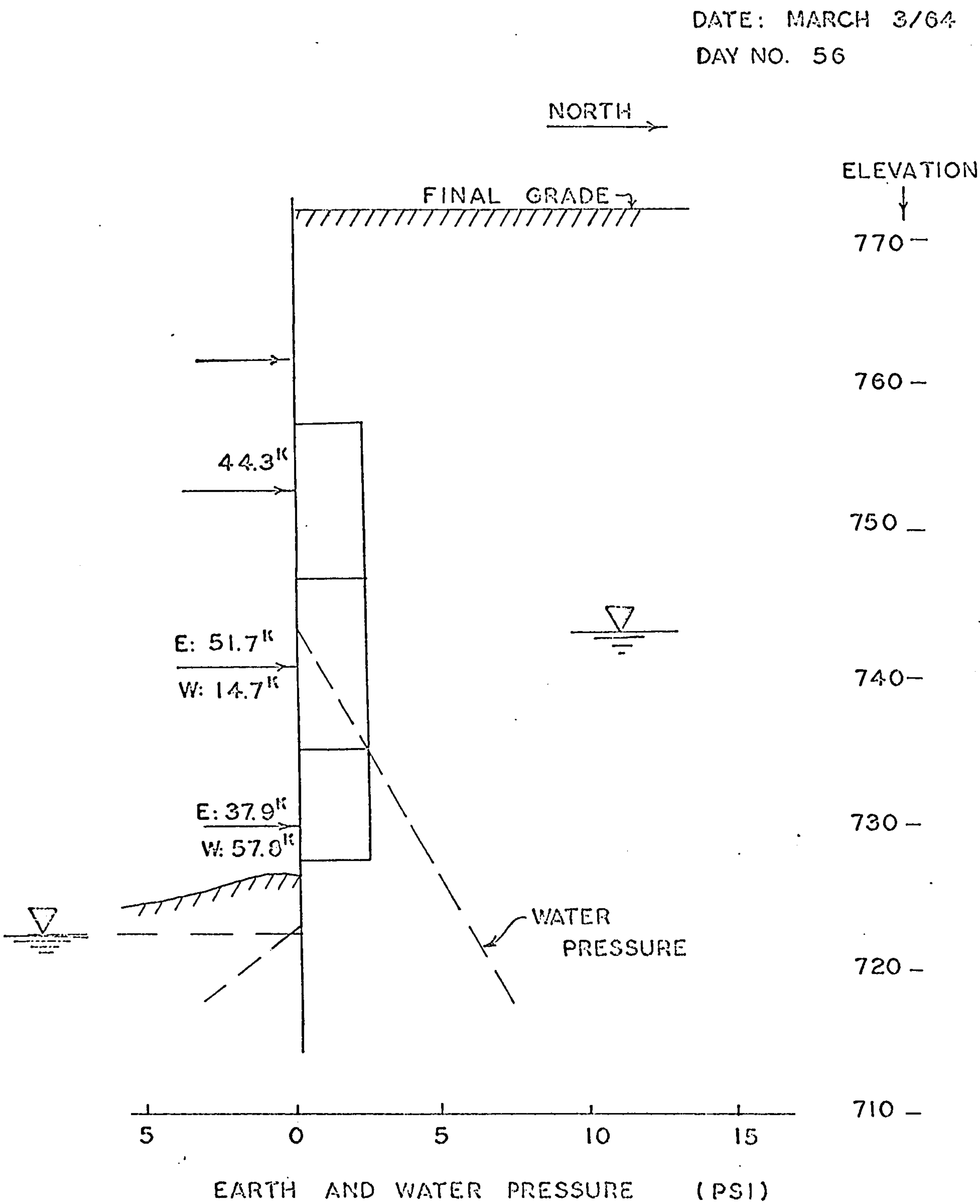

FIG. 5.2.26 STRUT LOADS

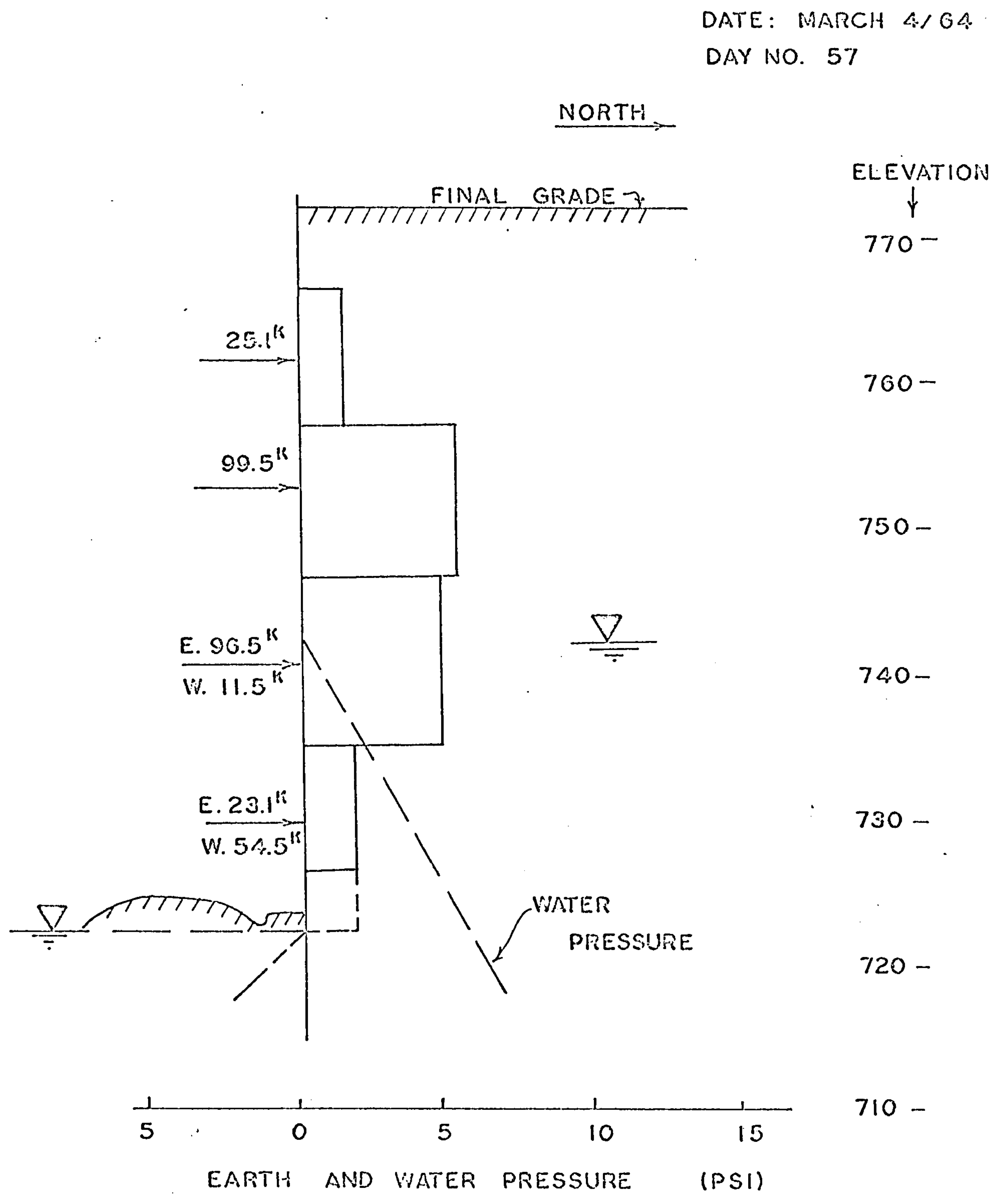

FIG. 5.2.27 STRUT LOADS

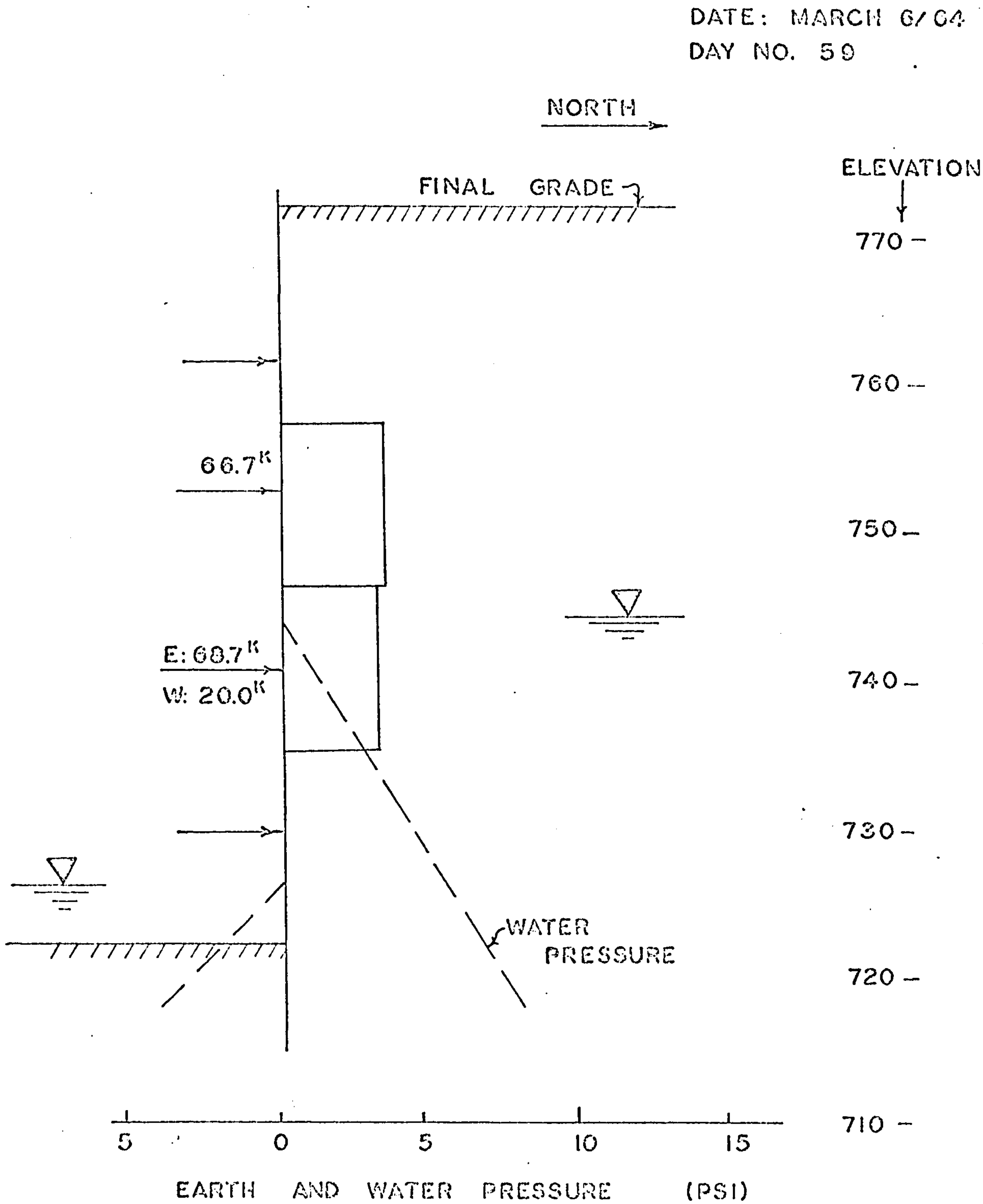

FIG. 5.2.28 STRUT LOADS

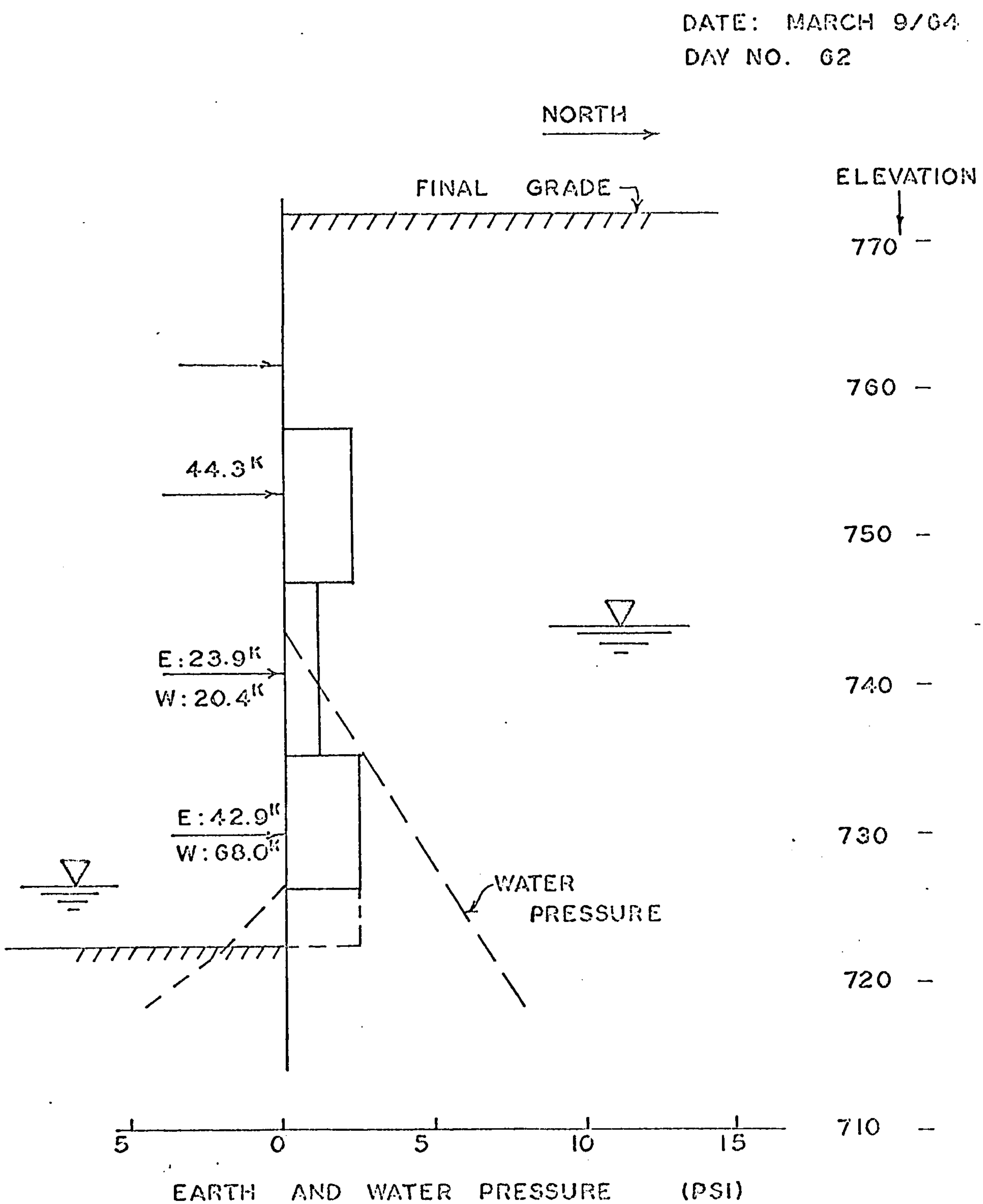

FIG. 5.2.29 STRUT LOADS

DATE: MARCH 11/64
DAY NO. 64

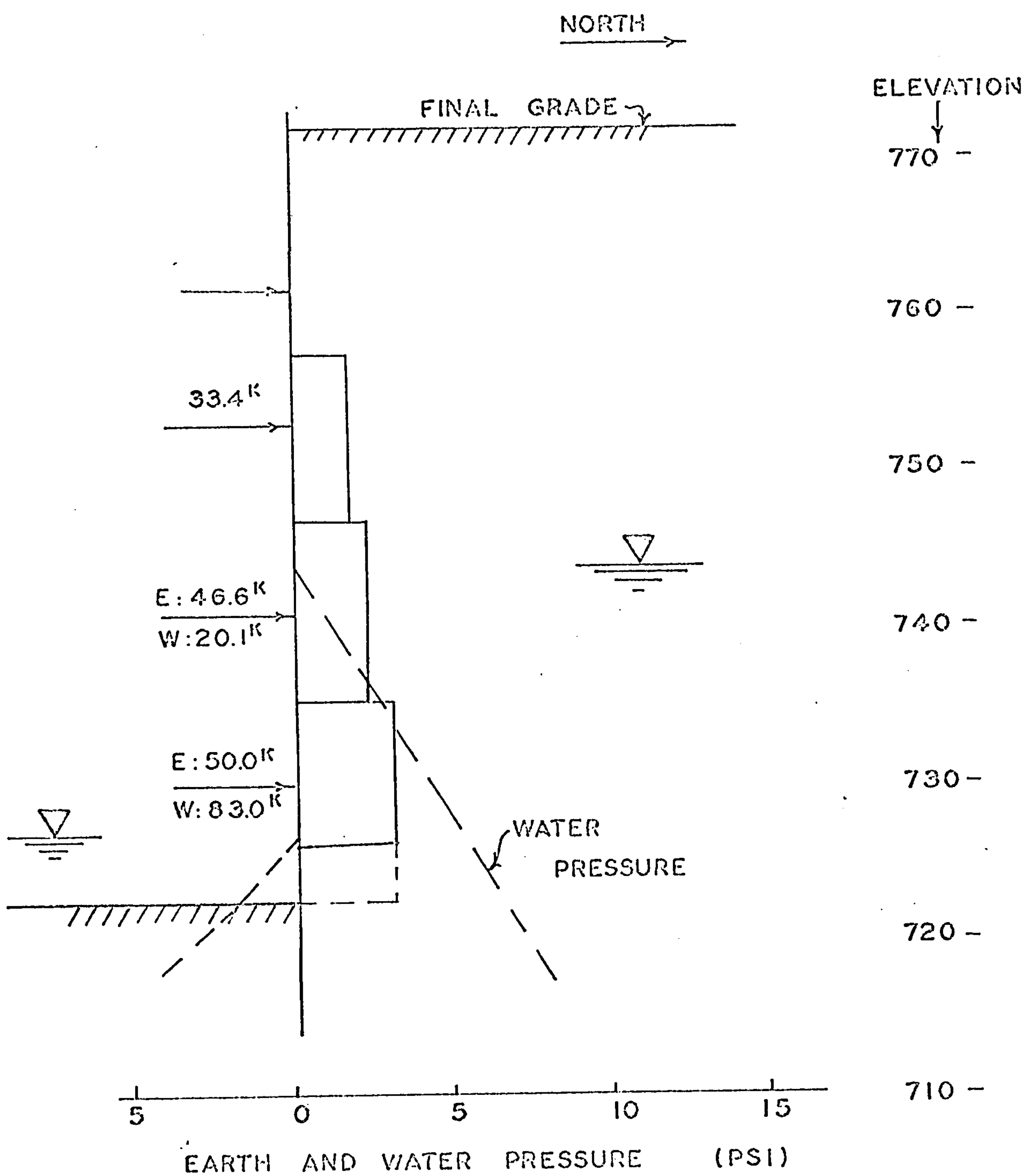

FIG. 5.2.30 STRUT LOADS

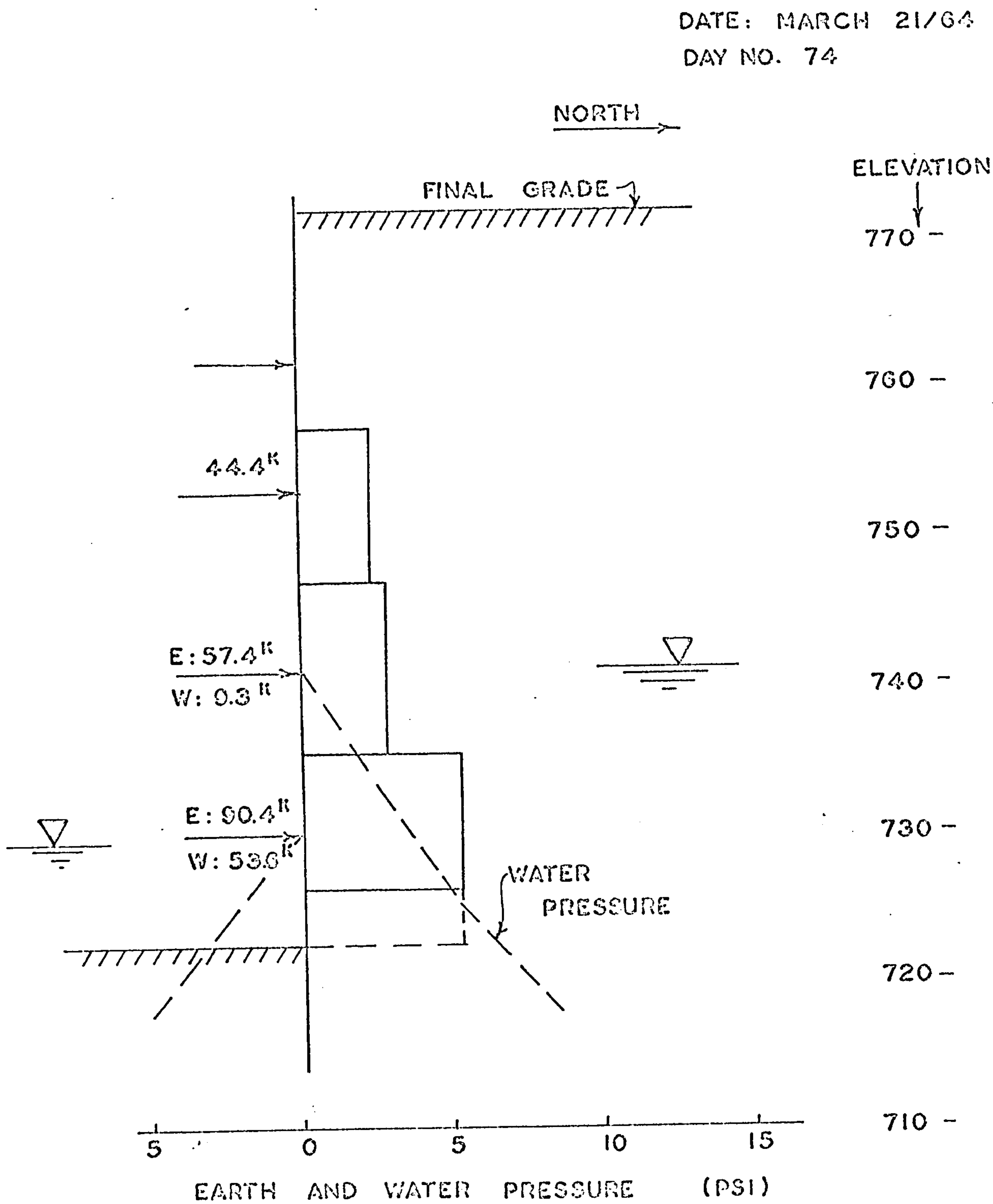

FIG. 5.2.31 STRUT LOADS

DATE: MARCH 23/64
DAY NO. 76

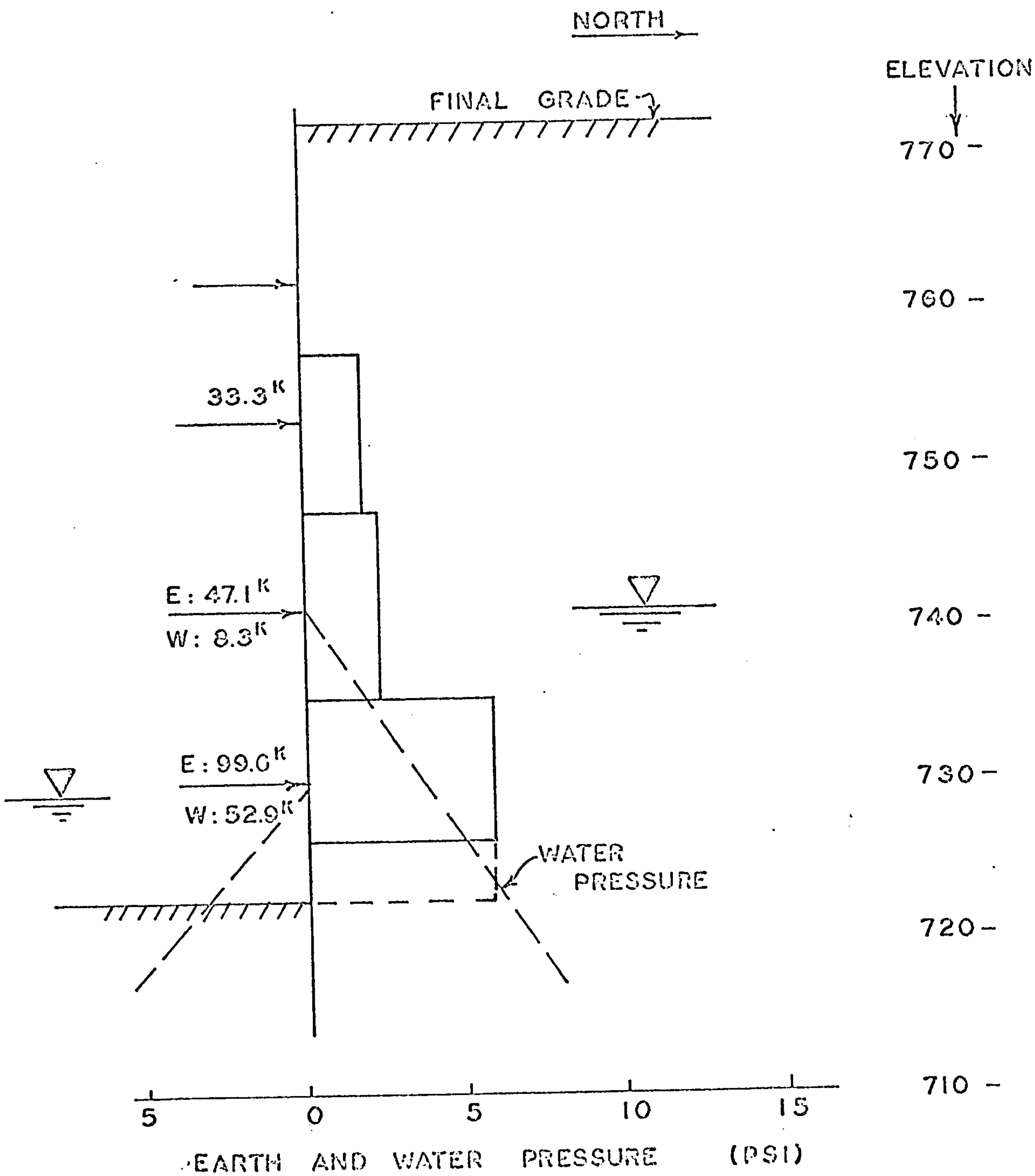

FIG. 5.2.32 STRUT LOADS

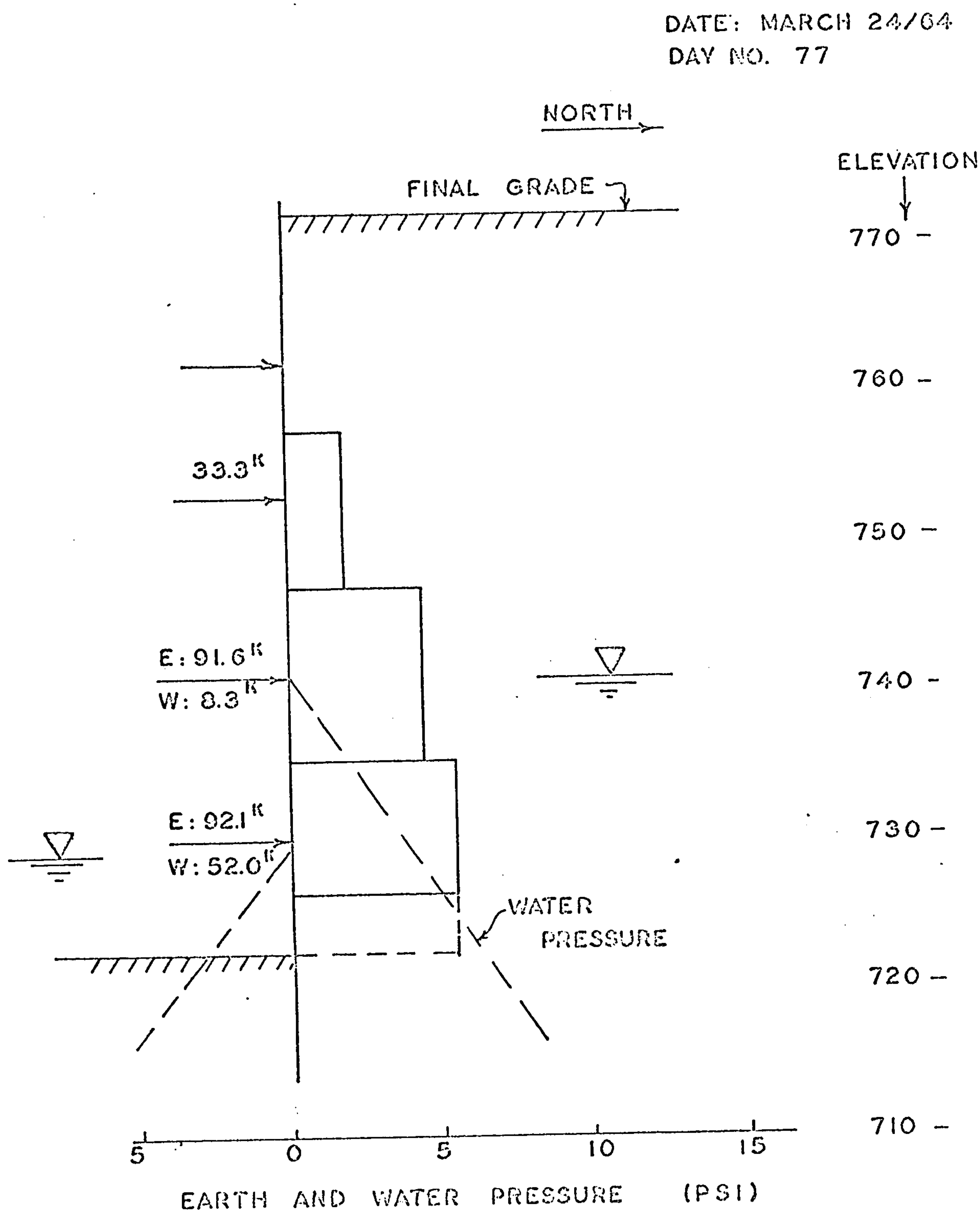

FIG. 5.2.33 STRUT LOADS

DATE: APRIL 1/64
DAY NO. 85

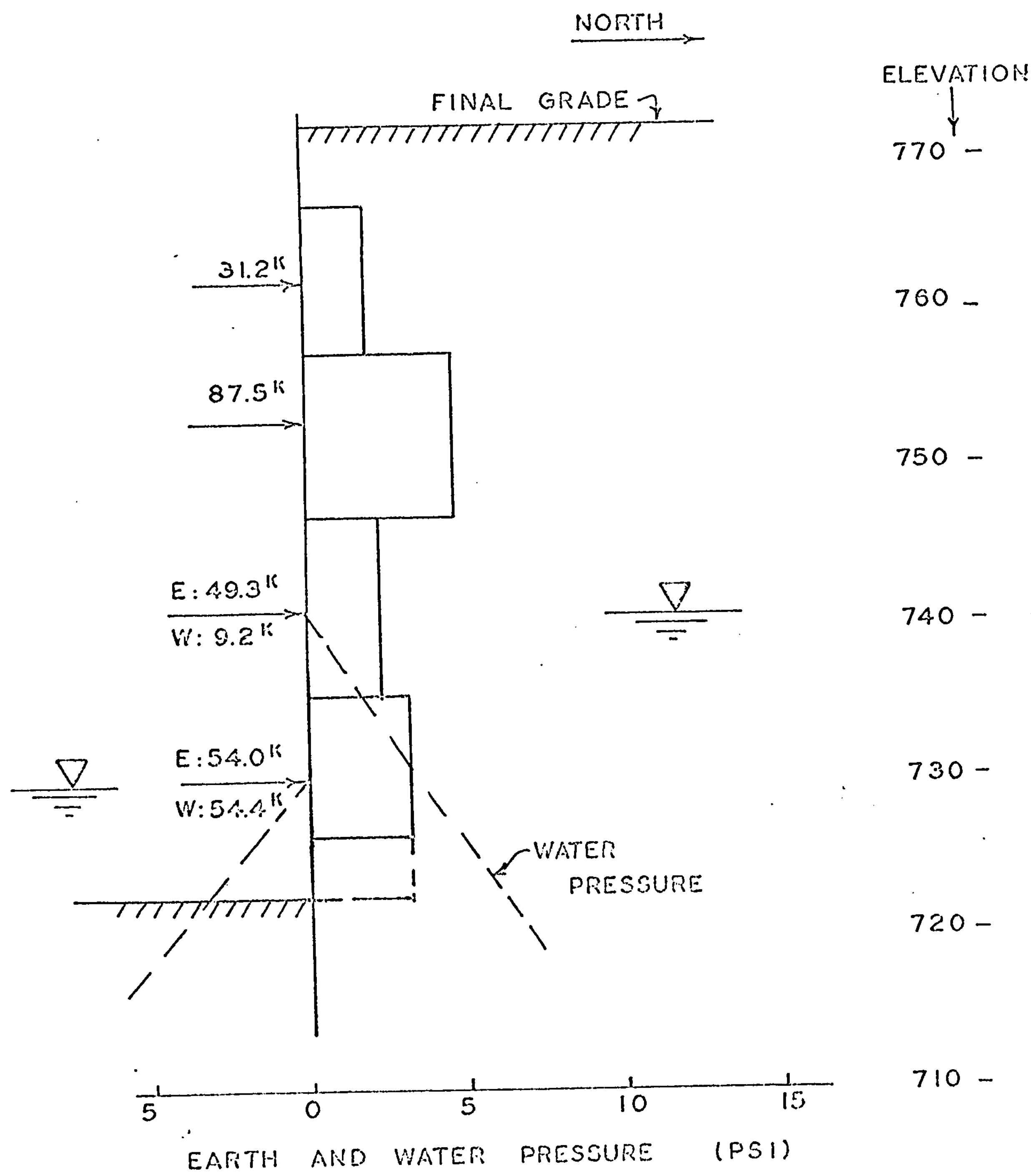

FIG. 5.2.34 STRUT LOADS

DATE: APRIL 2/64
DAY NO. 86

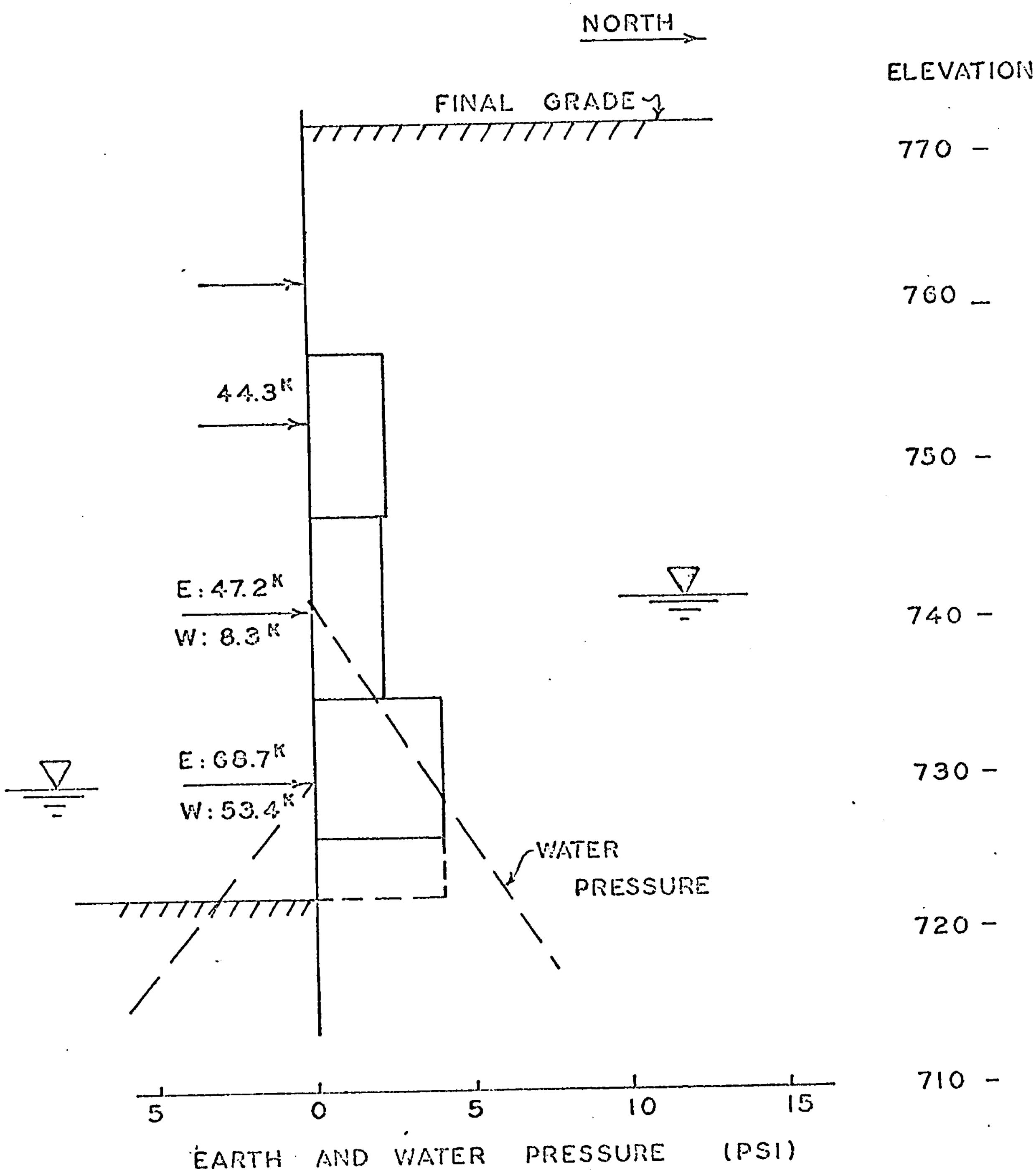

FIG. 5.2.35 STRUT LOADS

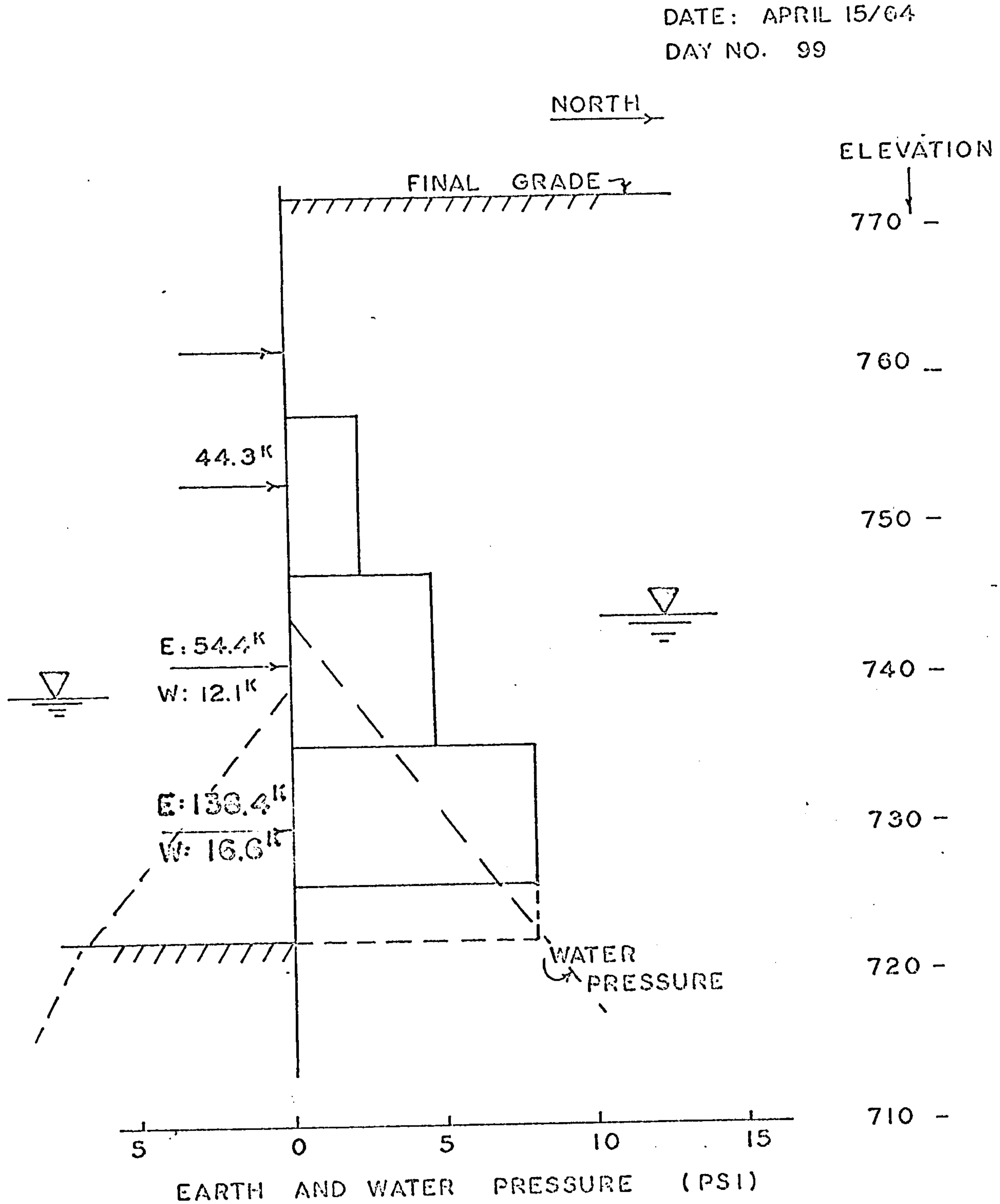

FIG. 5.2.36 STRUT LOADS

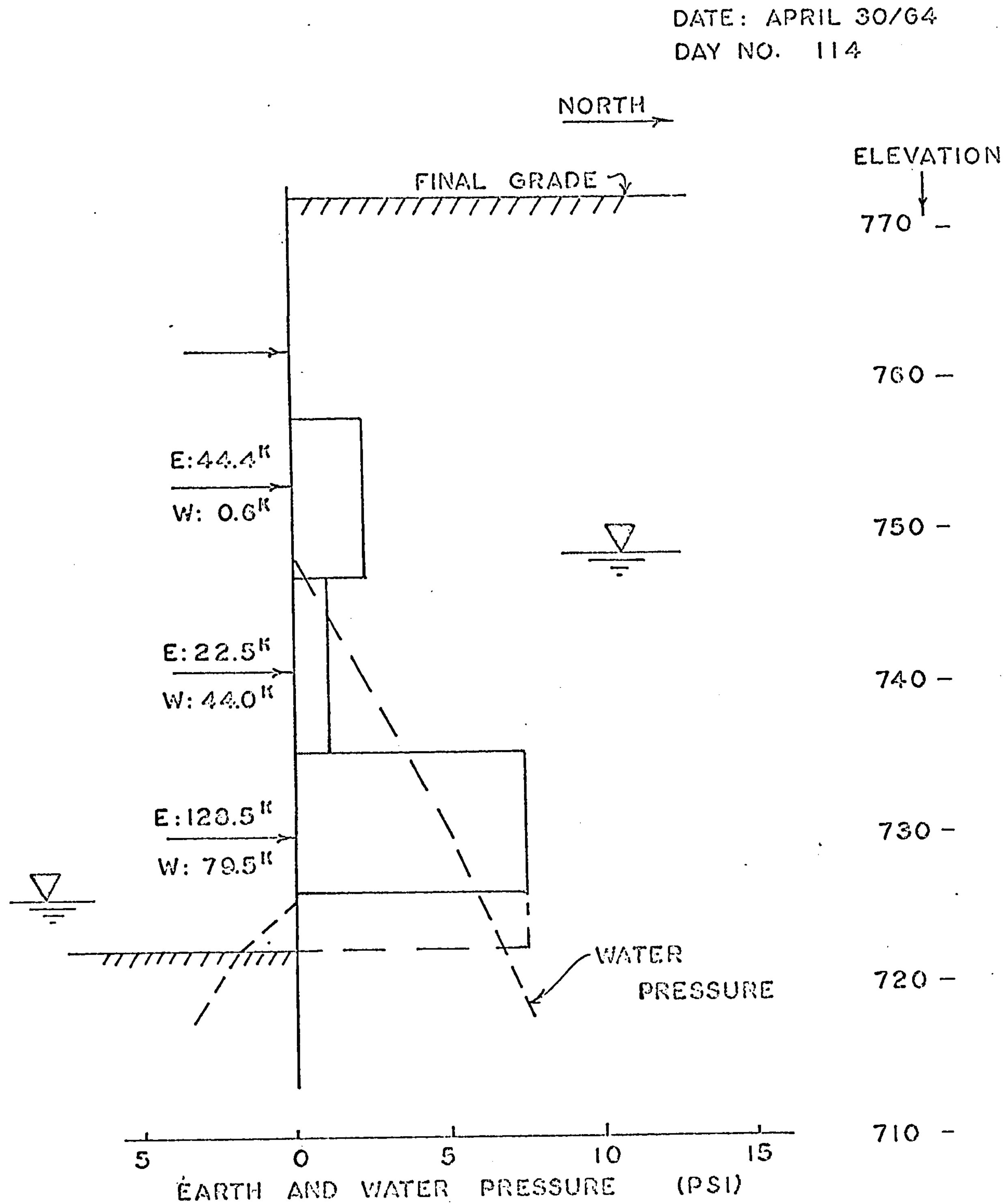

FIG. 5.2.37 STRUT LOADS

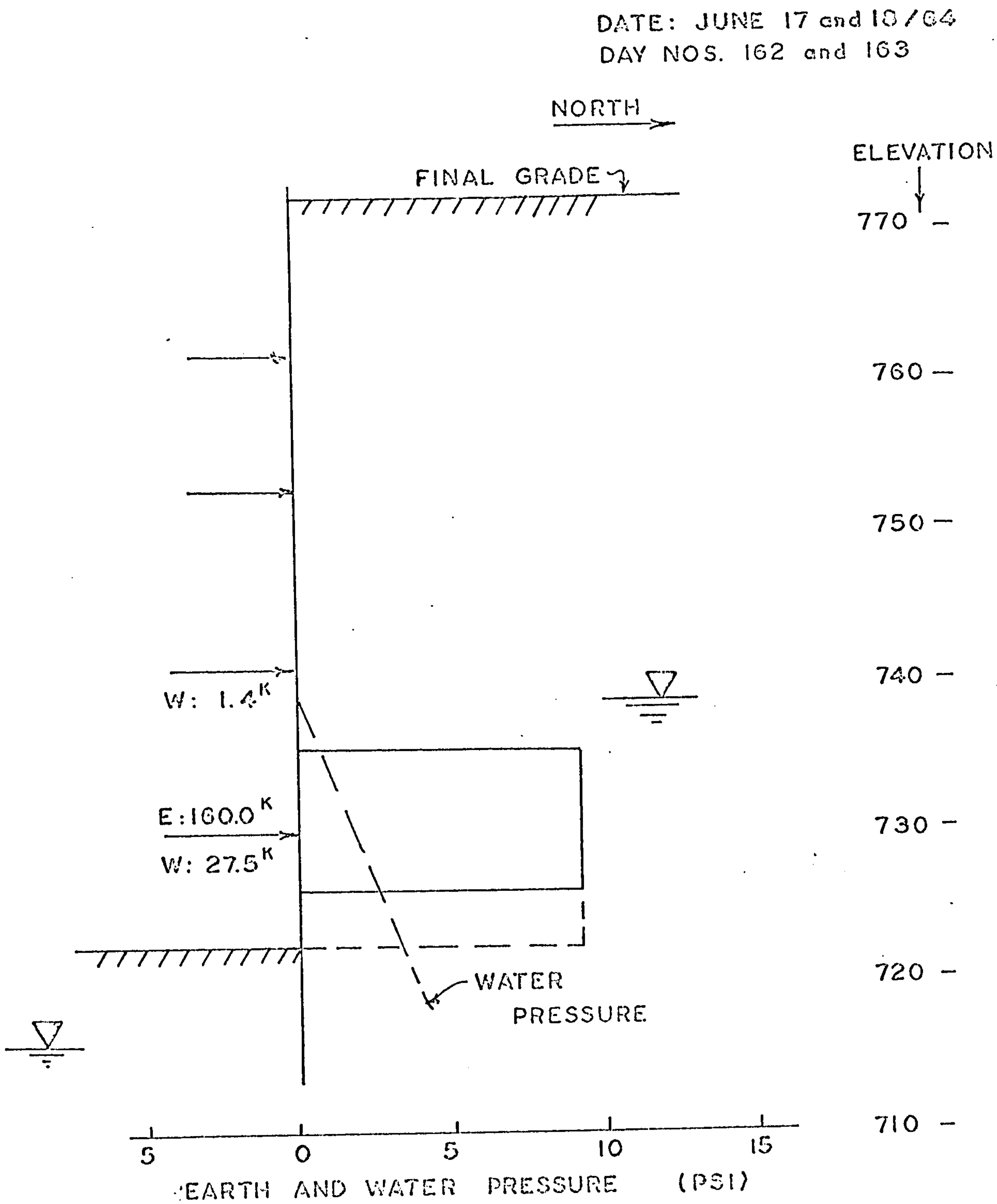

FIG. 5.2.38 STRUT LOADS

east and west strut enclosing the centre bay of the north wall. The strut load component due to the earth pressure and the component due to the water pressure are indicated at each strut level. At times it was not possible to obtain strain readings at each strut level because of the high water level within the excavation or the loss of a set of gauges. The missing strut loads were therefore interpolated from the readings before and after in order to determine the sum of the strut loads over the whole section. The forces in the struts corresponding to the water pressure were calculated from flow net analyses as outlined in Section 5.2.4 below. Table 5.2.2 lists the strut load measurements.

To give a more realistic interpretation of these results the progress of excavation and water levels have also been indicated on the figures. An attempt was made to draw an apparent pressure distribution curve representing the lateral earth pressure on the sheet pile wall based on the strut load measurements. Fig. 5.2.39 shows the variation of net strut forces in kips with time. The contribution of the water pressure where applicable, is also shown.

5.2.4 Water Pressures

The hydrodynamics of steady-state water flow into an excavation has been dealt with in Chapter 4, Section 4.5. Due to the geometric complexity of the problem and the present lack of mathematical solutions

Day	Date 1964	EL. 762		EL. 753 Level A		EL. 741 Level B		EL. 730 Level C	
		Earth	Water	Earth	Water	Earth	Water	Earth	Water
28	Feb. 4	12.8	0						
30	Feb. 6	5.2	0	28.6	0				
38	Feb. 14	39.0	0	94.9	0				
45	Feb. 21	20.0	0	79.6	0	3.5	30.3		
46	Feb. 22			33.3	0	0.7	32.6		
49	Feb. 25			33.3	0	33.1	17.4		
50	Feb. 26	15.7	0	82.6	0	69.6	22.1		
51	Feb. 27			89.0	0	98.3	20.7		
55	Mar. 2							3.3	62.1
56	Mar. 3			44.3	0	51.7	14.7	37.9	57.8
57	Mar. 4	25.1	0	99.5	0	96.5	11.5	23.1	54.5
59	Mar. 6			66.7	0	68.7	20.0		
62	Mar. 9			44.3	0	23.9	20.4	42.9	68.0
64	Mar. 11			33.4	0	46.6	20.1	50.0	83.0
74	Mar. 21			44.4	0	57.4	9.3	90.4	53.6
76	Mar. 23			33.3	0	47.1	8.3	99.6	52.9
77	Mar. 24			33.3	0	91.6	8.3	92.1	52.0
85	Ap. 1	31.2	0	87.5	0	49.3	9.2	54.0	54.4
86	Ap. 2			44.3	0	47.2	8.3	68.7	53.4
99	Ap. 15			44.3	0	54.4	12.1		
114	Ap. 30			44.4	0.6	22.5	44.0	128.5	79.5
162	June 17						1.4	148.5	27.5
163	June 18						1.4	171.5	27.5

TABLE 5.2.2

STRUT LOADS IN KIPS

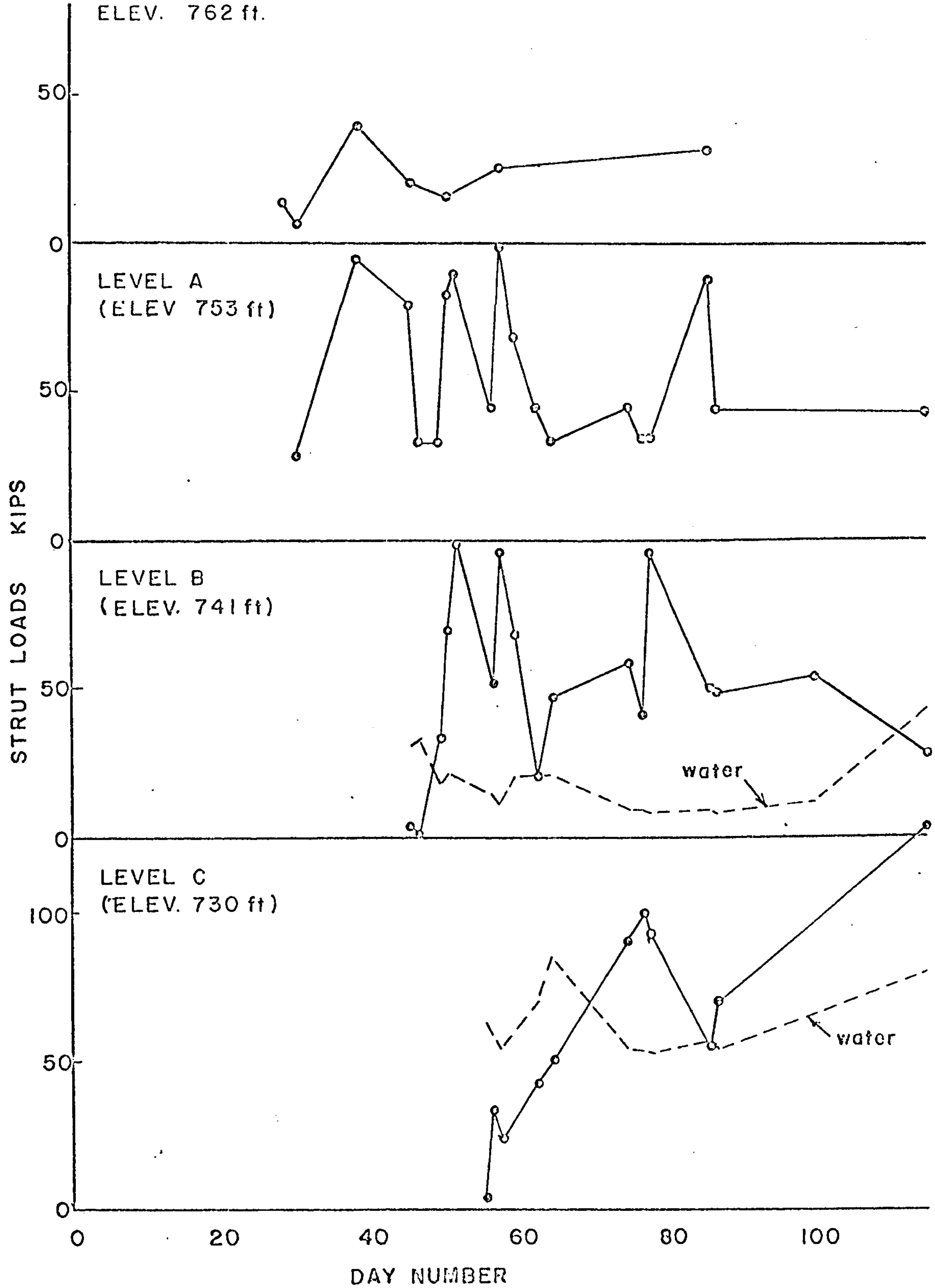

FIG. 5:2·39 INDIVIDUAL STRUT LOADS

the sketch flow-net method was used throughout in determining the steady-state seepage conditions. Flow nets are an extremely powerful and useful engineering tool even for persons possessing moderate skill and they develop a clear physical understanding of the hydrodynamics involved. The flow nets constructed for the different hydraulic conditions were considered sufficiently accurate in determining the water pressures on the back of the sheeted excavation. The water pressure acting directly on the retaining structure was obtained from three piezometers, P 10, P 11, and P 12, which were of the standpipe type mounted on sheet pile No. 13. The piezometers were located at elevations 743.8 feet, 733.5 feet, and 725.0 feet, respectively. There were also several standpipes north of the wall and inside the pit to allow a reasonable accurate location of the potential lines inside and outside the excavation. A continuous record of the water levels of the 25 piezometers located around the periphery and inside the excavation and of the level of the Thames River were obtained during the month of March. Fig. 5.2.40 shows the location of these standpipes and Fig. 5.2.41 indicated the fluctuation of the water levels of Thames River and the water level inside and outside of the excavation at the north wall. Of particular interest, of course, were the water level observations directly behind the north wall at the same time as pressure cell readings were taken. Flownets were constructed for every earth pressure or strut strain

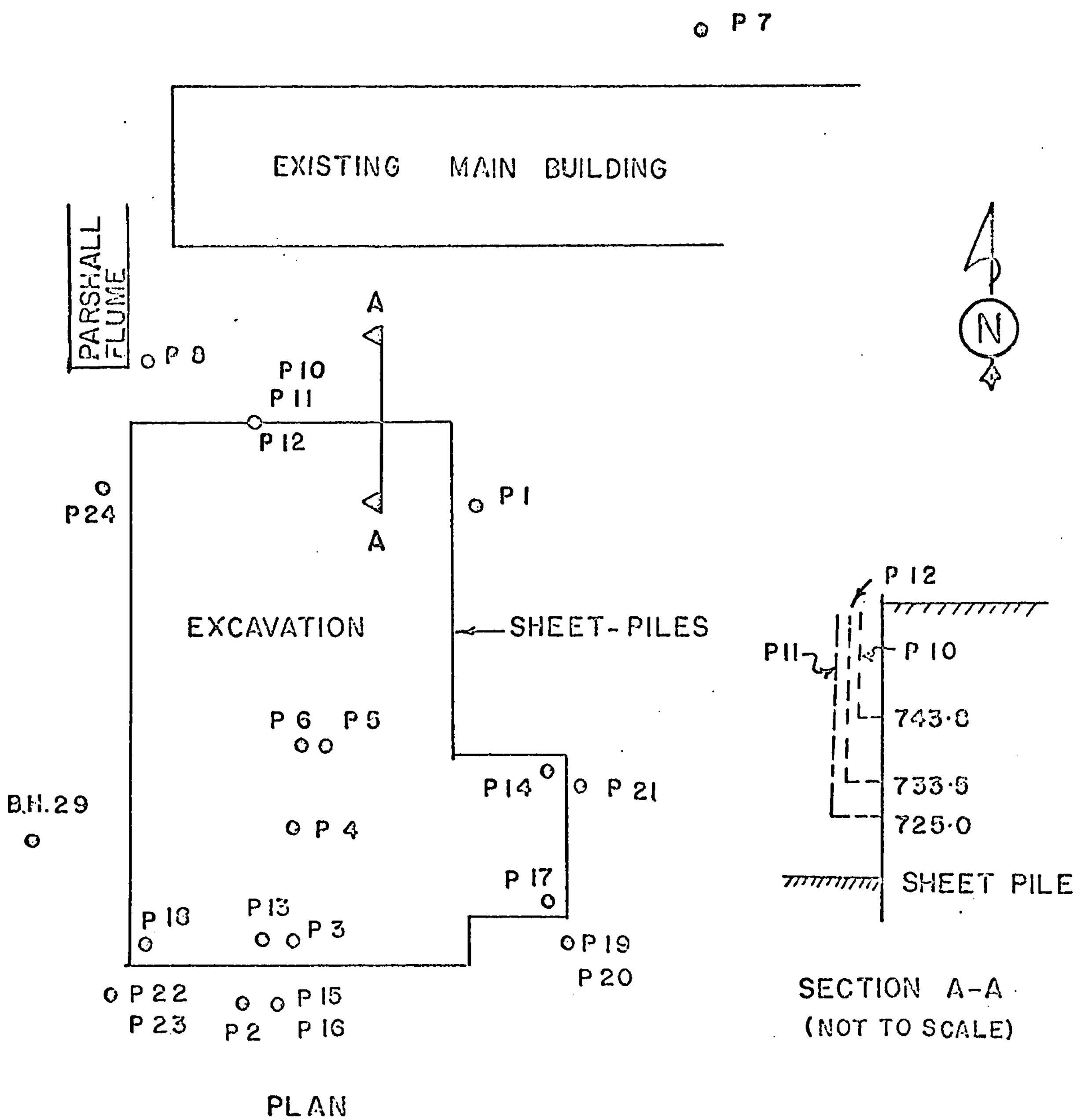

NOTE: THAMES RIVER LOCATED APPROXIMATELY 250' NORTH OF EXCAVATION

FIG. 5.2.40 LOCATION OF PIEZOMETERS

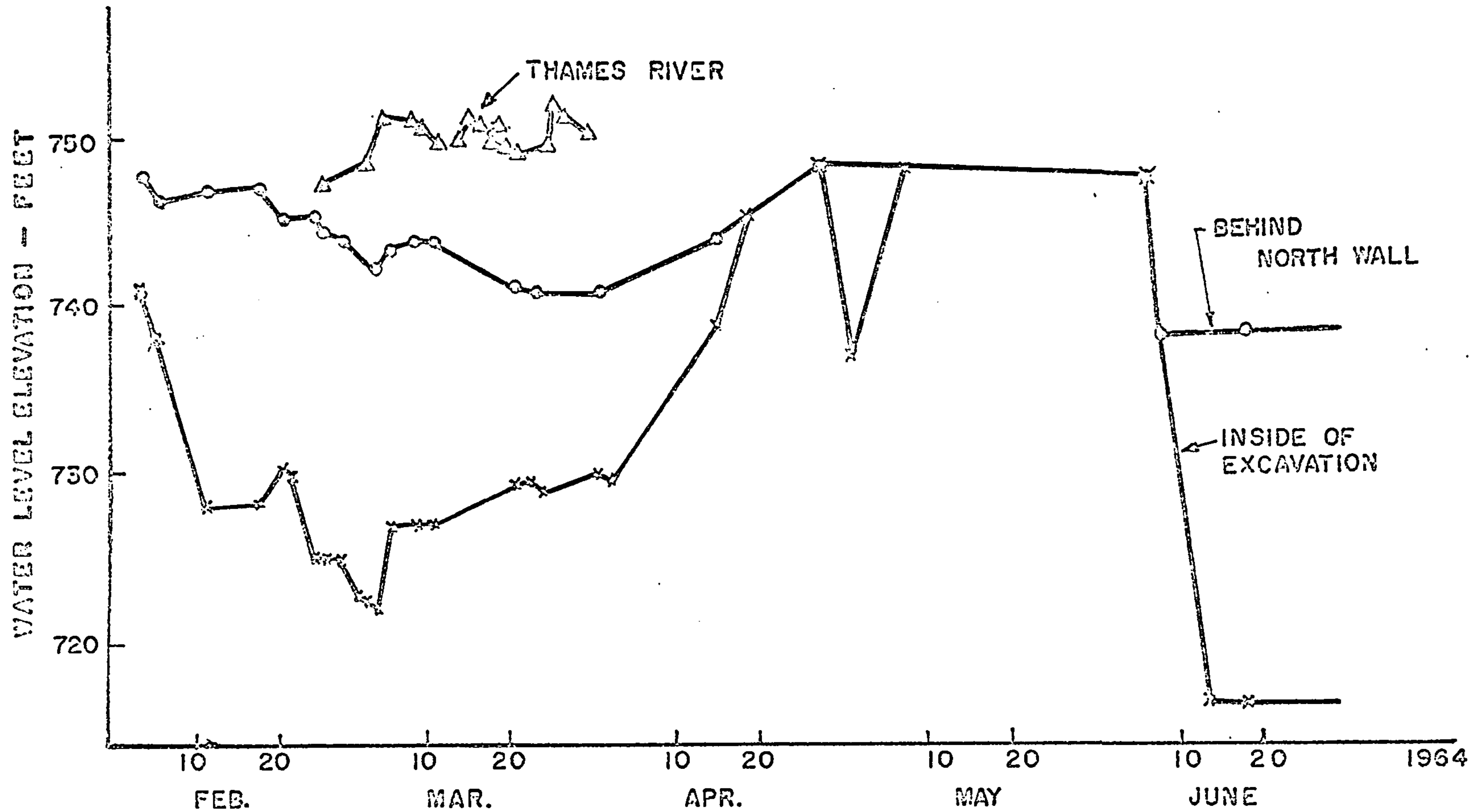

FIG. 5.2.41 CHANGE OF WATER LEVELS

gauge reading, twenty-five in total. Because of the similarity of these diagrams, only five have been shown in Figs. 5.2.42 to 5.2.46. These indicate the major changes of the free water surface inside and outside of the excavation at the north wall. The drawdown of the free water surface behind the sheet pile wall was surprisingly minimal and generally could be considered negligible especially when the difference of water levels between the outside and the inside of the excavation was small.

All the flownets were drawn disregarding the effect of the well point systems. The first well point system was inadequate and the discharge from it was so small that it was assumed that the flow pattern was as shown in Figs. 5.2.42 to 5.2.45. Only two sets of earth pressure readings were taken after the new well point system had been installed. For both sets of readings the water level inside the excavation was well below cell G-7 at elevation 618.5 feet.

5.2.5 Sheet Pile Movement

The deformation behaviour of two sheet piles, No. 13 and No. 15, were observed over a five month period. The bottom of the excavation was reached on March 7th (day 59) and readings of lateral deflections and movement of pile tops were continued until June 23rd (day 168).

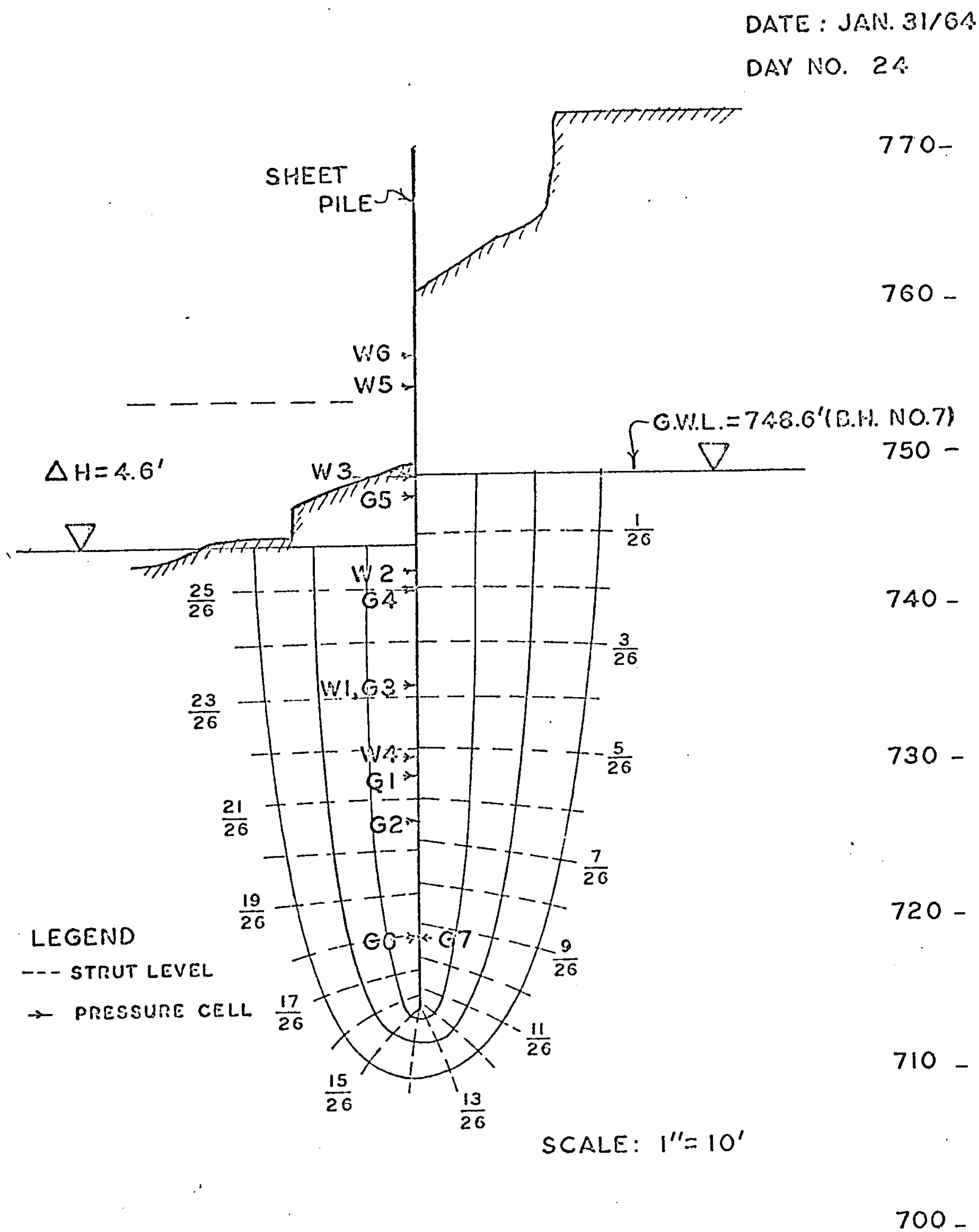

FIG. 5.2.42 SEEPAGE PRESSURES ON SHEET PILES NO. 13, NO.14 AND NO.15

DATE: FEB. 12/64
DAY NO. 36

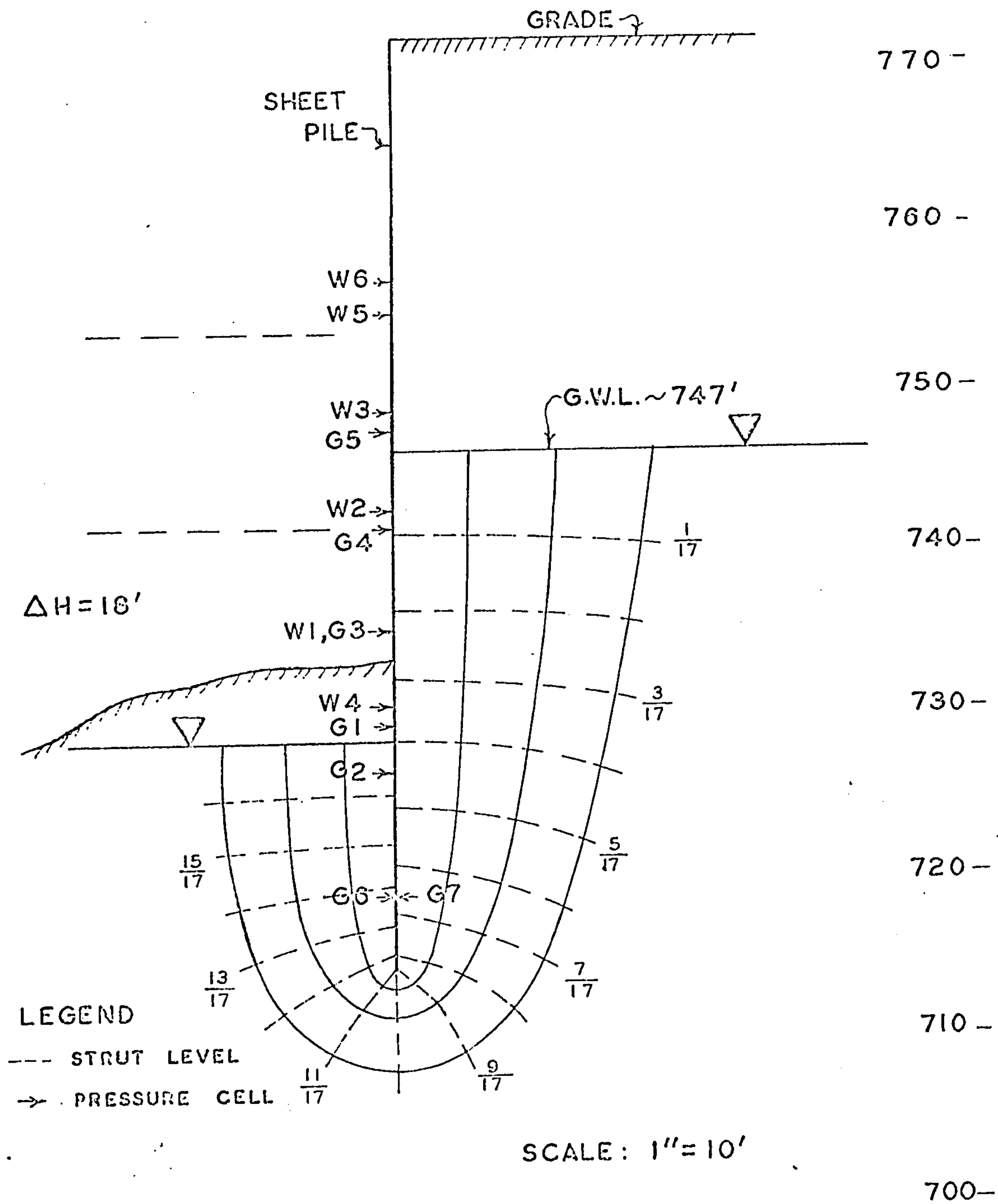

FIG. 5.2.43 SEEPAGE PRESSURES ON SHEET PILES NO. 13, NO. 14 AND NO. 15

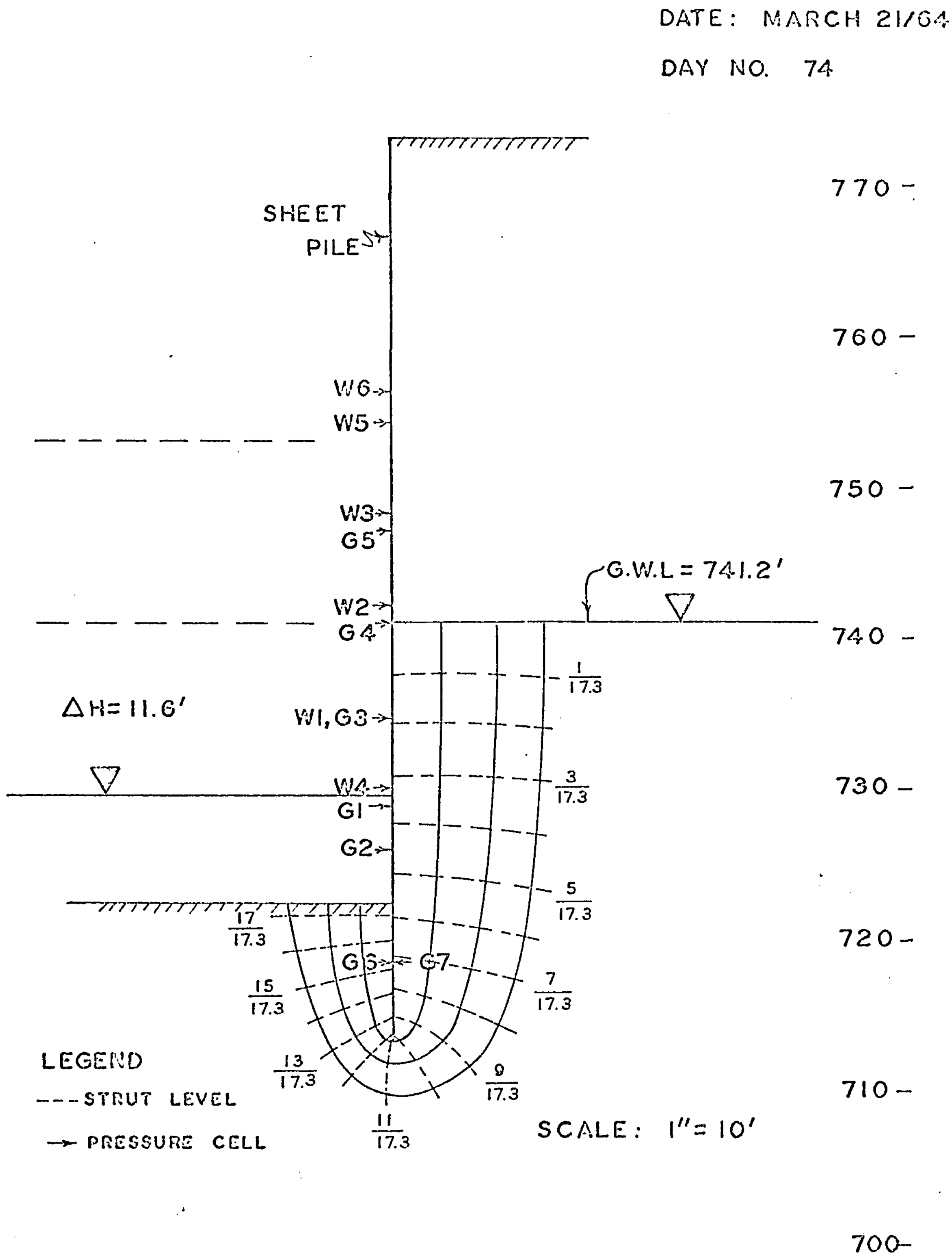

FIG. 5.2.44 SEEPAGE PRESSURES ON SHEET PILES NO. 13, NO. 14 AND NO. 15

DATE: APRIL 30/64
DAY NO. 114

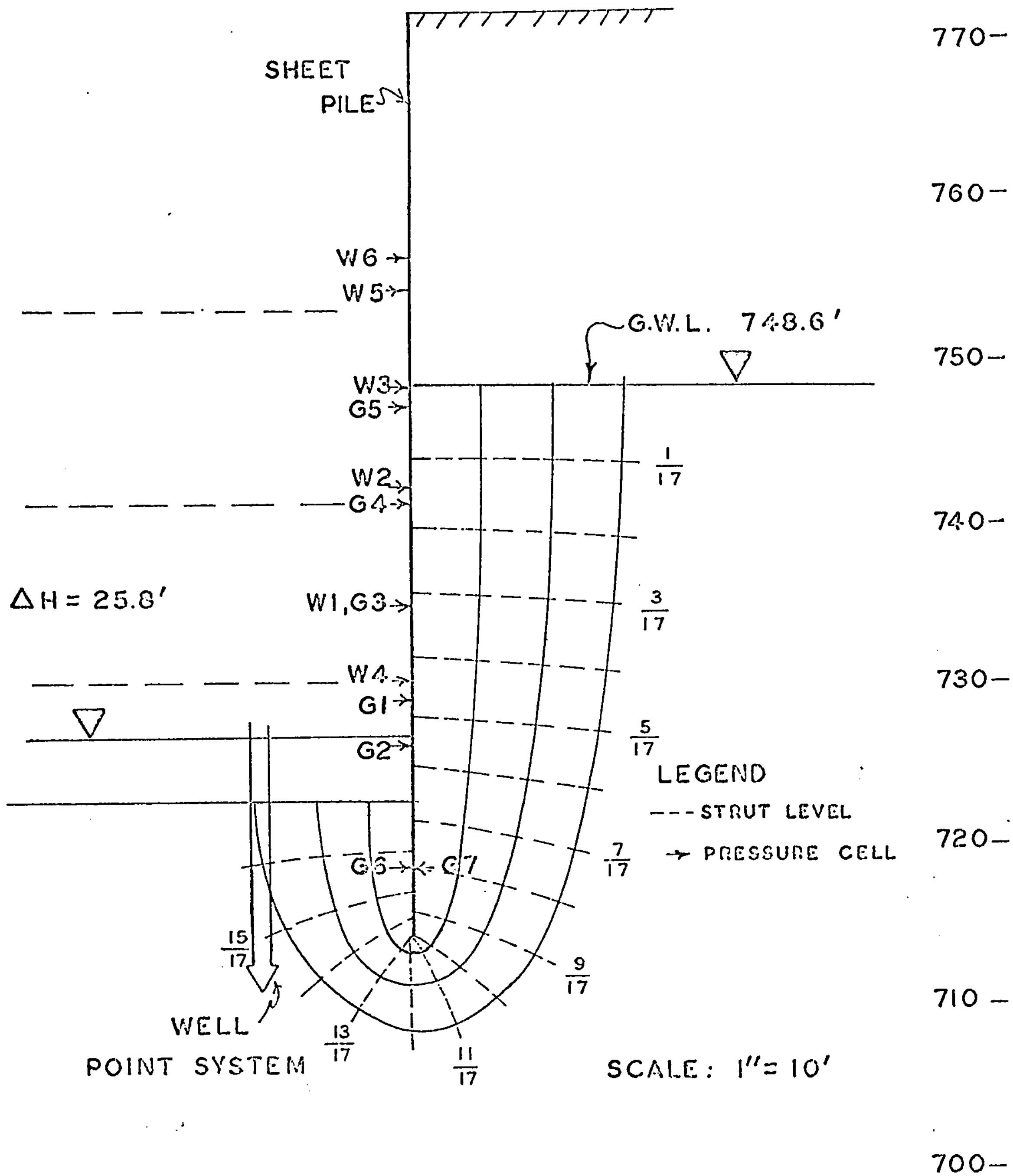

FIG. 5.2.45 SEEPAGE PRESSURES ON SHEET PILES NO. 13, NO. 14 AND NO. 15

DATE: JUNE 17,18/64

DAY NO. 162, 163

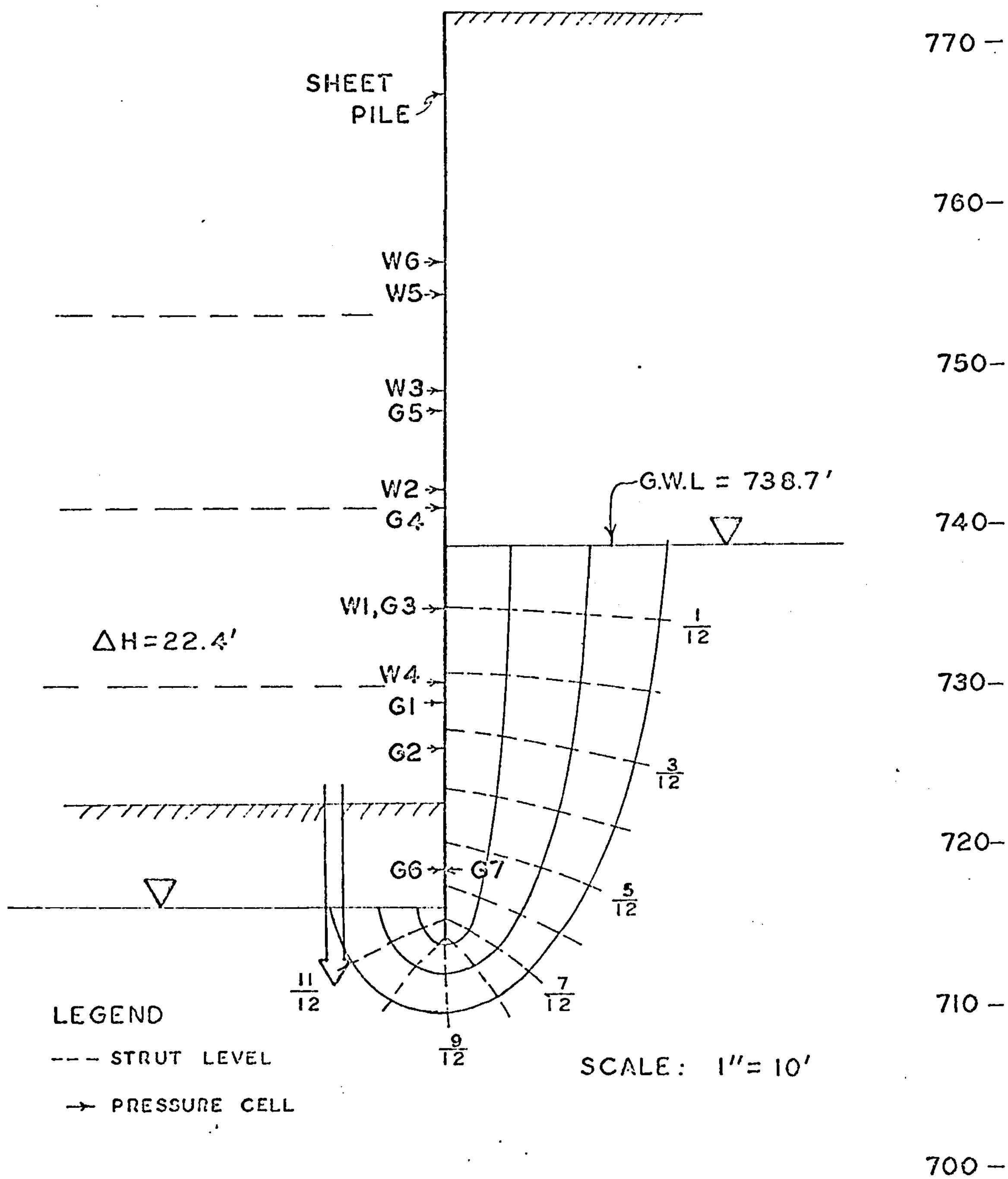

FIG. 5.2.46 SEEPAGE PRESSURES ON SHEET PILES NO. 13, NO. 14 AND NO. 15

Fig. 5.2.47a shows the position of pile No. 13 and Fig. 5.2.47b shows the position of pile No. 15 throughout the observation period. On day 21 (Jan. 28) the piles were fully driven and excavation had not commenced. The pile tops were approximately five feet above the ground surface at elevation 763 feet.

The position of the two piles from the baseline was established on day 11 when the piles were driven only 14 feet into the ground. The piles were held in vertical alignment by a steel template consisting of two horizontal steel beams spaced 20 feet apart vertically. The stiff interlocking pile sections were guided during driving by this steel template. The completed excavation showed that the piles were very straight with very little curvature. The maximum offset from a chord connecting the top and bottom of the 50 foot sheet piles was 2 inches. From the above observations it was held that the relative positions of the piles when partially driven and when fully driven did not change appreciably. Therefore the initial position of the two test piles was obtained by superimposing the measured position of day 11 onto the exposed portion of the piles of day 21. The total movement from the assumed initial position to the measured final position was similar for the two piles and confirmed the validity of the assumption of the initial position of the piles.

Initially there was a difference of six inches between the tips of piles No. 13 and No. 15 as measured from the baseline whereas

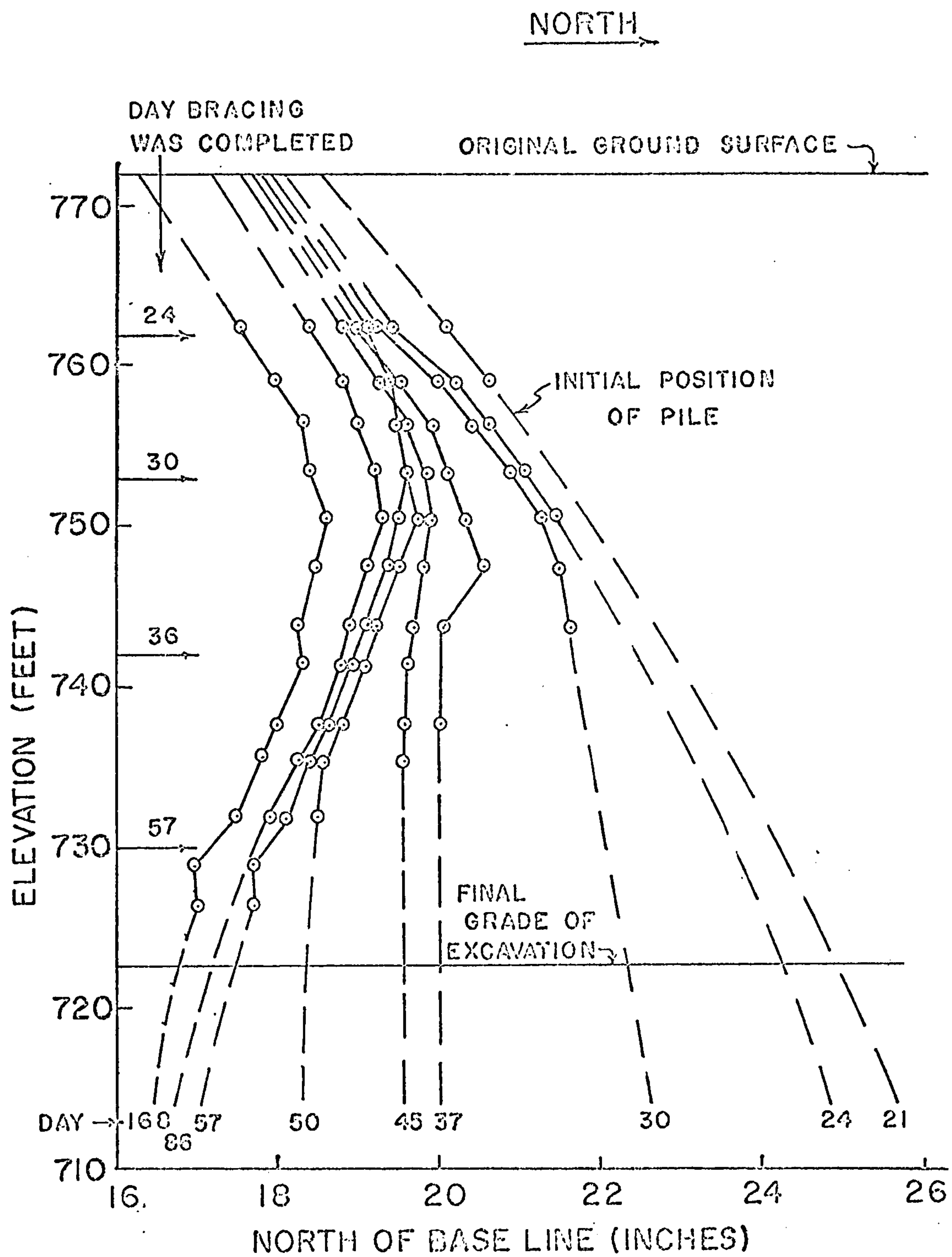

FIG. 5.2.47 a POSITION OF PILE NO. 13

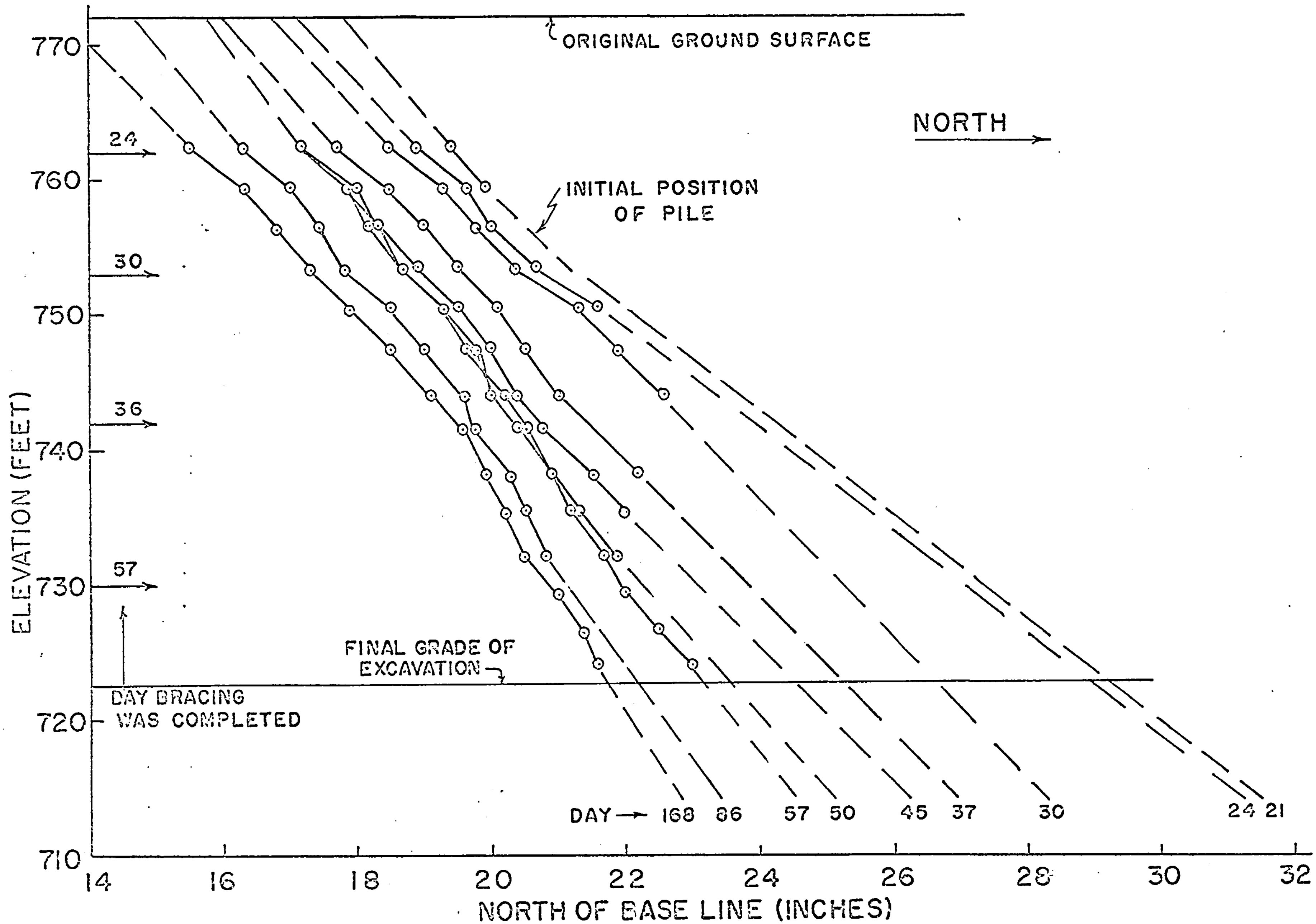

FIG. 5.2.47b POSITION OF PILE NO. 15

for the pile tops this difference was only one inch. The difference of initial pile position was caused by pile No. 14 which had to be kept away from the guiding template in order to prevent the attached pressure cells from being scraped off. Pile No. 13 was 7 inches and pile No. 15 was 14 inches off plumb initially. These batters were hardly noticeable with the naked eye considering that they occurred over a 58 foot pile length. Both pile tops were leaning towards the future excavation.

Figs. 5.2.48a and 5.2.48b show the movement of piles No. 13 and No. 15 respectively. It is assumed that the movement of the two test piles can be considered to be representative of, at least, the centre portion of the wall. The general trend of deformation of the wall was initially a pronounced translational movement towards the excavation. The top strut at elevation 762 feet was placed at day 24. By this time the wall at this elevation had moved 0.5 of an inch. It deformed an additional 3 inches on the average by day 168. Therefore the installation of the struts at this level did not prevent the top of the wall from moving further towards the excavation. This was mainly due to poor wedging. Wooden wedges were driven from one direction only resulting in a small contact area and crushing of the wedges. Some wedges fell out during the construction period giving more room for the sheet piles to move. The two inclined struts at elevation 762 feet were

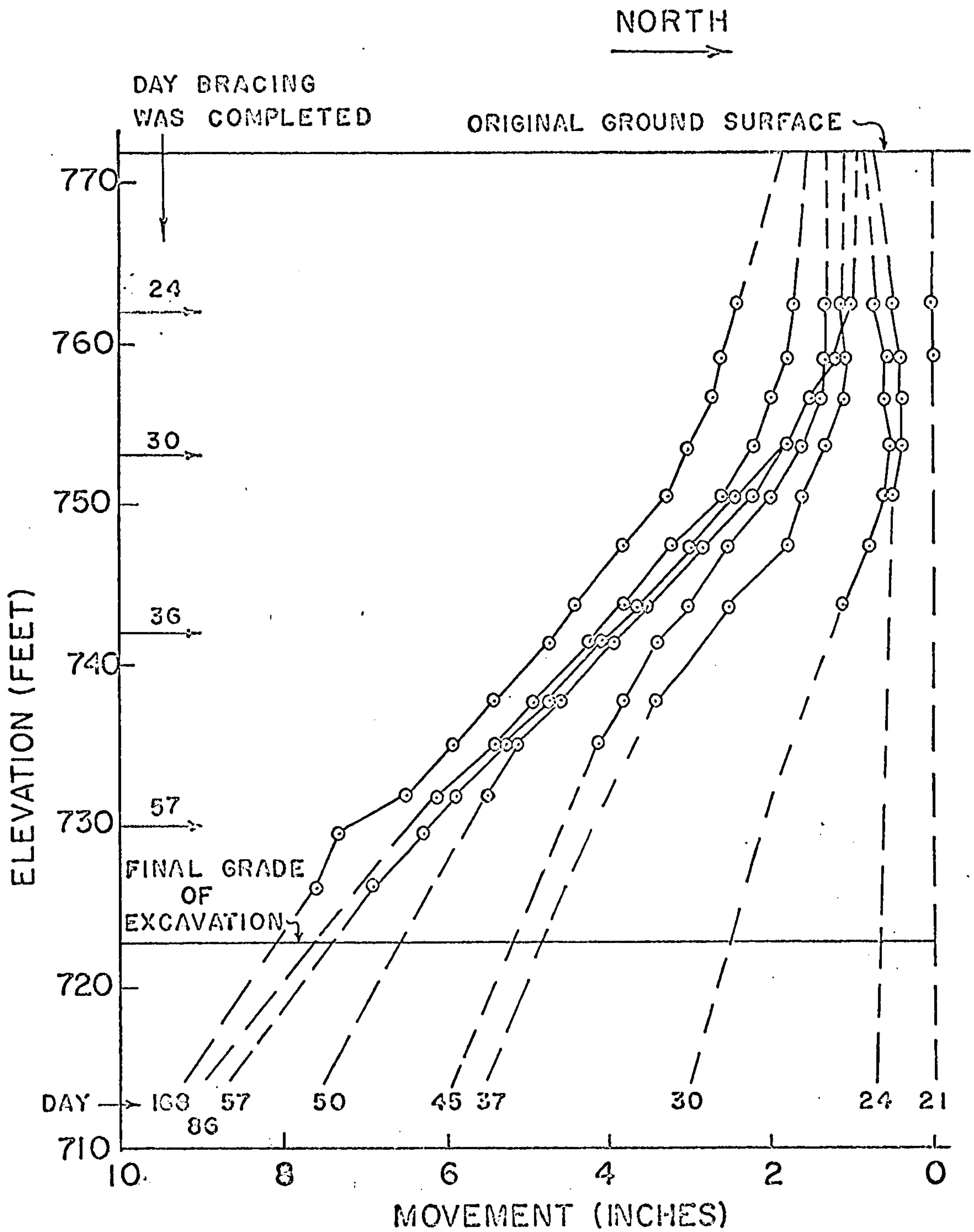

FIG. 5.2.48 a MOVEMENT OF PILE NO. 13

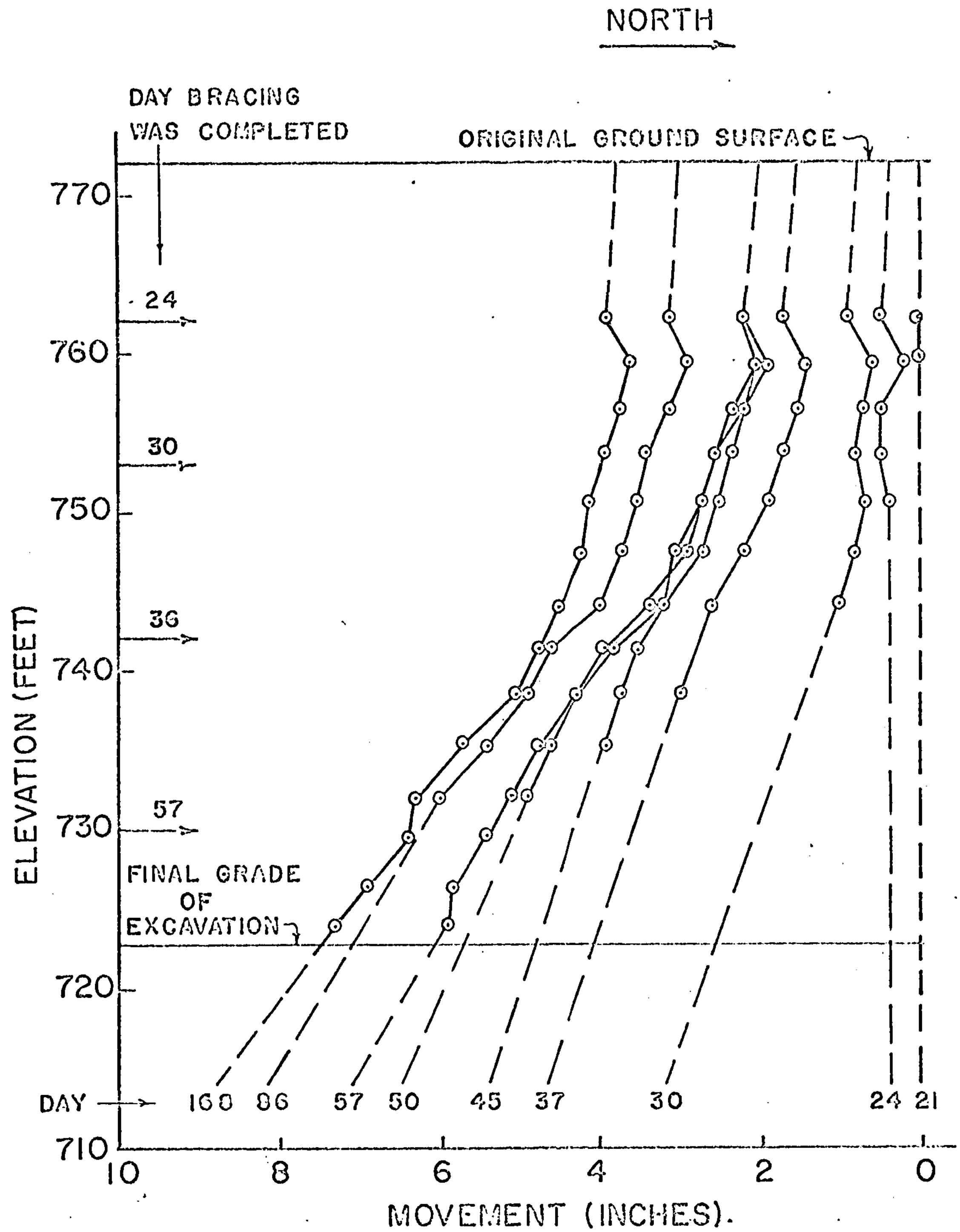

FIG. 5.2.48 b MOVEMENT OF PILE NO. 15

braced against the sheet piles of the east and west wall respectively and did not provide adequate supports. This arrangement of bracing was probably responsible for the large movement (three inches) of the upper part of the north wall occurring after installation of the struts. The ground surface behind the north wall was approximately 12 feet higher than behind the other three sides of the excavation and the higher pressure on the north wall tended to shift the bracing system southward.

As the excavation proceeded below elevation 750 feet, a distinct rotational movement of the piles towards the excavation was measured having a pivot at the second strut level (elevation 753 feet). For the lower part of the wall most of the movement did occur before the struts were installed at their respective levels. The final movement of the two sheet piles is shown by the curves of day 168 in Figs. 5.2.48a and 5.2.48b and resembles approximately the movement of a rigid wall translating and at the same time rotating about its top point.

Fig. 5.2.49 shows the movement of the pile tops at elevation 763 of the entire north wall. Initially the piles terminated at this elevation. Later, additional sections were welded on to extend the wall to elevation 772 feet, the original ground surface. The position of the pile tops on day 21 (Jan. 28) were taken as zero position. Only the movement of the tops of the even numbered piles and piles No. 13 and

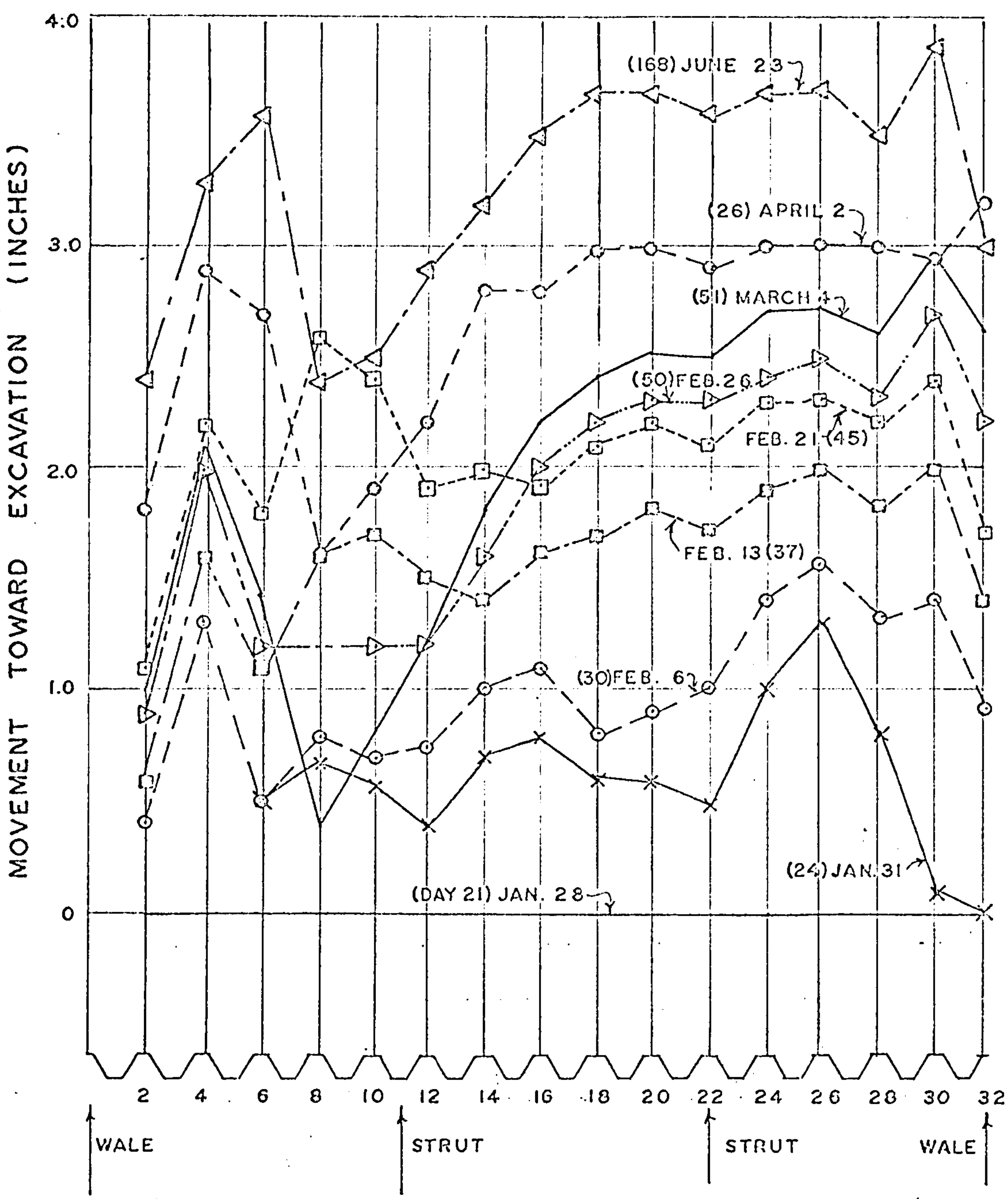

FIG. 5.2.49 MOVEMENT OF PILE TOPS

No. 15 were measured. The top of pile No. 13 deflected 2.4 inches whereas the top of pile No. 15 moved 3.9 inches towards the open cut. The average of these two movements is 3.2 inches which is exactly the distance the top of pile No. 14 had moved during the same time. The movement of the pile tops at the centre bay of the north wall over the five month period averaged 3.5 inches, one inch of it occurring after the excavation had reached final grade.

The measured positions and movements of the piles are tabulated in Tables 5.2.3 and 5.2.4.

A more detailed discussion and interpretation of the wall deformation will be given in Chapter 6.

5.3 Results of Laboratory Measurements

5.3.1 General

Seven field samples from different depths within the excavation were obtained in order to evaluate the relevant index properties and to establish representative shear strength parameters.

The soil consisted of closely graded cohesionless sand having the grading curve shown in Fig. 5.1.2 (page 136). The grains under the microscope appeared round and polished, the predominant mineral being colourless quartz. The index properties which were determined were the specific gravity and the relative density. The in situ dry

Pile No.	Pile Elev-Ft	Jan 28	Jan 31	Feb 6	Feb 13	Feb 21	Feb 26	Mar 4	Ap 2	June 23
	Date / Day	21	24	30	37	45	50	57	86	168
13	762.3	0	0.5	0.7	1.1	1.3	1.0	1.0	1.7	2.4
	759.0	0	0.4	0.6	1.1	1.3	1.2	1.2	1.8	2.6
	756.5	0	0.4	0.6	1.1	1.4	1.5	1.5	2.0	2.7
	753.5	0	0.4	0.5	1.3	1.6	1.8	1.8	2.2	3.0
	750.5	0	0.5	0.6	1.6	2.0	2.2	2.4	2.6	3.3
	747.3	0		0.8	1.8	2.5	2.8	2.9	3.2	3.8
	743.8	0		1.1	2.7	3.0	3.5	3.6	3.8	4.4
	741.3	0				3.4	3.9	4.1	4.2	4.7
	737.8	0			3.4	3.8	4.6	4.7	4.9	5.4
	735.3	0				4.1	5.1	5.3	5.4	5.9
	731.8	0					5.5	5.9	6.1	6.5
	729.3	0						6.3		7.3
	726.3	0						6.9		7.6
15	762.4	0	0.5	0.9	1.7	2.2	2.2	2.2	3.1	3.9
	759.2	0	0.2	0.6	1.4	2.0	2.0	1.9	2.9	3.6
	756.6	0	0.5	0.7	1.5	2.2	2.3	2.2	3.1	3.7
	753.7	0	0.5	0.8	1.7	2.3	2.5	2.5	3.4	3.9
	750.7	0	0.4	0.7	1.9	2.5	2.7	2.7	3.5	4.1
	747.5	0		0.8	2.2	2.7	2.9	3.0	3.7	4.2
	744.0	0		1.0	2.6	3.2	3.6	3.4	4.0	4.5
	741.5	0				3.5	3.9	3.8	4.6	4.7
	738.0	0			3.0	3.7	4.3	4.3	4.9	5.0
	735.5	0				3.9	4.6	4.7	5.4	5.7
	732.0	0					4.9	5.1	6.0	6.3
	729.5	0						5.4		6.4
	726.5	0						5.8		6.9
	724	0						5.9		7.3

Total Movement of Piles - inches

TABLE 5.2.3

MOVEMENT OF PILES NO. 13 AND NO. 15

Pile No.	Day Date	21 Jan 28	24 Jan 31	30 Feb 6	37 Feb 13	45 Feb 21	50 Feb 26	57 Mar 4	86 Ap 2	168 June 23
		Total Movement of Pile Tops - inches								
2		0		0.4	0.6	1.1	0.9	1.0	1.8	2.4
4		0		1.3	1.6	2.2	2.0	2.1	2.9	3.4
6		0	0.5	0.5	1.1	1.8	1.2	1.4	2.7	3.6
8		0	0.7	0.8	1.6	2.6	0.8	0.4	1.6	2.4
10		0	0.6	0.7	1.7	2.4	1.2	0.8	1.9	2.5
12		0	0.4	0.6	1.5	1.9	1.2	1.2	2.2	2.9
13		0	0.5	0.7	1.1	1.3	1.0	1.0	1.7	2.4
14		0	0.7	1.0	1.4	2.0	1.6	1.8	2.8	3.2
15		0	0.5	0.9	1.7	2.2	2.1	2.2	3.1	3.9
16		0	0.8	1.1	1.6	1.9	2.0	2.2	2.8	3.5
18		0	0.6	0.8	1.7	2.1	2.2	2.4	3.0	3.7
20		0	0.6	0.9	1.8	2.2	2.3	2.5	3.0	3.7
22		0	0.5	1.0	1.7	2.1	2.3	2.5	2.9	3.6
24		0	1.0	1.4	1.9	2.3	2.4	2.7	3.0	3.7
26		0	1.3	1.6	2.0	2.3	2.5	2.7	3.0	3.7
28		0	0.8	1.3	1.8	2.2	2.3	2.6	3.0	3.5
30		0	0.1	1.4	2.0	2.4	2.7	3.0	2.9	3.9
32		0	0	0.9	1.4	1.7	2.2	2.6	3.2	3.0

TABLE 5.2.4

MOVEMENT OF PILE TOPS OF NORTH WALL

unit weights were established in the field by the sand cone and rubber balloon method. The maximum and minimum densities were obtained in the laboratory as will be outlined in Section 5.3.3.

The internal angle of friction was established from direct shear box and triaxial compression tests. Two different sizes of shear boxes were used, a large shear box with a 5 inch square box and a 2.5 inch diameter round box. All direct shear tests were carried out on dry samples. Drained triaxial tests were performed on sand samples in the dry state as well as in the saturated state with volume change measurements. It was realized that a correction had to be made to the results of the symmetric strain triaxial tests in order to apply these to the plane strain conditions in the field. It was felt that the results from the versatile and comparatively simple triaxial tests were more consistent and these were favoured in adopting respective shear strength values.

5.3.2 Specific Gravity

The true or absolute specific gravity (the specific gravity of the soil solids) of the seven samples were determined by the pycnometer bottle method. The results are listed in Table 5.1 (page 138). They ranged from 2.69 to 2.71. Each sample was tested at least three times, the specific gravity of each sample listed in column 4 of Table 5.1 is the average of these three determinations. The overall average of specific gravity of all seven sand samples was 2.70. This value was used in all calculations.

5.3.3. Relative Density

It is common to describe certain soils as having a high or low density depending on whether the particles are closely or loosely packed. It is evident that among other things, soil density is an index of compressibility, the loosely packed soils being far more compressible than those with greater density. Soil density, as used in this thesis, is measured in terms of weight of soil solids and voids per unit of soil volume. The term dry density or unit dry weight is defined as the weight of the soil solids per unit of soil volume. To judge whether a soil at a given void ratio, e, is to be described as dense or loose, it is necessary to establish its existing void ratio with respect to the range of possible void ratios for the particular soil. This is expressed by the term relative density, D_r, defined as,

$$D_r = \frac{e_{max} - e_{nat.}}{e_{max} - e_{min}} \tag{5.3.1}$$

There are certain practical difficulties in determining void ratios, one of which is the problem in measuring solid volumes. For this reason, it is sometimes advantageous to express relative density in terms of unit dry weight of soil, by substituting for e in Eq. (5.3.1) using the relation

$$\gamma_d = \frac{G\,\gamma_w}{1 + e} \tag{5.3.2}$$

thus

$$D_r = \frac{1/\gamma\ \text{min} - 1/\gamma\ \text{nat.}}{1/\gamma\ \text{min} - 1/\gamma\ \text{max}} \tag{5.3.3}$$

It is realized that Eqs. (5.3.1, 5.3.2, and 5.3.3) are basic equations of elementary Soil Mechanics, but because of the existence of different definitions it was believed that these terms should be redefined here for clarification.

There are unfortunately no standard tests for determining the maximum and minimum dry unit weights of sand, and hence a number of the more commonly recommended tests were used. The most expedient method and the most consistent results for the minimum dry density, that is, maximum porosity, were obtained by dry deposition (Kolbuszewski 1948).

To obtain the maximum dry density several methods were employed such as the standard and modified Proctor test and the vibro-flotation method (Pettibone and Hardin 1964), but they all failed to yield densities equal to or higher than the field densities. The only method which seemed to be successful for this type of sand was dynamic compaction using a compaction energy much higher than the standard Proctor test energy.

At a given moisture content, the density of a given soil varies with compaction effort. Usually as the compaction effort increases the maximum density increases until an absolute density is attained (assuming that the soil grains are not broken under high compaction efforts). The optimum moisture content is also variable, decreasing with increasing compaction effort. A slight variation of moisture content up to two per cent from optimum or either side did not seem to have any appreciable effect on the dry density of this sand. Therefore the sand samples were compacted at an arbitrary two per cent dry of the modified Proctor optimum water content, which was 12 per cent. Six tests were performed on each of the seven samples, successively increasing the compaction effort. At a compaction effort of 115 ft-kips per cu ft., more than nine times the compaction energy of the standard Proctor test, the maximum dry densities listed in Table 5.1 (page 139) were obtained. One test was carried out at a higher compaction energy but crushing of the sand grains occurred. It was held that the values listed in Table 5.1 are the absolute maximum dry densities for this particular sand. They were used in calculating the relative densities also shown in Table 5.1.

The minimum dry density found was 85.5 pcf and the maximum dry density was 127.1 pcf. Above an elevation of 740 feet the soil was medium dense with the relative density varying between 41 and 56 per cent, whereas below this level the soil was very dense with a range of D_r values between 95 and 100 per cent.

5.3.4 Shear Strength

All seven sand samples were mixed throughly together and a representative sample passing the No. 40 sieve was used for testing purposes. As mentioned in the foregoing section two distinctly different sand densities existed in situ. One averaged 103 pcf, the other one 123 pcf. Testing was done to find the shear strength parameters at these two densities and also to show how a slight variation of the test specimen density from the above two values would affect the strength parameters.

Because of the phenomenon of interlocking the strength of a dense cohesionless soil tends to be greater at small displacements than at large displacements where the effect of interlocking has been overcome. For a dense sand the stress-strain curve obtained in the laboratory shows a definite peak and then decreases to an ultimate or residual value at a higher strain. The angle of internal friction, ϕ, exhibits a similar behaviour when plotted against strain. The question whether to use the peak or the ultimate strength parameter depends on the particular problem. For any large scale model test or full-scale retaining wall for which measurements have been made it was always observed that the earth pressure reached a minimum value (active case) after the structure had yielded a certain amount. Any further yield of the wall did not change the earth pressure. A decrease of the shear strength parameter, ϕ, as exhibited for dense sand in the laboratory would necessitate an increase in the total active pressure. Therefore, the shear strength does not appear to decrease with large strains in model or field tests.

Another reason for using peak strength parameters is to facilitate comparison of results with the work of other researchers (Terzaghi 1934, Ohde 1938, Spilker 1937, and Klenner 1942) who based their calculations on the maximum strength values. When the term "strength" is used in this thesis, the peak strength is meant unless otherwise stated.

The direct shear box tests were performed on dry sand only. The sand was poured into the assembled box, a normal pressure was applied and then the whole assembly was vibrated until the desired density was achieved. The density was calculated from the weight and linear dimensions after assembly and compaction. After completion of the test the density was recalculated. The circular 2.5 inch diameter shear box gave consistently lower angles of internal friction than the large square box. For a density of 115 pcf this difference was as high as 7.5°. The sample thickness in the round box was only 0.5 inch and it was extremely difficult to measure the volume of the sand specimen due to the penetrating teeth of the bottom and the top cap of the shear box. It was believed that as the shearing strain was applied and the top half of the box started overlapping the bottom half, some of the normal pressure was transferred through the thick side walls of the box rather than the soil sample. Applying an area correction did not change the results markedly. The results from the small direct shear box were considered to be unrealistic and were not given further consideration.

The stress-strain curves and the corresponding volume changes for the large direct shear box tests are shown in Fig. 5.3.1. As seen from the curves the dense samples show a heavily dilatant structure, resulting in a net volume increase during shear. They failed at a low strain, about 1 to 1.5 per cent. The loose samples show, on the contrary, a volume reduction and the strain at failure was about 4 per cent. The normal stress on the samples was approximately 2 psi on all five specimens and the strain rate was 0.01 inch per minute. The internal angle of friction was determined for each density assuming a zero cohesion intercept.

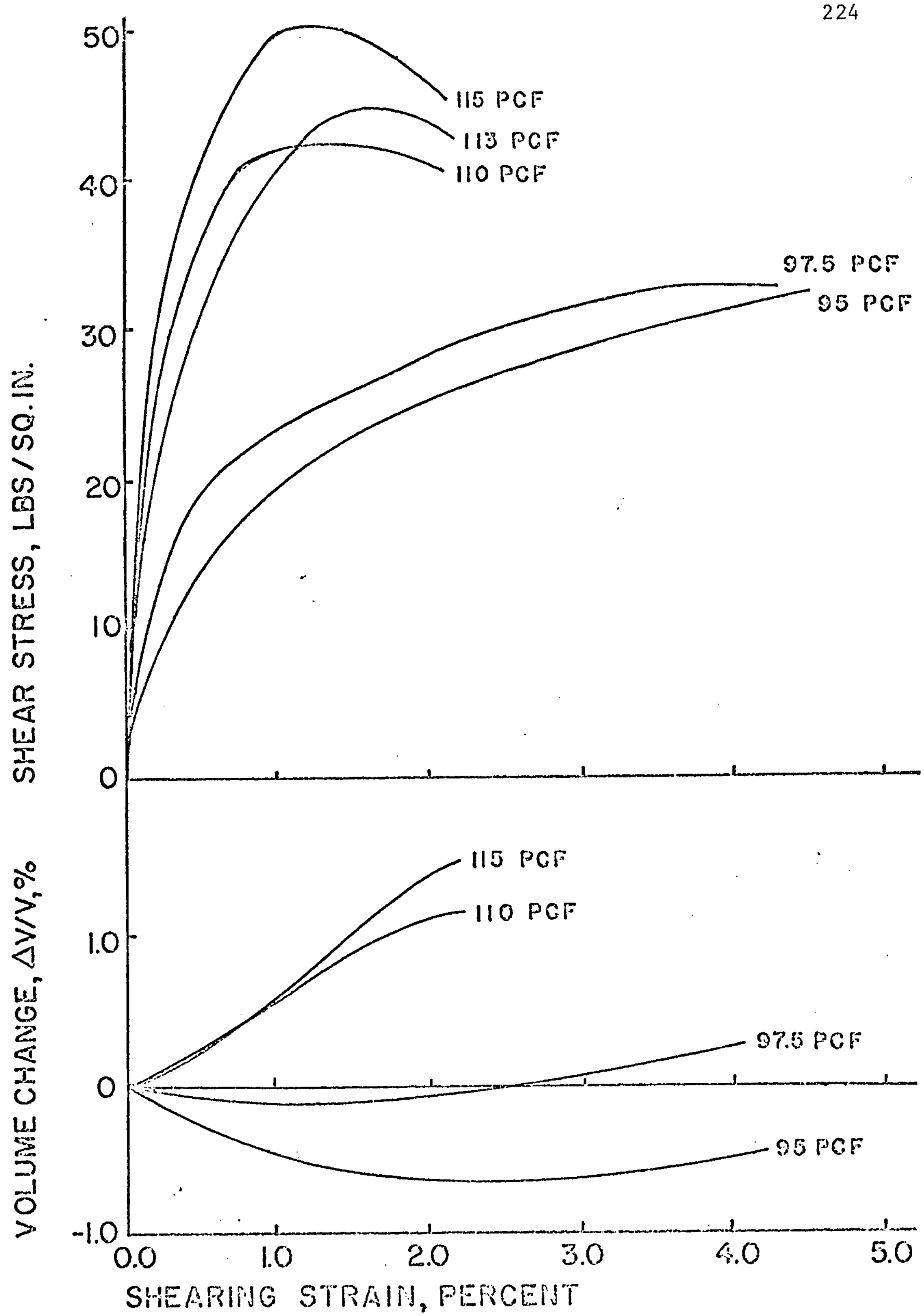

FIG. 5.3.1 STRESS STRAIN CURVES FOR DIRECT SHEAR BOX

To determine the shear strength parameters in a triaxial compression test, it is usually necessary to test specimens at different confining pressures. All the triaxial tests were done by multi-stage tests. As reported by Kenney and Watson (1961) and by Lumb (1964) this method of testing compares favourably to conventional testing procedures in the case of insensitive soils. The advantage of testing one specimen only instead of at least three is self-evident. The sample is prepared and consolidated as usual but the deviator stress is released once failure has commenced, that is, peak stress is reached. The lateral pressure is changed and the deviator stress is increased again until failure occurs. The sequence is repeated until sufficient results are obtained or until the deformation of the specimen is too great for reliable results to be expected.

Consolidated drained triaxial tests were carried out on dry and saturated sand samples. It was particularly difficult to prepare the dense samples. It was not possible for the saturated specimens to saturate the sand prior to compaction. In all instances where a density of more than 110 pcf was desired, the samples liquified in the mould during compaction. To overcome this the sand was compacted in layers in a split mould at 10 per cent moisture content. Compaction was achieved by a hand tamper and at the same time a vacuum of 14 psi was applied to the bottom of the sample. Care was taken to make the sample homogeneous. The maximum density which could be obtained by this method was 118 pcf. A further increase in compaction effort resulted in opening of the split mould. The samples were saturated by forcing de-aired water, under gravity flow, into the bottom of the sample and simultaneously applying a slight vacuum at the top drain. Six dry and two saturated samples having different densities were tested. Typical stress-strain curves are shown in Figs. 5.3.2 and 5.3.3. The dilatant characteristics for both dense saturated samples were almost identical. In the second stage ($\sigma_3 = 20$ psi) the maximum net volume increase was two per cent for a density of 115 pcf (Fig. 5.3.3.) and 2.5 per cent for a density of 117 pcf. The Mohr - Coulomb failure envelopes for the eight determinations are depicted in Figs. 5.3.4 and 5.3.5.

In Fig. 5.3.6 the angle of shearing resistance, ϕ, obtained from both testing methods are plotted against porosity and dry density. From this it can be seen that the triaxial and direct shear box tests give the same angle of shearing resistance for a density of 118 pcf (initial porosity: 29.9 per cent). Above this density the extrapolated shear box values are slightly higher than the triaxial. Below this the triaxial values are higher. Similar observations were made by Nash (1953). He also found that there was no appreciable difference in the angle ϕ for wet and dry tests. For a density of 123 pcf the extrapolated friction angles were 49° and 50.5° for the triaxial and direct shear tests

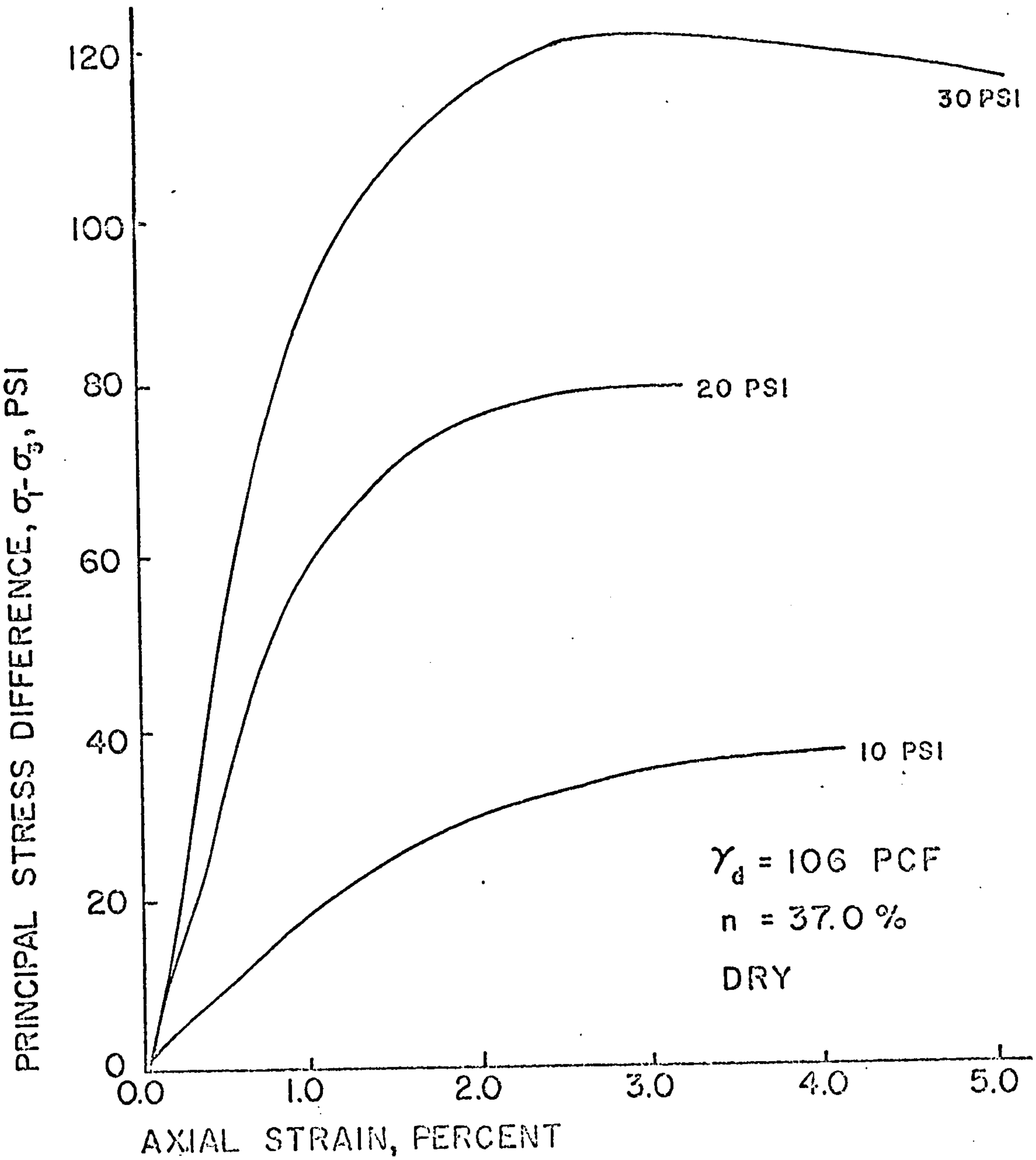

FIG. 5.3.2 STRESS STRAIN CURVES FOR DRAINED TRIAXIAL TESTS (DRY)

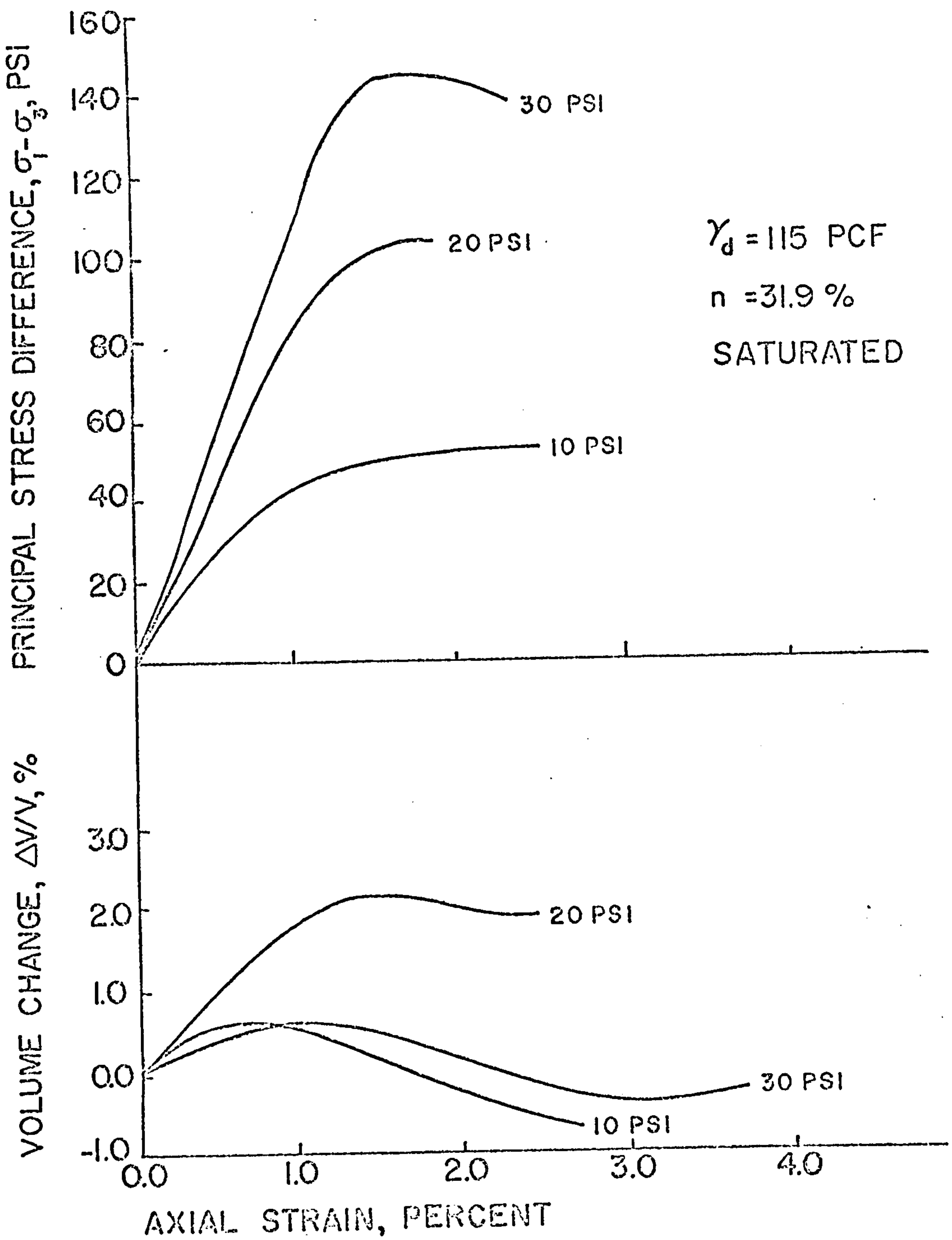

FIG 5.3.3 STRESS STRAIN CURVES FOR DRAINED TRIAXIAL TESTS (SATURATED)

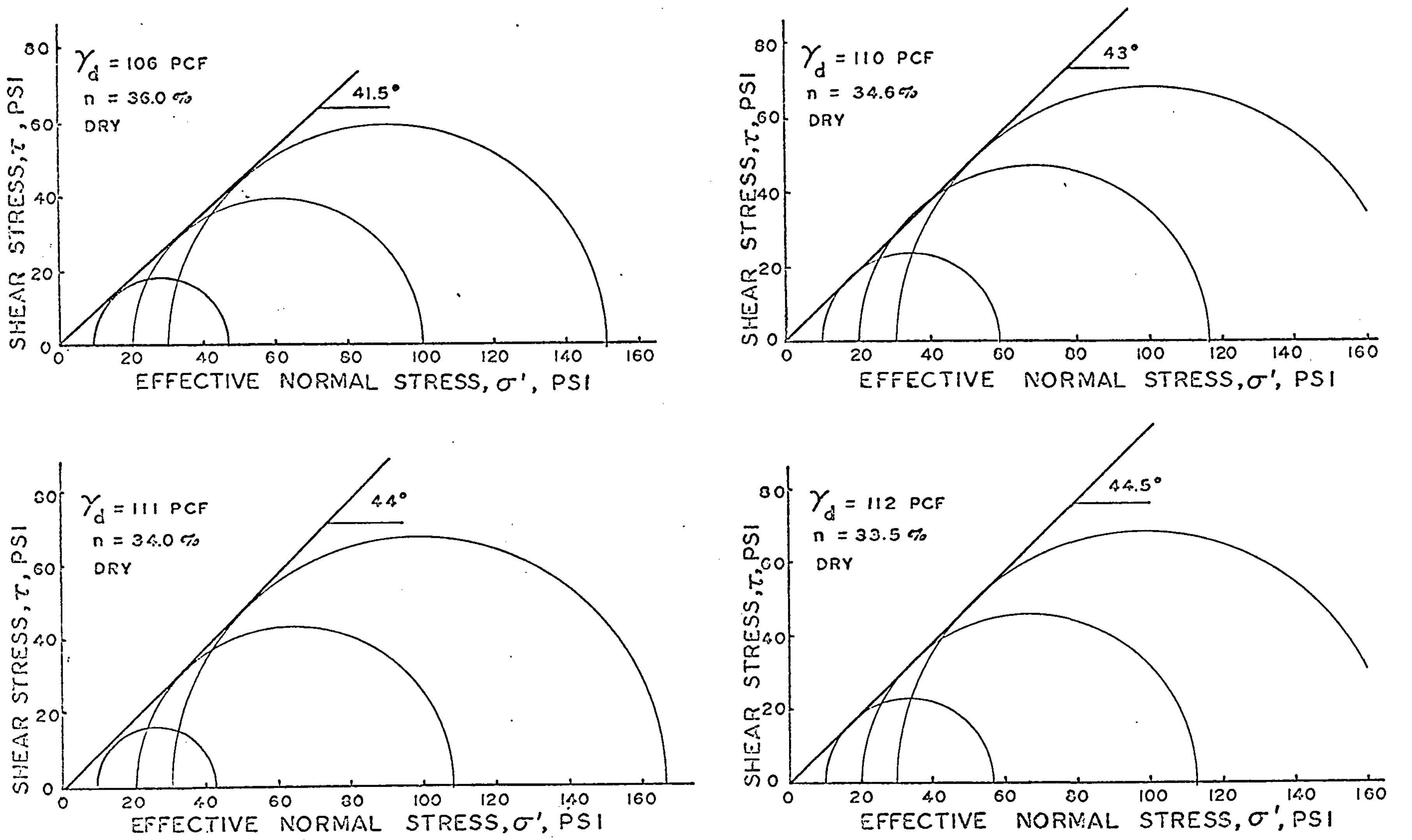

FIG. 5.3.4. MOHR DIAGRAMS FOR TRIAXIAL COMPRESSION TEST

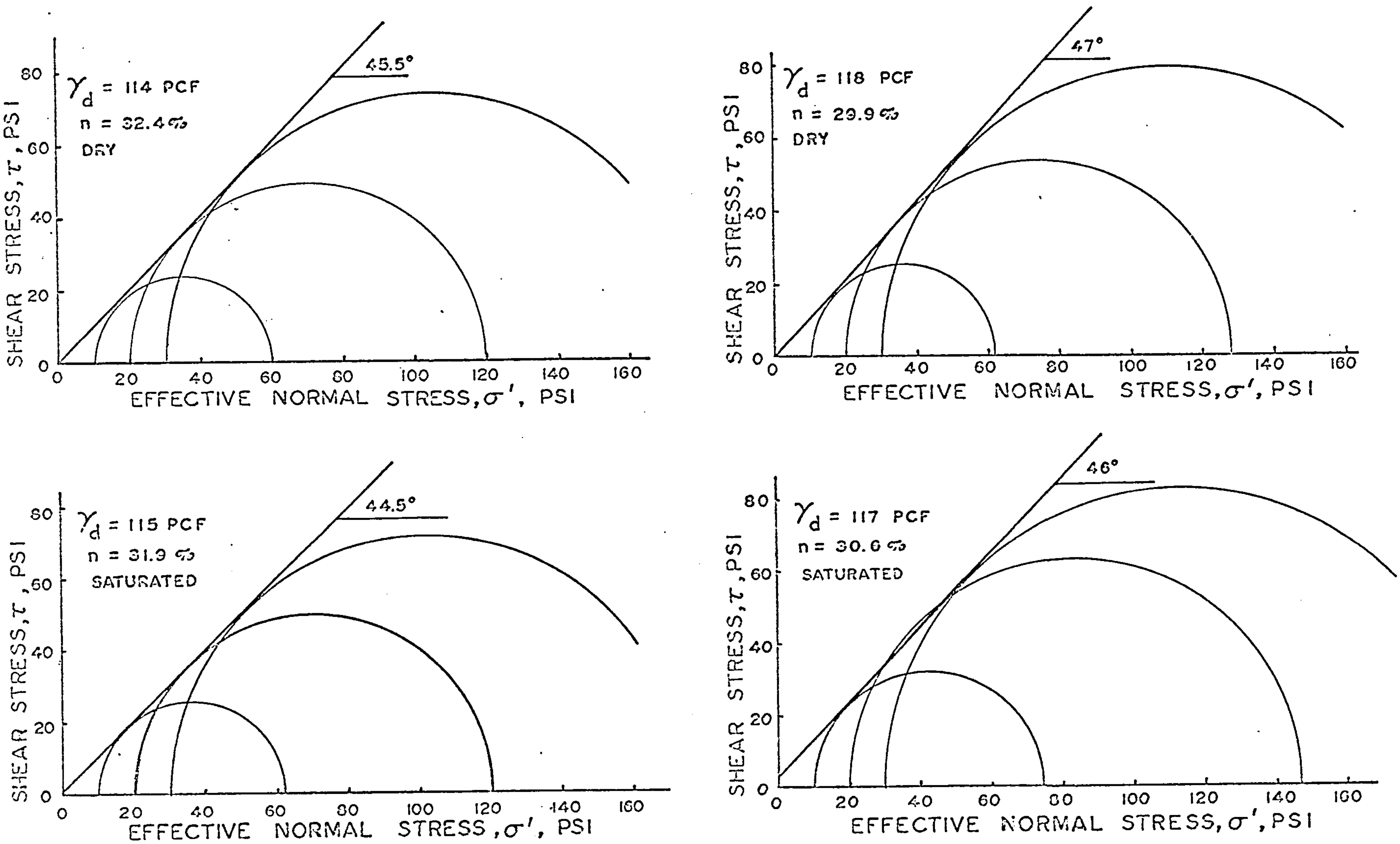

FIG. 5.3.5 MOHR DIAGRAMS FOR TRIAXIAL COMPRESSION TEST

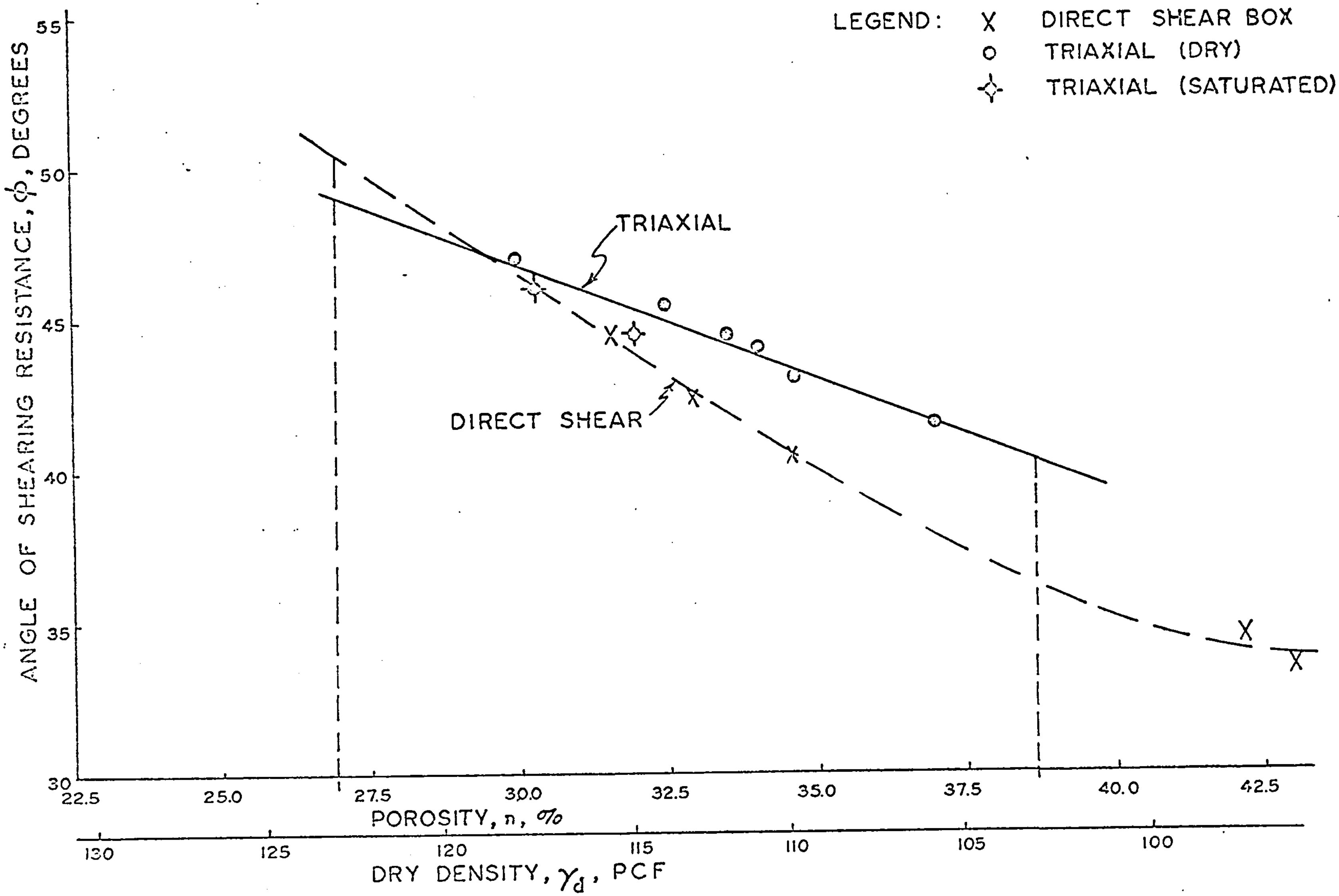

FIG. 5.3.6 VARIATION OF ϕ WITH POROSITY AND DRY DENSITY

respectively. The corresponding values for a dry density of 103 pcf were 40.5° and 36°.

Cornforth (1964) compared the results of triaxial compression tests with those from a plane strain apparatus for a poorly graded medium sand. Constructional details of this apparatus have been presented by Wood (1958). Cornforth found from these tests that the strength of the plane strain specimens were always greater than the strength of the corresponding triaxial specimens at the same density. The difference varied from $1/2^{\circ}$ at the looser densities to about 4° for the dense samples. The shape of both strength density curves were slightly concave upwards. Therefore it seems to be more realistic to increase the angle of shearing resistance from triaxial compression tests for calculation purposes involving plane strain problems. In accordance with this the following values were used:

For a dry density of 123 pcf, $\phi = (49.0^{\circ} + 3.0^{\circ}) = 52^{\circ}$.

For a dry density of 103 pcf, $\phi = (40.5^{\circ} + 1.5^{\circ}) = 42^{\circ}$.

CHAPTER 6

INTERPRETATION AND DISCUSSION OF EXPERIMENTAL MEASUREMENTS

6.1 General

In order to evaluate and generalize the results of the earth pressure measurements, it is desirable to determine a theoretical basis upon which the results can be compared. For many years the so-called classical earth pressure theories have been used for homogeneous materials whose shearing resistance is composed of both cohesion and internal friction.

At the London site the soil profile consisted exclusively of a cohesionless fine uniform sand of two distinct densities. Above an elevation of approximately 740 feet the relative density was medium and below this the relative density was very dense reaching 100 per cent at one location. Also below the water table the unit weight of the soil reduces to the buyant unit weight. Generally speaking then the soil behind the retaining structure consisted of a three-layered system; considering the soil below the water table as a separate stratum. This was reduced to a two-layered system when the waterlevel coincided with the interface of the medium and dense sand deposits. In order to refer easily to the different layers, the top medium dense sand deposit is referred to as layer 1, and the very dense layer as layer 2. Even within one layer the density was not quite uniform, as can be expected from any natural deposit. The average density for each sand layer was determined from the individual field density measurements.

The theoretical expressions for total lateral earth pressure as presented in Chapter 4 must be modified to take into account different soil parameters over the depth of the cut. The theory is adequate to serve, nevertheless, as the starting point in the analysis of the experimental results.

6.2 Earth Pressure and Deformations

6.2.1 Earth Pressure at Rest

Fig. 6.1 shows the soil profile and initial water level at the London site after the sheet piles were driven to grade and before excavation started. This is a typical example of an at-rest condition, assuming that the driving of the piles did not disturb the soil appreciably. The ground water table was established in a bore-hole at an elevation of 750 feet. Above the water table the soil was partially saturated, as established by the field density tests, whereas below the water table the soil was taken as completely saturated. At elevation 740 feet a definite change in density occurred. This was determined by field density tests. The different densities for the two

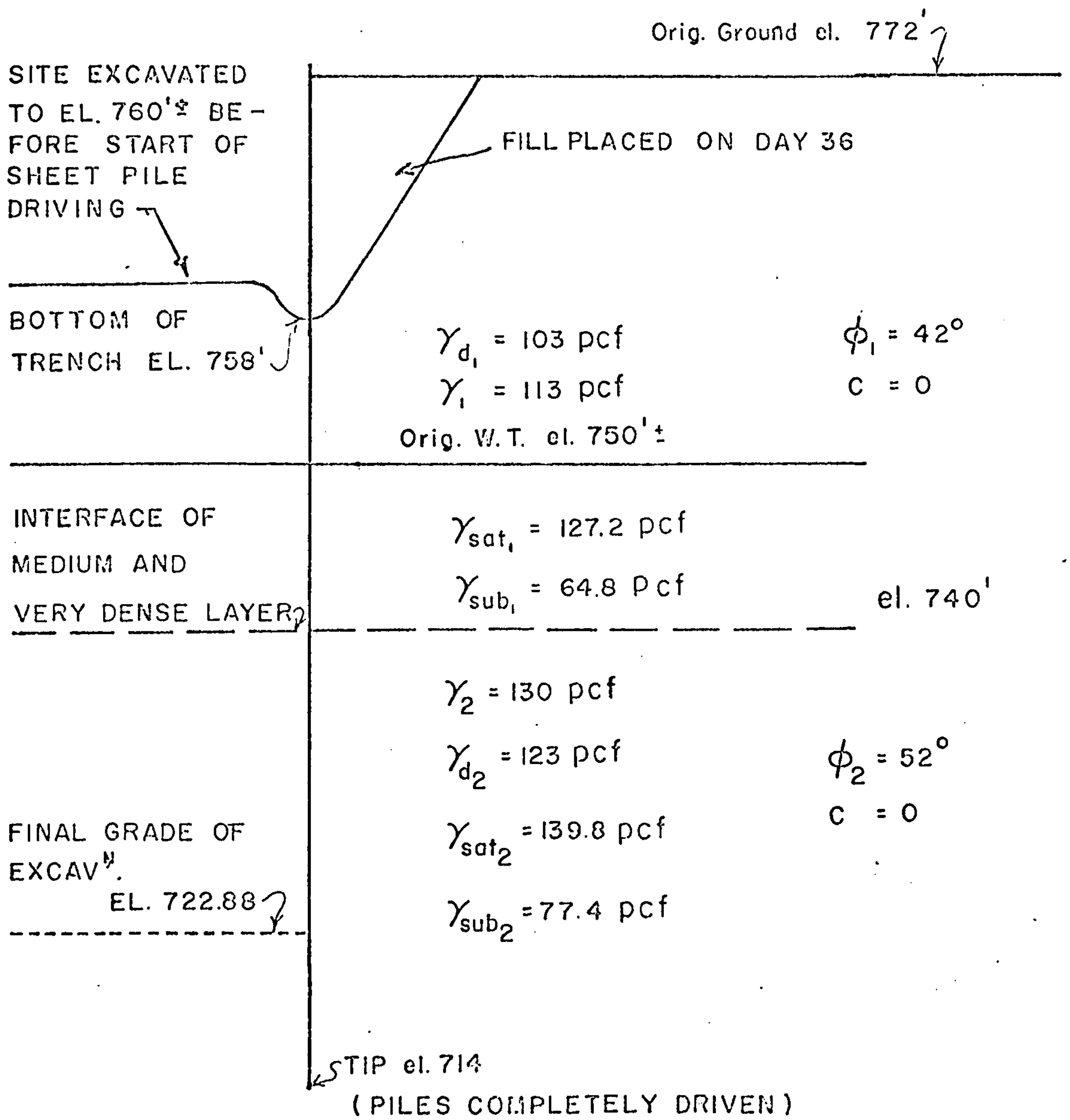

SCALE: HOR. = VERT.: 1" = 10'

FIG 6.1 SOIL PROFILE AND PROPERTIES

sand strata are indicated in Fig. 6.1. The fully saturated unit weight and its buoyed or submerged weight could be readily computed, according to Eqs. (6.1) and (6.2).

$$\gamma_{sat} = (1 - \frac{1}{G})\, \gamma_d + \gamma_w \tag{6.1}$$

and

$$\gamma_{sub} = (1 - \frac{1}{G})\, \gamma_d \tag{6.2}$$

The lateral pressures were measured by the pressure transducers attached to the two test piles. In the profile illustrated in Fig. 6.1 where the free water table is approximately ten feet below the ground surface, differentiation is essential between the following two methods of calculation. First, both the vertical pressure, σ_1', and the lateral pressure σ_3' are purely effective or intergranular pressures, their ratio being Ko. Second, both σ_1 and σ_3 include a component of free water pressure which is transmitted through the water in the voids of the soil quite independently of its grain skeleton; their ratio is designated by Ko_w. The w subscript indicated that the water pressure is included.

If the full water pressure is included in both the horizontal (measured directly) and vertical (computed) component of pressure, their ratio at depth z, will be equal to

$$Ko_w = \frac{\sigma_3}{\sigma_1} = \frac{P_h}{P_v} = \frac{P_h}{\gamma . z} = \frac{P_h \ (1+e)}{z \ (G+e)} \tag{6.3}$$

On the other hand, if only the intergranular pressures are taken into account, that is, if the full water pressure is to be subtracted from both the horizontal and vertical pressures, their ratio will be

$$Ko = \frac{\sigma_3'}{\sigma_1'} = \frac{P_h - \gamma_w z}{P_v - \gamma_w z} = \frac{P_h - \gamma_w z}{z(G+e/1+e) - \gamma_w z} \tag{6.4}$$

The latter equation is generally used because the problem is easier to study when effective stresses are considered.

The measured Ko values shown in Table 6.1, column 7, are based upon intergranular pressures. These experimental values are indicated in Fig. 6.2. The theoretical curves are identical to those shown in Fig. 4.2.26 (page 89) and are repeated for comparison with the experimental results. Only a few values agree approximately with the theoretical values proposed by Jaky (Eq. 4.2.30) or Hendron (Eq. 4.2.31). The majority of the experimental values lie in the range of 0.60 to 0.75. Terzaghi found from his large scale retaining wall tests (1934), prior to any displacement of the wall, that is, in the at-rest

Day	Date 1964	Cell No.	Meas. Lat. Earth Press. (psi)	Height of overburden (ft)	Overb. press (psi)	Meas. σ_3/σ_1=Ko	sin ϕ	Jaky Ko=1-sinϕ	Hendron
1	Jan 7	G-2	3.5	1.5	1.1	3.18	0.669	0.331	0.266
1	Jan 7	G-6	4.6	9.0	6.5	0.71	0.669	0.331	0.266
8	Jan 15	G-7	9.5	9.0	6.5	1.46	0.669	0.331	0.266
14	Jan 21	G-3	1.4	6.0	4.3	0.33	0.669	0.331	0.266
14	Jan 21	G-1	5.0	12.0	8.1	0.63	0.669	0.331	0.266
14	Jan 21	G-2	8.9	15.0	9.5	0.92	0.669	0.331	0.266
14	Jan 21	G-6	10.1	23.5	13.6	0.74	0.788	0.212	0.205
14	Jan 21	W-1	1.2	4.0	2.9	0.42	0.669	0.331	0.266
14	Jan 21	W-4	4.6	9.0	6.4	0.73	0.669	0.331	0.266
14	Jan 21	G-7	9.6	20.5	12.0	0.80	0.669	0.331	0.266
21	Jan 28	W-6	2.0	4.0	2.9	0.69	0.669	0.331	0.266
21	Jan 28	G-5	2.6	13.0	8.5	0.31	0.669	0.331	0.266
21	Jan 28	G-4	3.3	19.0	11.2	0.30	0.669	0.331	0.266
21	Jan 28	G-3	9.0	25.0	14.4	0.63	0.788	0.212	0.205
21	Jan 28	G-1	13.8	31.0	17.6	0.78	0.788	0.212	0.205
21	Jan 28	G-2	11.7	34.0	19.2	0.61	0.788	0.212	0.205
21	Jan 28	G-6	15.6	41.5	23.3	0.67	0.788	0.212	0.205
21	Jan 28	W-5	2.2	5.5	4.0	0.55	0.669	0.331	0.266
21	Jan 28	W-13	2.0	6.0	4.4	0.46	0.669	0.331	0.266
21	Jan 28	W-2	3.7	17.5	10.3	0.36	0.669	0.331	0.266
21	Jan 28	W-4	7.5	29.5	16.8	0.45	0.788	0.212	0.205
21	Jan 28	G-7	7.6	41.5	23.3	0.33	0.788	0.212	0.205

TABLE 6.1

EXPERIMENTAL AND THEORETICAL Ko VALUES

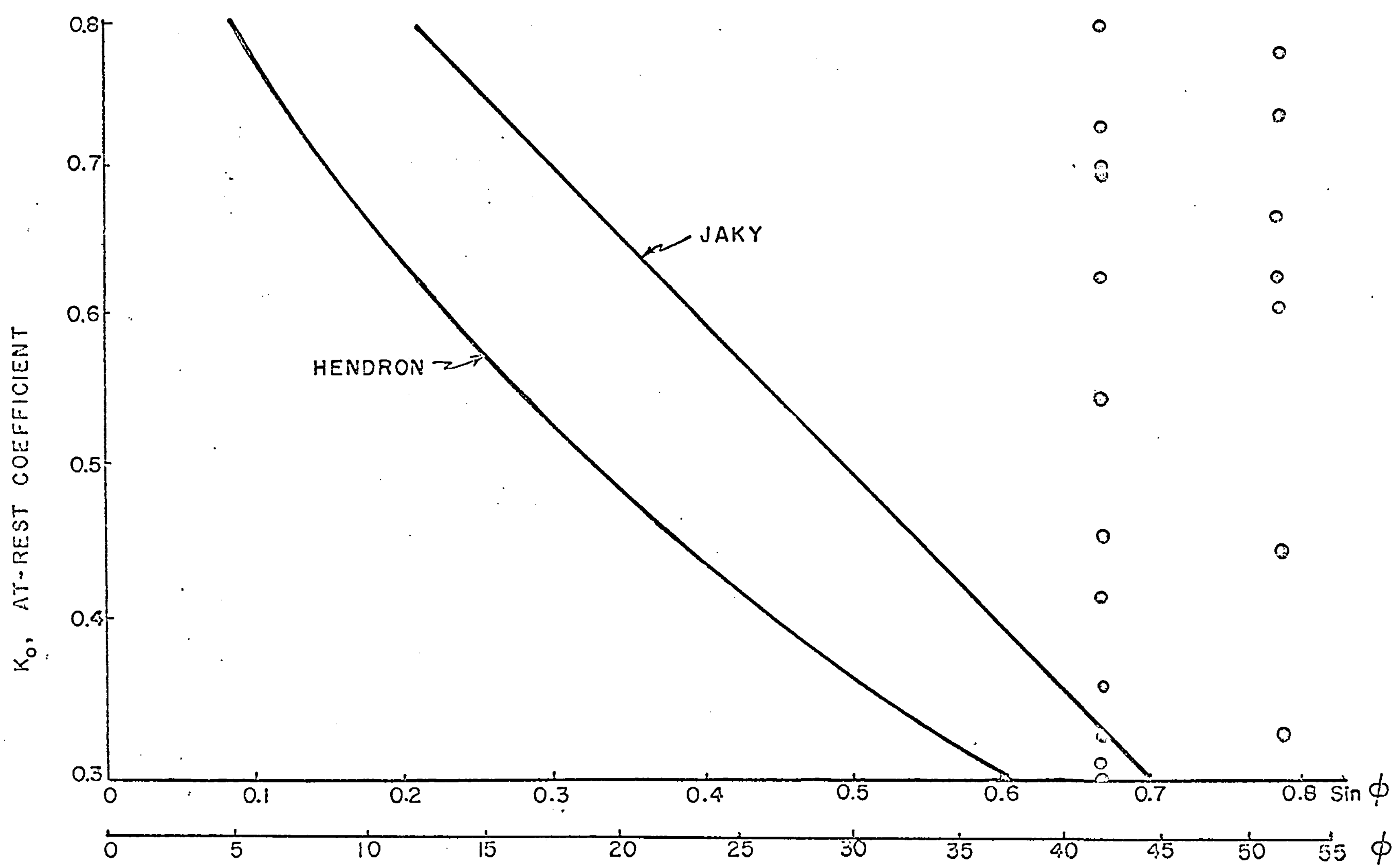

FIG 6-2 COMPARISON OF EXPERIMENTAL AND THEORETICAL K_o-VALUES

condition, the earth pressure coefficient Ko to be 0.70 for a compacted dense backfill. Ko values of 3.18 and 1.46 were measured at the beginning of driving of the test piles; the overburden heights for these measurements were 1.5 feet and 9 feet, respectively. It is quite possible that the long free standing pile was not properly aligned in the vertical direction or that bending of the pile caused the pressure transducer to be pushed into the soil thus bringing about a passive pressure condition. Ten of the twenty-two Ko values obtained experimentally lie between 0.60 and 0.80. Five values ranged between 0.30 and 0.40. The low lateral earth pressures resulting in these low Ko values are possibly caused by the effect of jetting the piles into position. The soil might have been loosened by this operation, but the cell readings after movement of the wall began were not affected by the "pocket action" due to the reorientation of the soil grains.

The theoretical solutions (Eqs. 4.2.30 and 4.2.31) yield Ko values between one-half and one third of the experimental values, except for the values discussed above. The theory may well agree with experimental values obtained in the laboratory for normally consolidated sands, but cannot be applied to heavily overconsolidated natural sand deposits. Since all dense sands are overconsolidated, otherwise they would not be in such a dense state, it is further argued that the theories for predicting Ko values do not apply to granular material in a dense condition. It appears therefore, that in natural deposits, the coefficient of earth pressure at rest will be governed by the nature of the sedimentation processes which have produced the soil and by the stress history of the deposit, differing according to the degree of overconsolidation. In man-made fills and deposits, the method and intensity of compaction will affect the principal stress ratio.

On the other hand if one assumes a mode coefficient of earth pressure at rest of Ko = 0.70, this would correspond to an internal friction angle, ϕ, of 17.5° according to Eq. (4.2.30) and approximately to 9° using Eq. (4.2.31). Such low friction angles have never been obtained on dense sands by any type of tests. It is therefore questionable that the coefficient Ko at rest is influenced at all by the interlocking or sliding of grains, since the phenomenon depends on motion to be fully mobilized whereas Ko is fully active prior to any motion or strain within the soil.

6.2.2 Deformation

In Chapter 4, Section 4.2.4, the importance of the effect of wall deformation on the lateral earth pressure distribution has been emphasized. There it has been shown theoretically that the pressure distribution is contingent on the nature and degree of movement permitted. The agreement among soils engineers is universal that the difference between distribution of pressure for rigid retaining structures and flexible ones is simply a function of displacement that occurs over the height of the structure. Therefore all earth pressure measurements have to be interpreted with respect to deformation.

In Fig. 4.2.4 (page 53) four possible deformation patterns of a braced cut were illustrated. Figs. 5.2.47 and 5.2.48 show the position and actual movement of piles No. 13 and No. 15. Fig. 5.2.49 shows the measured movement of the pile tops of the north wall. The reason for observing the movement of the whole north wall was to determine if arching effect would occur between struts. But from Fig. 5.2.49 it is clear that the entire wall moved towards the excavation bringing about plane strain conditions without arching effect occurring.

As the excavation proceeded to about an elevation of 750 feet there was a distinct inward translational movement of the wall. The upper part of the wall kept on moving inwards as the excavation proceeded below elevation 750 feet but the part of the wall below this elevation moved inwards at a greater rate. In the final stage (day 168) the deformations were similar to movement D of Fig. 4.2.4, which illustrates the deformation of a stiff retaining wall rotating about the top and at the same time moving horizontally inwards.

On June 23 (day 168) the top of sheet piles No. 13 and No. 15 had moved an average of 3.2 inches or 0.005 H, where H is the depth to the bottom of the excavation, whereas the piles at the bottom of the excavation had moved out about 7.8 inches or 0.013 H.

Terzaghi (1934) had observed from his large retaining wall tests on dense compacted sand, that slip occurred after the wall moved through an average distance of 0.0027 H for tilting about the foot and 0.005 H for a translational movement. Here H is also the total height of the retaining wall. He further observed that the average movement (about 0.007 H) of the wall that reduced the lateral pressure to a minimum was independent of the type of the movement. This leads to the conclusion that Coulombs active state in the sand had been reached after this minimal deformation has occurred.

This deformation requirement was satisfied for the portion of the pile exposed by excavation at all stages of excavation at the London site. Even as soon as the depth of excavation reached thirteen feet, the average movement of the sheeting was 0.0027 H, four times the movement required to bring about active failure conditions. Therefore it can be assumed that at any stage of excavation a failure or slip plane was formed passing through the respective bottom of the cut. Jakobsen (1958) concluded from a theoretical analysis, based on the theory of elasticity, that the necessary movement of a wall for active pressure development has to be regarded in relation to the height of the wall raised to the power of about 1.5. He also concluded that the deflection of a wall increases only with the square root of height. Thus the higher a wall is, the more will the earth pressure against the wall approach the earth pressure at rest. The first conclusion depends on the selection of a value for Poisson's ratio and modulus of elasticity. These parameters cannot be measured directly and are also not necessarily constant with depths, especially after some deformation has occurred, therefore the practical validity of this theory could be doubted. The second conclusion could hold true for rigid retaining walls, but the observed deformation values agreed much better with those observed by Terzaghi.

6.2.3 Comparison of Strut Loads with Cell Pressures

The measured total strut loads are shown in Figs. 5.2.17 to 5.2.39. The maximum and average strut loads are indicated in Fig. 6.3. From the strut loads an earth pressure distribution diagram has been drawn based on the reasonable approximation proposed by Terzaghi and Peck (1967) that the load in each strut corresponds to the pressure contributed by a rectangular area extending horizontally half the distance to the next set of struts on either side, and vertically half the

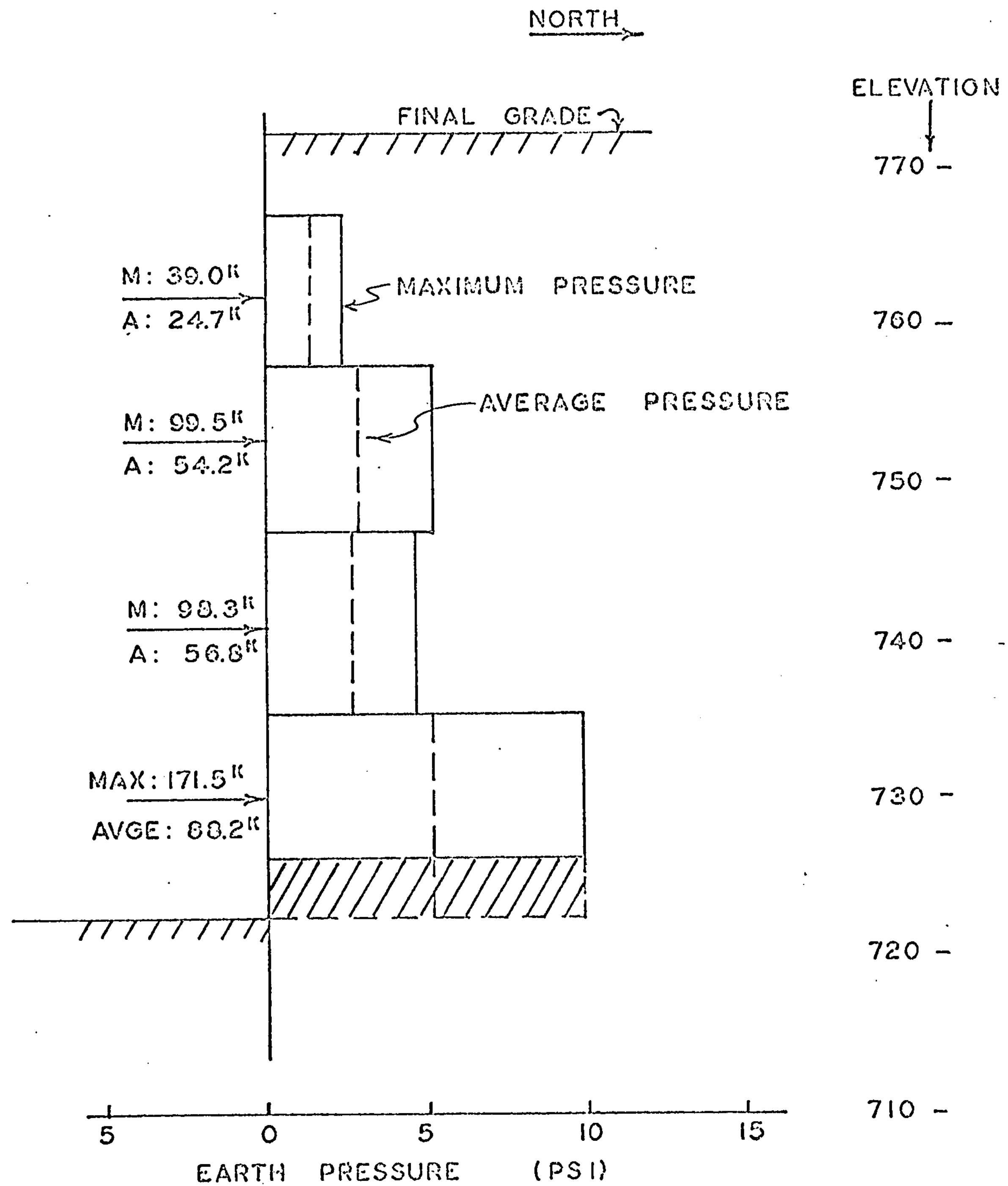

FIG. 6.3 MAXIMUM AND AVERAGE STRUT LOADS

distance to the next level of struts below and above. The earth pressure is assumed to be uniformly distributed over this area.

The real distribution of the earth pressure may differ appreciably from the calculated distribution. The discrepancies are of course the result of neglecting the continuity of the sheet piling. However, if both the shear and the moment in the sheet piles at the excavation level are known the magnitude and position of the resultant earth pressure can be calculated.

For a given pressure distribution on the wall, the loads carried by the individual struts can be very different, because they depend on many accidental factors which can be rarely controlled. Factors such as the time necessary between excavation and insertion of the struts (the longer the elapsed time the greater the stress relaxation will be), the rate and procedure with which the construction is carried out, the uniformity and method of prestressing, if the struts are prestressed, and last but not least the local variations of the soil behind the sheeting play a major part. This fact was illustrated by the measurements of strut loads of eight identical test sections of the Chicago subway (Terzaghi and Peck, 1967). The cuts contained five levels of struts. Excavation was carried out systematically from one level to the next on all eight sections. Yet, in spite of the unusually uniform construction procedure, individual strut loads in each level varied as much as $\pm$ 60 per cent from the average. Similar variations were characteristic for all the cuts in which enough strut loads were measured to justify a statistical evaluation.

To determine the total earth thrust from the measured strut loads, it is necessary to know the bottom reaction or shear force in the sheet pile at the depth of the excavation. Whether or not the value of this quantity is important enough to include in the total strut load depends on the deformation of the cut. As was illustrated in Figs. 5.2.47 and 5.2.48, the greatest deflection of the sheeting occurred at the bottom of the excavation. This type of deflection corresponds to a pressure distribution having small values at the bottom, and the bottom reaction is likely to be small. At the Chicago subway construction Peck (1943) measured the magnitude of the bottom reaction by a hydraulic jack by first cutting the H-pile at depth H. It was found that the bottom reaction was not too important except for one case where the vertical H-pile terminated in a stiff clay layer which induced a deflection curve with a maximum value at some distance above the bottom of the cut.

It therefore seems conservative to assume that the magnitude of the bottom reaction is equal to the resultant force of a rectangular pressure distribution. The vertical side of the pressure diagram being half the distance from the bottom of the cut to the lower most strut and the horizontal side being equal to the pressure intensity of the lowest strut. This is represented by the area enclosed by the dashed lines in Figs. 5.2.27 to 5.2.38 and by the shaded area in Fig. 6.3.

The estimated error in reading the strut loads is approximately 10 kips which corresponds to one dial division on the mechanical strain gauge. Since the water levels were not always read at the same time as the strut loads, they had to be interpolated for certain particular days. The error of interpolation should not have exceeded one foot, which would correspond to a seven kip error of the total strut load at the lowest strut level if the water level was approximately at an elevation 745 behind the sheet pile wall. The closeness of superimposed loads to the excavation is not indicated in the cross-sections of the north wall. The existing main office building consisted of a one storey brick building 115.5 feet long and 48.5 feet wide. Its closest wall was located approximately 20 feet away from the test wall. The general elevation of the underside of the six inch floor slab was at elevation 772 feet. The west wing of the building had a deep basement with the floor located at elevation 759 feet. This deep section was located 20 feet north of the test section. However, the basement was small in area and the load of the building was considered to be equal to the weight of the removed soil.

Fig. 6.4 shows the total earth pressures obtained from the strut loads and from the cell pressure readings plotted against time. Table 6.2 lists the total strut loads from the effective weight of the soil and other pertinent information. A corresponding bottom

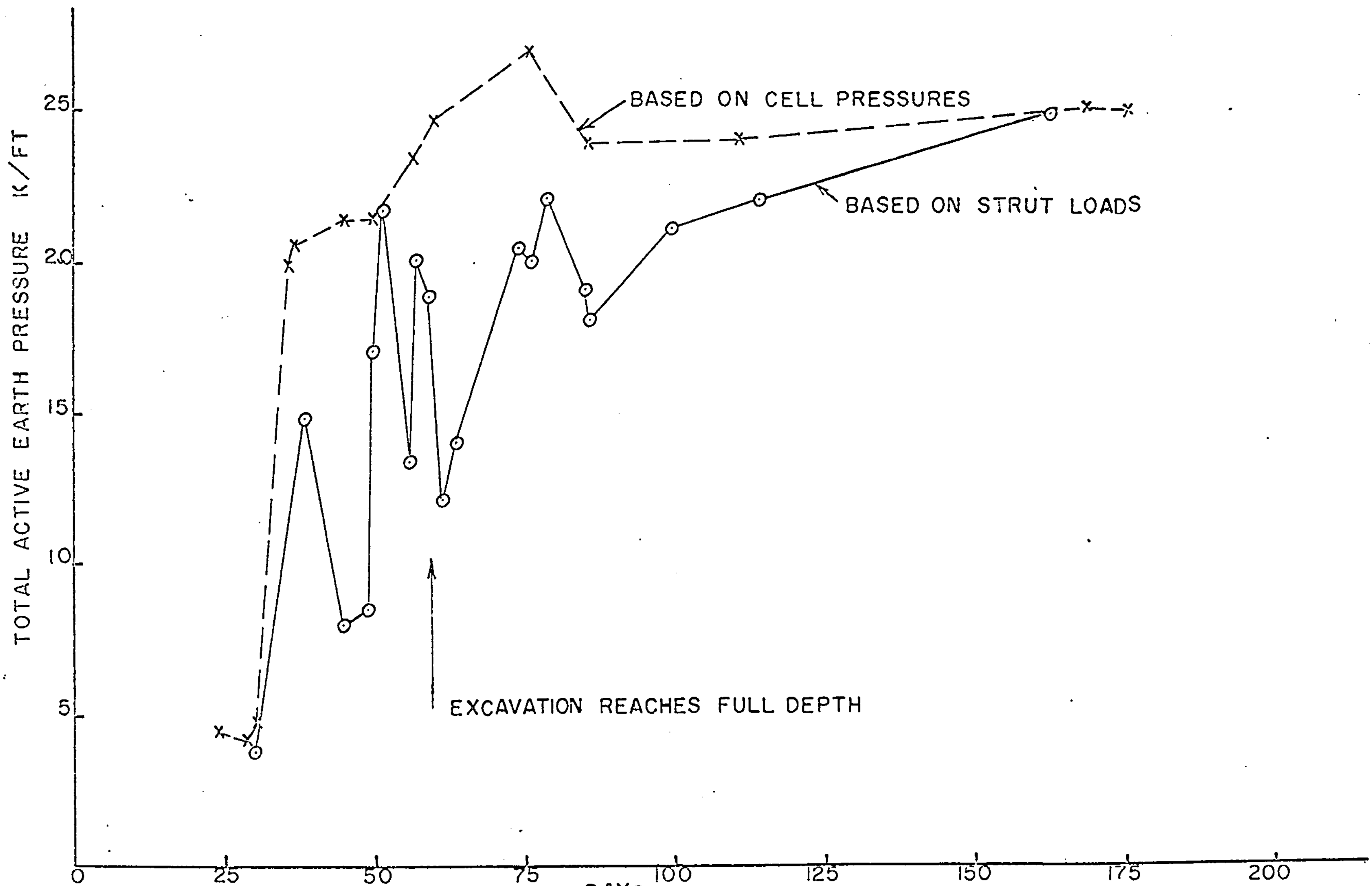

FIG 6.4 COMPARISON OF MEASURED EARTH PRESSURES

Day	Date 1964	Level of Excav^{n}	Total Strut Load From Effective Soil Weight	Strut Load per lineal ft	Bottom Reaction Total	Bottom Reaction Per lineal ft	Calc. Earth Press.
		EL (FT)	K	K/FT	K	K/FT	K/FT
30	Feb. 6	742	48.2	3.7	14.4	1.1	4.1
38	Feb. 14	732	191.1	14.7	68.1	5.3	16.3
45	Feb. 21	732	101.5	7.9	2.0	0.2	16.1
49	Feb. 25	727.5	107.6	8.4	24.0	1.9	19.5
50	Feb. 26	727.0	219.5	16.9	51.6	4.0	21.1
51	Feb. 27	727	279.2	21.7	75.2	5.8	21.1
56	Mar 3	725	173.9	13.4	15.2	1.2	22.8
57	Mar 4	724	258.1	20.0	10.9	0.8	23.1
59	Mar 6	723	241.8	18.8	81.4	6.3	23.0
62	Mar 9	723	154.4	12.0	19.2	1.5	23.0
64	Mar 11	723	181.4	14.1	22.2	1.7	23.0
74	Mar 21	723	263.6	20.5	40.2	3.1	25.1
76	Mar 23	723	255.4	19.8	44.3	3.4	25.1
77	Mar 24	723	288.2	22.5	41.0	3.2	25.1
85	Apr 1	723	246.0	19.1	24.0	1.9	25.1
86	Apr 2	723	231.9	18.0	30.5	2.4	25.0
99	Apr 15	723	272.2	21.1	43.7	3.4	24.7
114	Apr 30	723	282.6	22.0	56.0	4.3	22.2
163	June 18	723	329.1	24.8	71.0	5.5	24.9

TABLE 6.2

STRUT LOADS

reaction, as outlined in the preceeding pages, has been added to the strut loads in order to obtain a total earth pressure. Even so the strut loads yield consistently lower earth pressures than the cell readings, sometimes registering only one third or one half the earth pressure recorded by the pressure cells. The strut load readings themselves change erratically, for instance, from 8.4 kips per foot to 21.7 per foot and back to 13.4 kips per foot all within one week. The relatively few strut load readings do not warrant a statistical evaluation of the data. The strut loads were measured on the two centre 14 WF 87 strut sections, whereas the end sections consisted of relatively stiff and heavy 33 WF 130 beams. It is quite possible that a general load transfer from the lighter centre sections to the more rigid end sections did occur, which would explain the lower strut load readings as compared to the pressure cell readings. The inconsistent variation in strut load readings seems to represent a fundamental weakness of such measurements and a probable explanation for this behaviour could be the non-uniform deformation of the wall in a horizontal plane (Fig. 5.2.49) which could result in abrupt load adjustments in the relatively rigid bracing system.

In contrast the earth pressures from the cell readings are very stable and consistent. The pressures increased with increasing depth of excavation, and after the final grade had been reached the readings remain relatively constant, changing only when the fluctuating water table caused a change in total earth pressures.

In summary it can be said, that the earth pressure cells yielded very consistent readings corresponding to the excavation progress and change in water levels. They are therefore used in the comparison of the experimental to the theoretical values as discussed in the following section.

6.2.4 Active Earth Pressure

6.2.4.1 Passive Arching Effect

The measured earth pressures shown in Figs. 5.2.3 to 5.2.16 can be considered to be active pressures because of the magnitude of the soil deformation. Initially the earth pressure readings on both test piles were numerically similar (Figs. 5.2.3 to 5.2.8). After day 50 when the excavation depth was still four feet above final grade, the cells on pile No. 14 showed consistently higher readings until day No. 168 when the corresponding cell readings of the two test piles became similar again.

Following is a possible explanation for the difference in readings on the two test piles. The cells of pile No. 14 were located on the recessed face of the pile and with the movement of the wall the lateral earth pressure decreased from the at-rest pressure to the active one. Fig. 6.5 depicts an enlarged horizontal section through the two test piles. σ_3 is the pressure acting on plane ab ef, this pressure was measured by the cell mounted on the front face of pile No. 15. Due to the expansion of the soil σ_3 was reduced and shear stresses mobilized along the oblique sides of the piles acting in a direction as shown. These shear stresses tend to prevent a reduction of pressure on the recessed plane cd of pile No. 14. There the pressure readings should reduce only a small amount even after expansive strains have occurred in the sand. The normal stress on plane cd should be equal to σ_3 plus $\tau \cos (90 - \alpha)$, where τ is the shear stress mobilized along the oblique sides, bc and de, of the piles. This phenomenon is commonly called "passive arching" (Whitman and Luscher 1962, Triandafilidas et al 1964), which simply means that the pressure exerted on a soil structure interface is higher than the applied pressure. Where the readings from the cells on the two test piles agreed within reason all readings were averaged, but between day 50 and 111 for which period the cells on pile No. 14 recorded much higher readings than the corresponding cells on pile No. 15, due to arching effect occurring across the trough of the pile, the cell readings of pile No. 15 were taken.

The passive arching effect was demonstrated experimentally in a laboratory test (Appendix A 1.3). One earth pressure transducer

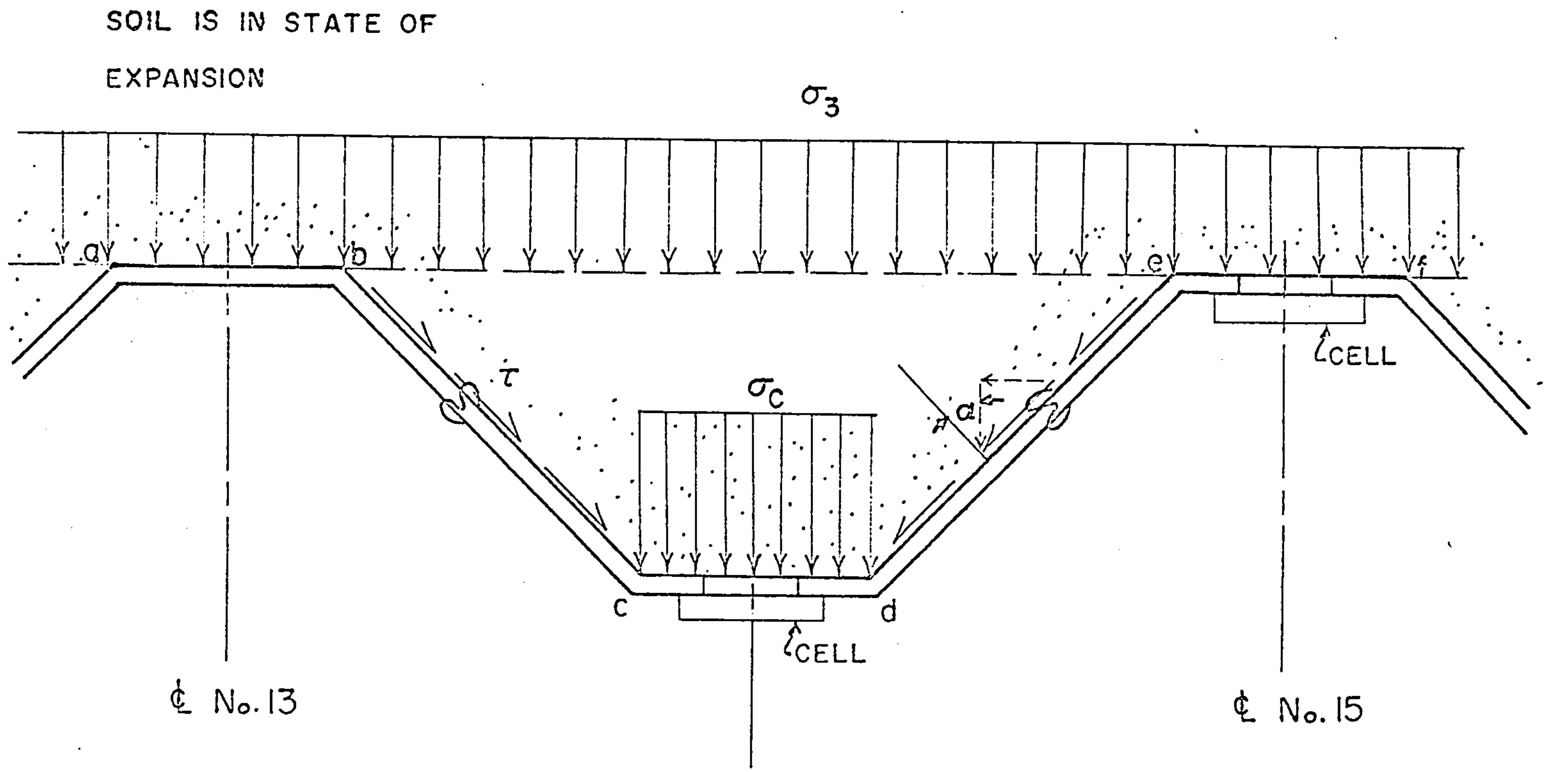

$$\sigma_c = \sigma_3 - \tau \cos(90 - \alpha)$$

$$\tau = \sigma_n \tan \delta$$

FIG 6.5 EARTH PRESSURES ACTING ON FRONT AND RECESSED FACE OF PILES.

was installed having its diaphragm flush with the bottom of a 10 inch diameter steel tank. A six inch high layer of sand was surcharge loaded by air pressure. Then the tank was vibrated shortly in order to minimize the effect of side friction. The known applied pressure agreed with the pressure recorded by the pressure cell. When the applied air pressure was reduced, the cell pressure readings were consistently higher than the corresponding applied pressures. Finally the air pressure was reduced to zero but the cell reading was still very much in excess of the overburden pressure exerted by the sand layer. Vibration destroyed the arching effect. Therefore it can be concluded from the field observations and the laboratory tests that passive arching did occur across the troughs of the sheet piles.

6.2.4.2 Magnitude of Active Earth Pressure

The measured active earth pressures and the theoretical Coulomb earth pressures together with other pertinent information have been summarized in Table 6.3. The height of the wall was always taken as the distance from the ground surface to the respective bottom of the cut. In the Coulomb analysis the failure has been assumed to pass through the point of intersection of the bottom of the excavation and the wall. The active earth pressure, P_A, was calculated over this

Day	Date 1964	Depth of Cut Feet	G.W.T. EL. Feet	W.T. Inside Excav. El. Feet	Depth of Cut El. Feet	P_A (measured) Kips/LFT	P_A (Coulomb) Kips/LFT
24	Jan 31	18	748.6	744.0	747	4.35	3.73
28	Feb 4	18	748.0	74.10	747	4.18	3.73
30	Feb 6	21	747.8	738.1	742	4.67	4.07
36	Feb 12	39	747.0	728.0	732	19.85	16.31
37	Feb 13	39	742.2	728.0	732	20.50	16.31
45	Feb 21	40	745.5	731.0	732	21.30	16.14
50	Feb 26	45	744.3	725.0	727	21.46	21.09
57	Mar 4	48	742.5	723.0	724	23.34	23.05
60	Mar 7	49	744.0	727.0	722.9	24.60	24.51
76	Mar 23	49	741.0	729.3	722.9	26.70	25.14
86	Apr 2	49	741.0	729.5	722.9	23.70	24.99
111	Apr 27	49	749.0	748.0	722.9	24.01	23.54
168	June 23	49	736.5	716.5	722.9	24.87	25.14
175	June 30	49	737.5	716.5	722.9	24.87	25.14

TABLE 6.3

EXPERIMENTAL AND THEORETICAL

ACTIVE EARTH PRESSURES

height. The soil properties for calculation purposes are indicated in Fig. 6.1 and the magnitude of the theoretical active earth pressure for a layered sand was calculated by the equation shown in Fig. 6.6.

As shown in Fig. 4.2.25 (page 83) the wall friction had little effect on the total active earth pressure and has therefore been taken as zero. If Coulomb's theory is valid, the measured earth pressure should agree with the theoretical earth pressure. Fig. 6.7 shows both these values plotted against time. The measured values are higher except for day 86 where the theoretical value was about six per cent higher and on days 173 and 175 where the theoretical values were about two per cent higher. Before day 45 the measured earth pressures exceeded the theoretical ones by an average of 20 per cent. After this the measured values were about five per cent above the theoretical ones. Assuming a value of wall friction of $\delta = 1/2\ \phi$ would lower the theoretical pressures by an additional five per cent. It should also be noted that the earth pressure cells were spaced on the test piles at 6-foot intervals and a linear distribution was assumed between the cells. The full depth of excavation was reached on day 59 when the wall had deflected an average distance of 0.006 H, where H is the full depth of the cut. The agreement from there on between the measured and theoretical pressures is very good. Therefore

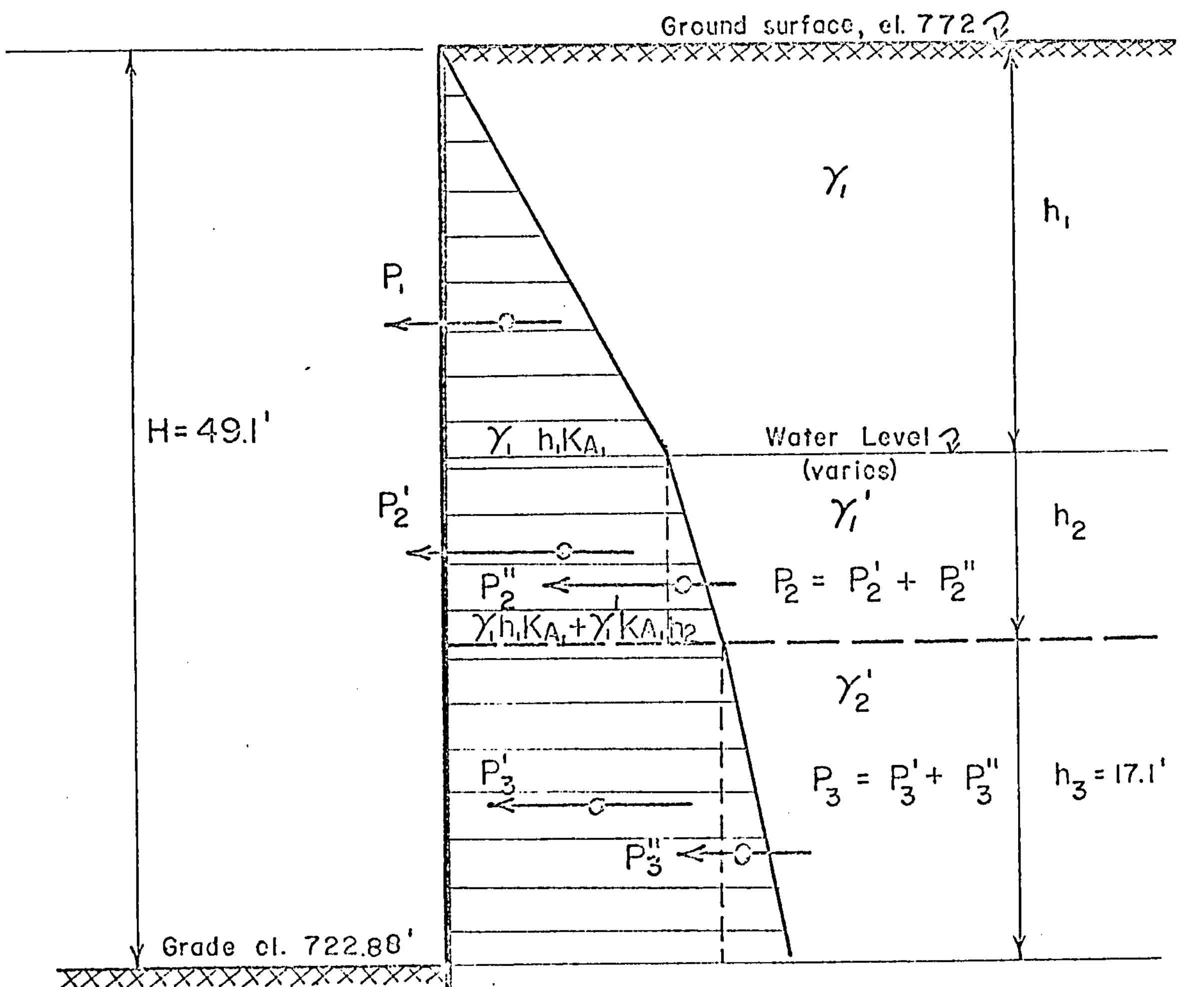

$$P_1 = \frac{1}{2} K_{A_1} \gamma_1 h_1^2$$

$$P_2 = P_2' + P_2'' = K_{A_1} h_2 (\gamma_1 h_1 + \tfrac{1}{2} h_2 \gamma_1')$$

$$P_3 = P_3' + P_3'' = K_{A_1} h_3 (\gamma_1 h_1 + \gamma' h_2) + \tfrac{1}{2} K_{A_2} \gamma_2' h_3^2$$

FIG 6.6 MAGNITUDES FOR EARTH PRESSURES FOR A LAYERED SYSTEM

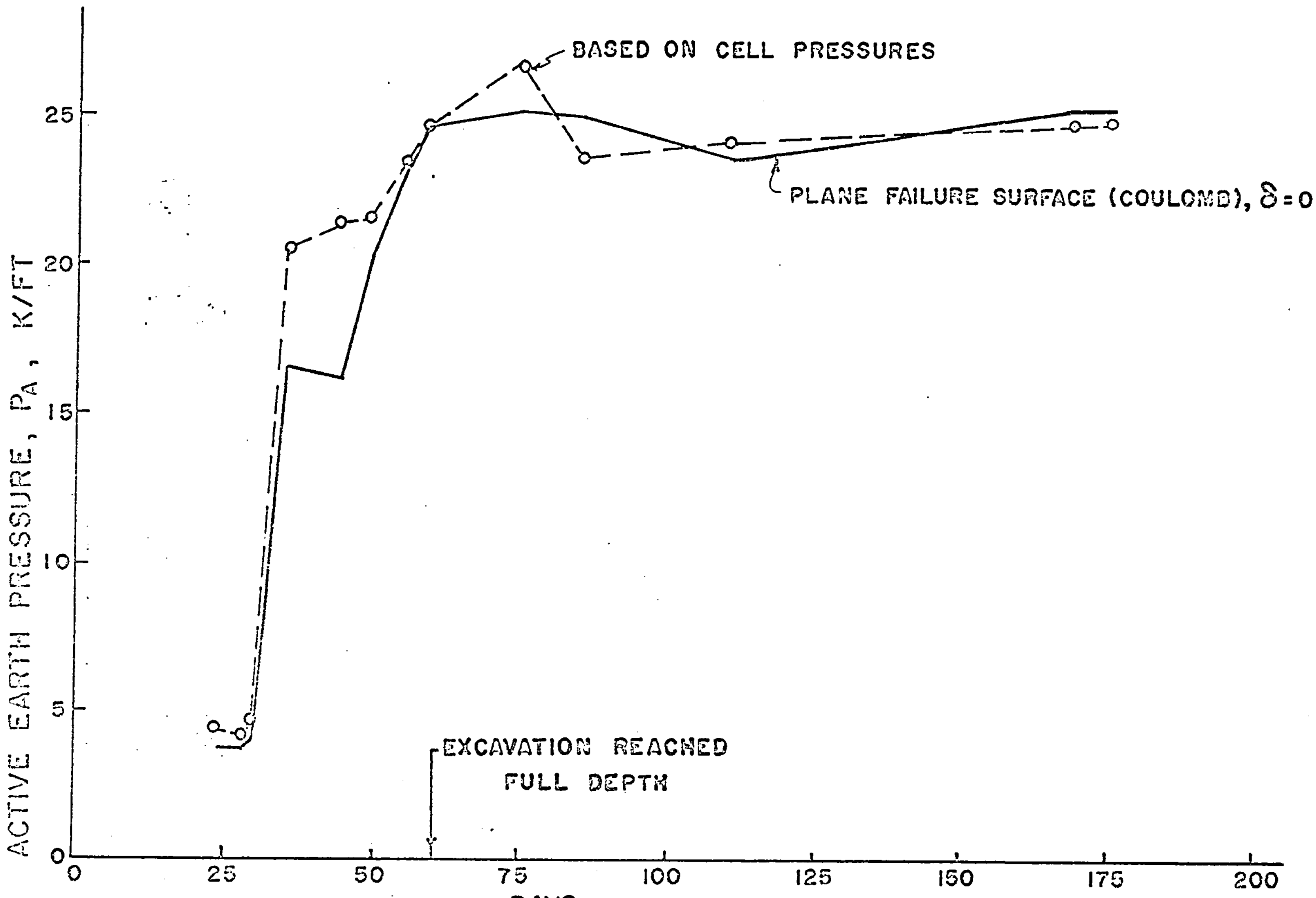

FIG. 6.7 VARIATION OF THEORETICAL AND MEASURED ACTIVE EARTH PRESSURE

it can be assumed that the active condition for the full depth of the cut was realized as soon as the cut reached its full depth. After day 86 the total active pressure remained relatively constant regardless of the continuing wall deformation. The slight variations were due to fluctuations in the water table which are reflected in both the calculated and the theoretical pressures. It, therefore, can be concluded that Coulomb's theory can be used to calculate the total active earth thrust on a braced cut in sand provided the soil has been strained the required amount.

Fig. 6.8 shows the variation of K_A with depth. The theoretical K_A value was defined in Chapter 4 by Eq. (4.2.7). The measured K_A values were calculated as follows:

$$K_A = \frac{p_A}{\sum \gamma_i \; h_i} \tag{6.5}$$

in which p_A is the lateral earth pressure measured by a respective cell and $\sum \gamma_i \; h_i$ is the corresponding overburden pressure. The theoretical K_A value above elevation 740 feet was 0.200 and below that elevation 0.125 as shown by the dashed-dotted lines in Fig. 6.8. The K_A values during the excavation period of the cut were averaged as shown by curve days 24 to 57. The second curve illustrates the average

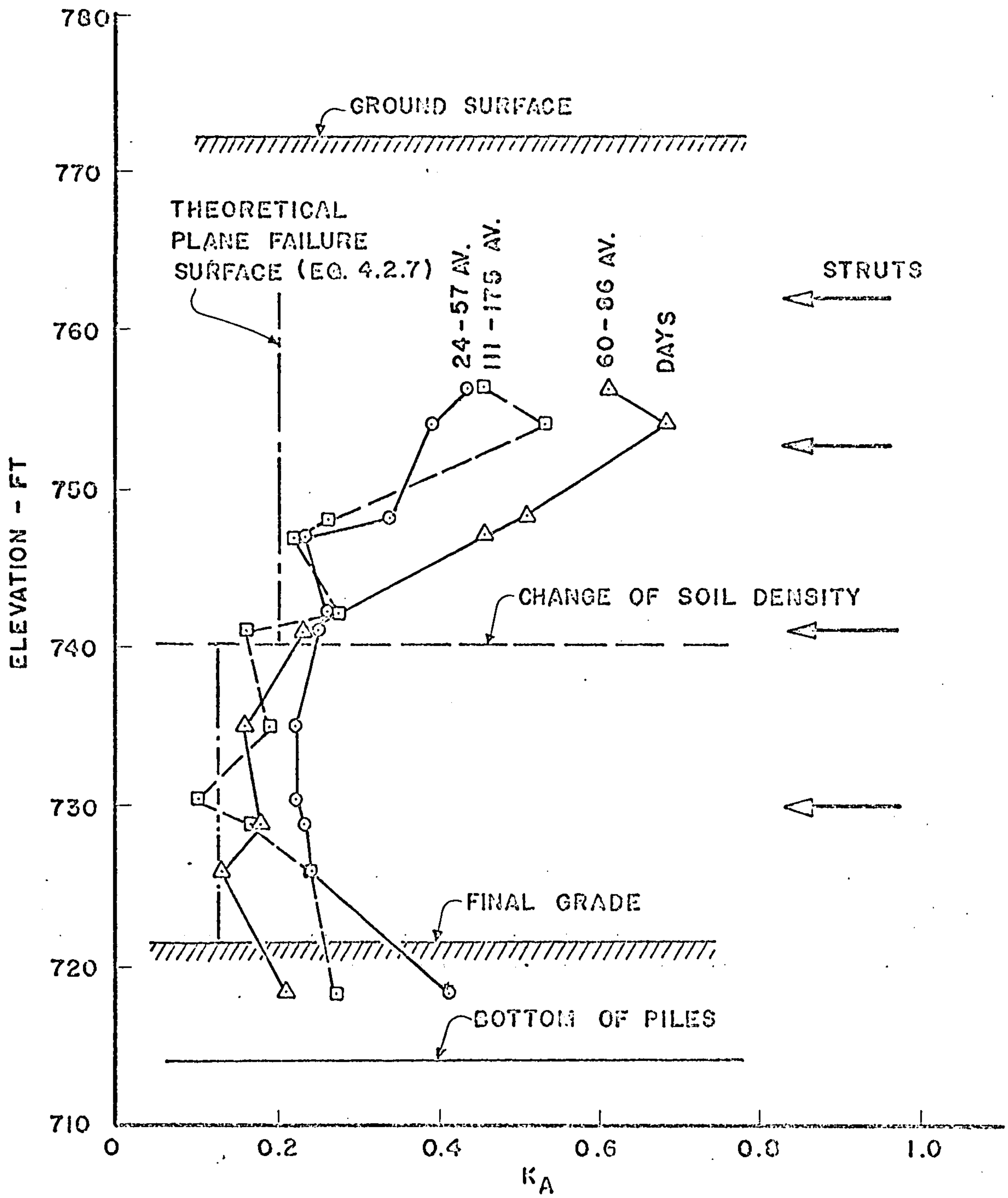

FIG. 6.8 VARIATION OF MEASURED AND THEORETICAL K_A-VALUES WITH DEPTH

of days 60 to 86 and the third curve the average of days 111 to 175, corresponding to definite construction stages. For the upper part of the wall the measured K_A-values are two to three times larger than the theoretical values. This is brought about by the special deformation behaviour of the wall. The soil in the lower portion of the cut is expanding at a greater rate and a stress transfer (arching effect) takes place from the yielding parts to the stationary or less yielding parts of the wall, resulting in higher pressures in the upper portion. This agrees with the observations made by previous engineers and researchers (Meem 1908, Spilker 1936, Peck 1943, and Müller-Haude et al 1965).

The measured K_A-values appear to decrease with increasing depth of excavation down to elevation 740 feet. Below this depth the variation is not as pronounced, the values range between 0.13 and 0.23 as compared to 0.125 for the theoretical K_A-value. It is interesting to note that the first period (day 24 to 57) K_A-values above elevation 740 feet were lowest and below this depth were largest of the three periods. It is quite likely that the deformation of the wall (for the first period) was not sufficient to bring about the full active condition below elevation 740 feet. This is explained by the deformation pattern of the wall during this period. Initially most of the movement occurred in the upper part of the wall, because the lower part of the piles were still embedded. From then on the lower portion of the wall was yielding to a much greater degree than the upper part and a stress transfer (arching effect) occurred from the yielding parts to the stationary or less yielding parts of the cut. This is reflected by an increase of K_A-values at the top and a decrease of K_A-values at the lower part as shown by the second curve (days 60 to 86).

As discussed in Section 6.2.2 much of the wall movement occurred after the struts were installed and the deformation consisted of a translational movement and of a rotational movement with its pivot point about the strut level at elevation 762 feet. This continuing deformation decreased the K_A-values in the first sand layer to approximately the same values as in the initial stage and to an average constant value of 0.18 in the dense sand layer. This is shown by curve days 111 to 175. The theoretical K_A-value in the dense layer (K_A = 0.125) can be considered as the lower limit for the measured values which averaged to 0.20. The measured K_A-values are not constant throughout the entire depth of the cut as suggested by Eq. 4.2.7 which is also proof of the non-linear pressure distribution. Nevertheless the theoretical K_A-values can be employed to predict the total active earth pressure acting on the cut.

6.2.4.3 K-Strain Relationship

Fig. 6.9 shows the variation of K-values vs. horizontal strain after day 24. The K-values were calculated according to Eq. 6.5. The strain of the soil at the elevation of a cell is obtained by the measured inward movement of that cell divided by the horizontal distance from the cell to the rupture surface of the retained soil mass. A logarithmic spiral was chosen as rupture surface as suggested by Terzaghi (1941). The spiral intersected the sheet pile wall at the excavation level.

Up to a horizontal strain of five per cent a considerable scatter of K-values occurred ranging from 0.12 to 0.70. It can only be suspected that up to such a strain the strain conditions in the soil were not yet uniform within the deforming soil. Beyond a strain of five per cent the K-values range from 0.10 to 0.19 with an average K-value of 0.15. At this point it is proper to draw the attention again to the Coulomb values, which were 0.125 for the dense and 0.200 for the medium dense sand stratum and are indicated in Fig. 6.9. Therefore it can be concluded that for this particular soil the active state has been brought about when the horizontal soil strain reaches a value of five per cent.

A tentative curve has been drawn through these points to

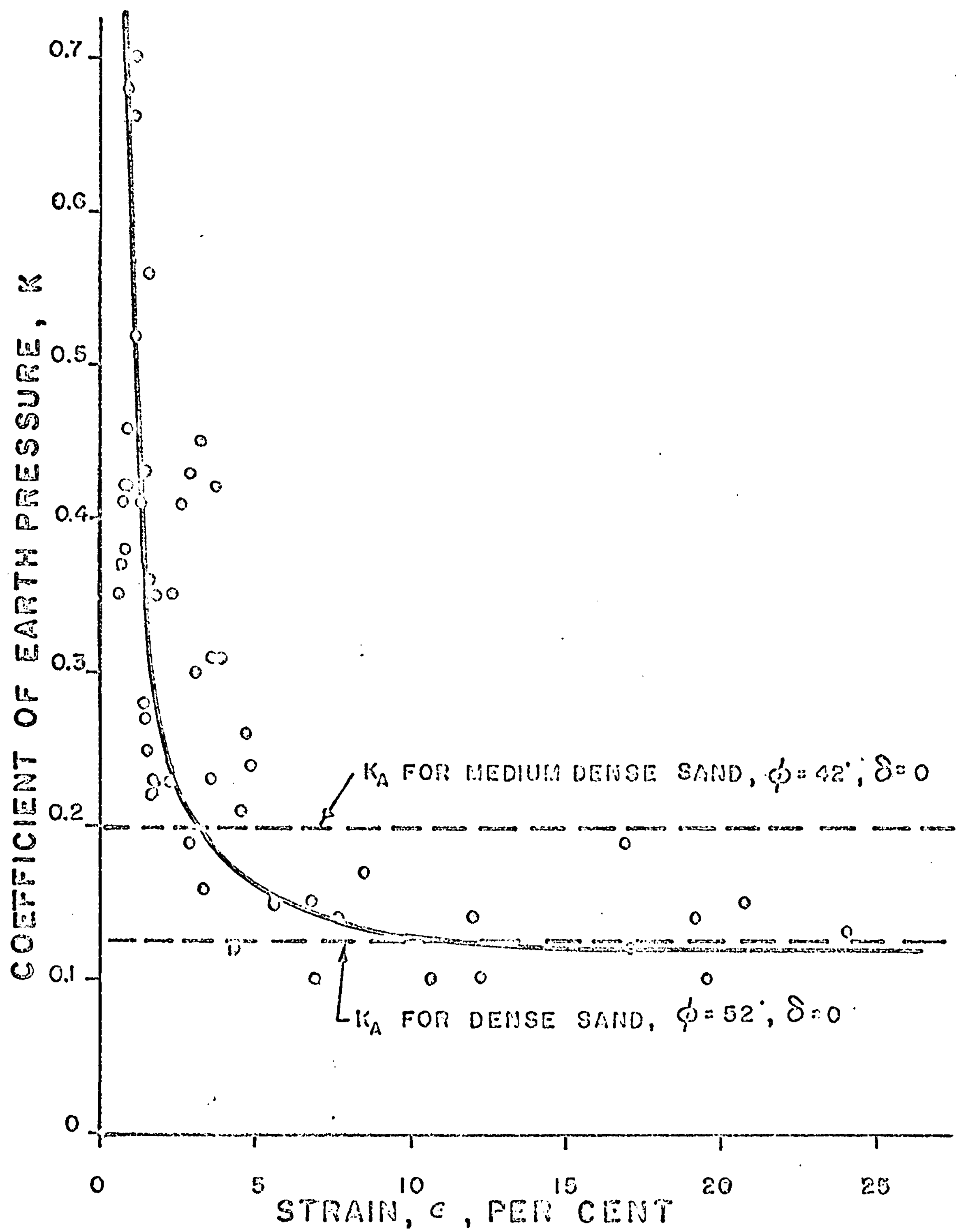

FIG. 6.9 VARIATION OF K WITH STRAIN

show more clearly how abruptly the K-values assumed a constant minimum value after the soil strain exceeded five per cent.

6.2.5 Passive Earth Pressure

For a smooth wall where no shearing stresses are developed between the soil and the wall, the passive resistance can conveniently be calculated by either Coulomb's or Rankine's equation, assuming a plane rupture or slip surface. Coulomb's general expression for the passive coefficient of earth pressure is given by:

$$K_p = \frac{\sin^2(\alpha - \phi)\cos\delta}{\sin\alpha\,\sin(\alpha + \delta)\left[1 - \sqrt{\dfrac{\sin(\phi+\delta)\,\sin(\phi+i)}{\sin(\alpha+\delta)\,\sin(\alpha+i)}}\right]^2} \qquad (6.6)$$

where $\alpha \overset{=}{<} 90^{\circ}$ is the angle between the horizontal and the back of the wall; the other terms have been defined previously. This equation is based on the simplifying assumption of a plane surface of sliding.

Fig. 6.10 shows the variation of K_p with the angle of internal friction ϕ and the angle of wall friction δ for the case where the wall is vertical and the soil surface is horizontal. δ is considered to be positive in Eq. (6.6), that is, the resultant passive

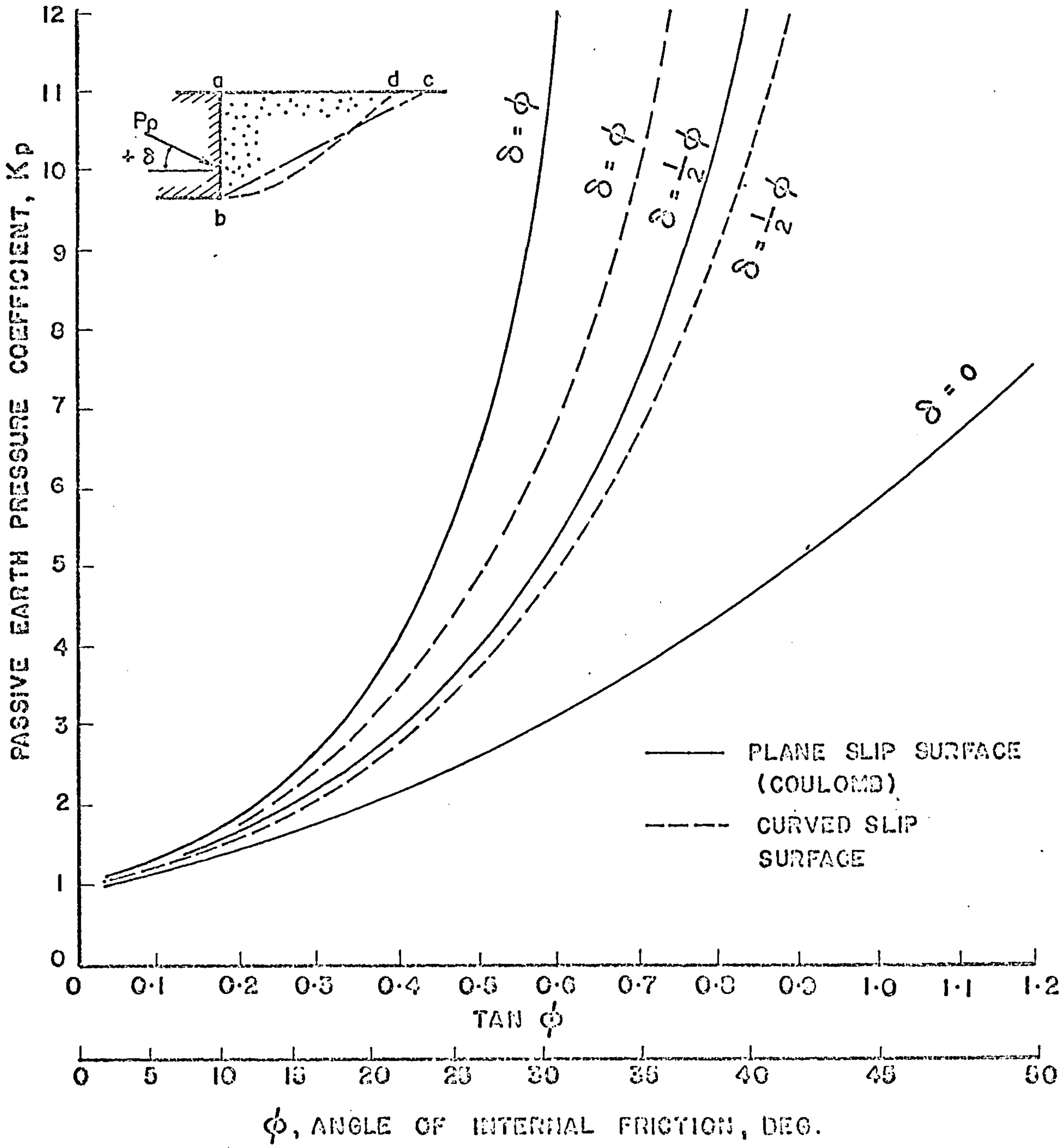

FIG. 6.10 VARIATION OF K WITH δ AND φ FOR PLANE AND CURVED SURFACES OF SLIDING

pressure acts as indicated on the inset of Fig. 6.10. This corresponds to most practical cases in which the wall is pushed into the soil resulting in an upward movement of the soil with respect to the wall. Curves have been plotted for three cases of wall friction, namely $\delta = 0$, $\delta = 1/2\phi$ and $\delta = \phi$. They indicate that for a given value of ϕ the value K_p increases rapidly with increasing value of δ. As δ increases so does the curvature of the surface of sliding and for a large δ it can no longer be approximated by a plane. Therefore a second set of dashed curves have been shown in Fig. 6.10 based on a more realistic curved surface of sliding as indicated by curve bd on the inset of Fig. 6.10. The values of K_p for the curved rupture surface were obtained from tables developed by Caquot and Kerisel (1948). For values $\phi = \delta = 30^o$, a horizontal backfill and a vertical wall it has been found that the value of the passive earth pressure as determined by means of a curved sliding surface is more than 30 per cent smaller than the corresponding Coulomb value computed by Eq. (6.6). For higher values of ϕ and δ the error becomes prohibitively large. For values $\phi = \delta = 40^o$, the corresponding values of K_p for a plane and curved surface of sliding are 92.3 and 17.5 respectively. This error is on the unsafe side. However, with decreasing values of δ the curvature decreases rapidly and becomes plane when $\delta = 0$. If δ is smaller than $\phi/3$, the difference between the real sliding surface and Coulomb's plane surface is small (as can be seen in Fig. 6.10) and Coulomb's equation is adequate. If δ is larger than $\phi/3$ a method should be used which takes the curvature of the slip surface into consideration.

The passive earth pressure at London was measured by cell G-7, mounted on the excavation side of pile No. 14 at an elevation of 618.5 feet. Therefore, the overburden was approximately 4.5 feet after the excavation had reached grade. Since the passive earth pressure acts at an angle δ to the normal on the contact face the following expression for the total passive resistance is valid.

$$P_p = \tfrac{1}{2} \gamma D^2 \frac{K_p}{\cos \delta} \tag{6.7}$$

in which D is taken as the distance from the excavation level at the test pile to the bottom of pile and K_p is the coefficient of passive earth pressure defined by Eq. (6.6). Cell G-7 measured the horizontal or lateral component of the passive resistance. Therefore, for the purpose of comparison of the theoretical with the actual values, the horizontal component of the passive pressure given in Eq. (6.7) should be used, which is

$$P_{p(h)} = \tfrac{1}{2} \gamma D^2 K_p \tag{6.8}$$

It will be understood in the following discussion when reference is made to the passive earth pressure it is the lateral component given by Eq. (6.8) which is meant unless otherwise stated.

The passive pressures measured by cell G-7 are shown in Figs. 5.2.4 to 5.2.16 inclusively. Fig. 6.11 shows the variation of the measured passive earth pressure and the theoretical values. At any time the measured passive resistance was well below the corresponding calculated value. To calculate the theoretical values the assumption of a failure plane passing through the bottom of the sheet piles was made. For a curved failure surface and $\delta = 1/2\ \phi$ the passive resistance increased approximately fourfold compared to the resistance obtained assuming a smooth wall. After day 59 when the excavation had reached its final grade the measured value varied between 1.36 kips per foot and 12.25 kips per foot. The high pressures were obtained in the final week of the experimental programme. The corresponding theoretical value for $\phi = 52$ was 23.0 kips per foot for a frictionless wall and 91 kips per foot assuming $\delta = 1/2\ \phi$ and a curved rupture surface. As a general rule the strain that is required to bring about a passive failure condition is about ten times the strain requirement for the active case. The maximum wall deformation at the elevation of cell G-7 occurred on day 175 and corresponded to 8.3 inches. This amount of yield should have been sufficient to cause the passive condition but as was pointed

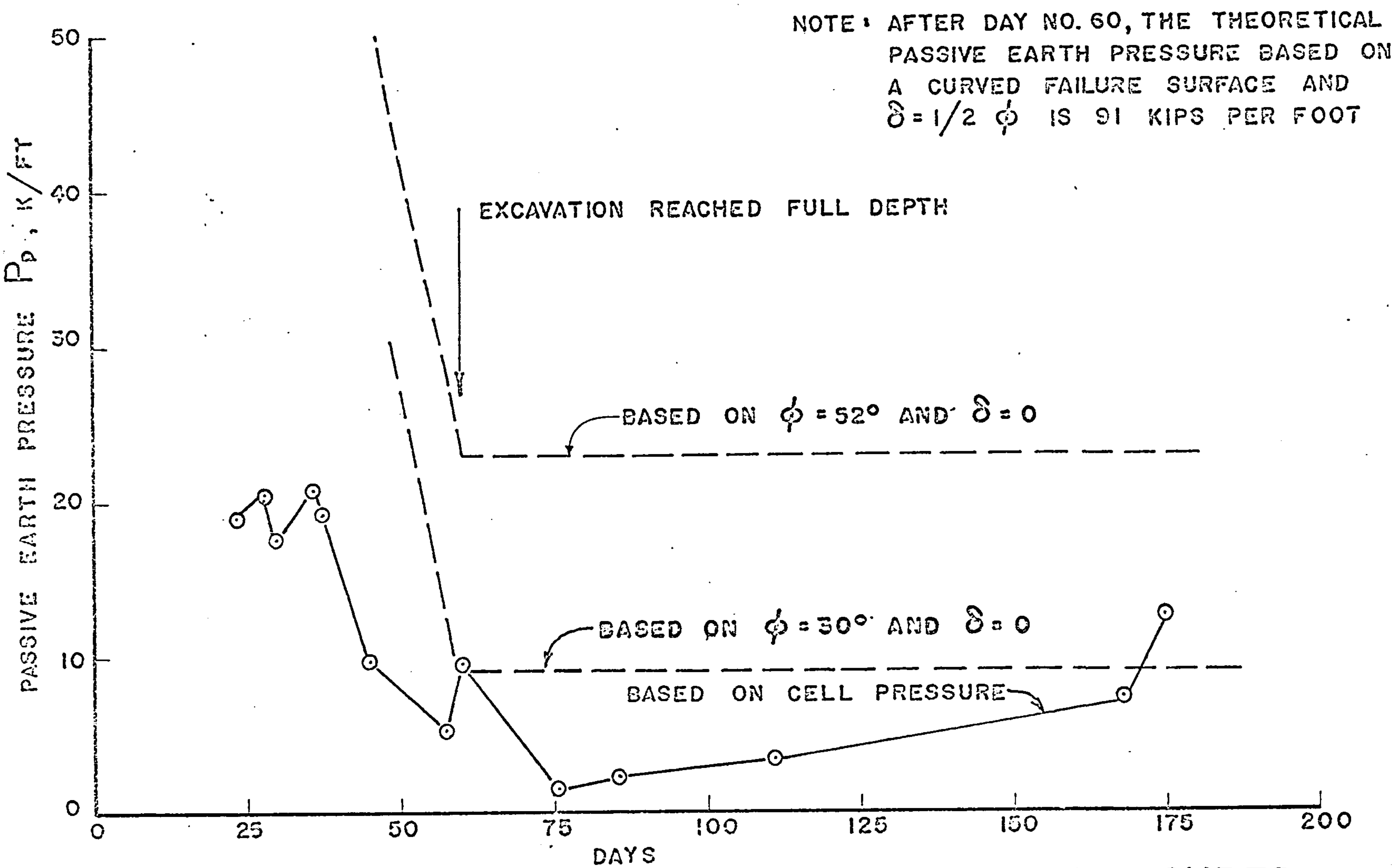

FIG 6.11 VARIATION OF THEORETICAL AND MEASURED PASSIVE EARTH PRESSURES

out above the measured passive pressures were much smaller than the theoretical values. In order for the theoretical value to agree with measured value the failure surface should pass through a point three feet above the tip of the pile or the angle of internal friction of the soil should have been approximately 30 degrees. The theoretical curve for $\phi = 30^{\circ}$ and $\delta = 0$ is also indicated in Fig. 6.11.

In Chapter 4, Section 4.5, the hydrodynamic analysis showed that the factor of safety against boiling or piping was close to unity for the most critical stage. As early as day 39 local boiling was observed at the bottom of the excavation. Boiling or quicking decreases the effective stress which in turn causes a decrease in shear strength and reduces the passive earth pressure. The passive resistance should become equal to zero if boiling were to occur homogeneously throughout the excavation. The measured low passive earth pressures lead to the conclusion that the angle of internal friction ϕ within the excavation was reduced from an initial value of 52 degrees to a value of approximately 30 degrees. This reduction came about because of the prevailing upward seepage conditions causing the soil to loosen.

Fig. 6.12 shows the variation of the measured coefficient of passive earth pressure with the deformation of cell G-7. On day 24 and day 28 the values of K_p were 0.35 and 0.37 respectively which are even lower than the K_o-values usually assumed for such a dense soil.

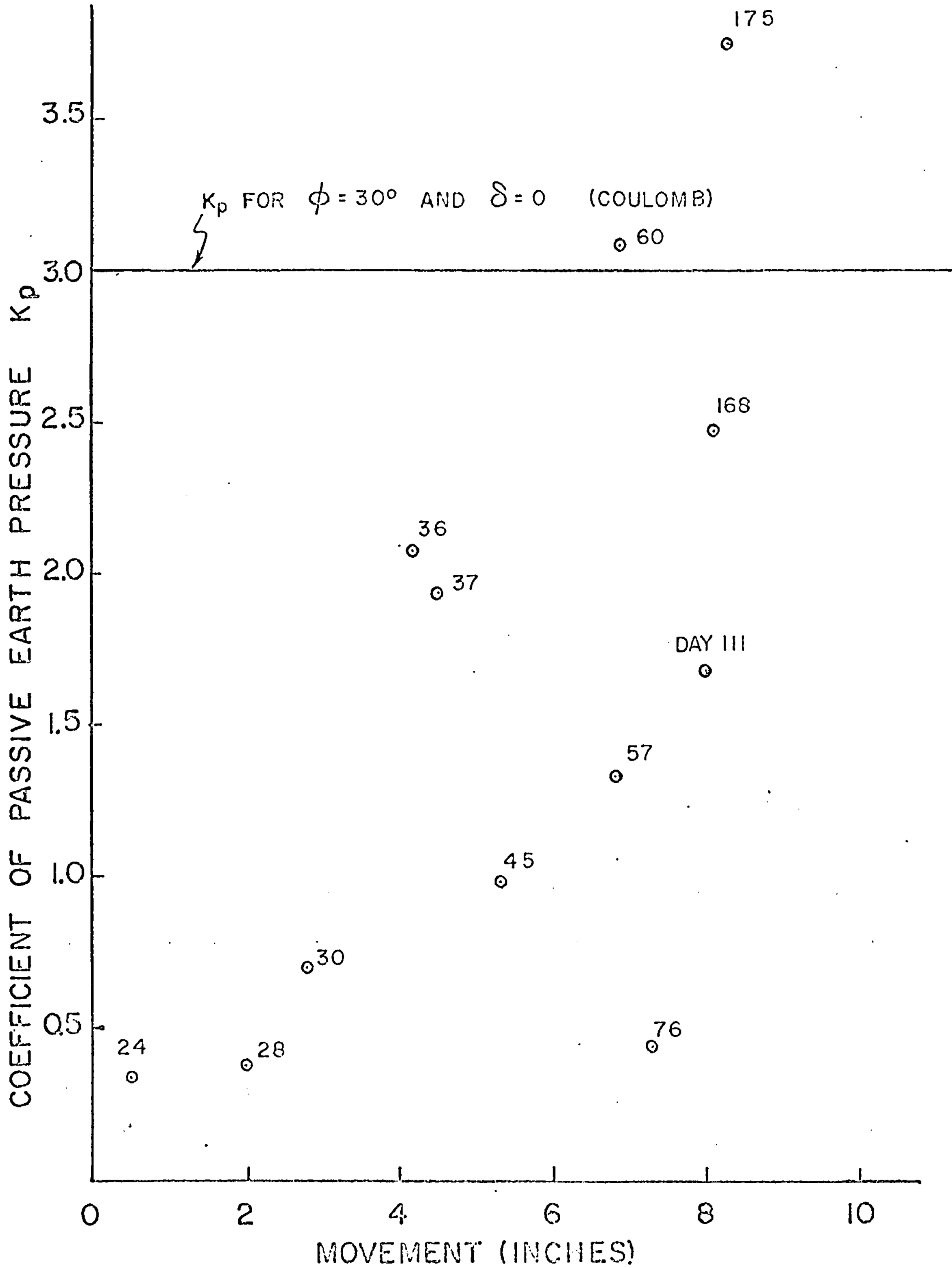

FIG. 6.12 VARIATION OF K_p WITH DEFORMATION

This suggests that the soil around cell G-7 was still in a loose condition due to jetting the piles into position. With increasing deformation the K_p- values also increased except for such days when boiling within the excavation was imminent. The last cell reading was obtained on day 175 when the water level inside the excavation was about two feet below the cell. The measured K_p-value was 3.75 this would correspond to an angle of internal friction of about 36 degrees neglecting wall friction. The K_p-value for $\phi = 52^{\circ}$ and $\delta = 0$ is 7.55 and for $\phi = 30^{\circ}$ and $\delta = 30^{\circ}$ is 3.00. The latter value is also indicated in Fig. 6.12. From this figure it can be concluded that the attainment of the coefficient of passive earth pressure is dependent on the wall deformation and that a change in soil density due to upward seepage will affect this coefficient markedly.

6.3 Earth Pressure Distribution

The earth pressure distributions are shown in Figs. 5.2.1 to 5.2.16 for different construction stages. Figs. 5.2.1 and 5.2.2 show a linear increase of pressure with depth for the at-rest condition.

During the period of excavation the measured earth pressures were larger in the centre and upper part of the cut. The distribution of pressure during this stage may also be interpreted from the curves of K_A vs. depth in Fig. 6.8, which indicate that the K_A-values for the top portion in some instances were twice the corresponding Coulomb value. The height of the resultant pressure above the bottom of the excavation for this stage was found to range between 0.42 H and 0.50 H with an average of approximately 0.46 H, which also reflects a non-triangular distribution. For a purely triangular distribution the centre of pressure would be at 0.33 H.

Fig. 6.13 shows the distribution of average earth pressure during the second period, that is, after the excavation had reached grade. The centre of pressure for this average distribution was 0.40 H. Thus it is evident that a significant redistribution of earth pressures had taken place during this latter period.

As mentioned in Section 6.2.2 the deformation behaviour matched approximately the wall movement D of Fig. 4.2.4. The theoretical earth pressure distribution corresponding to this type of deformation was plotted in dimensionless form in Fig. 4.2.15. To adopt this distribution for a multi-layered system the corresponding soil parameters had to be substituted. The average water level for the second stage was taken at elevation 742 feet. The change from the medium dense to the dense layer was also assumed to occur at this elevation, which corresponds to 0.6 of the depth of the cut. For the upper stratum (medium dense layer)

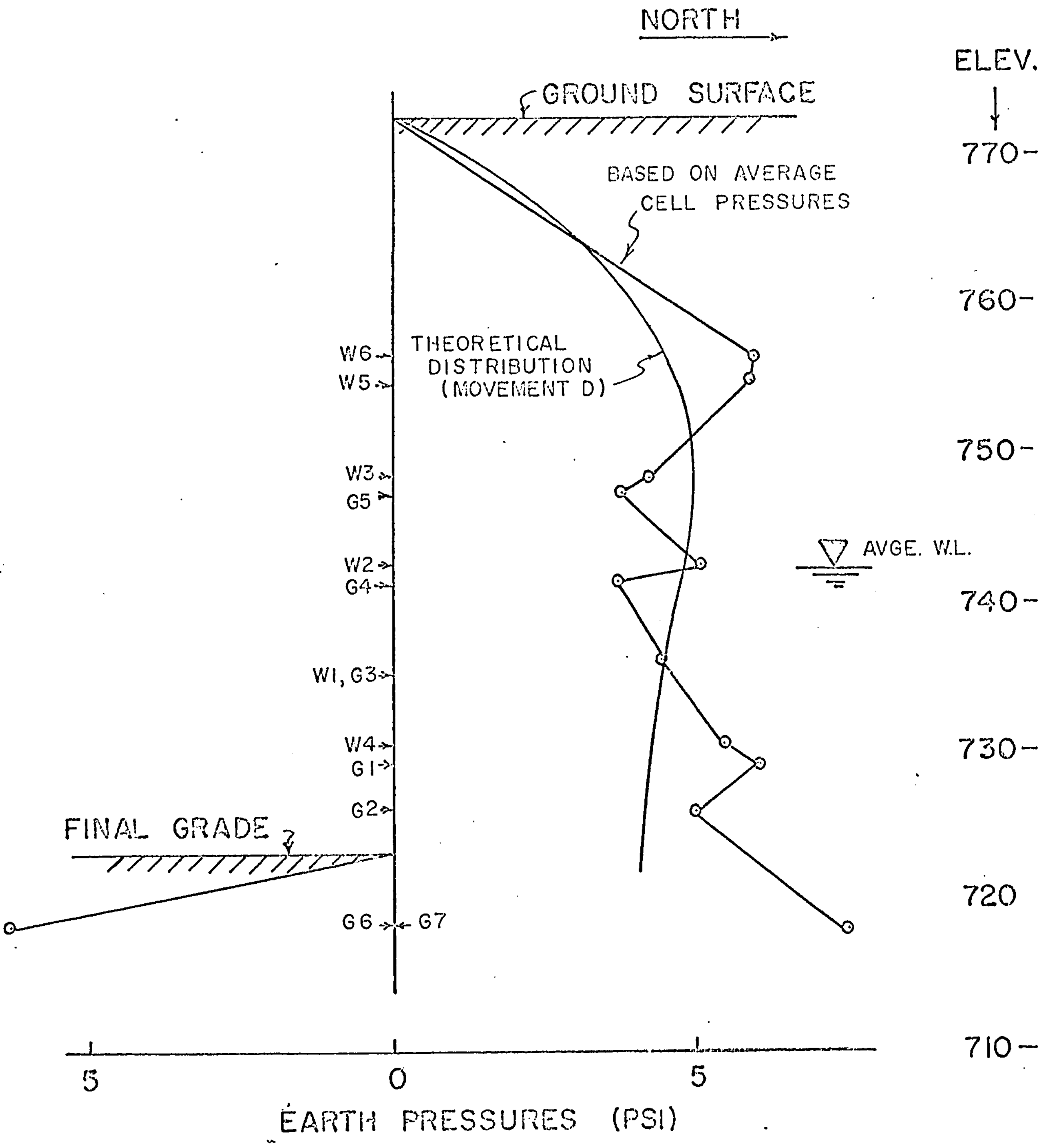

FIG. 6.13 EARTH PRESSURE DISTRIBUTION CURVES

the theoretical curve for $\phi = 42^{o}$ was plotted. The theoretical curve for the dense layer was plotted for $\phi = 52^{o}$ considering the soil above elevation 742 feet as surcharge and the pressure intensities for the dense layer were increased by this surcharge effect. Below the water table the submerged unit weight was used.

The comparison between the theoretical and the average measured lateral earth pressure distribution is shown in Fig. 6.13. The pressure intensity of the theoretical curve decreases below the depth of 748 feet. Below elevation 736 feet the measured values are in excess of the corresponding theoretical values. Above an elevation of approximately 757 feet no cells had been installed and a linear decreases in pressure is assumed with zero pressure at the ground surface. This assumption appeared reasonable because the soil against the sheet piles above elevation 760 was a loose backfill.

The theoretical distribution curve can be taken as a good fit of the experimental curve. The areas under each curve are approximately the same and are equal to the active Coulomb value.

The comparison between the theoretical and the measured average distribution shown in Fig. 6.13 leads to the conclusion that if the deformation of a wall can be predicted and can be controlled during construction the lateral pressure distribution on the wall can be predicted. The magnitude of the total earth thrust can be calculated by Coulomb's theory as discussed in Section 6.2.4.2.

CHAPTER 7

SUMMARY AND CONCLUSIONS

7.1 Summary

An experimental and analytical investigation has been conducted with the objective of finding a general relationship between the deformation of a braced cut in dense sand and the corresponding earth pressure distribution. The presently existing theories were scrutinized with respect to their applicability to the problem presented. A new solution is presented in Chapter 4 based on Dubrova's analysis (1963) which relates qualitatively and quantitatively the active earth pressure distribution to the mode of deformation of the cut. The theoretical solution gives expressions for four different deformation patterns which can be possibly expected on a braced excavation. Different values of angles of internal friction and different wall friction angles are considered. In each type of movement the total active pressure is equal to the Coulomb value. The analytical investigation further examines the solutions for the coefficient of earth pressure at rest as proposed by Timoshenko (1934), Jaky (1944) and Hendron (1963).

The passive earth pressure is evaluated theoretically taking into account the roughness of the wall, plane and curved surfaces of sliding.

The phenomenon of soil arching is investigated and the two different concepts suggested by Terzaghi (1954) and Tschebotarioff (1952) are clarified.

The hydrodynamic conditions of the braced excavation are examined and compared to the theoretical and empirical solutions proposed by Bazant (1963), Marsland (1953), McNamee (1949), and Ordujanz (1954).

The experimental investigation served three purposes: The first and main purpose was to collect reasonably accurate data with respect to earth pressure distribution and the total earth pressure acting on the braced cut and to record the corresponding deformation of the wall. Secondly, it provided information during and after construction concerning the effects of construction operations on the subsoil, and the corresponding effects of these changes in the subsoil upon the structure. Thirdly, it served as a safeguard to detect signs of impending danger during construction and to correct defects in design due to inevitable gaps in knowledge of subsoil conditions at the time the design criteria were laid down.

The experimental part was carried out on a full scale braced excavation which reached a depth of 50 feet. The quantities measured were, the earth pressures on two test piles, the pore water pressures, the horizontal deformations of the test section, and the strut loads. Field and laboratory tests supplied the necessary soil data.

7.2 Significance of Measurements

Comprehensive measurements of this kind in deep cuts in sand, prior to this London investigation, have only been made in Berlin, Munich, and New York. But at London it was the first time that the actual distribution of earth pressures in sand have been measured on a full-scale braced wall. It was also for the first time that earth pressure readings, strut loads and corresponding wall deformations on a braced wall retaining fine dense sand were recorded and systematically analysed.

The measurements are a valuable addition to the existing records of field measurements in braced excavations and should play an important part in reducing the cost of construction by improving future designs.

No new theory in soil mechanics should be accepted for practical use without ample demonstration by field observations that it is at least reasonably accurate under various conditions. Even small projects occasionally offer exceptional opportunities for significant additions to our knowledge, although some of the resulting interpretations may require modification in the light of future measurements.

7.3 Conclusions

The following conclusions are based on the experimental test results, theoretical analysis, and the preceding discussions and interpretations of the behaviour of earth pressures on braced walls.

1 - A theoretical solution, based on Dubrova's work (1963), relating the wall deformation and the corresponding lateral earth pressure distribution of a granular material on retaining structures has been presented. Five major modes of deformations which a retaining structure can be expected to undergo, have been considered. The final solution has been presented in graphical form (refer to Figs. 4.2.15 to 4.2.24) considering a wide range of angles of internal friction and angles of wall friction. The four possible types of deformation of a braced cut for which a graphical solution has been given all result in parabolic or pear-shaped lateral earth pressure distribution curves.

The experimental distribution of the lateral earth pressure on the braced cut was approximately parabolic with the maximum pressures occurring in the upper half of the cut. The average height of the resultant pressure above the bottom of the excavation was 0.46 H during excavation and approximately 0.40 H after the excavation had reached final grade. For a purely triangular distribution the centre of pressure would be at 0.33 H above the bottom of the cut. The actual deformation of the braced wall matched approximately the wall movement D of Fig. 4.2.4 and the agreement between the experimental lateral pressure distribution curve and the corresponding theoretical curve is fairly good. The agreement between the theoretical and the measured average earth pressure distribution leads to the conclusion that if the deformation of a wall can be predicted and can also be controlled during construction the pressure distribution on the wall can be predicted.

2 - There was a fairly good agreement between the total active earth pressure obtained from the pressure cells and the corresponding Coulomb value. During excavation the experimental values were often higher, in one instance as much as 30 per cent. After the cut had reached its final depth (day 59) the agreement was within 10 per cent. By this time the wall had deflected an average distance of 0.006 H and the measured total earth pressure remained relatively constant regardless of the continuing deformation of the wall and was consistent

with that computed by Coulomb's theory. It therefore can be concluded that if certain deformation requirements are met the total active earth pressure of dense sand on open cuts can be predicted by Coulomb's theory.

3 - The theoretical K_A-values as given by

$$K_A = \left[\frac{\cos \phi}{1 + \sin \phi}\right]^2 = \tan^2 (45 - \frac{\phi}{2}) \qquad (4.2.8)$$

necessitates a triangular pressure distribution over the entire depth of the cut. The measured K-values at different depths after the cut had reached its final grade were not constant. The experimental values were higher in the upper half of the cut compared to the theoretical values, as is found from a parabolic earth pressure distribution.

An experimental relationship between the horizontal soil strain and the variation of K-values has been established (Fig. 69). After the horizontal strain of the soil had reached five per cent the K-values assumed a minimum ranging between 0.19 and 0.10 with an average value of 0.15. It is especially noteworthy how suddenly the K-values approached a constant value after this soil strain had been exceeded. It is therefore concluded that when the horizontal strain within the retained soil mass exceeded five per cent the soil was in a completely active state. It is held that this relationship will be similar for other cuts in dense sand having similar soil properties and deformation behaviour.

4 - The theories for predicting Ko-values as proposed by Jaky (1944) and Hendron (1963) do not apply to overconsolidated dense sand deposits. It appears therefore, that in natural deposits, the coefficient of earth pressure at rest will be governed by the nature of the sedimentation processes which have produced the deposit and by the stress history of the formation.

A mode coefficient of earth pressure at rest of 0.70 was measured which is identical to values obtained by Terzaghi (1934) for a similar dense sand. This value would correspond to an internal friction angle of 17.5° (according to Jaky) and approximately to 9° (according to Hendron). Such low friction angles have never been obtained on dense sands by any test. It is therefore questionable that Ko is influenced at all by the interlocking or sliding of grains, since this phenomenon depends on motion to be fully mobilized whereas Ko is fully active prior to any motion or strain within the soil.

5 - The deformation of the imbedded part of the wall should have been sufficiently large in order to mobilize the full passive resistance.

The measured passives pressures were consistently lower than the calculated values based on the initial soil density. It is therefore concluded that the prevailing upward seepage conditions reduced the soil density within the excavation and the angle of internal friction was correspondingly decreased from an initial value of 52 degrees to a value of about 30 degrees.

6 - For any large-scale model test or full-scale retaining wall for which measurements have been made it was always observed that the active earth pressure reached a minimum value after the structure had yielded a certain amount. Any further yield of the wall did not change the earth pressure. A decrease of the shear strength parameter ϕ with increasing strain as exhibited for dense sand in the laboratory would necessitate an increase in the total active earth pressure. Since the shear strength does not appear to decrease with large strains in model or field tests the peak shear strength should be used.

7 - The total earth pressures obtained from the strut load measurements were lower than the corresponding pressures from the earth pressure cells or the corresponding Coulomb values. The strut load readings were somewhat erratic, not necessarily corresponding to the excavation progress.

8 - The sheet pile penetration depth and the installed well point system did not prove entirely sufficient to prevent local boiling with the excavation.

7.4 Suggestions for Further Research

The foregoing investigation appears to warrant several lines of future research.

1) A few sets of field observations on braced cuts cannot be considered as absolute conclusive evidence that future excavations under similar conditions will perform similarly. Therefore future field instrumentation should be attempted on structures but only where the soil conditions are thoroughly known and relatively simple.

2) Regardless of the method used in measuring strut loads and earth pressures, the observations should be made on several independent profiles, in order to get a conception of the deviation of the loads on individual profiles from the average.

3) The deflection of the struts induces arching effect in the soil adjoining the deflecting supports and relieves the pressure to an unknown extent. It was shown qualitatively in the foregoing chapters, that arching effect did occur, but its magnitude and relation to strain is not yet known. This should be investigated, possibly in the laboratory where conditions are more controllable.

4) Further research should be devoted to the testing of soils under plane strain conditions in order that the shear strength parameters are compatible to those mobilized in the field under the same strain conditions.

5) A large scale model study of a braced cut seems to be warranted to further correlate the theories proposed in Chapter 4 with actual behaviour.

BIBLIOGRAPHY

Bazant, Z., 1963. Ergebnisse der Berechnung der Stabilitaet gegen Hydraulischen Grundbruch mit Hilfe der Elektronen-Rechenanlage. Proc. Int. Conf. on Soil Mech. and Found. Eng., Budapest, September.

Belidore, B.F., 1729. La Science des Ingénieurs. Paris, (1st edition), 1813 ed. edited by Navier.

Bierbaumer, A., 1913. Die Dimensierung des Tunnelmauerwerkes. Leipzig, W. Engelmann.

Bishop, A.W. and G. Eldin, 1950. Undrained triaxial tests on saturated sand and their significance in the general theory of shear strength. Géotechnique II,

Bishop, A.W. and D.J. Henkel, 1957. The measurements of soil properties in the triaxial test. Edward Arnold (Publishers) Limited, London.

Bjerrum, Kringstad and Kummeneje, 1961. The shear strength of a fine sand. Proc. 5th Int. Conf., I, 29.

Bjerrum, L., Kenney, T.C. and B. Kjaernsli, 1965. Measuring instruments for strutted excavations. Journal of Soil Mechanics and Foundation Division, Proc. A.S.C.E. SM 1, January, 111.

Caquot, A., 1934. Equilibre des Massifs à Frottement Interne. Paris, Gauthier-Villard.

Caquot, A. and J. Kerisel, 1948. Tables for the calculation of passive pressures, active pressure and bearing capacity of foundations. Translation from French by Maurice Bec, (revis. translation by Chief Scientific Advisers Div. Min. of Works, London), Gauthier-Villard, 120.

Chapman, L.J. and D.F. Putman, 1966. The Physiography of Southern Ontario, 2nd ed. University of Toronto Press.

Chen, L.S., 1948. An investigation of stress-strain and strength characteristics of cohesionless soils. Proc. 2nd Int. Conf. on Soil Mech. and Found. Eng., 5:35.

Collin, A., 1848. Recherches Expérimentalles sur le Glissement des Terres. (Translatéd into German), 1848, Ingénieur, I:309.

Constable, C., 1874. Retaining walls, theory and practice. Transactions, A.S.C.E., 3:67.

Cornforth, D.H., 1964. Some experiments on the influence of strain conditions on the strength of sand. Géotechnique XIX, 2:143-167.

Coulomb, C.A., 1776. Essai sur une Application des Règles des Maximis et Minimis à quelques Problèmes de Statique. Mémoire Académie Royal des Sciences, 7, Paris.

Darcy, H., 1856. Les Fontaines Publiques de la Ville de Dijon. Dijon.

Donath, A.D., 1891. Untersuchungen ueber den Erddruck auf Stuetzwaende. Zeitschrift fuer Bauwesen, Berlin.

Drucker, D.C. and W. Prager, 1951. Soil Mechanics and Plastic Analysis or Limit Design. Office of Naval Research, Techn. Rep. No. 64, Providence, November.

Dubrova, G.A., 1963. Interaction of Soil and Structures. Izd. Rechnoy Transport, Moscow.

Engesser, F., 1882. Ueber den Erddruck gegen innere Stuetzwaende. Deut. Bauzeigt., 16:91-93.

Feld, J., 1923. Accurate experimental determination of lateral earth pressure. Trans. A.S.C.E., 86:1448.

Feld, J., 1940. Review of pioneer work in earth pressure determination and recommendation for earth pressure evaluation. Proc. Highway Research Board, U.S.A.

Fellenius, W., 1927. Erdstatische Berechnungen mit Reibung und Koheasion und unter Annahme Kreiszylindrisher Gleitflaechen. Wilh. Ernst, Berlin.

Flaate, K.S., 1966. Stresses and movements in connections with braced cuts in sand and clay. Ph.D. Thesis, University of Illinois, Urbana, pp. 264.

Forchheimer, Ph., 1882. Ueber Sanddruck und Bewegungserscheinigungen im Inneren Trockenen Sandes. Zeits. Oesterreich Ing. u. Arch. Vienna, 34:111, and 35:103.

Franzius, O., 1924. Versuche mit Passivem Erddruck. Der Bauingenieur, p. 314, 554.

Franzius, O., 1928. Apparatus for earth pressure experiments. Der Bauingenieur, Hefte 7 and 8.

Gauthey, E.M., 1816. Oeuvres. Published by Navier, Traité de la Construction des Ponts. 1:1809-1818, Paris.

Hagen, G.H.L., 1852. Druck und Bewegung des Trockenen Sandes. Ber K. Preus, Akad. Wissenschaften, p. 35, Berlin.

Hansen, J. Brinch, 1953. Earth pressure calculation. The Danish Technical Press, Copenhagen.

Hansen, J. Brinch, 1953. A general earth pressure theory. Proc. 3rd Int. Conf. on Soil Mech. and Found. Eng., II.

Harr, M.E., 1966. Foundations of Theoretical Soil Mechanics. McGraw-Hill Book Company, p. 217.

Hendron, Jr. A.J., 1963. The behaviour of sand in one-dimensional compression. Ph.D. Thesis, University of Illinois, Urbana.

Hertwig, A., 1939. Bemerkungen ueber neuere Erddruckuntersuchungen. Veroeffentlichungen der Degebo, Heft 7, Berlin.

Hope, Ltt., 1845. Experiments on the pressure of earth. London, Royal Engineers Papers, 7:69.

Jakobsen, B., 1957. Some fundamental properties of sand. Proc. 4th Int. Conf., I:167.

Jaky, J., 1944. The coefficient of earth pressure at rest. Journal of the Society of Hungarian Architects and Engineers, Budapest, p. 355-358.

Jenkins, C.F., 1932. Pressure on retaining walls. Proc. Inst. C.E., 234:103.

Karman, Th.v., 1926. Ueber elastische Grenzzustaende. Proc. Sec. Int. Congress, Applied Mechanics, Zurich.

Kenney, T.C. and G.H. Watson, 1961. Multi-stage triaxial test for determining c' and ϕ' of saturated soils. 5th Int. Conf. I:191-195.

Kirkpatrick, W.M., 1957. The condition of failure for sands. Proc. 4th Int. Conf. on Soil Mech. and Found. Eng., I:172.

Karafláth, L., 1953. Angewandte Bodenmechanik. Épitésügyi Kiadó, Budapest.

Kolbuszewski, J.J., 1948. An experimental study of the maximum and minimum porosities of sand. Proc. 2nd Int. Conf. on Soil Mech. and Found. Eng., I:158-165.

Kötter, F., 1892. Die Entwicklungen der Lehre vom Erddruck. Jahresber. deutsch. Math. Ver., Vol. 2.

Krey, H., 1923. Groesse und Richtung des Erddruckes. Bautechnik, p. 219, 338. 1924, p. 462.

Lee, I.K., 1960. The application of vibrating wire measuring principle to the measurement of soil pressure. Austr. Journal of Applied Science, II:65.

Lehmann, H., 1942. Die Verteilung des Erddruckes an einer oben drehbar gelagerten Wand. Bautechnik, Heft 31/32.

Lumb, P., 1964. Multi-stage triaxial tests on undisturbed soils. Civil Engineering and Public Works, Review, p. 591-595.

Mandel, J., 1951. Wasserstroemung unter einer Spundwand (Hydraulischer Grundbruch), Travaux.

Marsland, A., 1953. Model experiments to study the influence of seepage on the stability into a sheeted excavation in sand. Géotechnique III, 6:53.

Mayniel, E., 1808. Traité Expérimental, Analytique et Pratique de la Poussée des Terres et Murs de Revêtement. p. 316, Paris.

McNamee, J., 1949. Seepage into a sheeted excavation. Géotechnique I:229-241.

Meem, J.C., 1910. Pressure resistance and stability of earth. Trans. A.S.C.E., 70:352-411, New York.

Mises, R. von, 1913. Mechanik der festen Koerper im plastisch-deformablen Zustand. Nachr. Ges. d. Wiss. zu Goettingen.

Molnar, L., 1957. Bestimmung der Gesetzmaessigkeiten der Fluessigkeitsgstroemungen mit Hilfe der Elektrischen Analogie. Hidrologiai Kozlemenyck, Budapest, No. 4.

Moulton, H.G., 1920. Earth and rock pressure. Trans. American Institute of Mining and Metallurgy Engs., p. 20.

Müller-Breslau, H., 1906. Erddruck auf Stuetzmauern. Berlin, 159 pp.

Müller-Haude and V. Schreiber, 1965. Neue Bodendruckmessungen an Baugruben und Tunnelbauten der Berliner U-Bahn. Bautechnik, Heft 9, September.

Nadai, A., 1928. Plasticitaet und Erddruck. Handbuch der Physik. VI, Ch. 6.

Nash, J., 1953. The shearing resistance of a fine closely graded sand. Proc. 3rd Int. Conf., 1953, Vol. I, p. 160.

Norwegian Geotechnical Inst., 1962. Measurements at a strutted excavation. Oslo Subway, Vaterland 1, N.G.I. Technical Report No. 6.

Odquist, F., 1934. Plasticitetsteori med Tillampningar. Ingeniør vetenskapsakademien, Stockholm.

Øien, K., 1958. An earth pressure cell for use on sheet piles: Oslo Subway. Brussels Conference on Earth Pressures Problems. 2:118-126, Belgium.

Ordujanz, K.S., 1954. Gruendungen fuer Bauwerke. Berlin.

Peck, R.B., 1943. Earth pressure measurements in open cuts, Chicago Subway. Trans. A.S.C.E., 108:1008-1036.

Pettibone, H.C. and J. Hardin, 1964. Research on vibratory maximum test for cohesionless soils.

Prandtl, L., 1920. Ueber die Haerte plastischer Koerper. Nachr. der Ges. der Wiss., Goettingen.

Rankine, W.J.M., 1857. On the stability of loose earth. Trans. Royal Soc., London, Vol. 147.

Rendulic, L., 1935. Ein Beitrag zur Bestimmung der Gleitsicherheit. Bauingenieur, Heft 19/20.

Rendulic, L., 1940. Gleitflaechen Prueflachen und Erddruck. Bautechnik Heft 13/14.

Rowe, P.W., 1952. Anchored sheet pile walls. Proc. Inst. Civ. Eng., Paper 5788, London.

Rowe, P.W., and A. Briggs, 1961. Measurements on model strutted sheet pile excavation. Proc. of the 5th Int. Conf. on Soil Mech. and Found. Eng., II, Paris.

Siegler, M., 1887. Expériences Nouvelles sur la Poussée des Terres. Annales des Ponts et Chaussées, 13:488.

Spilker, A., 1937. Mitteilung ueber die Messung der Kraefte in einer Baugrubenaussteifung. Bautechnik, Heft. 1.

Skempton, A.W., and W.H. Ward, 1952-53. Investigations concerning a deep cofferdam in the Thames Estuary clay at Shellhaven. Géotechnique, III:119-139.

Sokolovsky, V.V., 1942. Statics of Soil Media. Moscow. (Transl. by D.H. Jones and A.N. Schofield, 1960).

Stroyer, P.R.N., 1935. Earth pressure on flexible walls. Journal Inst. Civil Eng., November, paper No. 5024.

Terzaghi, K., 1934. Large retaining wall test. I-V. Engineering News Record, Vol. 112.

Terzaghi, K., 1936. A fundamental fallacy in earth pressure computations. Journal, Boston Society of Civil Eng., April, p. 78.

Terzaghi, K., 1936. Distribution of the lateral pressure of sand on the timbering of cuts. Proc. 1st Int. Conf. on Soil Mech., I.

Terzaghi, K., 1941. General wedge theory of earth pressure. Trans. A.S.C.E. Paper No. 2099, 106:68-97.

Terzaghi, K., 1954. Theoretical Soil Mechanics. John Wiley & Sons, Inc., New York.

Terzaghi, K., 1954. Anchored bulkheads. Trans. A.S.C.E., 119:1243-1280.

Terzaghi, K., and R.B. Peck, 1967. Soil Mechanics in Engineering Practice. John Wiley & Sons, Inc., 2nd ed., Art. 48.

Timoshenko, S., 1934. Theory of Elasticity. McGraw-Hill, p. 416.

Trollope, D.H., and I.K. Lee, 1957. The performance of a laboratory earth pressure cell. Austr. Journal of Applied Science, 8, 2:84.

Tschebotarioff, G.P., 1948. Large scale model earth pressure tests on flexible bulkheads. Proc. A.S.C.E. , Jan. p. 9-48.

Tschebotarioff, G.P., and J.D. Welch, 1948. Lateral earth pressures and friction between minerals. Proc. 2nd Int. Conf. on Soil Mech. VII:135-148.

Tschebotarioff, G.P., 1951. Soil Mechanics, Foundations and Earth Structures. New York, McGraw-Hill.

Tschebotarioff, G.P., 1952. Einfluss der Gewoelbebildung auf die Erddruckverteilung. Bautechnik-Archiv, Heft 8.

Triandafilidas, G.E. et al, 1964. An experimental evaluation of soil arching. Proc. of the Symposium on Soil Structure Interaction, University of Arizona, Tucson, Arizona, September.

Vernant, B. de Saint, 1870. Comptes Rendus. 70, 73, 74, Gauthier-Villard, Paris.

Vollmy, A., 1937. Eingebettete Rohre. Mitt. Inst. Baustatik, Eidgen. Tech. Hochschule, Zurich, Mitt. No. 9.

Whitman, R.V. and U. Luscher, 1962. Basic experiment into soil-structure interactions. Journ. of Soil Mech. and Found. Div. Proc. A.S.C.E., 88. December.

Woltmann, R., 1794. Beitraege zur Hydraulischen Architektur. 3, 4 (1799).

Wood, C.C., 1958. Shear strength and volume change characteristics of compacted soil under conditions of plane strain. Ph.D. Thesis, University of London.

APPENDIX A

PERFORMANCE AND RELIABILITY OF THE VIBRATING WIRE EARTH PRESSURE CELLS

A.1 General.

During the period from December 1963 to July 1964 readings were obtained on thirteen pressure cells installed on two test piles of a five-storey basement excavation for a $8-million expansion of London, Ontario's Greenway Pollution Control Centre, a project designed to triple the city's sewage treatment capacity.

The pressure cells were installed on two adjacent sheet piles, No. 14 and No. 15, respectively, on the 42 - ft. wide north wall of the cofferdam (Fig. A.1). Waterlevel standpipes were also installed on the two piles in order to measure the water pressures. Sheet pile movements and strut loads were also measured as discussed in Chapter 5, but will only be discussed here with respect to effects on pressure cell readings.

The vibrating-wire pressure cells have many advantages over other types of pressure transducers and were chosen for the following reasons:

(i) They were considered to be more stable and accurate than other conventional transducers used before.

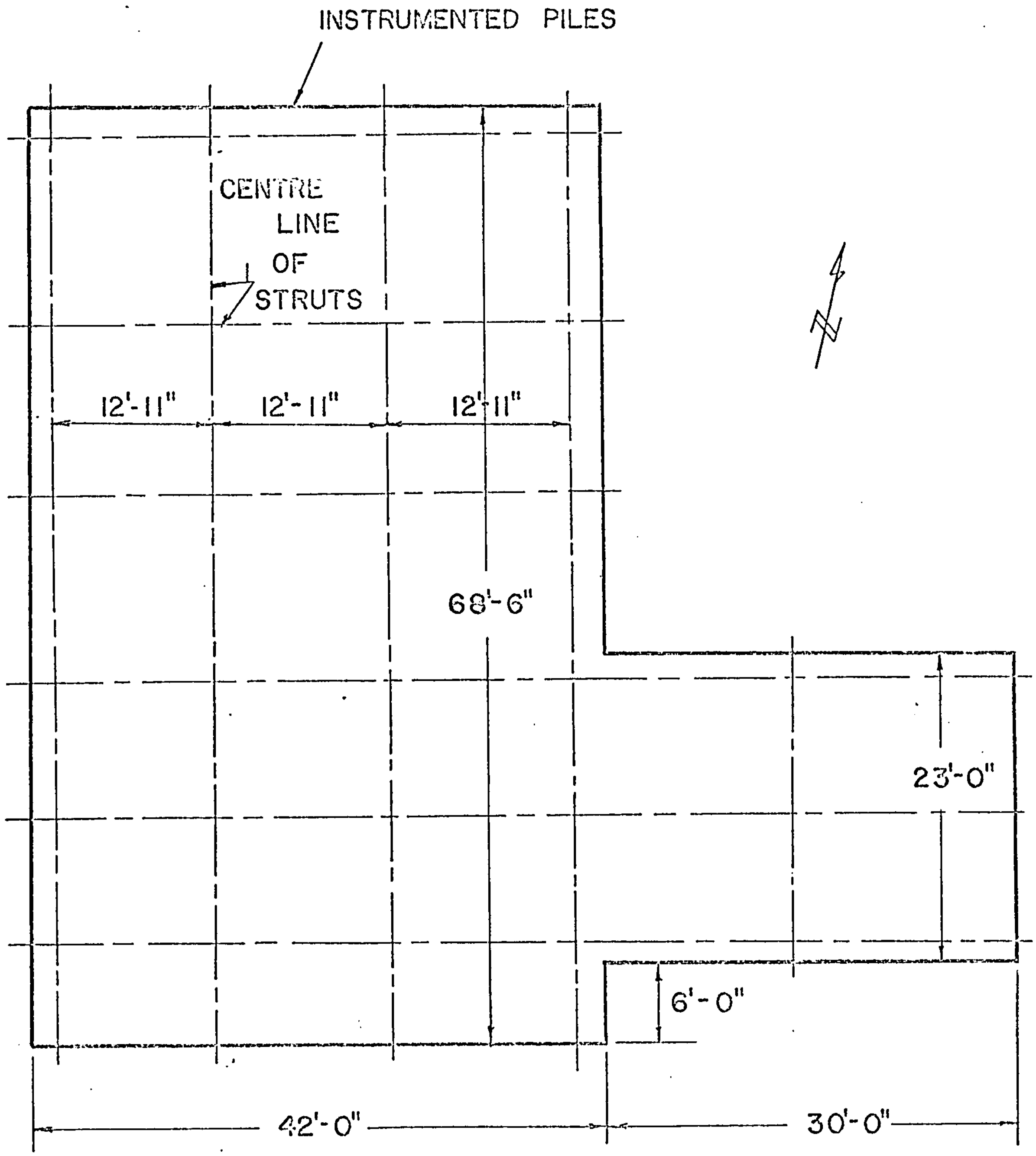

FIG.A.I LAYOUT OF EXCAVATION

(ii) The past favourable experience gained by the Norwegian Geotechnical Institute with these instruments.

(iii) The National Research Council's willingness to loan seven of these cells and the electronic read-out instrument for this project.

(iv) The fact that the cells could be read at a remote station and so did not interfere with the excavation and construction operations.

(v) The possibility of retrieving the cells easily at the end of construction.

A.2 Principle of the Vibrating-Wire Earth Pressure Cell

The method depends upon the measurement of the pitch or vibration of a stretched wire, which in turn is a measure of the tension applied. The fundamental natural frequency of a stretched wire is:

$$f_o = \frac{1}{2L}\sqrt{\frac{\sigma_o}{\rho}} \quad \text{OR} \quad f_o^{\,2} = \frac{1}{4L^2\rho}\,\sigma_o \qquad (1)$$

Where f_o = natural frequency (pitch of emitted sound)

L = length of the wire between grips

σ_o = tensile stress in the wire, and

ρ = density of the wire (mass per unit volume)

A change of the stress in the wire from σ_o to σ, causes a change in the frequency from f_o to f and Eq. (1) takes the following form:

$$(f^2 - f_o^2) = \frac{1}{4L\rho} (\sigma - \sigma_o), \text{ since } \sigma - \sigma_o = \Delta\sigma$$

we get

$$\Delta\sigma = 4L^2\rho \, (f^2 - f_o^2) \tag{2}$$

For a given $\Delta\sigma$, the sensitivity, Δf, is increased by decreasing L and σ. The lower limit for σ is reached when the wire no longer emits a pure tone owing to its own lack of stiffness. Similarly if the length of the wire L is too short, end conditions become too important. Naturally the actual relationship between Δf and $\Delta\sigma$ is obtained by calibration and not by using Eq. (2). The accuracy of the vibrating wire method depends largely on the accuracy of measuring the vibration frequency of the wire.

A.3 Description of the Cell

The cell (Type V) is discussed in detail by the Norwegian Geotechnical Institute's Technical Report No. 9, 1962 and only a short description will be given here with reference to Fig. A.2.

The cell is machined from mild steel and consists essentially of a housing (12) and a diaphragm (2) which is a 2.5 mm steel plate with two posts set a distance of 57 mm apart and an outer ring of 10 mm thickness and a total height of 14 mm. The diaphragm rested on three

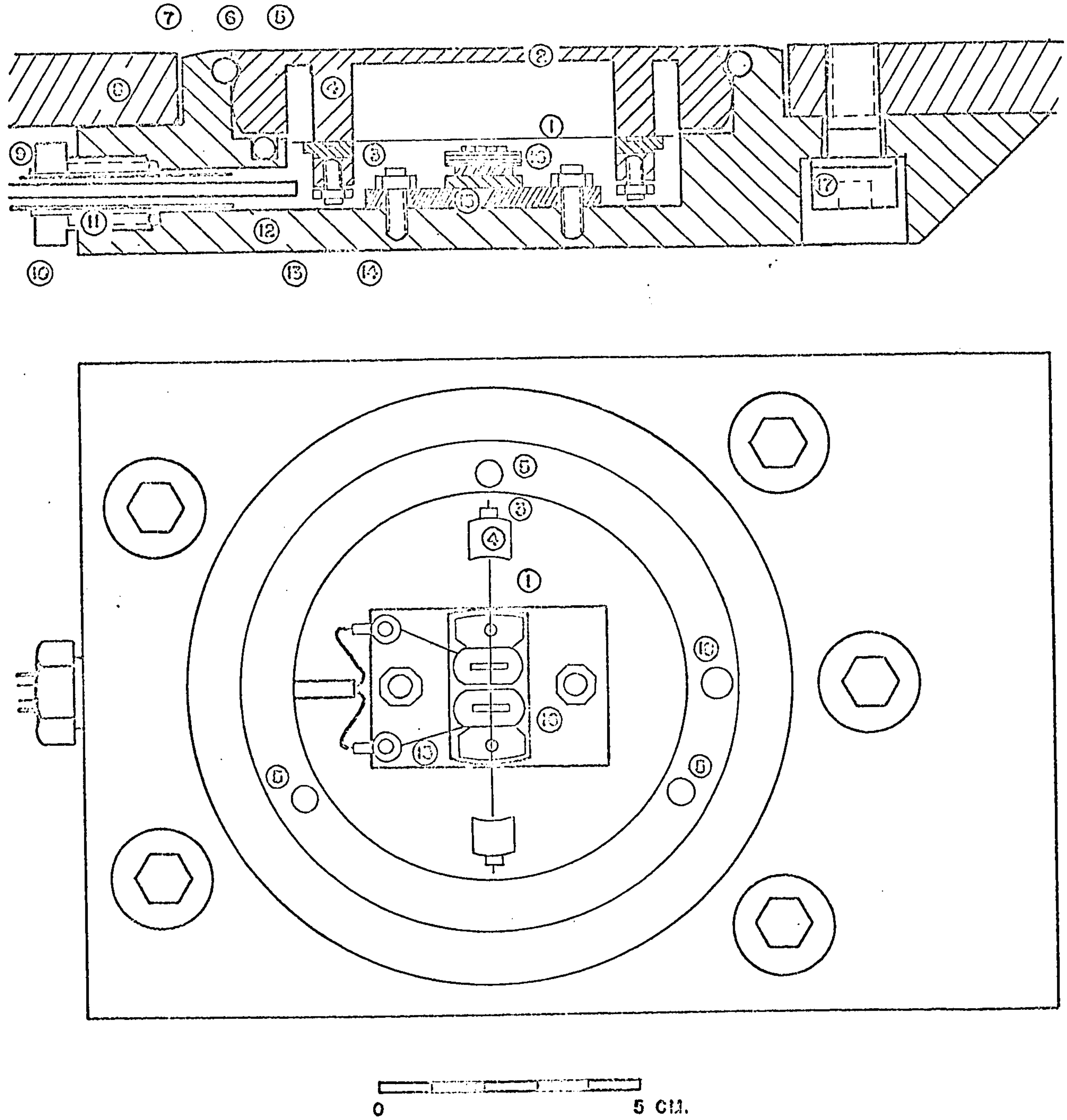

1. Steel wire
2. Diaphragm
3. Clamping pin
4. Arm
5. Steel ball
6. O-ring
7. O-ring
8. Sheetpile
9. Cable
10. Copper tube
11. Fitting screw
12. Housing
13. Locking nut
14. Unbrako Z screw
15. Insulation strip
16. Electromagnet
17. Screw
18. Hole for a guide pin

FIG. A.2 VIBRATING-WIRE PRESSURE CELL

steel balls (5) at a mutual angular spacing of 120° on the shoulder of the housing. The inclusion of the steel ball support made the cell more sensitive and different degrees of tightening of the cell bolts did not affect the readings. At a pressure of 35 psi the diameter/deflection ratio is about 2000. The diameter/deflection ratio should be $\cong$ 1000 according to an investigation carried out by the U.S. Waterways Experiment Station (1944) for a pressure cell mounted flush with the surface of a rigid wall retaining loose sand. The diaphragm is bearing on the housing by three steel balls (5) and is sealed off by an O-ring. An electromagnet (16) is mounted on the bottom of the housing and plucks the wire stretched between the two posts of the diaphragm. The induced back-emf by the vibrating wire is read out and compared to a reference vibrating quartz crystal by an electrical instrument. A change of pressure on the diaphragm gives a corresponding change of tension in the wire, that is, a change of natural frequency.

The cells were mounted flush with the face of the sheet pile by means of 5 bolts. The housing is fitted into a hole cut in the sheet pile by a torch and bolted tight. The bolts were torqued to a maximum of 60 ft - lb to prevent the stripping of the threads. The electrical cables were brought up to the ground surface inside a plastic or copper tubing protected by a steel angle welded to the sheetpile.

A.4 Calibration of the Cells

A.4.1 Laboratory Calibration

From Eq. (2) it is seen that the changes of stress in the wire is directly proportional to the square of the corresponding frequency change. The constant of proportionality for each cell had to be determined by calibrating the gauge against known pressures. Since the cells were to be used to measure the pressure of dense fine sand against sheet piling they should be calibrated against sand pressures. The result of this calibration test is shown in Fig. A.3 together with calibration curves for the same cell calibrated against known water and air pressures. Owing to the negligible difference in results the calibration against water pressure was generally adopted for simplicity sake for all thirteen earth pressure cells.

The calibration of the cells against sand pressure was done in an 8 in. inside diameter and 10 in. high tank with the cell mounted to the bottom of the tank. The five bolts were tightened to a uniform torque of 60 ft - lb. Calibrations were made with sand layers compacted to heights of 2 in., 4 in., and 6 in., respectively, in order to evaluate the influence of tank wall friction on the cell reading. The inside of the wall was polished and lined with a polyethylene sheet to minimize the side friction effect. A thin rubber membrane was placed over the sand and a known air pressure was applied for calibration purposes.

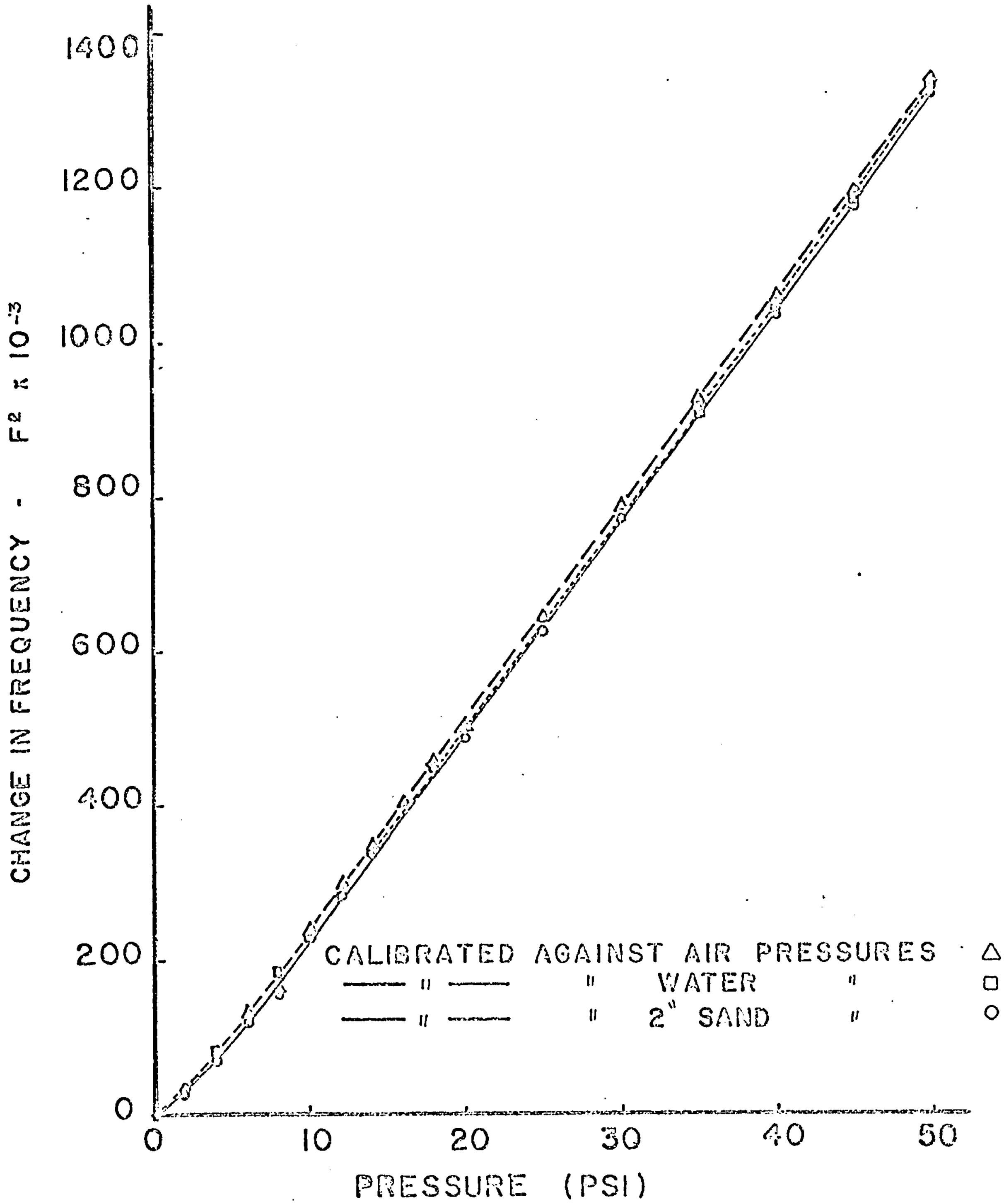

FIG. A3 CALIBRATION CURVES FOR CELL W-6 CALIBRATED AGAINST AIR-, WATER-, AND SAND PRESSURES

Five cells of the Waterloo series were calibrated using this method and a typical test result is shown in Fig. A.4.

The cell reading decreased considerably for the same applied loading pressure due to the influence of wall friction as the sand height became greater than one half of the tank diameter. Arching effect in the soil took place in two forms. Firstly, arching effect could be expected across the diaphragm due to its deflection and secondly, arching effect across the whole tank due to the friction of the side walls. For the unloading cycle the reverse effect was observed, the actual pressure on the cell was greater than the applied pressure since the friction force was acting now in the opposite direction.

The calibration of the cells is extremely important since once driven into the ground there is no way of checking the zero frequency. A shift in zero frequency can only be detected when the cell is still above ground or after it is recovered and recalibrated. Eleven cells were recovered and recalibrated and most of the cells showed a decrease in zero frequency due to factors which will be discussed later. However, all the recalibration curves coincided with the original calibration as shown in Fig. A.5, for one cell G-5. This was expected since the squares of the difference of frequency was plotted against pressure in order to give a straight line relationship. Even an appreciable change of the zero frequency will hardly affect the squares of the difference of the frequency to a large extent. Two cells, G-6, and G-7, were below excavation grade and could not be retrieved.

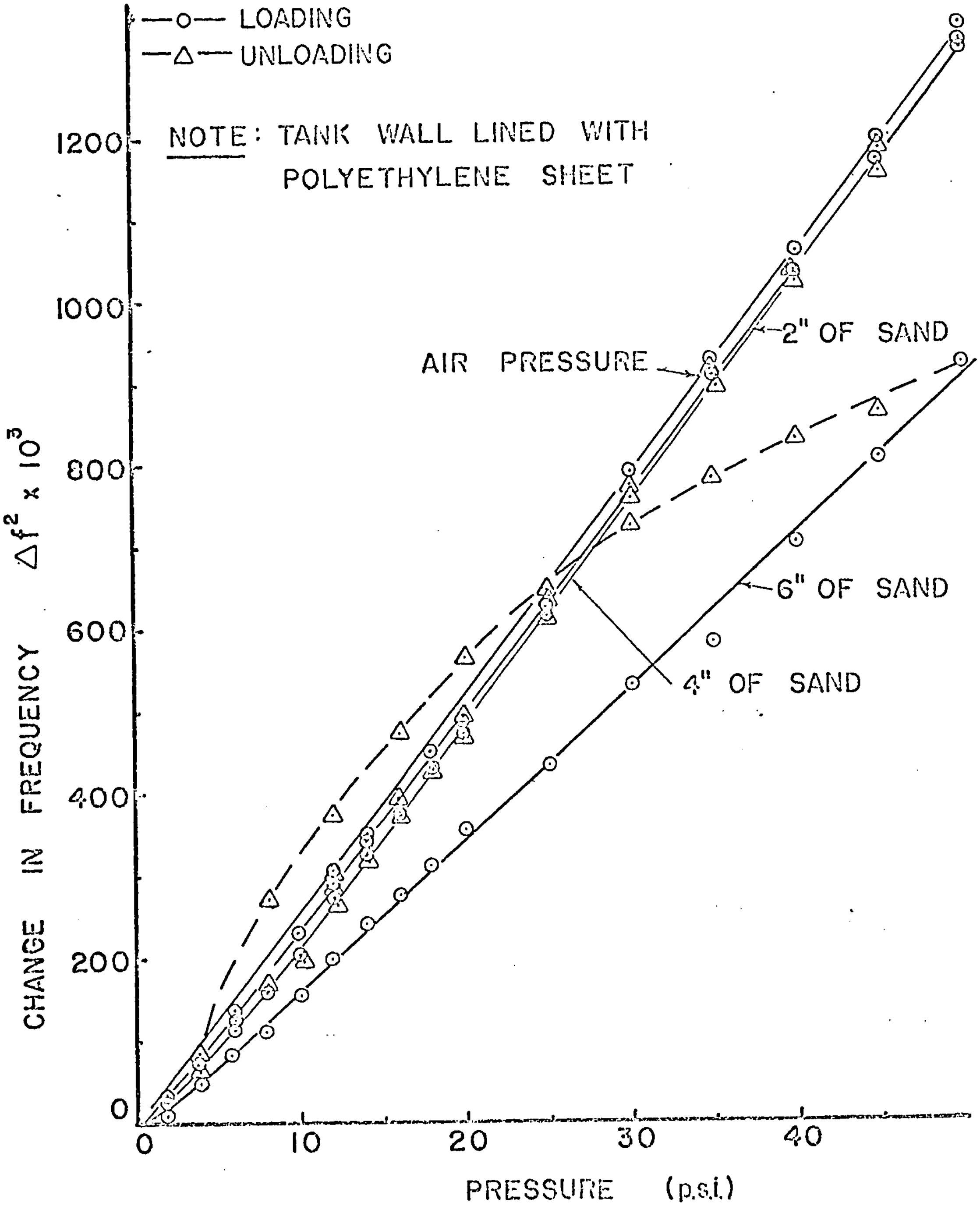

FIG. A.4 CALIBRATION ON SAND TANK CELL W-6.

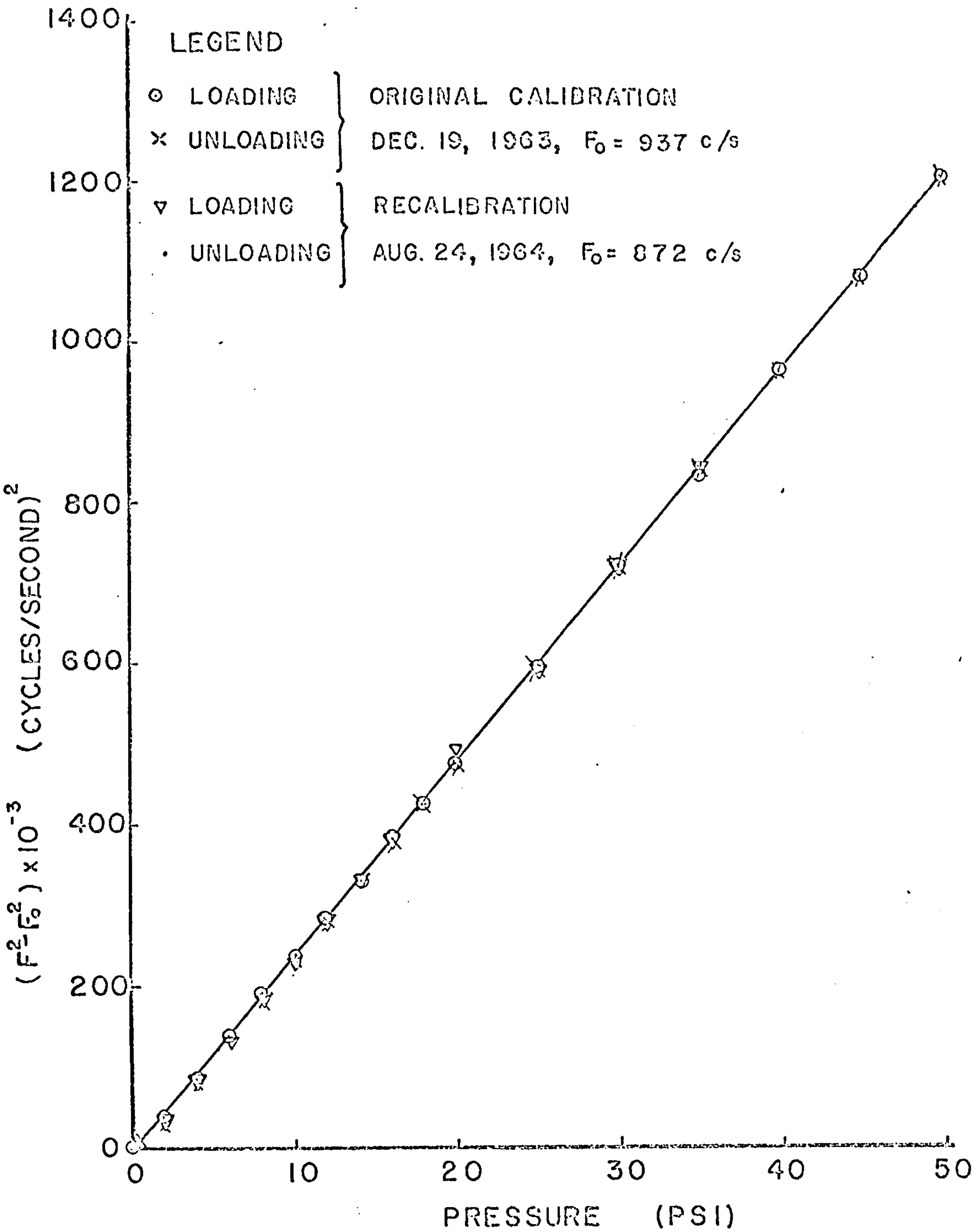

FIG. A.5 CALIBRATION AND RECALIBRATION OF PRESSURE CELL G-5

A.4.2 Field Calibration

The sheet piles were driven through dense fine sand and it was feared that because of the severe driving conditions slippage of the wire in the grips would occur i.e. a decrease of wire tension. Later this was found to be true. Two earth pressure cells, G-6, and G-7, were below the bottom of the excavation and were not retrieved for recalibration after completion of the program. These two pressure cells were installed at the tips of the respective sheet piles and were the first ones to go underground when driving started. To check their zero frequency at the end of driving the following procedure was used:

Each of the thirteen cells was connected with either a plastic tube for the Waterloo cells, or a copper tube for the Geonor cells. The purpose of the tubing was two-fold, firstly, to protect the electrical lead wires that ran inside the polyethylene tube, and secondly, to keep the inside of the cell at atmospheric pressure. The copper tube for cells G-6 and G-7 was hooked up to a vacuum pump and/or compressor and the pressure inside the cell was decreased or increased at will. If the inside cell pressure was equal to the external pressure exerted on the diaphragm by the soil, then the membrane should be undeflected and one would have theoretically a state of initial stress in the wire or the zero frequency of the transducer.

The pressure inside the cell was varied from -14 psi to +25 psi for cell G-6 and to +50 psi for cell G-7. The upper limit was reached when the transmitter ceased to emit a clear signal. These two tests are shown in Fig. A.6a and A.6b for cells G-6 and G-7 respectively.

In Fig. A.6a the inside cell pressure was increased at intervals from -14 psi and corresponding frequency readings were taken. A marked change of slope occurred at point B, after which the slope flattened out and eventually became horizontal. It was assumed that at this point the outside earth pressure and the inside cell pressure were equal. A further increase of the inside cell pressure pushed the diaphragm into the soil and mobilized the passive condition. At an inside cell pressure of 25 psi the transmitter stopped emitting a distinguishable signal; apparently the diaphragm was pushed out too far. The zero frequency decreased from 876 cps to 802 cps due to driving of the sheet piles. Cell G-6 was measuring the active earth pressure whereas cell G-7 was facing the excavation to record the passive earth pressure.

Fig. A.6b depicts the behaviour of cell G-7 when the inside cell pressure was increased from -14 to +50 psi, points B and C indicate two points where the slope changes abruptly. The reasons why it was assumed that the point of zero frequency was at B rather than C were the following: After the excavation to grade and bracing of the sheet piles little movement of the wall took place except for the lower part of the piles below the last strut level tending to move into the excavation. The movement was restricted only by the piles own rigidity as well as the

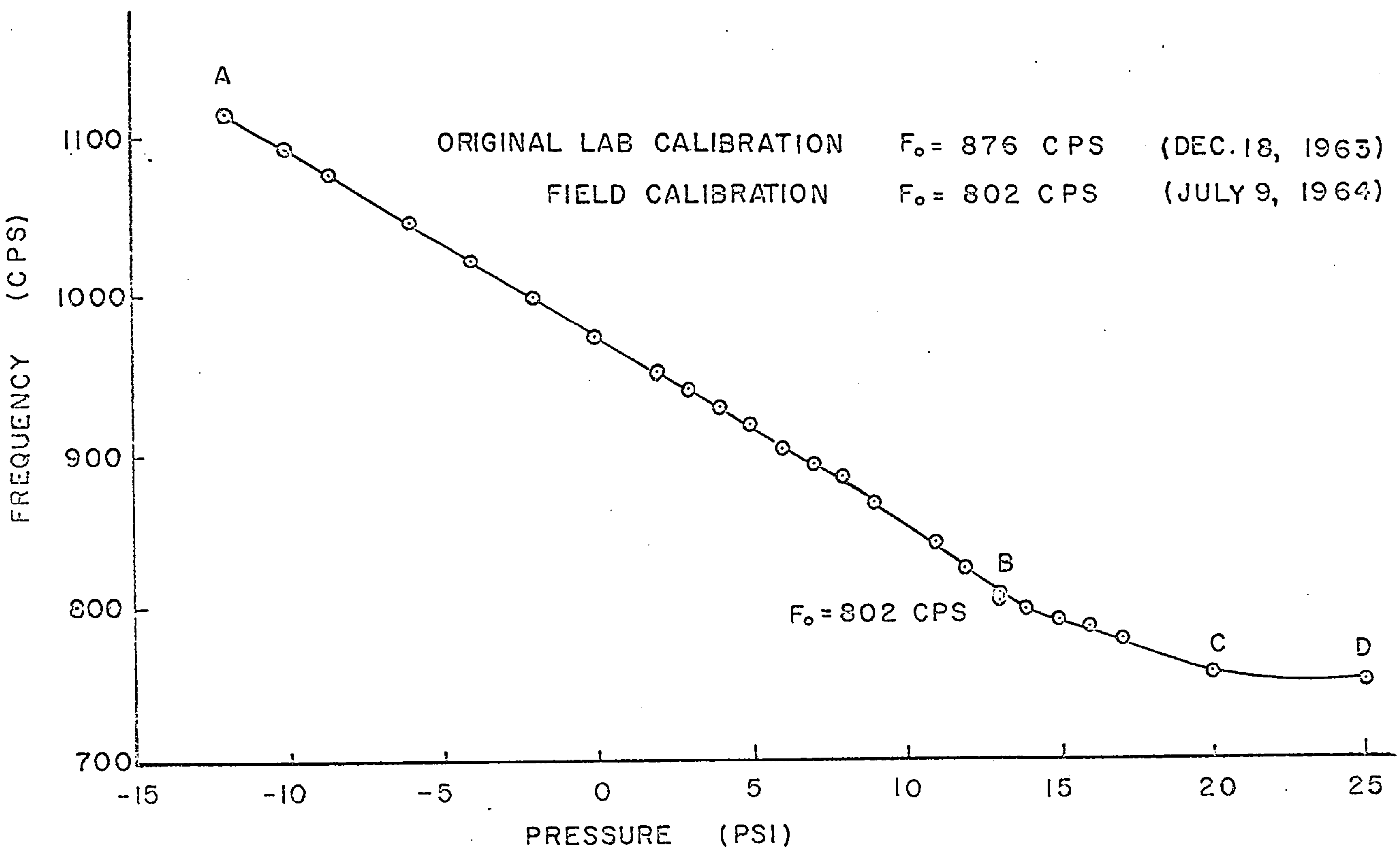

FIG. A.6.a FIELD RECALIBRATION OF CELL G-6

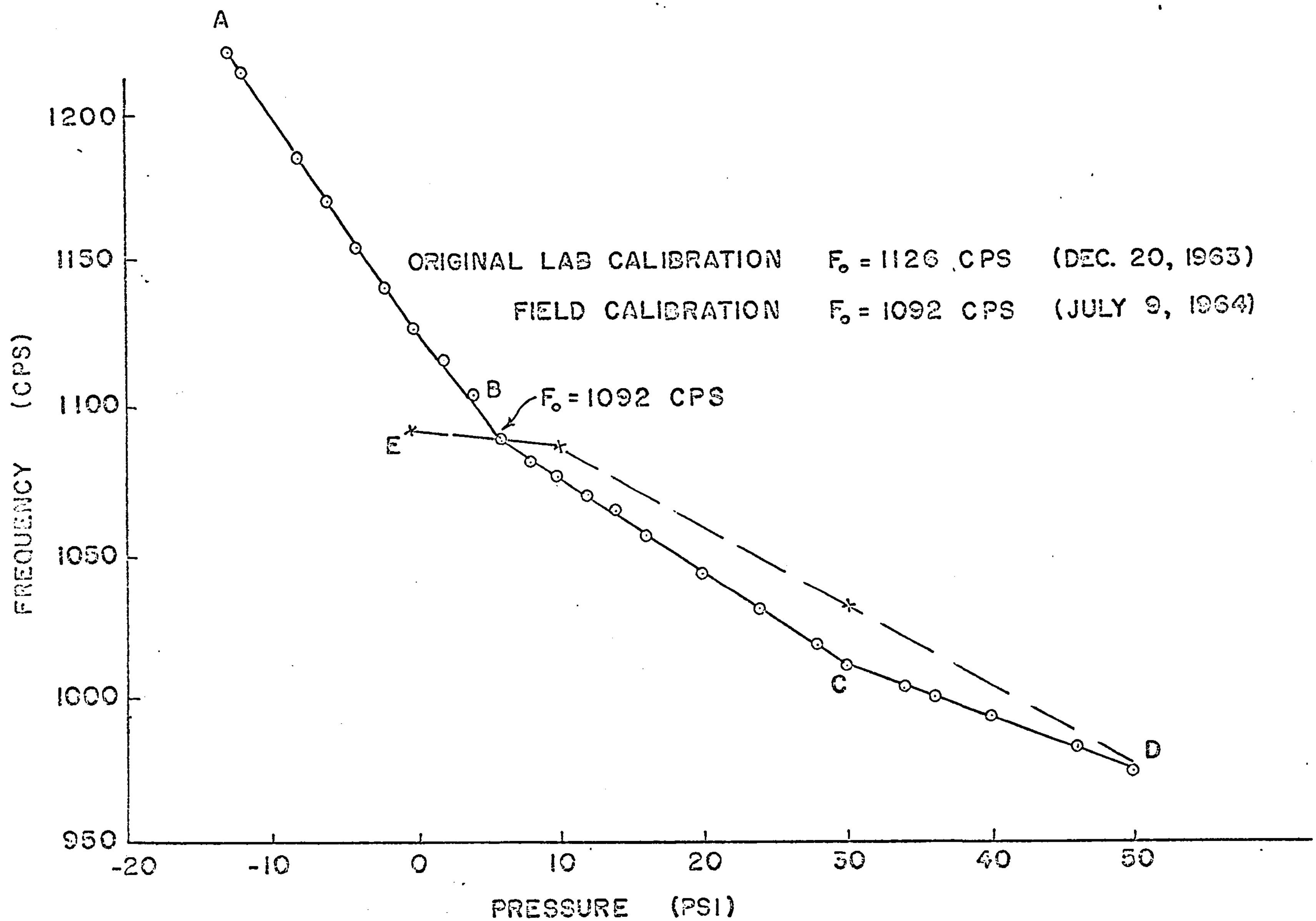

FIG. A.6.b FIELD RECALIBRATION OF CELL G-7 passive earth pressure of the sand in front of it. Due to bottom heave and "boiling" this passive resistance was decreased quite considerably and the lower parts of the piles probably deflected some more towards the excavation. So in July 1964 when the field calibration was performed there was no tendency for the piles to move (or to be moved) any further to mobilize the full passive resistance of the "re-deposited" sand and cell G-7 was just measuring the at rest-pressure due to the 5 ft of overburden plus, of course, the water pressure acting on it. Thus the total pressure as can be seen from Fig. A.6b was approximately 5 psi. As the inside cell pressure was increased beyond point B, the diaphragm deflected further outwards and the passive condition was reached at point C which is indicated by a change in slope of the calibration curve. When the pressure was decreased the curve passed through point B again which is another verification that this was the point of zero frequency. A decrease of zero frequency by 34 cps was observed due to driving of the pile.

A.5 Factors Affecting Cell Reading

A.5.1 Temperature

It was known from the experiments done by N.G.I. that changes in gauge temperature will cause a shift in the zero frequency. To obtain the magnitude and direction of this shift several cells were tested and the zero-frequency measured at different temperatures. Fig. A.7 shows the result of one cell, G-5, for which the temperature was varied from $-12^{o}F$ to $+90^{o}F$, the corresponding maximum frequency change was 47 cycles per second. The temperature of the cell was measured by a thermometer and a thermocouple placed inside the housing. The gauge was considered to have reached equilibrium with respect to temperature when both the cell as well as the surrounding air indicated the same temperature and only then a frequency reading was taken. For below freezing point temperatures the cells were placed in a freezer compartment and for higher temperatures in a drying oven, respectively.

The frequency squared with regard to temperature changes is given in Fig. A.8, from which the temperature coefficient α was obtained as 0.7×10^{-3} $sec^{-2} \times {}^{o}F^{-1}$; this means a temperature change of $10^{o}F$ will result in an error of less than 0.3 psi in the pressure measurement. The air temperature at the site varied from below $0^{o}F$ in December 1963 to over $100^{o}F$ in June 1964. The temperatures given in Figure A.9 are daily maximum, minimum, and mean temperatures of London as recorded by the Meteorological Branch of the Department of Transport. The temperatures of the excavation were slightly higher in the summer months since the north wall was exposed to direct sunlight during part of the day. Although the cells were shaded from direct sunlight, the air temperatures on that side of the excavation were high. In the initial pile driving stage when the pressure cells were above ground surface their temperature was

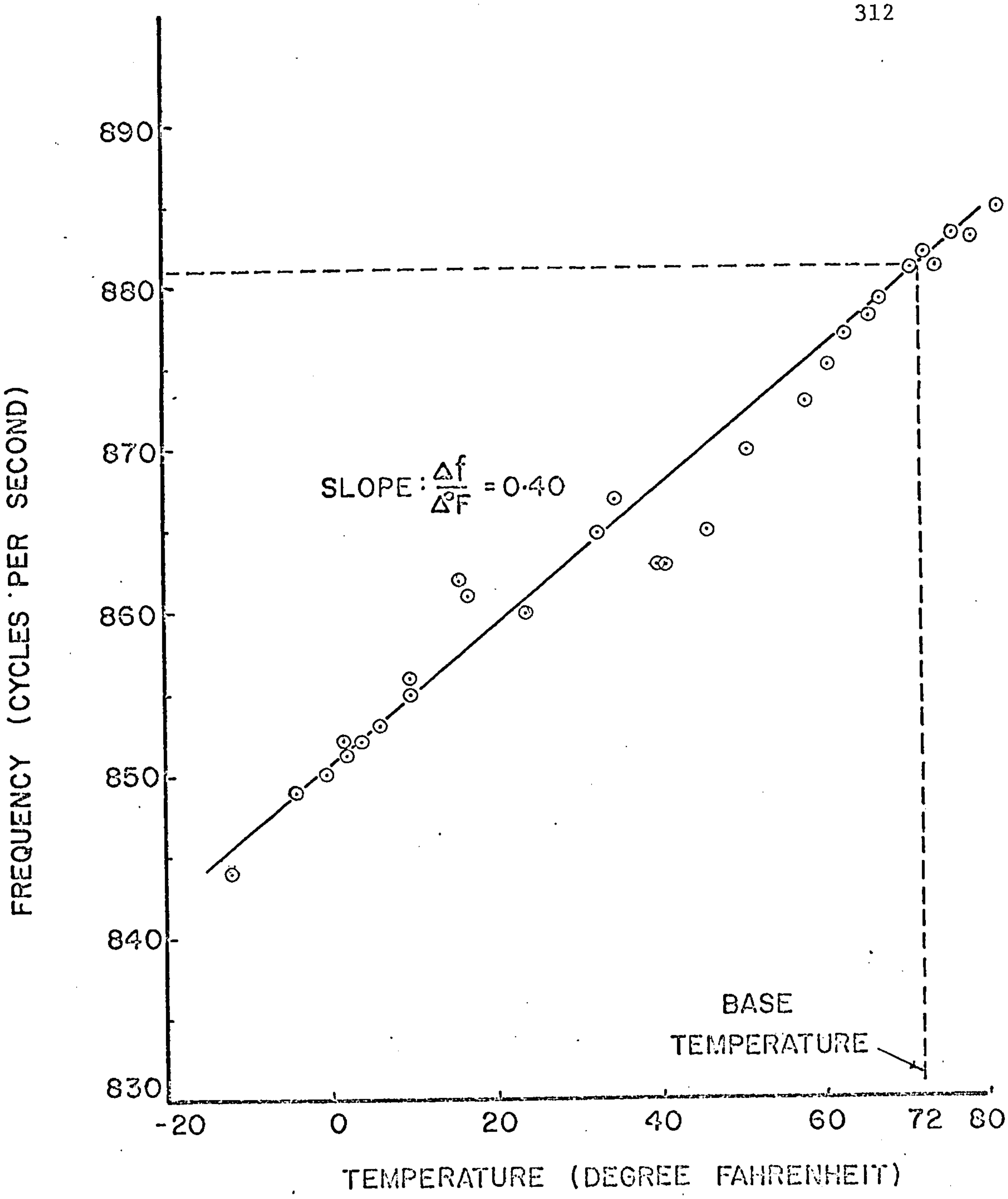

FIG. A.7 EFFECT OF TEMPERATURE ON ZERO-FREQUENCY READING CELL G-5

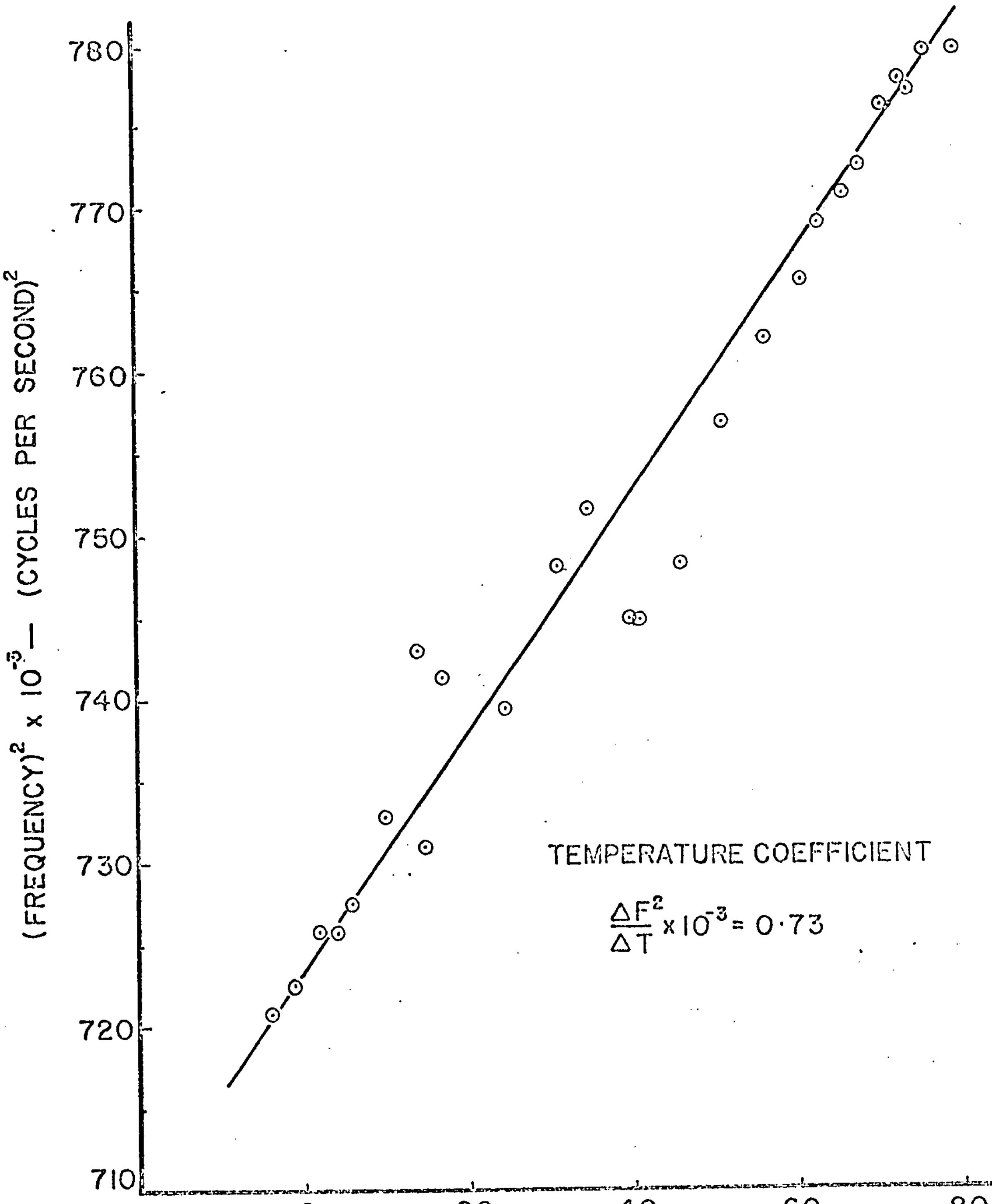

FIG. A.8 DETERMINATION OF TEMPERATURE COEFFICIENT α (CYCLES / SEC.)^2/ °F

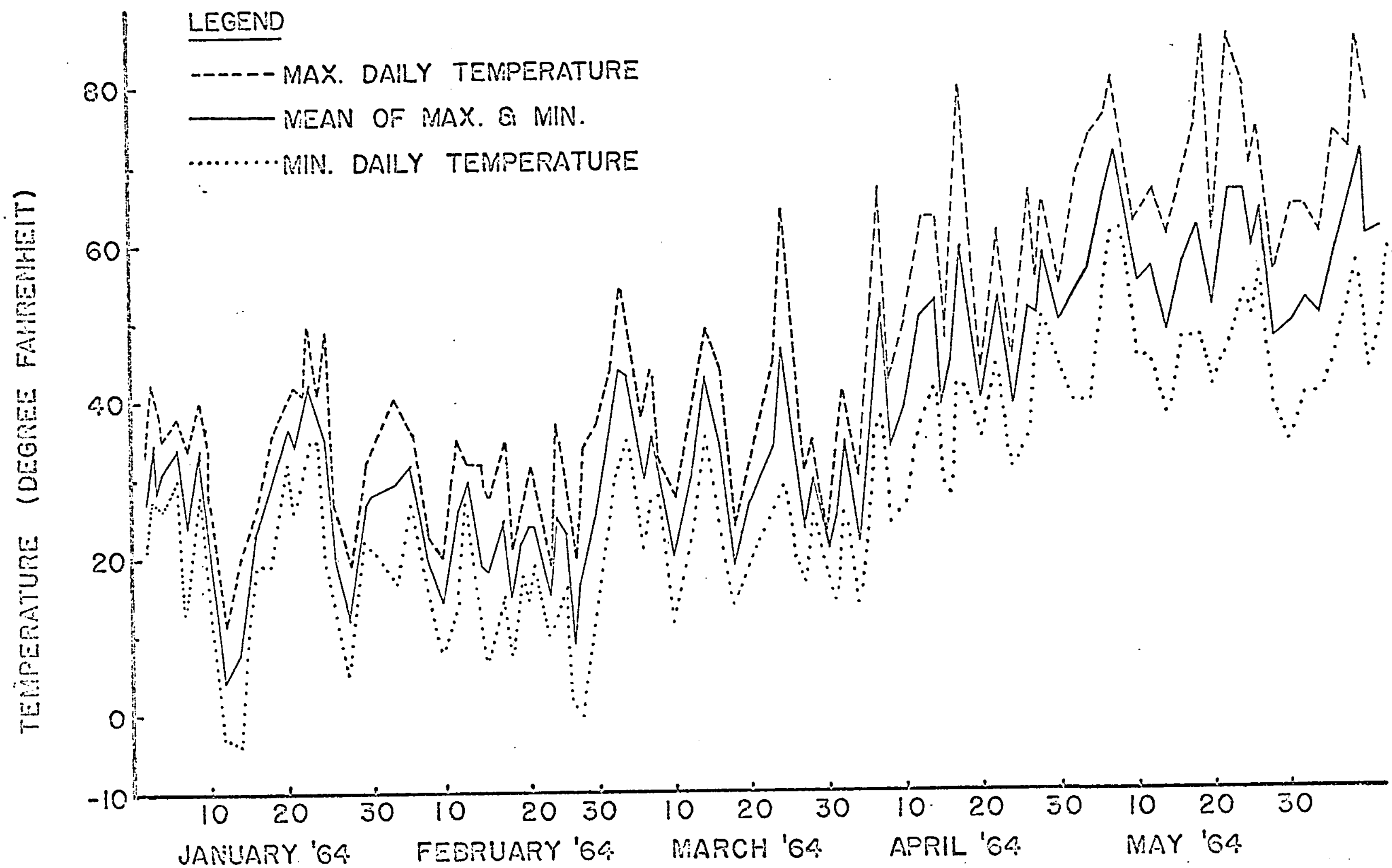

FIG. A.9 VARIATION OF DAILY TEMPERATURES FOR LONDON, ONT.

taken to be equal to the surrounding air temperature and was assumed to be identical with the soil temperature when completely buried. Unfortunately only a few soil temperatures were measured at the site, it varied from a low 35°F to a high of 70°F (when the air temperature was 94°F), for soil located directly behind the sheet piles. It never went below the freezing point (32°F), since even during the coldest day water was observed seeping through the interlocking joints. As the excavation proceeded the back or excavation side of the cells became exposed to the air. For this condition the cell temperature was taken as the average of the mean air temperature and the soil temperature, assuming an uniform temperature gradient across the cell.

This assumption was substantiated by a laboratory test where a cell was mounted to the water tank, the back of the cell was kept at room temperature (72°F) and the face of the cell (diaphragm) at a constant water temperature of 40°F, the corresponding frequency reading indicated that the cell should be at 57°F, the actual temperature measurement of the inside of the cell was 59°F.

All field frequency readings were corrected to a base temperature of 72°F corresponding to the initial and final calibration temperature in the laboratory, For both calibratiors the water in the tank was kept at room temperature to avoid any temperature difference across the cell walls.

The applied frequency corrections were obtained using the following relationship:

$$F_{72} = F_g + k\ (72 - T_g) \tag{3}$$

where
F_{72} = corrected cell frequency
F_g = measured cell frequency
T_g = actual cell temperature
k = 0.4 (average slope of graph frequency vs. temperature)

For an extreme air temperature of $-10^{\circ}F$ and a soil temperature of $40^{\circ}F$ the cell temperature would be $(-10^{\circ} + 40)^{\circ}F/2 = 15^{\circ}F$ for a cell exposed to soil at one side and to air on the other. The corresponding frequency correction from Eq. 3 would amount to 0.4 (72 - 12) = 23 cycles per second which would affect the pressure measurement by less than 0.4 psi on the average.

The frequency measurements were made with an instrument Oscar V, built by the Central Institute for Industrial Research, Norway. The apparatus consisted of a power supply, a Wienbridge oscillator with adjustable frequency, a cathode tube, two amplifiers, one for the oscillator signal and one for the quartz crystal signal, and a crystal oscillator. All these components are assembled in a sturdy sheet metal box. The crystal oscillator was set to supply a constant reference frequency of 1000 cycles/second indicated on the oscilloscope by an elliptical Lissajous figure. It was observed that the instrument temperature had a marked effect on the frequency reading. When the instrument was checked for its reference frequency at $+20^{o}F$ the deviation was 32 cycles per second and decreased to -2 cycles per second at an instrument temperature of $+83^{o}F$. The temperature was measured by a thermometer placed in the recess beneath the chassis inside the metal box.

In a similar test the pressure cell W-7 was connected to the oscilloscope and reference readings at various temperatures were taken with the pressure gauge being kept at room temperature throughout this procedure. The results of both tests are shown in Fig. A.10. In both cases the relationship of frequency deviation and instrument temperature is a straight line. The curve for the readout instrument and the curve for the instrument with the cell attached to it coincide at a temperature of $80^{o}F$. Ideally the two curves should coincide with one another if the instrument were unaffected by temperature changes. The difference in ordinates between corresponding points of the two curves is the correction which has to be applied as shown by the dashed-dotted curve in Fig. A.10. Since the working temperature of the instrument was usually between 50 and $80^{o}F$ the maximum error introduced was in the order of 6 cycles per second. At $80^{o}F$ the correction was zero cycles per second and there was also no deviation from the reference frequency. It appears therefore that the instrument was set for a base temperature of $80^{o}F$.

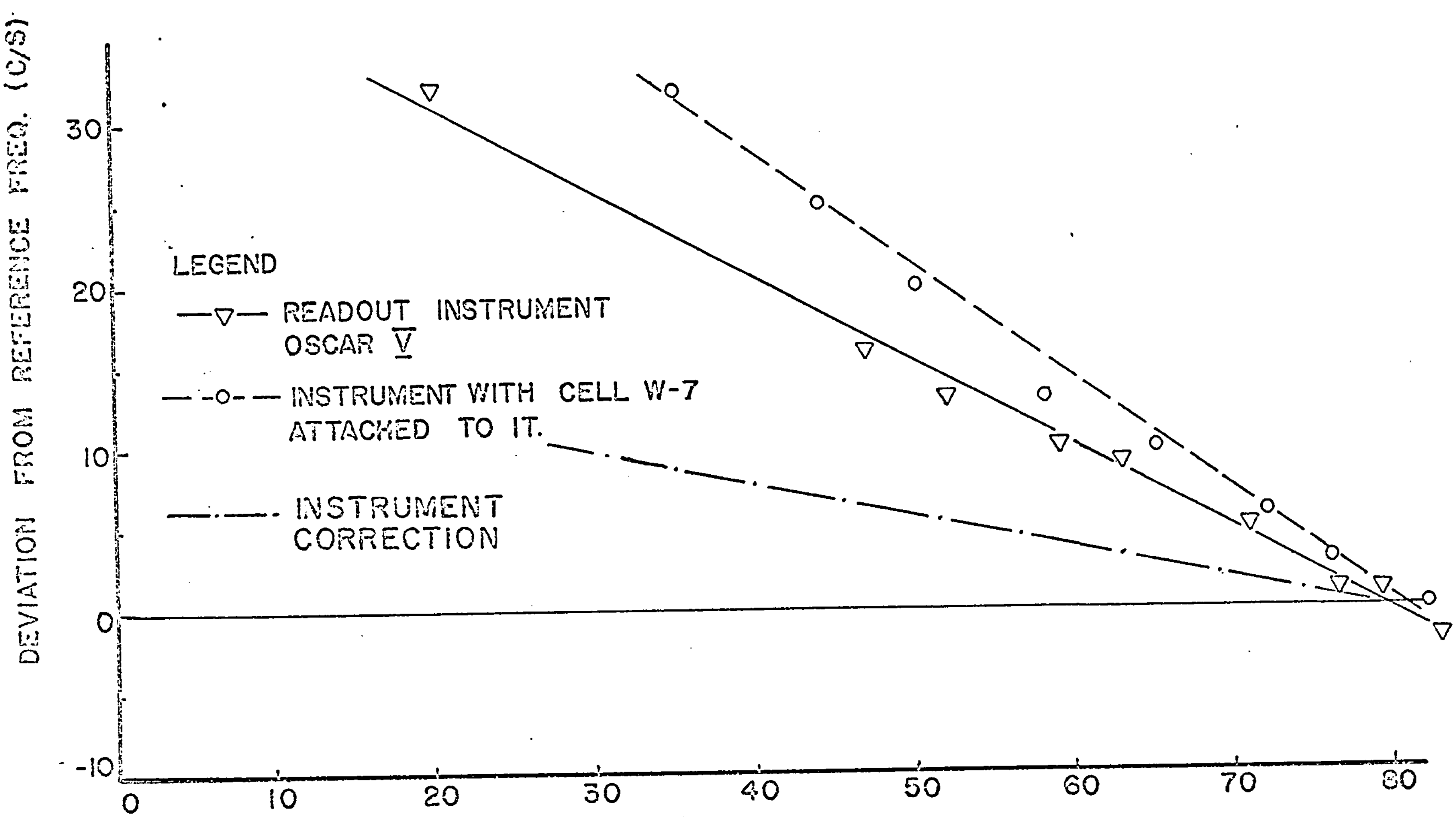

FIG. A.10 EFFECT OF INSTRUMENT TEMPERATURE ON FREQUENCY READING

A.5.2 Distance of Wire to Magnet

The excited wire is vibrating in a magnetic field and according to laws of electricity the damping force increases as the distance of the wire to magnet decreases. The change of this distance was due to two factors. Firstly, the deflection of the diaphragm necessitated a change in distance and secondly, a change of distance could be expected during installation of the cells since the diaphragm was fitted loosely in the housing held in place by a rubber O-ring. To investigate the effect of wire distance from magnet poles, tests were made on two cells the results of which are shown in Figs. A.11.a, and A.11.b, respectively. In Fig. A.11.a a N.G.I. test is also shown for comparison. The frequency of the two cells decreased rapidly as the distance of wire to poles became less than 1.0 mm. Above 1.1 mm the frequency remained constant but the emitted signal became less clear as the distance was increased. The clearest signal of the induced e.m.f. was recorded on the oscilloscope when the distance was greater than 0.9 mm but less than 1.1 mm, this was true for both cells. The Norwegian Geotechnical Institute concluded from their test that the distance should be somewhat smaller than 1 mm but not less than 0.6 mm.

All of the recovered cells were taken apart after recalibration and their distance of wire to magnet poles was measured and the condition of the cell checked. The distance varied from 0.4 mm to 1.1 mm.

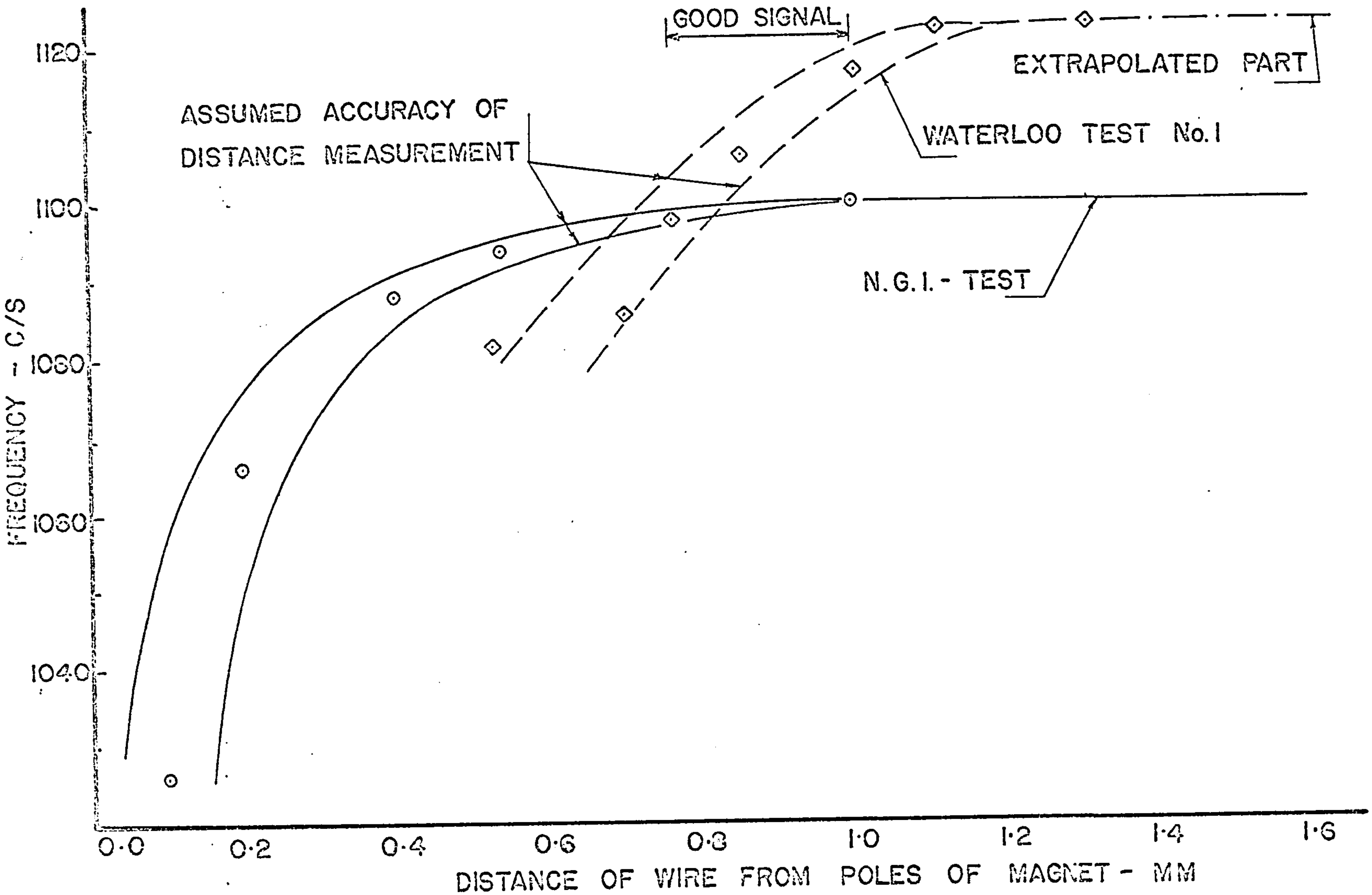

FIG.A.IIa VARIATION OF DISTANCE BETWEEN WIRE TO MAGNET AND ITS EFFECT ON FREQUENCY

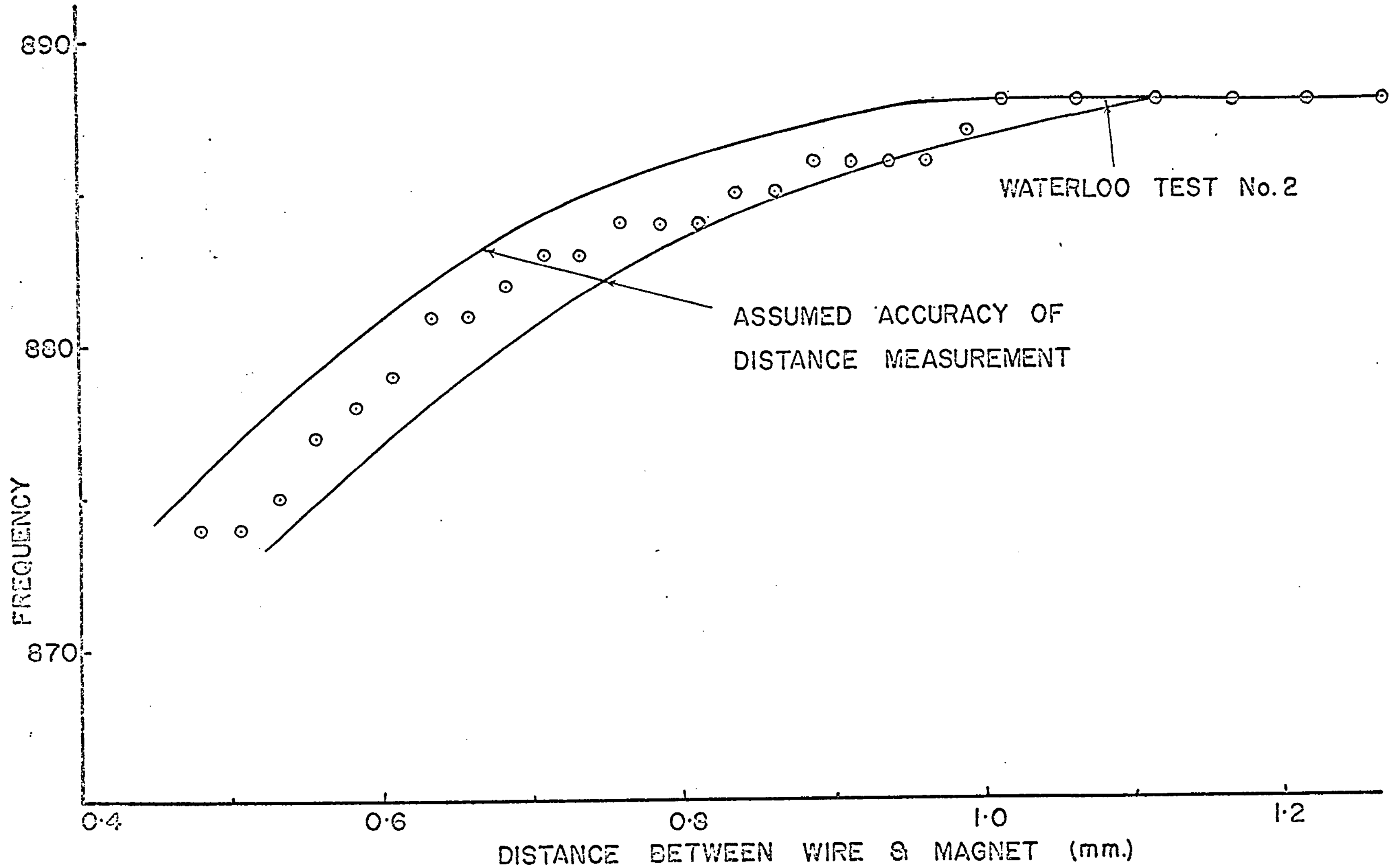

FIG. A.II.b FREQUENCY vs. DISTANCE BETWEEN WIRE & MAGNET

Surprisingly the three cells whose distance of wire to magnet was between 0.4 mm and 0.5 mm yielded good to excellent amplitude readings when recalibrated as compared to a very poor amplitude for the cell having a distance of 1.1 mm. This was attributed to the possible different field strength of the magnets.

Upon recovery all of the wires and magnets were found to be covered with slime and rust despite the inside of the cell having been sprayed with a rust inhibitor "Araldite Resin D" and given a coating of silicone grease excluding the wire and the magnet poles before final assembly. The O-rings and grooves were also coated with silicone grease. The maximum thickness of residue measured on the magnet was 0.15 mm. and on the piano wire was 0.0.8 mm. In all cells fine sand was found deposited between the diaphragm and the housing shoulder mixed with some slimy black substance probably caused by the partial deterioration of the rubber O-ring.

A.5.3 Effect of Kinks in Wire

The wires were slightly stretched before installation to insure their straightness. Although the wire is subjected to a tensile stress it has been found that some curvature is generally present, even if special straightening processes are carried out before the wire is installed in the gauge. For this reasons the measured sensitivities are less than the theoretical values (Lee 1957). After recovery and disassembly of the cells three wires had kinks a distance of 1/8 to 3/8 inches from the lock nuts. The effect of these kinks is to reduce further the sensitivity of the transducers. The calibration relationship between pressure and receiver response varied from unit to unit depending on the extent of the kinks and the initial curvature.

A.5.4 Effect of Pile Driving

The piles used on the project were positioned at the site and driven down approximately 10 ft by a Delmag D-12 driver, then a vibratory driver, Model Foster Vibro, weighing 5½ tons and capable of doing anywhere from 700 to 1,000 vibrations per minute, was used to drive the piles to their required tip elevation of 714.0 feet. In some instances the severe resistance to driving was overcome by jetting, i.e. sinking a 2-inch pipe with a 1-inch nozzle down to the tip of the pile and loosening up the soil ahead of the pile by a jet of water. It should be pointed out again that the soil through which the piles had to be driven consisted of very dense and fine uniform sand. Field densities of up to 125 pcf (dry unit weight) were recorded. For the first 10 ft the N values varied between 10 and 20. Below 20 ft they exceeded 100 blows per foot penetration.

Both test piles were made up of two sections each, a 12 ft and a 41 ft section which were welded together in the field after some initial driving. For pile No. 14 the short 12 ft section was driven first whereas, for pile No. 15 the 41 ft section was driven first. The bottom section of pile No. 14 was driven initially 3 feet by dropping the top 41 ft section on it using 10 blows with 15 ft drop. The long part of pile No. 15 was driven first after it was dropped into place. The tip elevations of piles No. 14 and No. 15 were 754.0 and 756.0 feet respectively. Both piles were then driven together with the Delmag D-12 hammer to a tip elevation of 746.0 feet. The driving was continued with vibratory equipment. The vibratory head works on following principle. Electric motors, powered by a portable generator set or commercial power, drive eccentrically loaded shafts at high speed. The resultant centrifugal force developed by the synchronized eccentrics, generator vertical motion in the main chassis of the Vibro Driver. This motion is transmitted undiminished to the sheet piles by the hydraulics clamping system. Frequency, amplitude and driving forces are easily adjusted to correspond to soil conditions. The vibratory action is transmitted through the pile to the soil to minimize friction and permit the soil grains to be more readily displaced by the tip of the pile being dirven. It was also resorted to jetting to further facilitate the ease of driving. Except for pile No. 15, at elevation 713 feet, driving was very hard despite jetting.

Table A.1 summarizes the pile driving operation for the two test piles. Fig. A.12shows graphically the effect of pile driving on the change of zero frequency for the gauges mounted on pile No. 14 and

Date 1964	Pile No.	Pile Tip Elevation Ft Start	End	Jetting	Relative Ease of Driving	Time Sec.	Type of Driving Equipment	Remarks
Jan 7	14	757	to 754	no	10 blow @15'	-	dropping 41 ft sect. on 12 ft section	
	15	757	to 756	no		-		dropped pile in place by own weight
Jan 15	15	756	to 754	no	tapped easily		Delmag D-12	
	14 & 15 together	754	to 749.5	no	22 blows for last $1\frac{1}{2}$ ft	-	Delmag D-12	
	13 & 14 together	749.5	to 746	no	47 blows for last foot	-	Delmag D-12	driving stopped as pile tops started bending
	15 & 16	749.5	to 746	no	45 blows for last foot	-	Delmag D-12	
	14	746	to 742	no	fairly easy	-	Vibratory	
Jan 21	13 & 14 together	742	to 732	yes	easy	90 sec.	Vibratory	
	15	746	to 730	yes	easy very hard @ 730	45 sec.	Vibratory	no visible damage to earth pressure cells
Jan 23	14	732	to 723	yes	easy	45 sec.	Vibratory	no visible
	15	730	to 721	yes	very easy	25 sec.	Vibratory	damage to cells
Jan 26	14	723	to 114	yes	fairly easy		Vibratory	
	15	721	to 714	yes	fairly easy		Vibratory	

TABLE A.1

Progress of Pile Driving for Piles No. 14 and No. 15

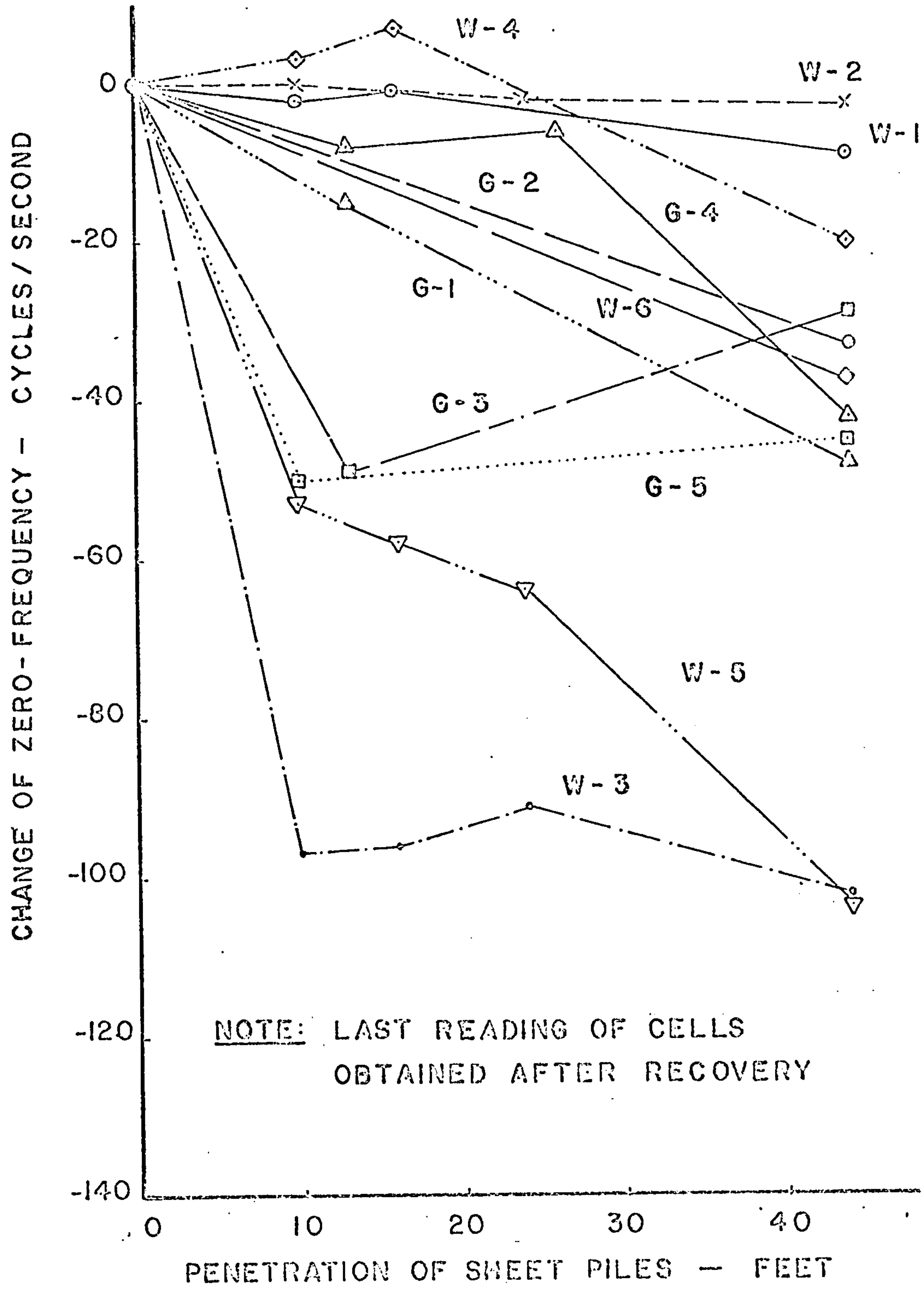

FIG. A.12 VARIATION OF ZERO FREQUENCY -- DEPTH OF PENETRATION

No. 15, respectively. The final zero frequencies were obtained at the end of construction operations when the cells were recovered and recalibrated in the laboratory. The Geonor cells showed an average negative zero drift of 51 cycles/second and a maximum of 74 cycles per second. The cells from the Waterloo series had an average change of 53 cycles per second and a maximum negative change of 134 cycles per second for cell W-3. Most of the decrease occurred in the first 10 ft of pile driving or when the Delmag D-12 hammer was in operation. A decrease in frequency is equivalent to a decrease in wire tension presumably due to a slip of the wire in the grips of the post.

For the evaluation of earth pressures zero frequencies from the laboratory recalibration were used after January 28th, 1964, the date when the pile driving was completed. For readings before that corresponding corrections were applied assuming a linear decrease between the last two zero frequencies. The readings of cells G-6 and G-7 were corrected by 74 and 34 cycles per second, respectively, based upon the change obtained from the field calibration.

A.5.5 Radio Interference

For the first few field frequency readings no clear signal could be obtained on the oscilloscope due to interference of the local radio station. A 50 ft lead cable, with both strands shielded and grounded, was used between the end of the cell leads and the frequency readout instrument to eliminate most of the static.

A.6 Factors Causing the Breakdown of the Cells

1. The inside of the cells were sprayed with a rust inhibitor and as the wire vibrated in the magnetic field it touched and adhered to the magnet poles in some instances. A hammer blow on the back of the cell usually freed the wire again but this remedy was only possible where the cells were accessible. Ths problem can be avoided in future installations using a different, non-sticky rust inhibitor or not putting it on the magnet face.

2. Most of the cells were located below the ground water table and were sealed against infiltration of water by an O-ring fitted around the collar of the flexible steel diaphragm (refer to Fig. A.2). This method did not prove adequate for some cells where the inside of the gauge became flooded and short circuited the electrical system. Attempts to drain one cell, W-1, by drilling a hole in the back of the cell and blowing out the water were only partly successful.

3. Severe pounding with pile driving equipment will decrease the zero frequency but not enough to make the transducer inoperative.

A.7 Conclusion and Recommendations

1. Of the thirteen cells which were in operation for six months two cells, W-1, and W-3, stopped working. W-1 quit emitting signals one month after installation on the sheet piles and could not be brought back into

operation until the completion of the programme when the cell was dismantled and cleaned. The inside was completely rust covered and full of water. W-3 stopped transmitting several times, every time it was submerged under water, i.e. by the rising water table, water penetrated into the cell and short circuited the electrical system. When the water level fell below the cell's elevation water drained out from the cell and it went back into operation. It is recommended to improve the water-tightness by installing a better seal, such as a double O-ring.

2. The driving of the sheet piles influenced the zero frequency of the cell the most. An average decrease of about 50 cps was observed. As an improvement a better gripping arrangement of the wire at the post is suggested.

3. Another disadvantage of the cell is, that once installed there is no possibility to get at the inside of the transducers without taking them off the sheet piles and by doing so the soil in front of the diaphragm is unavoidably disturbed. A different design which provides for an opening at the back of the cell will be recommended.

4. The calibration was carried out using fluid (water) pressure and it was established that under fluid pressure each gauge gave a stable, linear calibration curve, both in loading and unloading cycles with negligible hysteresis, thus providing a constant fluid calibration factor.

5. The behaviour of the sand over the gauge in unloading cycle was shown

to differ markedly from the behaviour of the loading cycle. This was attributed to arching of the soil across the calibration tank and to a lesser extent to arching across the diaphragm.

6. The temperature has a definite effect on the reading of the gauge but variations in zero frequency could easily be corrected for once the temperature of the transmitter was known.

7. The ratio of central deflection to the diameter of the gauge diaphragm is about 2000 for a pressure of 35 psi. According to an investigation carried out by U.S. Waterways Experiment Station (1944), the diameter deflection ratio should exceed 1000, for a pressure cell mounted flush with the surface of a rigid wall facing up to a loose sand mass.

8. On the whole the earth pressure cells have proved themselves to be satisfactory and dependable for the purpose intended.

VITA

Gunther E.A. Bauer was born in Michelstadt, West-Germany on April 22nd, 1936. He graduated from the City High School in 1957 in which year he came to Canada. From 1957 to autumn 1959 he worked as a miner for Lacnor Mines, Elliott Lake, Ontario.

He enrolled at the University of Toronto in September 1959, and received a Bachelor of Applied Science Degree in Civil Engineering in June 1964. During the summer of 1960 he was employed as an instrument man by the consulting firm of Gordon Urwin Limited, Oakville, Ontario. For the summers of 1961 and 1962 he worked as an intermediate and senior draughtsman for the consulting firm W.S. Atkins & Associates in Toronto.

In the summer of 1963 he did research work for the Civil Engineering Department of the University of Toronto under the supervision of Professor W. Huggins on a project sponsored by the National Research Council.

During the summer of 1964 he was employed by the consulting firm of Kilborn Engineering Limited in Toronto, in the capacity of a design engineer.

In the autumn of 1964 he started studies in the Graduate School of the University of Waterloo from which he obtained his Master of Applied Science Degree in 1965.

He was awarded a teaching assistantship by the Civil Engineering Department and a Studentship by the National Research Council.

He continued his graduate study towards the Degree of Doctor of Philosophy in Civil Engineering at the University of Ottawa and was appointed a lecturer in the Department of Civil Engineering in 1967 which position he presently holds.

He is a licenced Professional Engineer in the Province of Ontario, a member of the Engineering Institute of Canada, a member of the International Society for Soil Mechanics and Foundation Engineering, an Associate Member of the American Society of Civil Engineers and a member of the Canadian Institute of Surveying.